

University of Nevada, Reno

**Application of Polymer Concrete and Non-Proprietary Ultra-High Performance  
Concrete for Pre-fabricated Bridge Decks Field Joints**

A dissertation submitted in partial fulfillment of the  
requirements for the degree of Doctor of Philosophy

in

Civil and Environmental Engineering

by

Mohamed Abokifa

Dr. Mohamed A. Moustafa / Dissertation Advisor

December 2021

© 2021, Mohamed Abokifa



THE GRADUATE SCHOOL

We recommend that the dissertation  
prepared under our supervision by

**Mohamed Abokifa**

entitled

**Application of Polymer Concrete and Non-Proprietary Ultra-High  
Performance Concrete for Prefabricated Bridge Decks Field Joints**

be accepted in partial fulfillment of the  
requirements for the degree of

**Doctor of Philosophy**

Mohamed A. Moustafa, Ph.D.

*Advisor*

Ahmad M. Itani, Ph.D.

*Committee Member*

Floriana Petrone, Ph.D.

*Committee Member*

Elnaz Esmailzadeh Seylabi, Ph.D.

*Committee Member*

Michael H. Gardner, Ph.D.

*Graduate School Representative*

David W. Zeh, Ph.D., Dean

*Graduate School*

December, 2021

## ABSTRACT

Pre-fabricated full-depth bridge deck panels are widely used to expedite bridge deck erection and accelerate bridge construction. However, these pre-fabricated deck panels dictates the need for field cast joints at least in one direction of the bridge. Currently, ultra-high performance concrete (UHPC) full-depth deck joints with concave shear key are commonly used in bridge decks. The robust UHPC mixes have gained popularity for deck field joint applications because of their unparalleled mechanical properties, high early strength, high bond strength and high durability. However, the proprietary nature and relatively expensive cost of these mixes may restrain their implementation in the US bridge industry. Therefore, many research efforts have considered addressing these major drawbacks and have searched for other alternative advanced materials, like this doctoral study presented herein. The overarching goal of this study is to identify alternative materials to UHPC and experimentally proof-test their suitability for use in the deck field joints. Poly-methyl methacrylate polymer concrete (PMMA-PC) along with non-proprietary UHPC mix (NP-UHPC) developed using locally available materials in the western states were identified as the alternatives for deck field joint materials. To accomplish this goal, experimental investigation of nine full-scale specimens was done to study the structural performance of deck systems with PMMA-PC and NP-UHPC field joints and compare them with reference systems with proprietary UHPC (P-UHPC) field joints. The experimental program included testing of six specimens with transverse field joints, and three other specimens that represent the longitudinal field joints in typical deck-bulb tee girders (DBTs). The specimens were subjected to vertical static loading up to failure to investigate the overall structural behavior of the deck specimens and the performance of the field joints. The results demonstrated that the PMMA-PC and the developed NP-UHPC mix can be efficiently used for full-depth bridge deck field joints with comparable performance to the proprietary UHPC joints. The study has also considered developing and updating design guidelines for the design of full-depth deck panels with PMMA-PC and UHPC field joints. Thus, based on the results and assessment of all specimens, the study is concluded with design and construction recommendations for both field joints with emerging materials and the deck panels.

## ACKNOWLEDGMENTS

This dissertation would not have been possible without the support, help, and encouragement I received over the past four years from many individuals, to whom I am sincerely thankful.

First and foremost, I would like to express my deepest and most sincere gratitude to Dr. Mohamed Moustafa, my Ph.D. advisor and the chair of my dissertation committee. I have been tremendously fortunate and honored to have him as my advisor, and I truly cannot thank him enough for his continuous guidance, support, and encouragement throughout my graduate studies at University of Nevada, Reno. He provided me with the freedom to explore my own research interests and motivated me to pursue my goals on every step of the way. What I learned from him has sure spanned beyond academia, and he will always serve as my inspiration for excellence as I move ahead in my professional career.

I would also like to express my sincere gratitude to my dissertation committee members, Prof. Ahmad Itani, Dr. Elnaz Seylabi, Dr. Floriana Petrone, and Dr. Michael Gardner for providing valuable inputs to improve this dissertation and for all the guidance and support they provided throughout my doctoral research. I deeply appreciated our fruitful discussions about my future career plans.

I would like to thank Dr. Patrick Laplace, Chad Lyttle, Todd Lyttle, Wendy Freeman, and Mark Lattin for their time and hard work in the UNR laboratory. I am also thankful for all the sources that funded my research, especially the ABC-UTC.

Many thanks and appreciation to all friends, colleagues in the Earthquake Engineering Laboratory at UNR for making my graduate school experience so memorable. It is a great honor for me to share this bond with the past, present, and future members of EEL. I would specially thank Dr. Mahmoud Aboukifa, Michael Abdelmalak, Hussein Sadek, Omar Shabrawy and Karim Moustafa for their friendship, company, support and guidance through the years at Reno. I am also thankful to Dr. Luna Ngeljaratan, Dr. Azin Ghaffary, Mohamed Shaker, Mohamed Hosny, Milana Cimeša, Rolando Grijalva, Stephen Waldvogel, and Sagar Acharya for their friendship and support.

Finally, I would especially like to thank my father, Prof. Amin Abokifa, who is my role model and my inspiration for excellence. I also want to express my special gratitude to my family; my mother Maha Hanafy, my lovely wife Mariam Soliman and daughters Noureen and Nelly, and my siblings Dr. Ahmed Abokifa, Dr. Mahmoud Aboukifa, and Nada Abokifa for their continued support and endless motivation and support through all these years.

## TABLE OF CONTENTS

Acknowledgments.....	ii
Table of Contents.....	iv
List of Tables .....	x
List of Figures.....	xii
<b>1 Introduction.....</b>	<b>1</b>
1.1 Background and Problem Statement.....	1
1.2 Motivation .....	6
1.3 Research Objectives .....	9
1.4 Research Methodology.....	11
1.5 Dissertation Outline.....	14
References.....	15
<b>2 Comparative Structural Behavior of Bridge Deck Panels with Polymer Concrete and UHPC Transverse Field Joints.....</b>	<b>17</b>
Abstract.....	17
2.1 Introduction .....	17
2.2 Experimental Program.....	22
2.2.1 Specimen Design and Test Matrix .....	22
2.2.2 Test Setup and Instrumentation Plan .....	27
2.2.3 Loading Protocol.....	31
2.2.4 Specimen Construction.....	32
2.2.5 Material Properties.....	33
2.3 Test Results and Discussion.....	36
2.3.1 Damage Progression and Mode of Failure.....	36

2.3.2	Load-Deflection Relationship.....	40
2.3.3	Reinforcement Strains.....	46
2.3.4	Interface Opening.....	51
2.3.5	Comparative PC and UHPC application cost .....	53
2.4	Concluding Remarks .....	54
	Acknowledgment .....	55
	References.....	55
3	Experimental Behavior of Poly Methyl Methacrylate Polymer Concrete for Bridge Deck Bulb Tee Girders Longitudinal Field Joints .....	60
	Abstract.....	60
3.1	Introduction .....	60
3.2	PMMA-PC Mechanical Properties .....	65
3.2.1	Material Mixing .....	66
3.2.2	Compressive Strength.....	68
3.2.3	Flexural Strength.....	69
3.2.4	Direct Tension Strength .....	71
3.3	Experimental Program.....	72
3.3.1	Specimens Design and Test Matrix .....	72
3.3.2	Test Setup and Instrumentation Plan .....	76
3.3.3	Loading Protocol.....	79
3.3.4	Specimens Construction.....	80
3.3.5	Material Properties.....	81
3.4	Test Results and Discussion.....	83
3.4.1	Damage Progression and Mode of Failure.....	83
3.4.2	Load-Deflection Relationship.....	87



3.4.3	Reinforcement Strains.....	93
3.4.4	Interface Opening.....	99
3.5	Summary and Conclusion .....	100
	Acknowledgment .....	102
	References.....	102
4	Mechanical Characterization and Material Variability Effects of Emerging Non-Proprietary UHPC Mixes for Accelerated Bridge Construction Field Joints.....	107
	Abstract.....	107
4.1	Introduction .....	107
4.2	Background on Developing Non-proprietary UHPC.....	110
4.2.1	Mix Design.....	110
4.2.2	Mixing Proportions .....	110
4.2.3	Material Constituents .....	111
4.2.4	Mixing Methodology .....	114
4.3	Variability Study .....	114
4.3.1	Material Sources Variability.....	115
4.3.2	Aggregate Types and Grading Variability .....	115
4.3.3	NP-UHPC Mixes Summary .....	118
4.4	Test Results and Discussion.....	119
4.4.1	Flow Tests.....	119
4.4.2	Compression Tests .....	121
4.4.3	Flexure Tests.....	131
4.4.4	Direct Tension Test.....	135
4.5	Summary and Concluding Remarks.....	139
	Acknowledgments.....	141

References .....	141
5 Experimental Behavior of Precast Bridge Deck Systems with Non-Proprietary UHPC Transverse Field Joints .....	146
Abstract .....	146
5.1 Introduction .....	147
5.2 Background .....	150
5.2.1 NP-UHPC Mix .....	150
5.2.2 Reference Specimen with P-UHPC Joint .....	152
5.3 Experimental Program .....	154
5.3.1 Specimens Design and Test Matrix .....	154
5.3.2 Test Setup and Instrumentations .....	158
5.3.3 Loading Protocol .....	160
5.3.4 Fabrication of Test Specimens .....	160
5.4 Test Results and Discussion .....	161
5.4.1 Key Results .....	161
5.4.2 Global Behavior of Specimens .....	162
5.4.3 Local Behavior of Specimens .....	167
5.5 Conclusions .....	174
Acknowledgment .....	176
References .....	176
6 Full-Scale Testing of Non-Proprietary Ultra-High Performance Concrete for Deck Bulb Tee Longitudinal Field Joints .....	181
Abstract .....	181
6.1 Introduction .....	181
6.2 Non-Proprietary UHPC Mix Design And Characterization .....	186

6.2.1	Non-proprietary UHPC mixing proportions and procedure .....	187
6.2.2	Non-Proprietary UHPC Material Testing .....	189
6.3	Experimental Program.....	191
6.3.1	Design and Fabrication of the Test Specimen .....	191
6.3.2	Test Setup and Loading Protocol.....	195
6.3.3	Instrumentation Plan .....	197
6.4	Test Results and Comparative Behavior .....	198
6.4.1	Global Behavior of Specimens .....	199
6.4.2	Local Behavior of Specimens .....	207
6.5	Summary and Conclusions.....	211
	Acknowledgments.....	213
	References.....	214
7	Comparisons and Design and Construction Recommendations .....	218
7.1	Comparison of the Transverse Specimens .....	218
7.1.1	Transverse specimens with straight splice .....	218
7.1.2	Transverse specimens with loop splice.....	222
7.2	Comparison of the Longitudinal Specimens .....	224
7.2.1	Summary of Results .....	224
7.2.2	Load-Deflection Relationship.....	227
7.3	Design and Construction Recommendations of the FDBD Field Joints .....	228
7.3.1	Field Joint Materials .....	229
7.3.2	Full-Depth Deck Panels (FDDP) .....	242
7.3.3	Field Joint Interface .....	244
7.3.4	Full-Depth Deck Field Joints .....	245

7.3.5	Target Performance of Precast Bridge Deck with Full-Depth Field Joints	247
	References.....	248
8	Summary, Conclusions and Future Work.....	252
8.1	Summary .....	252
8.2	Key Conclusions and Findings.....	257
8.3	Recommendations for Future Work.....	262

## LIST OF TABLES

<b>Table 2-1</b> Test matrix and specimen details (metric dimensions in cm).....	27
<b>Table 2-2</b> Summary of measured compressive strength of different materials used in this study .....	35
<b>Table 2-3</b> Summary of key experimental test results.....	36
<b>Table 2-4</b> Interface opening width of specimens S1-UHPC and S2-PC at service and ultimate loads .....	52
<b>Table 3-1</b> PMMA-PC mixing proportions per cubic meter. ....	66
<b>Table 3-2</b> Test matrix and specimen details. ....	75
<b>Table 3-3</b> Summary of measured compressive strength of different materials used in this study .....	83
<b>Table 3-4</b> Summary of key experimental test results.....	84
<b>Table 3-5</b> Summary of the measured reinforcement strain values at peak load. ....	97
<b>Table 3-6</b> Interface opening width of specimens S1-UHPC and S2-PC at service and ultimate loads .....	99
<b>Table 4-1</b> Material constituents and local suppliers of the NP-UHPC mixes used in this study.....	116
<b>Table 4-2</b> Summary of five different NP-UHPC mixes used in this study .....	118
<b>Table 5-1</b> Mixing Proportions and Material Sources of the NP-UHPC Mixes.....	151
<b>Table 5-2</b> Main Mechanical Properties Tested at 28 days for the NP-UHPC Mixes.....	152
<b>Table 5-3</b> Mixing Proportions of the P-UHPC and NP-UHPC Components. ....	153
<b>Table 5-4</b> Experimental Test Matrix and Specimen Design Details.....	154
<b>Table 5-5</b> Summary of Key Experimental Test Results.....	162
<b>Table 5-6</b> Summary of the Maximum Tensile Reinforcement Strains and Concrete Compressive Strains at the AASHTO LRFD Service and Ultimate Loads.....	167
<b>Table 6-1</b> Baseline non-proprietary UHPC mix design as developed by OU [24].....	188
<b>Table 6-2</b> Compressive strength results [psi (MPa)] of the UNR and the OU NP-UHPC mixes.....	191
<b>Table 6-3</b> Flexural strength results of the UNR and the OU NP-UHPC mixes. ....	191
<b>Table 6-4</b> Summary of main experimental test results.....	200

<b>Table 6-5</b> Interface crack opening at the AASHTO LRFD service and ultimate loads.	211
<b>Table 7-1</b> Summary of the experimental results of the transverse specimens with straight splices.....	219
<b>Table 7-2</b> Summary of the compressive strength and flexural strength of the utilized materials.....	219
<b>Table 7-3</b> Summary of the experimental results of the transverse specimens with loop splices.....	222
<b>Table 7-4</b> Summary of the experimental results of the longitudinal specimens .....	224
<b>Table 7-5</b> Normalization of the experimental results of the longitudinal specimens.....	225
<b>Table 7-6</b> Main material properties of the P-UHPC, i.e. Ductal <sup>®</sup> JS1000 .....	230
<b>Table 7-7</b> Ductal <sup>®</sup> UHPC mixing proportions according to the number of dry premix bags .....	231
<b>Table 7-8</b> Ductal <sup>®</sup> UHPC mixing proportions per cubic yard and cubic meter .....	232
<b>Table 7-9</b> Main material properties of the PMMA-PC, i.e. Transpo <sup>®</sup> T-17 PC.....	237
<b>Table 7-10</b> Transpo <sup>®</sup> T-17 PC mixing proportions according to number of powder bags .....	239
<b>Table 7-11</b> Transpo <sup>®</sup> T-17 PC proportions per cubic yard and cubic meter .....	239

## LIST OF FIGURES

<b>Figure 1-1</b> Precast deck panels and field joints (photo credit: Georgia DOT) .....	1
<b>Figure 1-2</b> Schematic view of a typical precast bridge deck system with transverse and longitudinal field joints. ....	4
<b>Figure 1-3</b> DBT girders with full-depth longitudinal field joints [3].....	4
<b>Figure 1-4</b> Location and number of US Bridges with UHPC connections .....	5
<b>Figure 1-5</b> Typical UHPC field joints with (a) straight lap splice, (b) loop splice, and (c) headed bar splice.....	7
<b>Figure 2-1</b> Field joints for precast bridge deck systems and schematic of test specimen used in this study.....	18
<b>Figure 2-2</b> Dimensions and design details of S1-UHPC and S2-PC specimens including two deck panels and a field joint shear key .....	24
<b>Figure 2-3</b> Dimensions and design details of S3-PC-Loop specimen deck panels and field joint shear key .....	25
<b>Figure 2-4</b> (a) Schematic drawing of test setup, and (b) photograph of actual setup at UNR (1 in = 2.54 cm).....	28
<b>Figure 2-5</b> Distribution of LVDTs and string potentiometers for displacement measurements for: (a) S1-UHPC/S2-PC, and (b) S3-PC-loop; locations of strain gages shown only for bottom reinforcement as a sample for: (c) S1-UHPC/S2-PC, and (d) S3-PC-loop .....	30
<b>Figure 2-6</b> Loading protocol for all tested specimens (1 kip = 4.448 kN).....	31
<b>Figure 2-7</b> Photographs that illustrate the various construction stages and sequence of precast deck assemblies with UHPC and PC field joints.....	33
<b>Figure 2-8</b> (a) Grinding of UHPC and PMMA-PC cylinders, and compression testing of: (b) 3×6 in (7.5×15 cm) UHPC cylinders, (c) 3×6 in (7.5×15 cm) PMMA-PC cylinders, (d) 2-inch (5.1 cm) PMMA-PC cubes, and (e) 6×12 in (15 × 30 cm) NSC cylinders .....	35
<b>Figure 2-9</b> Crack pattern, damage, and modes of failure at: (a) top side of S1-UHPC; (b) top side of S2-PC; (c) bottom side of S1-UHPC; and (d) bottom side of S2-PC. ....	37
<b>Figure 2-10</b> Crack pattern at the AASHTO ultimate load level at the bottom side of: (a) S1-UHPC; (b) S2-PC; and (c) S3-PC-Loop. ....	39

<b>Figure 2-11</b> Crack pattern, damage, and mode of failure of S3-PC-Loop as seen from: (a) top side; (b) west side; and (c) bottom side. ....	40
<b>Figure 2-12</b> Load-deflection relationship at mid-span of specimens S1-UHPC and S2-PC as measured at three different locations.....	41
<b>Figure 2-13</b> Comparison of load-deflection relationship of specimens S1-UHPC and S3-PC-Loop as measured at the mid-span at three different locations. ....	44
<b>Figure 2-14</b> Comparison of load and mid-span deflection relationship of specimens S1-UHPC, S2-PC, and S3-PC-Loop .....	45
<b>Figure 2-15</b> Load versus difference between mid-span deflection under the field joint and the east and west sides under the deck panels.....	46
<b>Figure 2-16</b> Force versus strain measured at the mid-span location of the bottom transverse reinforcement .....	49
<b>Figure 2-17</b> Load versus strain measured at the middle top longitudinal rebars for all three specimens.....	51
<b>Figure 3-1</b> Overview of precast DBT girders bridge deck system: (a) Construction of a DBT girders bridge of Route 31 Bridge in Lyons, New York (photo courtesy of NYSDOT [1]), and (b) schematic of field joints and test specimen adopted in this study (photo courtesy Peruchini et al. [2])......	61
<b>Figure 3-2</b> Different components of commercial PMMA-PC used in this study: (a) powder bags, (b) liquid component pails, and (c) mixing process .....	68
<b>Figure 3-3</b> Compressive stress-strain relationship of PMMA-PC cylinders (tested at 70 days).....	69
<b>Figure 3-4</b> Flexural load-deflection relationship of PMMA-PC beams at age of 70 days .....	70
<b>Figure 3-5</b> Direct tension stress-strain relationship of PMMA-PC dog-bone specimens at age of 70 days .....	72
<b>Figure 3-6</b> Dimensions and design details of S1-UHPC and S2-PC specimens including two representative deck panels of DBT girders and a field joint shear key .....	75
<b>Figure 3-7</b> (a) Schematic drawing of test setup, and (b) photograph of actual setup at UNR .....	78



<b>Figure 3-8</b> Instrumentation plan: (a) distribution of LVDTs and string potentiometers for displacement measurements, and (b) locations of strain gages shown only for bottom reinforcement as a sample.....	78
<b>Figure 3-9</b> Loading protocol for both tested specimens .....	79
<b>Figure 3-10</b> Photographs to illustrate the various construction stages and sequence of representative DBT flanges/slab assemblies with UHPC and PC field joints .....	80
<b>Figure 3-11</b> (a) Grinding of UHPC and PMMA-PC cylinders; and compression testing of: (b) $7.6 \times 15.2$ cm UHPC cylinders, (c) $7.6 \times 15.2$ cm PMMA-PC cylinders, (d) 5.1 cm PMMA-PC cubes, and (e) $15.2 \times 30.5$ cm conventional concrete cylinders.....	82
<b>Figure 3-12</b> Crack pattern, damage, and modes of failure at: (a) top side of S1-UHPC; (b) bottom side of S1-UHPC; (c) west side of S1-UHPC; and (d) interface crack of S1-UHPC .....	85
<b>Figure 3-13</b> Crack pattern, damage, and modes of failure at: (a) bottom side of S2-PC; (b) top side of S2-PC; and (c) east side of S2-PC .....	86
<b>Figure 3-14</b> Crack pattern at AASHTO ultimate load at the bottom side of (a) S1-UHPC and (b) S2-PC.....	87
<b>Figure 3-15</b> Load-deflection relationship at mid-span of specimens S1-UHPC and S2-PC as measured at three different locations.....	89
<b>Figure 3-16</b> Load-deflection relationship at quarter and mid span of specimens S1-UHPC and S2-PC .....	91
<b>Figure 3-17</b> Load versus difference between middle deflection and the deflections of north and south sides .....	92
<b>Figure 3-18</b> Load versus strain measured near the mid-span location of the bottom transverse reinforcement of specimen S1-UHPC .....	94
<b>Figure 3-19</b> Load versus strain measured near the mid-span location of the bottom transverse reinforcement of specimen S2-PC .....	94
<b>Figure 3-20</b> Load versus strain measured at the middle longitudinal bars for both test specimens.....	98

<b>Figure 4-1</b> (a) Test setup of precast deck assembly with longitudinal NP-UHPC field joint; (b) comparison of load-deflection relationships of specimens with proprietary UHPC and ABC-UTC NP-UHPC.....	109
<b>Figure 4-2</b> Mixing proportions of: (a, b) ABC-UTC NP-UHPC baseline mix with 1% and 2% steel fibers, (c) typical commercial UHPC mix reported in [4], and (d) FHWA NP-UHPC mixes reported in [8] .....	111
<b>Figure 4-3</b> Different sand types used in the various NP-UHPC mixes in this study: (a) UNR non-sieved crushed aggregate sand, (b) UNR sieved crushed aggregate sand, and (c) OU fine masonry sand. ....	118
<b>Figure 4-4</b> Static and dynamic flow table measurements of the five different fresh NP-UHPC mixes. ....	120
<b>Figure 4-5</b> Static flow of the fresh NP-UHPC mixes.....	121
<b>Figure 4-6</b> Compression testing of NP-UHPC cylinders: (a) test setup; (b) grinding machine for cylinder preparation; and (c) views of typical NP-UHPC cylinder through preparation sequence.....	122
<b>Figure 4-7</b> Compressive strength gain of NP-UHPC mixes in comparison with prediction equations [5, 42].....	125
<b>Figure 4-8</b> Compressive strength versus time for mixes with 2% (left) and 1% (right) steel fibers. ....	126
<b>Figure 4-9</b> Test setup of the compressive stress-strain behavior test.....	127
<b>Figure 4-10</b> Compressive stress-strain relationships of the five tested NP-UHPC mixes. ....	129
<b>Figure 4-11</b> Average axial strains measured at peak compressive stresses. ....	130
<b>Figure 4-12</b> Measured modulus of elasticity for the various NP-UHPC mixes and comparison against different predictions using selected equations from the literature and a new proposed equation. ....	131
<b>Figure 4-13</b> Flexural testing and instrumentation of the NP-UHPC prisms.....	133
<b>Figure 4-14</b> Flexural strength versus time for the NP-UHPC mixes .....	134
<b>Figure 4-15</b> Average flexural stress versus middle deflection relationships for the NP-UHPC prisms tested at different ages. ....	135

<b>Figure 4-16</b> Direct tension testing of NP-UHPC dog-bone specimens. ....	137
<b>Figure 4-17</b> Direct tensile strength versus time of the NP-UHPC mixes. ....	138
<b>Figure 4-18</b> Direct tension stress-strain relationships of all NP-UHPC mixes tested at 7 and 28 days. ....	139
<b>Figure 5-1</b> Types of field joints in a typical prefabricated bridge deck system. ....	148
<b>Figure 5-2</b> Experimental test results of the reference P-UHPC specimen: (a) Load versus mid-span deflection; (b) Load versus tensile strains at the middle of the bottom transverse reinforcement. ....	153
<b>Figure 5-3</b> Overall dimensions and structural design details of specimens (a) S1-Str-2%; (b) S2-Lop-2%; (c) S3-Str-1%; (d) close-up view of the field joint details. ....	156
<b>Figure 5-4</b> Experimental test setup (a) schematic drawing of the test setup; (b) photograph of the actual test setup at UNR. ....	159
<b>Figure 5-5</b> Instrumentation plan (a) plan view for the locations of the string potentiometers; (b) photograph of the instrumentations. ....	159
<b>Figure 5-6</b> Construction of the test specimens (a) fabrication of the deck panels; (b) alignment of the deck panels; (c) pouring the NP-UHPC inside the field joints. ....	161
<b>Figure 5-7</b> Crack pattern, damage and modes of failure at the top and bottom of specimens (a) S1-Str-2%; (b) S2-Lop-2%; (c) S3-Str-1%. ....	164
<b>Figure 5-8</b> Global Behavior of the NP-UHPC specimens: (a) Load versus mid-span deflection relationships of the tested specimens; (b) Stages of the flexural behavior of specimen S1-Str-2%. ....	165
<b>Figure 5-9</b> Load versus tensile strains of the bottom transverse reinforcement measured at mid-span of specimens (a) S1-Str-2%; (b) S2-Lop-2%; (c) S3-Str-1%. ....	169
<b>Figure 5-10</b> Load versus tensile strains of selected bottom longitudinal reinforcement of specimens (a) S1-Str-2%; (b) S2-Lop-2%; and (c) S3-Str-1%.; (d) close-up view for the locations of the strain gages. ....	171
<b>Figure 5-11</b> Load versus concrete compressive strain measured at mid-span of specimens (a) S1-Str-2%; (b) S2-Lop-2%; and (c) S3-Str-1%.; (d) sketch of the test specimens with the locations of the concrete strain gages. ....	173
<b>Figure 6-1</b> DBT girders with full-depth longitudinal field joints [2]. ....	183

<b>Figure 6-2</b> NP-UHPC mixing at UNR: (a) UHPC mix components; (b) UHPC high shear mixer .....	188
<b>Figure 6-3</b> NP-UHPC material testing at UNR: (a) slump test; (b) compression test; (c) flexure test.....	190
<b>Figure 6-4</b> General Dimensions and structural details of the test specimens and a cross sectional view of the longitudinal field joint (1 in = 2.54 cm, 1 ft = 30.48 cm).....	193
<b>Figure 6-5</b> Photographs from the fabrication process and illustration of the sequence of constructing test specimens.....	195
<b>Figure 6-6</b> Photograph and schematic drawing of the test setup (1 in = 2.54 cm, 1 ft = 30.48 cm). .....	196
<b>Figure 6-7</b> Reinforcement strain gages distribution for the bottom and top reinforcement of S1-NP-UHPC.....	197
<b>Figure 6-8</b> Photograph of some of the instrumentation devices used in this study. ....	198
<b>Figure 6-9</b> Flexural crack pattern and concrete crushing at: (a) bottom of S1-NP-UHPC; (b) bottom of S2-P-UHPC; (c) top of S1-NP-UHPC; and (d) top of S2-P-UHPC. ....	202
<b>Figure 6-10</b> Load versus vertical displacements at quarter- and mid-span locations of the non-proprietary S1-NP-UHPC specimen (left) and proprietary S2-P-UHPC specimen (right). .....	202
<b>Figure 6-11</b> Deflected shape of specimen S1-NP-UHPC at peak load.....	206
<b>Figure 6-12</b> Load versus strain of selected bottom transverse reinforcement. ....	207
<b>Figure 6-13</b> Load versus strain of selected transverse reinforcement inside and outside the joint .....	209
<b>Figure 6-14</b> Load versus strain at the middle of the top and bottom longitudinal bars. ....	210
<b>Figure 7-1</b> Load versus middle deflection relationships of the transverse specimens with straight lap splice. ....	221
<b>Figure 7-2</b> Load versus middle deflection relationships of transverse specimens with loop splice. ....	223
<b>Figure 7-3</b> Load versus difference between the middle and east side deflections relationships of the longitudinal specimens. ....	226
<b>Figure 7-4</b> Load versus middle deflection relationships of the longitudinal specimens.....	228

<b>Figure 7-5</b> Ductal <sup>®</sup> UHPC components (a) dry premix, (b) superplasticizer, and (c) steel fibers. ....	231
<b>Figure 7-6</b> Examples of the UHPC mixer types (a) IMER high shear mixer, (b) high shear pan mixer [13], and (c) portable concrete pan mixer [12]. ....	232
<b>Figure 7-7</b> Transpo <sup>®</sup> T-17 PC components (a) dry premix, and (b) liquid component. ....	238

# 1 INTRODUCTION

## 1.1 Background and Problem Statement

Time, cost, and quality are the three main aspects of every engineering project. Reducing the bridge construction time in addition to utilizing high-quality materials for the sake of having durable bridges will accomplish less construction and maintenance costs. The growing need for durable and resilient highway bridge construction/rehabilitation systems compels various research entities and departments of transportation (DOTs) to search for better construction techniques to facilitate rapid completion of on-site activities to minimize the impact on road commuters. As a result, hundreds of bridge projects around the nation have recently adopted one or more aspects of accelerated bridge construction (ABC) techniques, methods, and connections. Pre-fabricated bridge decks are one of the most common ABC applications which are widely implemented in many highway projects. Figure 1.1 shows precast deck panels of one of the Georgia DOT projects.

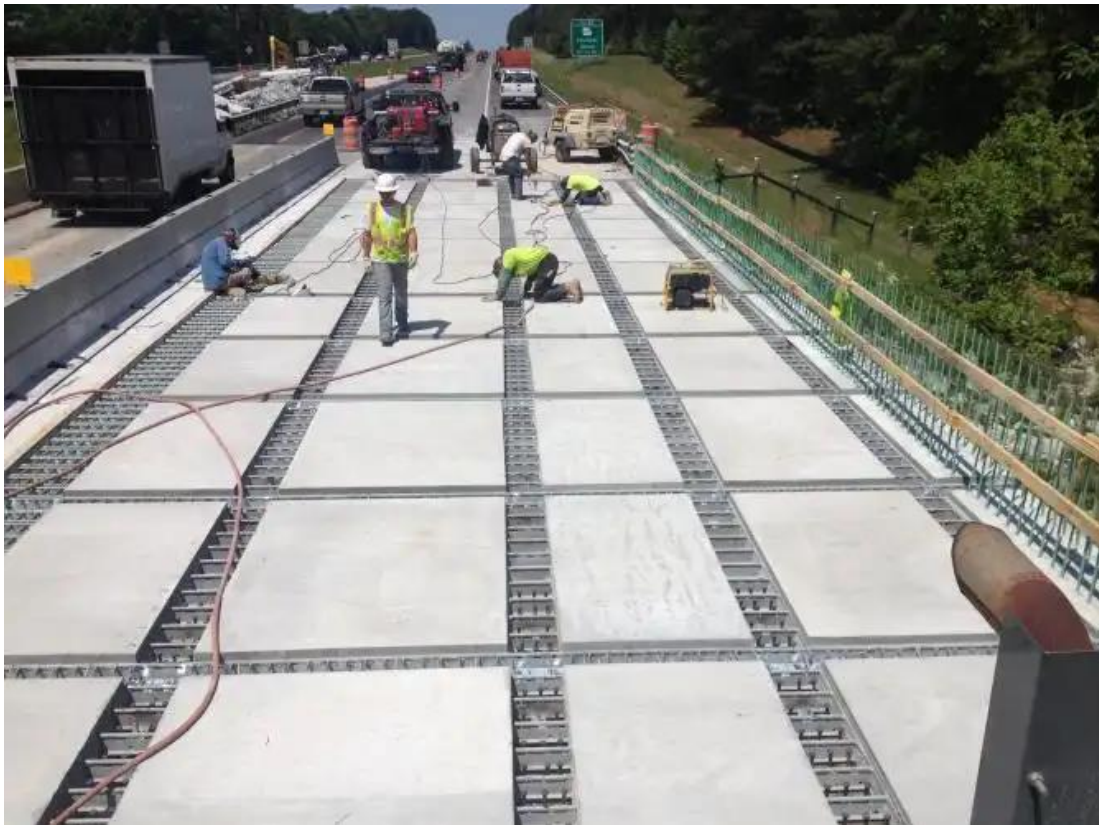


**Figure 1-1** Precast deck panels and field joints (photo credit: Georgia DOT)

Based on the records of the American Road and Transportation Builders Association (ARTBA), there are over 230,000 bridges in the United States (US) that need repair. Nearly 56,000 US bridges are considered structurally deficient [1]. Most of these bridges need a bridge deck replacement or rehabilitation as bridge decks are heavily stressed throughout their life span by both structural loadings and severe environmental conditions, such as the use of deicing salts during winter times, wearing due to traffic, etc. Hence, bridge decks deteriorate faster than the other bridge components. As a result, more than \$8 billion are spent annually on repairing or replacing the deteriorated bridge decks [1]. Approximately 85% of the US daily commuters travel on state-owned bridges, which makes it more difficult to use the traditional construction techniques or cast-in-place (CIP) methods in the replacement or rehabilitation of the deteriorated decks. As a result, this has paved the way for wider use of the precast elements to accelerate the deck erection. Pre-fabricated bridge elements and systems (PBES), which is one of the main ABC applications, can enhance constructability issues, offer higher quality, provide accelerated and safer construction, and minimize traffic disruption and safety concerns arising from detours and delays.

The implementation of PBES, especially full-depth precast deck panels (FPDP) and deck-bulb-tee girders (DBTs), has improved the quality and durability of the current bridge decks due to using advanced construction materials and quality control used for precast elements. However, the FPDP and DBTs require full-depth joints which usually require field casting and could form a weak link that affects the overall system performance. The construction of bridges using FPDP has increased dramatically in the last two decades [2]. The use of FPDP dictates the need for field joints in at least one direction. The field joints can be classified into two main types depending on the orientation of the joint with respect to the traffic flow of the bridge: (1) transverse joints, which run perpendicular to the traffic flow direction, and (2) longitudinal joints, which run along the longitudinal axis of the bridge, i.e. parallel to the traffic direction. Figure 1.2 shows both field joint types in a typical precast bridge deck system. DBTs are one of the attractive superstructure systems that have been implemented by many state DOTs such as Washington and New York DOTs over the last few decades. The DBT girders can also provide fast erection for the bridge superstructure, less on-site activities, less traffic disruption, and more feasible options for

bridge construction in rural areas. The I-shaped DBT girders have wide top flanges that establish the bridge deck. Such top flanges are connected in the longitudinal direction to form a continuous deck surface as illustrated in Figure 1.3 [3].

Full-depth deck joints can impose durability issues resulted from the weak quality control on the field joint concrete material and the interface cracking between the old and new concrete surfaces that may lead to corrosion of reinforcement. Therefore, using conventional construction materials for such joints can result in less durable joints compared to the precast joined parts. The history of these traditional field joints has often proved lacking and durability issues, resulting in less desirable overall system performance. Accordingly, many research studies have focused on identifying and implementing durable materials for such joints which feature high early strength and high bond strength. The implementation of durable closure pour with superior mechanical properties in the precast deck field joints can simplify the reinforcement splice details, enhance the joint durability, narrow down the width of the joints, save the time needed for formwork erection, and provide simpler reinforcement details inside the joints without requiring any post-tensioning [4]. Thus, emerging research efforts investigated the applicability of using modern advanced materials such as ultra-high performance concrete (UHPC) for such joints to maintain simpler joint configurations in addition to increased durability. The rising number of research efforts in this field has facilitated and expanded the use of UHPC in many projects around the nation. Figure 1.4 shows the number of US bridges with UHPC connections versus time in addition to the geographical distribution of these bridges according to the FHWA UHPC interactive map. As can be seen from Figure 1.4, most of the US bridges with UHPC connections are located in the eastern United States. This dictates the need for providing more attractive deck closure solutions to the state DOTs in the western states.



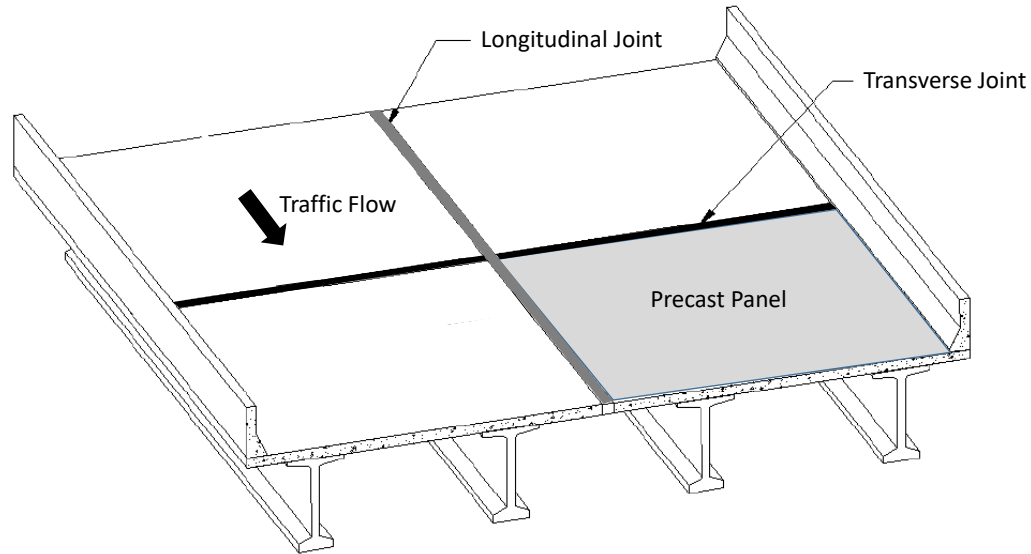


**Figure 1-2** Schematic view of a typical precast bridge deck system with transverse and longitudinal field joints.

UHPC is an advanced construction material that was developed in late 20<sup>th</sup> century. It is a cementitious material with steel fibers (typically 2 % by volume) and a low water-to-cement (w/c) ratio. The UHPC has a high compressive strength, which is typically 4-6 times higher than the normal strength concrete (NSC), in addition to other superior mechanical properties such as high sustained tensile cracking resistance and high bond strength. The unparalleled material properties of UHPC have made it a strong candidate in many bridge construction applications around the US.

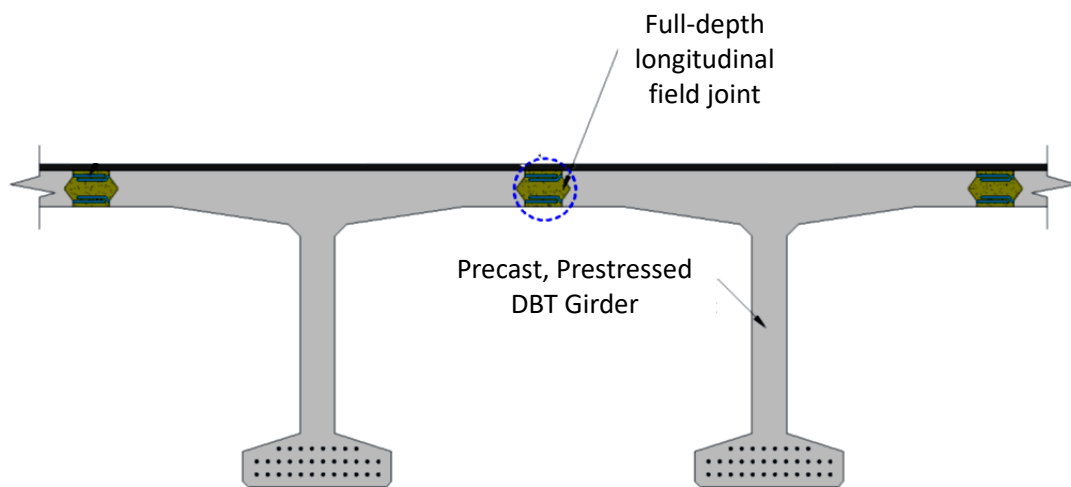


**Figure 1-3** DBT girders with full-depth longitudinal field joints [3].

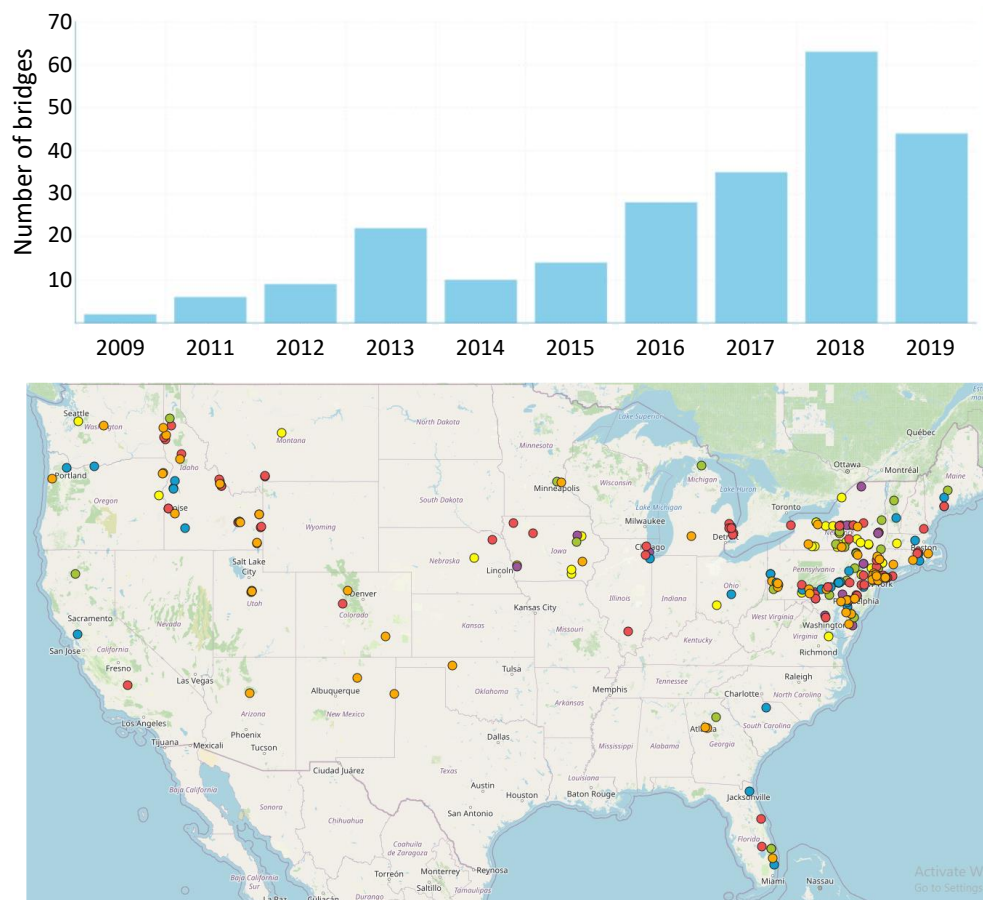


**Figure 1-4** Location and number of US Bridges with UHPC connections

UHPC has gained a great significance and reputation as a bridge deck joint material for the last decade. However, the use of UHPC comes with several challenges. First, the commercial UHPC products are very expensive as they are 20 times more expensive than conventional concrete. Moreover, UHPC might pose also bidding issues due to the limited number of suppliers and proprietary nature of most of the robust mixes. This often limits state DOTs that are trying to avoid sole-sourcing among other bidding issues to use UHPC. Another challenge is that the UHPC requires special expertise to mix and place because of the steel fibers. Hence, there is a growing interest from various state DOTs and research agencies in finding other advanced alternative materials to commercial or proprietary UHPC for use as a bridge deck joint material.

## 1.2 Motivation

As mentioned earlier, the superior mechanical properties of UHPC have made it an ideal deck joint material. However, there are some challenges associated with the use of commercial UHPC products that triggered the research need to find other doable alternatives. Before the recent introduction of UHPC as a filler material in bridge deck joints, many researchers have focused on improving the previously existed conventional joints. These research studies have examined the use of conventional construction materials for the full-depth deck joints such as conventional concrete, advanced grouts, and high-performance concrete (HPC). However, special reinforcement requirements such as mechanical splices and post-tensioning along with relatively wider joints have been associated with the use of these conventional materials inside the field joints. Nonetheless, the conventional materials have relatively lower rates for strength gain which may delay the bridge deck erection. Many of these previously provided solutions require more on-site work in addition to higher labor costs that are not viable for ABC. Although, after years of service, these proposed solutions have proven durability and performance issues. Hence, the main conclusion after experiencing many years of research and practical implementations is that advanced construction materials (especially UHPC) are the best solutions to most of these issues. The implementation of UHPC in the deck joints has been shown to solve most of the previously mentioned issues and can provide monolithic deck systems with higher performance and prolonged durability.

Since UHPC is a relatively new material that is recently introduced in the highway industry, a large number of research studies have focused mostly on the experimental testing and demonstration of the use of commercial UHPC products in the longitudinal and transverse full-depth deck field joints. Examples of these efforts include, but are not limited to, the work done by Graybeal [4], Hartwell et al. [5], Hwang and Park [6], and Vitek et al. [7]. In addition to testing the performance of the UHPC joints, other research studies considered different parameters of the field joints such as connections types, shear key shapes, details of reinforcement, types of reinforcement, and tested the various joint details under different loading conditions including cyclic and static loading. As a result of the large number of

studies in this area, several reports were published through the federal highway administration (FHWA) to summarize and synthesize the state-of-the-art for prefabricated concrete components and deck connections and detailing. Consequently, the synthesized practical and research projects converged on typical UHPC field joints that are 6 to 8 inches wide without post-tensioning and use simplified reinforcement configuration inside the joint with diamond-shaped shear key type as shown in Figure 1.5. These typical joint details have been demonstrated to develop sufficient shear and bending capacities to link the precast deck components together [4].

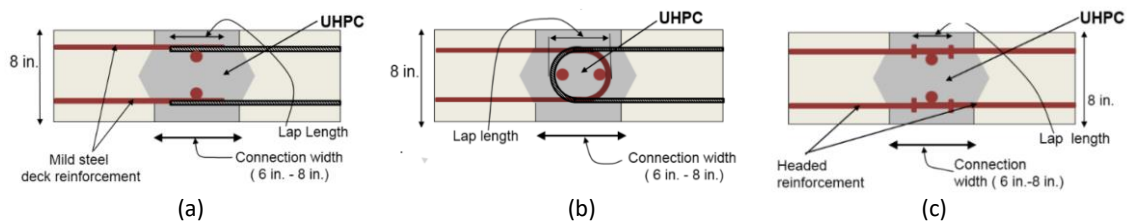


**Figure 1-5** Typical UHPC field joints with (a) straight lap splice, (b) loop splice, and (c) headed bar splice.

After the field implementation of UHPC in the bridge deck joints, other practical challenges were found. One of these challenges is the quality control for early strength characterization as UHPC cylinders require end grinding before compression testing, which is not possible to do on-site for the first 12-hour strength characterization and associated decisions for other ABC activities. UHPC also exhibits high early shrinkage that requires more time and additional labor costs to have an acceptable surface finish if no overlay is planned to be used. Moreover, UHPC is currently mixed in small-sized batches and requires a long mixing time. UHPC also requires special heat treatment to accelerate the strength gain if used in cold weather which may impose additional costs. Most of the aforementioned challenges can be tackled and their implications become less significant when compared to the benefits of the unparalleled superior mechanical properties of UHPC. Nonetheless, identifying other alternative materials that can provide acceptable solutions, i.e. maintaining simpler reinforcement configurations and avoid the use of post-tensioning, specifically for ABC applications and full-depth deck panel field joints could be very beneficial.

Poly Methyl Methacrylate (PMMA) polymer concrete (PC) is another advanced construction material that emerged over the past few decades and can provide a potential alternative to UHPC for bridge deck joints. PC features high bond strength, high early strength, high shear strength, adequate flowability, and high durability with respect to cycles of freezing and thawing. Furthermore, PC is corrosion-resistant, fast-curing, and has very low permeability and superior cracking resistance. The superior properties of PC make it a very attractive material for use in many industries and various structural engineering applications for more than four decades such as concrete patching and bridge repairs. PC is also a popular material for use in bridge deck overlays. Among the different types of PC, the PMMA-PC has been used for decades as bridge deck overlay and fast-permanent repair for runways and taxiways in many airports around the nation. PMMA-PC cylinders do not require special preparation before compression testing. PMMA-PC can gain a full-strength in less than 24 hours and does not require special heat treatment in cold weather, which makes it a very good candidate for various ABC applications.

Earlier research studies demonstrated that PMMA-PC beams have better fatigue strength than Portland cement concrete beams. A recent study showed that the PMMA-PC could provide shorter development and lap splice lengths than typical UHPC [8]. Moreover, the study showed that the PMMA-PC has almost double the shear strength of UHPC and one-half the cost of the UHPC. The study also concluded that PMMA-PC has the potential to be a good candidate or alternative for field joints in ABC deck field joints.

Some other research efforts have sought to make UHPC more accessible and less expensive through the development of non-proprietary UHPC (NP-UHPC) mixes using locally available material sources. A former study by Wille et al. [9] demonstrated that it is possible to develop NP-UHPC with a compressive strength greater than 30 ksi (200 Mpa) without requiring any special treatment conditions. Due to the high number of these research efforts, a FHWA report was published to summarize some of these research findings to accelerate the use of NP-UHPC and promote more resilient US transportation infrastructures [10]. As mentioned earlier, many state DOTs have initiated comprehensive experimental research on developing and material testing of several NP-UHPC mixes using

locally available materials in their states for use in different bridge applications, especially bridge deck joints. Up to the time of this writing, there are only limited experimental validations for NP-UHPC field joints behavior and implementation. Some of these experimental efforts provided guidance for the potential use of different NP-UHPC mixes in the field joints. However, the tested specimens were not in full-scale and they implemented the use of un-recommended flat shear key shape or the contact lap splice. However, these studies have concluded that different NP-UHPC mixes could provide comparable performance and can be an alternative to commercial UHPC products.

Based on the above summary, there is a knowledge gap in the experimental proof testing and validating the use of alternative emerging and advanced materials beyond UHPC for bridge deck field joints. Generally, and up to the date of this writing, no research studies have been conducted to understand the behavior of the PMMA-PC longitudinal and transverse field joints. Meanwhile, only limited studies have investigated the behavior of NP-UHPC mixes in the bridge deck joints, but none of these efforts were directed to the development and full-scale experimental testing of NP-UHPC mixes using locally available materials from the western states. Thus, PMMA-PC and NP-UHPC are the focus of this study as they seem to be viable candidates for use in the bridge deck joints with comparable performance to the currently accepted practice of the proprietary UHPC joints.

### **1.3 Research Objectives**

The overall objective of this study is to fill the abovementioned knowledge gaps and provide more choices for connecting the FPDP, especially on the west coast, through investigating and validating the structural performance of PMMA-PC and NP-UHPC transverse and longitudinal full-depth deck joints as compared to the proprietary UHPC. Moreover, this study aims at developing a better understanding of the structural behavior of the newly proposed joints at the AASHTO service and ultimate load levels and developing design tools for the future applications of the proposed joints. The following list comprise the specific objectives that contributed to fulfilling the overarching goals of this doctoral study:

1. Review the available and recent research efforts related to this field of study to select the best candidates from the wide array of advanced construction materials to allow for further multi-scale testing at the material and structural levels.
2. Investigate and examine the mechanical behavior of the PMMA-PC to develop an understanding of the PMMA-PC properties at the material level before further implementation in large-scale applications and to provide guidance for future finite element modeling.
3. Investigate the global and local structural behaviors in addition to service and ultimate performances of the full-depth precast deck panels with transverse PMMA-PC, NP-UHPC, and proprietary UHPC field joints with respect to the overall deck behavior compared to the monolithic deck systems, joint performance, damage schemes, and local behavior through assessment of the reinforcement strains.
4. Investigate the global and local structural behaviors in addition to service and ultimate performances of the longitudinal full-depth joints of the DBT girders using PMMA-PC, NP-UHPC, and proprietary UHPC closure materials. This is through establishing experimental assessment of the tested specimens with respect to the overall deck behavior compared to the monolithic deck systems, joint performance, damage schemes, and local behavior through assessment of the reinforcement strains.
5. Experimental validation and verification of the competency of the PMMA-PC and NP-UHPC transverse and longitudinal field joints through comparing their overall structural behaviors, peak loads and deflections, and joints performance with the currently implemented proprietary UHPC joints to provide guidance and offer more closure joint solutions for the highway industry and state DOTs nationwide.
6. Examine the applicability of using a new and innovative joint detail (i.e., modified diamond-shaped shear key) that is proposed to eliminate the time, cost, and labor associated with the formwork which is typically required for field casting of joints through the assessment of the overall structural behavior and joint performance.
7. Investigate the effect of varying the reinforcement splice types (i.e., loop splice versus straight splice) of the transverse field joints on the structural behavior and joint

- performance to examine various practically existed solutions for the deck-level connections and to provide future recommendations for the most effective splice type.
8. Provide more solutions to a variety of ABC applications on the west side of the US and facilitate the future implementation of the NP-UHPC through developing ultimately cheaper NP-UHPC mixes using locally available materials from Nevada and California States.
  9. Develop better understanding of the material behavior of the developed NP-UHPC mixes through investigating and comparing the main mechanical properties of various developed NP-UHPC mixes to determine the best closure material candidate for use in deck joints and to provide enough data for future replication or finite element modeling of the developed mixes.
  10. Investigate the effect of using different particle sand gradation on the main mechanical properties of the developed NP-UHPC mixes to verify the applicability of using different sand types for the future replication of the developed mixes when varying sources of sand.
  11. Establish a multi-scale engineered optimization of the NP-UHPC mixes to reduce the material cost through using a reduced amount of steel fibers (i.e., 1% versus 2% steel fibers) and experimenting them at the material level and structural level through using relatively wider joints and validate their performance with the typical 2% mixes.
  12. Evaluate the effect of providing denser reinforcement inside the transverse field joints through varying the reinforcing bar sizes on the overall structural behavior of the deck slab specimens to provide future recommendations for the best joint details.
  13. Provide guidance for the future implementations of the proposed joints using the new materials through developing design guidelines and recommendations for the transverse and longitudinal field joints fabricated using PMMA-PC and NP-UHPC mixes.

#### **1.4 Research Methodology**

The previously mentioned list of objectives are mainly accomplished through both material and large-scale experimental investigations and validations of the proposed deck joint



materials and field joint details. Then, evaluation and discussion of the experimental results are performed to provide design guidelines for the proposed deck joint systems. The details of the adopted research approach in this study is categorized into six parts that are outlined in the list below based on the different objectives:

1. The first research approach aimed at investigating and validating the structural behavior and joint performance of PMMA-PC transverse field joints as compared to proprietary UHPC. The specific objective was to conduct experimental testing of representative full-scale full-depth precast deck panel assemblies with PMMA-PC and proprietary UHPC transverse field joints under static vertical loading. Three large-scale tests were conducted and presented in detail in this part of the study. Two identical specimens that varied only in the field joint material, i.e. UHPC versus PMMA-PC, were tested. While the third specimen used PMMA-PC but with a different splice type (i.e., loop splice instead of straight splice) and a different shear key shape (i.e., modified diamond-shaped).
2. The main objective of the second part of the study was to investigate and validate the structural performance of PMMA-PC longitudinal field joints in DBT girders as compared to proprietary UHPC. This part is sub-divided into two sections as material tests were initially performed to characterize the main mechanical properties of PMMA-PC to provide a better understanding of the material behavior that helps interpret the large-scale application. The material tests included flowability, compression, flexure, and direct tension testing of PMMA-PC samples at 28 days. The provided material characterization can also be used for future analytical studies and finite element modeling of the extend the results of the test specimens presented herein. The second part also included the full-scale experimental testing of deck assemblies of representative DBT girder flanges (slabs) with PMMA-PC and UHPC longitudinal field joints under static vertical loading. Two identical specimens that varied only in the field joint material, i.e. UHPC versus PMMA-PC, were tested and presented in this part.
3. The overall objective of the third part of the study is to characterize and document the main physical and mechanical properties of the developed NP-UHPC mixes using local

- materials in the western states to facilitate the use of the developed mixes in various ABC applications, mainly bridge deck field joints. This study presented results from flow tests of the fresh mixes, compression, flexural, and direct tension tests of five different NP-UHPC mixes. Furthermore, this paper delivers more information on the mix design, sourcing of the material ingredients, and mixing of the developed NP-UHPC mixes. This part also investigated the variability effects that arose from using different material types and sources, using different sand types and sand particle grading, mixing and testing conducted by different research teams at different universities, and using different testing equipment on the main physical and mechanical properties of the developed NP-UHPC mixes.
4. The fourth part of study included the experimental testing of three full-scale specimens with three different full-depth transverse joint systems, but all using NP-UHPC mixes that were developed using local materials on the west coast. The main objectives of this study were to investigate the structural behavior of the NP-UHPC transverse joints with varying the reinforcement splice type, using dense reinforcement in the joint, and using wider joints with a NP-UHPC of 1 % by volume steel fibers. The first specimen utilized the NP-UHPC with 2% steel fibers and a straight lap splice. The second specimen was slightly different as it utilized a loop splice. However, the third specimen was designed to optimize the NP-UHPC through using 1% steel fibers with relatively wider joints and denser reinforcement in the joint. The structural behavior of the tested specimens was evaluated and compared with similar specimens with proprietary UHPC joints in terms of load and deflection capacities as well as the field joint performances at the AASHTO service and ultimate load levels.
  5. The objective of the fifth part is to leverage a readily developed NP-UHPC mix, but using local materials available in the western United States, and to proof-test it in DBTs full-depth longitudinal field joints. An experimental investigation was conducted to test one full-scale specimen of a representative DBT top flange section with NP-UHPC longitudinal field joint under static vertical loading. This part of the study presented a comparison of the structural behavior and joint performance between two identical deck specimens utilizing the developed non-proprietary UHPC and the robust

- commercial UHPC mix inside the longitudinal field joints. The structural behavior of both specimens was evaluated in terms of load and deflection capacities as well as the field joint performances at the AASHTO service and ultimate loads.
6. The last part of this study focused on analyzing, evaluating, and comparing the experimental results from the six full-scale bridge deck specimens with transverse joints and the three full-scale specimens with longitudinal field joints. The comparison and assessment aimed at providing design guidelines and recommendations for the future use of the proposed field joint systems.

### **1.5 Dissertation Outline**

This dissertation follows a paper-based format which encompass five standalone papers besides an introduction, design guidelines and recommendations, and conclusion chapters. Thus, the dissertation is organized into a total of eight chapters as follows. Chapter 1 presents the background of the research topic and discusses the problem statement in addition to providing the research objectives and approaches. Chapter 2 is standalone paper #1 and presents the experimental results and research findings along with a detailed discussion of the structural behavior and joint performance of the two transverse full-depth deck joints with PMMA-PC as compared to a similar proprietary UHPC specimen. Chapter 3 is standalone paper #2 and presents the results of the PMMA-PC material characterization tests in addition to the results and research findings of the comparative study of the PMMA-PC and proprietary UHPC longitudinal field joints in DBT girders. Chapter 4, i.e. standalone paper #3, provides information about the development and material characterization of the developed NP-UHPC mixes. Chapter 5, i.e. standalone paper #4, presents the experimental results and detailed discussion of the global and local behavior of three deck specimens with transverse NP-UHPC field joints. Chapter 6 is the last standalone paper #5 which presents the results from two full-scale experimental tests of deck assemblies of representative DBT girder flanges with non-proprietary and proprietary UHPC longitudinal field joints under static vertical loading in addition to providing a discussion on the developed NP-UHPC mix and material characterization. Chapter 7 presents comparison of the overall behavior of the nine full-scale specimens along with

providing design and construction guidelines and recommendations for the proposed field joints. An overall summary and concluding remarks of this doctoral research are presented in Chapter 8 along with recommendations for future work.

## References

- [1] American Road and Transportation Builders Association (ARTBA) 2020 bridge report.
- [2] Garber, D., & Shahrokhinasab, E. (2019). Performance Comparison of In-Service, Full-Depth Precast Concrete Deck Panels to Cast-in-Place Decks (No. ABC-UTC-2013-C3-FIU03-Final). Accelerated Bridge Construction University Transportation Center (ABC-UTC).
- [3] Haber, Z. B., & Graybeal, B. A. (2018). Performance of Grouted Connections for Prefabricated Bridge Deck Elements (No. FHWA-HIF-19-003). United States. Federal Highway Administration. Office of Infrastructure Research and Development.
- [4] Graybeal, B. Behavior of Field-Cast Ultra-High Performance Concrete Bridge Deck Connections Under Cyclic and Static Structural Loading; Report No. FHWA-HRT-11-023; Federal Highway Administration, McLean, VA, 2010
- [5] Hartwell, D. R. "Laboratory testing of Ultra High Performance Concrete deck joints for use in accelerated bridge construction" (2011). Graduate Theses and Dissertations. 10420.
- [6] Hwang H., Park S. Y. "A study on the flexural behavior of lap-spliced cast-in-place joints under static loading in ultra-high performance concrete bridge deck slabs" (2014). Canadian Journal of Civil Engineering, 41:615-623.
- [7] Vitek, J.L., Kolisko, J., Citek, D., Rehacek S., Coufal R. "UHPC connection of precast bridge deck" (2016). First International Interactive Symposium on UHPC.
- [8] Mantawy, I.; Chennareddy, R.; Genedy, M.; Taha, M.R. Polymer Concrete for Bridge Deck Closure Joints in Accelerated Bridge Construction. *Infrastructures* 2019, 4, 31.
- [9] Wille, K., Naaman, A. E., & Parra-Montesinos, G. J. (2011). Ultra-High Performance Concrete with Compressive Strength Exceeding 150 MPa (22 ksi): A Simpler Way. *ACI materials journal*, 108(1).

- [10] Graybeal, B. A. (2013). Development of Non-Proprietary Ultra-High Performance Concrete for Use in the Highway Bridge Sector: TechBrief (No. FHWA-HRT-13-100). United States. Federal Highway Administration.

## 2 COMPARATIVE STRUCTURAL BEHAVIOR OF BRIDGE DECK PANELS WITH POLYMER CONCRETE AND UHPC TRANSVERSE FIELD JOINTS

*This chapter is a standalone paper that has been published in the journal of Engineering Structures*

### **Abstract**

Precast bridge deck panels are widely used to accelerate bridge deck erection and provide cost savings, better durability, and solving many constructability challenges. Full-depth deck joints with diamond shear key type and ultra-high performance concrete (UHPC) are the most recent commonly used field joints in bridge decks. UHPC has superior mechanical properties and leads to simplified details and joints. However, UHPC might have some constructability and finishing as well as cost and bidding challenges. Thus, exploring the viability of alternative materials for field joints could be beneficial. Poly Methyl Methacrylate Polymer concrete (PMMA-PC) is another popular construction material with superior mechanical properties that have been used for overlays and can provide a potential alternative to UHPC for deck joints. The objective of this study is to investigate and compare the structural performance of using PMMA-PC and UHPC for full-depth precast deck panel transverse field joints. An experimental program was conducted to test three full-scale specimens under vertical loading at the University of Nevada, Reno. Two specimens were identical except for the material used in the joint, i.e. UHPC versus PMMA-PC, while the third specimen used a new proposed joint detail with PMMA-PC. The structural response was evaluated for connection performance under the AASHTO service and ultimate loads, peak strength, damage progression and mode of failure, and local steel reinforcement strains. The results demonstrated that PMMA-PC, and the proposed joint detail, can be successfully used for bridge deck field joints with comparable performance to UHPC field joints.

### **2.1 Introduction**

Bridge decks are traditionally constructed using cast-in-place (CIP) normal strength concrete to create a monolithic deck slab that might be divided only using expansion joints. Bridge decks are susceptible to rapid degradation due to many factors such as structural

and environmental loads, the use of deicing salts during winter times, wearing due to traffic, etc. The use of precast bridge deck slabs has improved the quality and durability of bridge decks due to the using of better materials and quality control used for precast elements. Another significant advantage of using precast bridge decks is the construction time and cost savings, which makes it one of the most popular applications for accelerated bridge construction (ABC). However, precast bridge deck connections, among other ABC connections, usually require field casting and could form a weak link that affect the overall system performance. The use of full-depth precast bridge deck systems dictates the need for field joints in at least one direction. The field joints can be classified into two main types depending on the orientation of the connection with respect to the traffic flow of the bridge. Transverse joints run perpendicular to the direction of traffic flow on the bridge, while longitudinal joints run along the longitudinal axis of the bridge, i.e. parallel to the traffic direction. Figure 1 shows both joint types and orientation on a precast bridge deck system. This paper focuses on transverse joints and a schematic of how the test specimens relate to the deck system is also illustrated in Figure 2.1.

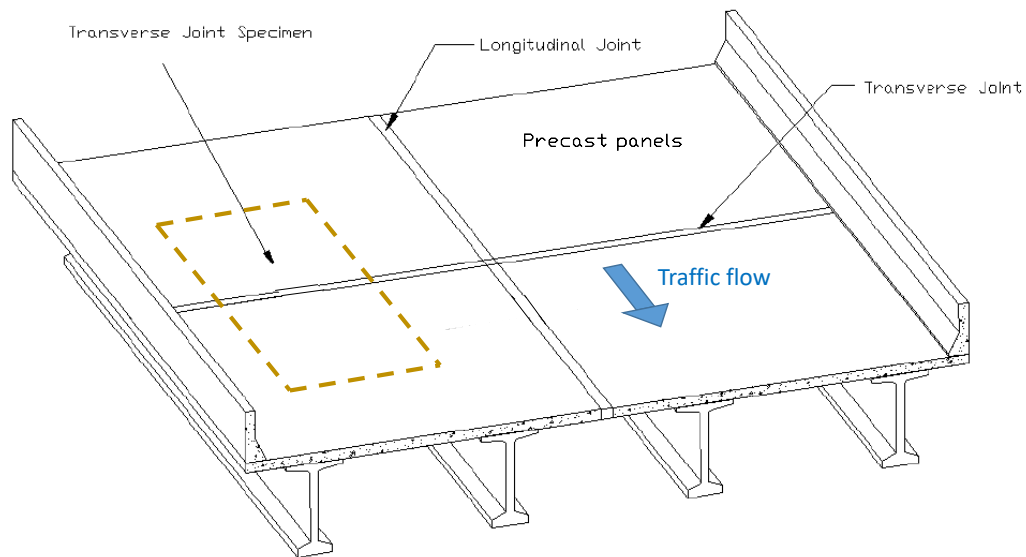


**Figure 2-1** Field joints for precast bridge deck systems and schematic of test specimen used in this study.

Field connections are one of the challenging issues in the ABC applications due to the durability issues resulted from the weak quality control on the field joint concrete material

and the interface cracking between the old and new concrete surfaces that may lead to corrosion of reinforcement. Therefore, using conventional construction materials for such joints can result in less durable connections compared to the precast joined parts. Accordingly, many research studies focused on identifying and implementing durable materials for such joints which feature high early strength and high bond strength. The implementation of durable closure pour with superior mechanical properties in the precast deck field joints can simplify the connection details, enhance the connection durability, narrow down the width of the connections, save the time needed for formwork erection, and provide simpler reinforcement details inside the connections without requiring any post-tensioning.

Large number of the recent research studies on precast deck panel joints focused on experimental testing and demonstration of the use of ultra-high performance concrete (UHPC) for field. Examples include the work done by Graybeal [1], Hartwell et al. [2], Hwang and Park [3], and Vitek et al. [4], among others. Earlier research studies considered more common materials and focused on investigating the behavior of field joints with advanced grouts, high performance concrete (HPC), and HPC with fiber reinforcement [5-7]. However, many of these research efforts demonstrated the need for reinforcement post-tensioning inside the joint or the use of mechanical splices or using of headed rebars or adding of rebar confinement inside the joint or increase joint width to maintain the desired performance of the deck field joints. Many of these solutions are not viable for ABC where durable systems with less erection time, cost, and labor are desired. In addition to exploring joint materials, other research studies considered different parameters of the field joints such as connections types, shear key shape, details of reinforcement, types of reinforcement, and tested the various connections details under different loading schemes. As a result of the large number of studies in this area, several reports were published through the national cooperative highway research program (NCHRP) to summarize and synthesize the state-of-the-art for prefabricated concrete components and deck connections and detailing. For example, NCHRP report 10-71 [8] focused on static and fatigue testing of both transverse and longitudinal field connections between precast concrete deck panels. Consequently, the synthesized practical and research projects converged on typical UHPC



field joints that are 6 to 8 inches (15.2 - 20.3 cm) wide without post-tensioning and use simplified reinforcement configuration inside the joint with diamond shaped shear key type. This typical connection has been demonstrated to develop sufficient shear and bending capacities to link the precast deck components together [1, 9, 10].

In the past decade, UHPC has been considered for field joints and closure pours between precast bridge deck panels in many projects around the nation because of its superior mechanical and durability properties. However, the use of UHPC comes with several challenges. First, UHPC might pose cost and bidding challenges due to the limited number of suppliers and proprietary nature of most of the robust mixes. This often limits state departments of transportation that are trying to avoid sole-sourcing among other bidding issues to use UHPC. Another challenge is that typical UHPC mixes use 2% steel fibers which require special expertise to mix and place UHPC in addition to the long mixing time. Moreover, some leading domestic steel fiber producers in the United States are exiting the country, which might challenge compliance with the Federal Buy America Act if no reliable domestic alternatives are identified. For ABC applications, UHPC comes with two additional challenges. The quality control for early strength characterization is an issue because properly prepared cylinders with end grinding are needed for UHPC testing as recommended by the ASTM C1856 [11] and other literature studies [12-14] to ensure adequate representation of the strength of UHPC. The required end grinding of the UHPC cylinders is not possible to do on-site for 10 or 12-hour strength characterization and associated decisions for other ABC activities. UHPC also exhibits high early shrinkage that requires more time and additional labor costs to have an acceptable surface finish if no overlay is planned to be used. Most of the aforementioned challenges can be tackled and their implications become less significant when compared to the benefits of the unparalleled superior mechanical properties of UHPC. Nonetheless, identifying other alternative materials that can provide acceptable solutions, i.e. maintaining simpler reinforcement configurations and avoid the use of post-tensioning, specifically for ABC applications and full-depth deck panel field joints could be very beneficial. Hence, some research studies were focused on developing and testing of several non-proprietary UHPC

mixes using locally available materials for use in the bridge deck joints and for different bridge applications [15-18].

Poly Methyl Methacrylate (PMMA) polymer concrete (PC) is another advanced construction material that emerged over the past few decades and can provide a potential alternative to UHPC for bridge deck joints. PC features high bond strength, high early strength, high shear strength, adequate flowability, and high durability with respect to cycles of freezing and thawing [19, 20]. Furthermore, PC is corrosion-resistant, fast curing, has very low permeability and superior cracking resistance [19-21]. The superior properties of PC make it a very attractive material for use in many industries and various structural engineering applications for more than four decades such as concrete patching and bridge repairs [22-25]. PC is also a popular material for use in bridge deck overlays [26]. Among the different types of PC, the PMMA-PC has been used for decades as bridge deck overlay and fast-permanent repair for runways and taxiways in many airports around the nation [27]. These applications are outcomes of earlier research studies that demonstrated that PMMA-PC beams have better fatigue strength than Portland cement concrete beams [28].

A recent study was conducted at the University of New Mexico [29] to characterize the mechanical properties of the PMMA-PC to explore its future applicability for field joints between precast bridge deck slabs. That study [29] focused on the development length and lap splice length and demonstrated that the PMMA-PC could provide shorter development and lap splice lengths than UHPC. The minimum development length required for steel rebars embedded in PMMA-PC is almost one-half that of the UHPC and ranges between 3.6 and 4.1 times the reinforcing bar diameter ( $d_b$ ) [29]. The minimum lap splice length required for uncoated rebar in PMMA-PC was slightly less than that of the UHPC as lap splice length of only  $4.1 d_b$  is sufficient to achieve yielding in the rebars [29]. Moreover, the study showed that the PMMA-PC has almost double the shear strength of UHPC and one-half the cost of the UHPC. The study concluded that PMMA-PC has the potential to be a good candidate or alternative for field joints in ABC deck field connections. The latter research project among other applications of PC motivated this study to further investigate and demonstrate the structural behavior of precast deck systems with PMMA-PC field joints.

Based on the above summary, there is a knowledge gap in testing and validating the use of alternative emerging and advanced materials beyond UHPC for ABC connections and field joints. While PMMA-PC seems to be a viable candidate, none of the previous efforts considered large or full-scale testing and demonstration of using PMMA-PC for deck joint connections. The overall goal of this study is to contribute towards filling the abovementioned knowledge gap through investigating and validating the structural performance of PMMA-PC field joints as compared to UHPC. The specific objective is to conduct experimental testing of representative full-scale full-depth precast deck panel assemblies with PMMA-PC and UHPC transverse field joints under static vertical loading. Three tests were conducted and presented in detail in this paper. Two identical specimens that varied only in the field joint material, i.e. UHPC versus PMMA-PC, were tested. The third specimen used PMMA-PC but with different reinforcement configurations in the joint. The paper comprises two main sections to first present the experimental program then provide the test results and discussions.

## **2.2 Experimental Program**

This section provides the details of test specimens design, testing parameters, setup and instrumentation, loading protocol, specimen construction, and material properties of the various components of test specimens.

### ***2.2.1 Specimen Design and Test Matrix***

The experimental program presented in this paper is a subset of a major ongoing research effort at the University of Nevada, Reno that aims at identifying and testing alternative materials for various ABC connections. The tests discussed here include three full-scale specimens that represent full-depth transverse field joints between two adjacent precast deck panels. The varied test parameters included the field joint material, i.e. PMMA-PC and UHPC, and reinforcement configuration. Although the compression strength of the UHPC is higher than that of the PMMA-PC, the PMMA-PC does still have comparable tensile, shear, and bond strengths to the UHPC that makes this material adequate as a closure joint material. The design of the specimens was done according to the AASHTO LRFD Bridge Design Specification [30]. The design moments were determined based on

the AASHTO Equivalent strip method. The moment values provided in this method takes into account the largest values that could be experienced by the deck slabs with respect to different loading conditions. The bridge example that was used to analyze the reinforced concrete deck in this study has a cross-section consisted of five steel girders spaced at 12 ft (3.66 m) on center and a deck slab of 8 in (20.3 cm) thickness.

Many design and practical considerations were taken into account during the design of the field connections to enhance constructability, accelerate bridge deck erection, and enhance the structural performance and durability of the field joints. (1) Two layers of steel were used inside the connection to transfer shear and provide moment continuity across the joint. (2) Staggered reinforcement was used inside the connection. (3) All the precast slabs were joined together through passive field connections without any reinforcement post-tensioning or welding inside the joints. (4) Straight and loop bar splices were used to provide simpler reinforcement details inside the connection. (5) A concave diamond-shaped shear key was used in this study given its previously demonstrated performance for transferring shear and bending and enhanced durability as compared to flat ends shear keys. (6) No protective coatings such as epoxy-coated reinforcement were used to maintain the full bond and in turn, minimize the lap splice length and field joint width.

The bottom concrete cover for deck panels was taken as 1 in (2.54 cm), and the top concrete cover as 2 in (5.1 cm) to represent normal condition exposure in a non-corrosive environment. The deck slabs were designed based on class two exposure, which also controls the spacing between the bottom main reinforcement to avoid the positive flexural cracking under the service limit state. For the test specimens, the transverse reinforcement was placed in the outer layers of the deck slabs to maximize the flexural capacity in the transverse direction and increase the demand in the joint. Grade 60 (420 MPa) reinforcing steel as specified by ASTM A706 was used in this study. Normal strength concrete was used for the precast panels with 5 ksi (35 MPa) specified compressive strength at 28 days.

To finalize the geometry, boundary conditions, and dimensions of the specimens, the effective span length of the test specimens was selected based on the expected distance between the flexural inflection points of the original bridge deck slabs. Usually, in the case

of bridge decks, it is hard to determine the exact location of such bending inflection points because of the numerous loading conditions. Thus, the effective span of the test specimens was estimated based on dead loads for simplicity and was adopted to be 8 ft (2.44 m), which is approximated as two-thirds of the original 12 ft (3.66 m) span. Since the effective span represents the positive flexural part of the slab and there is no negative moment in this part, the amount of negative reinforcement was taken as the same as the main positive reinforcement. Figure 2.2 shows the overall dimensions and reinforcement details of the first two specimens where a straight bar splice was used inside the joint. Both specimens were identical except for the field joint material and designated as S1-UHPC and S2-PC.

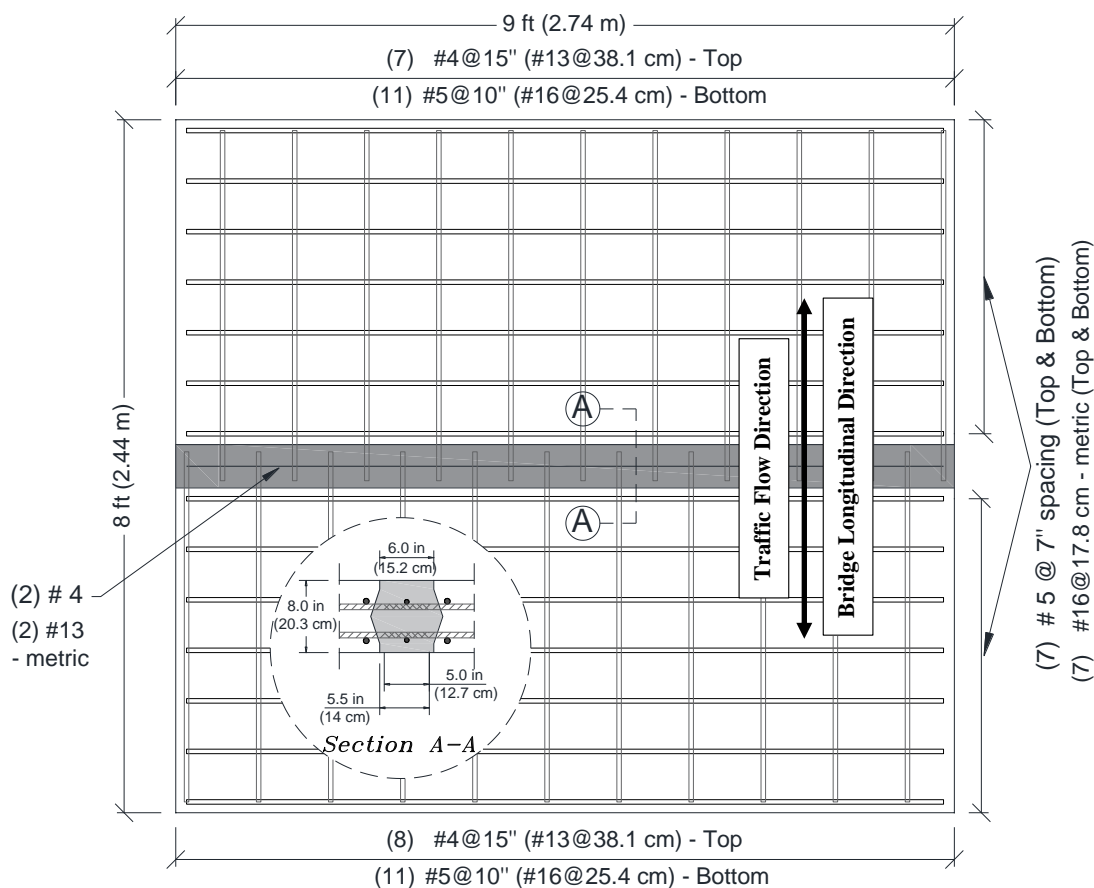


**Figure 2-2** Dimensions and design details of S1-UHPC and S2-PC specimens including two deck panels and a field joint shear key

The third specimen, designated as S3-PC-loop, used a PC field joint with different joint detail as shown in Figure 2.3. This third specimen varied from the other two specimens in two aspects. First, the shear key shape was different as it used a modified diamond-shaped

shear key with 6-inch width at the top surface and only half-inch gap at the bottom surface. This type of shear key was proposed to eliminate the time and labor needed in formwork erection at the bottom surface of the connection. Second, the straight non-contact lap splice was changed to a loop (U-bar) splice to investigate the difference in structural performance between these splice types.

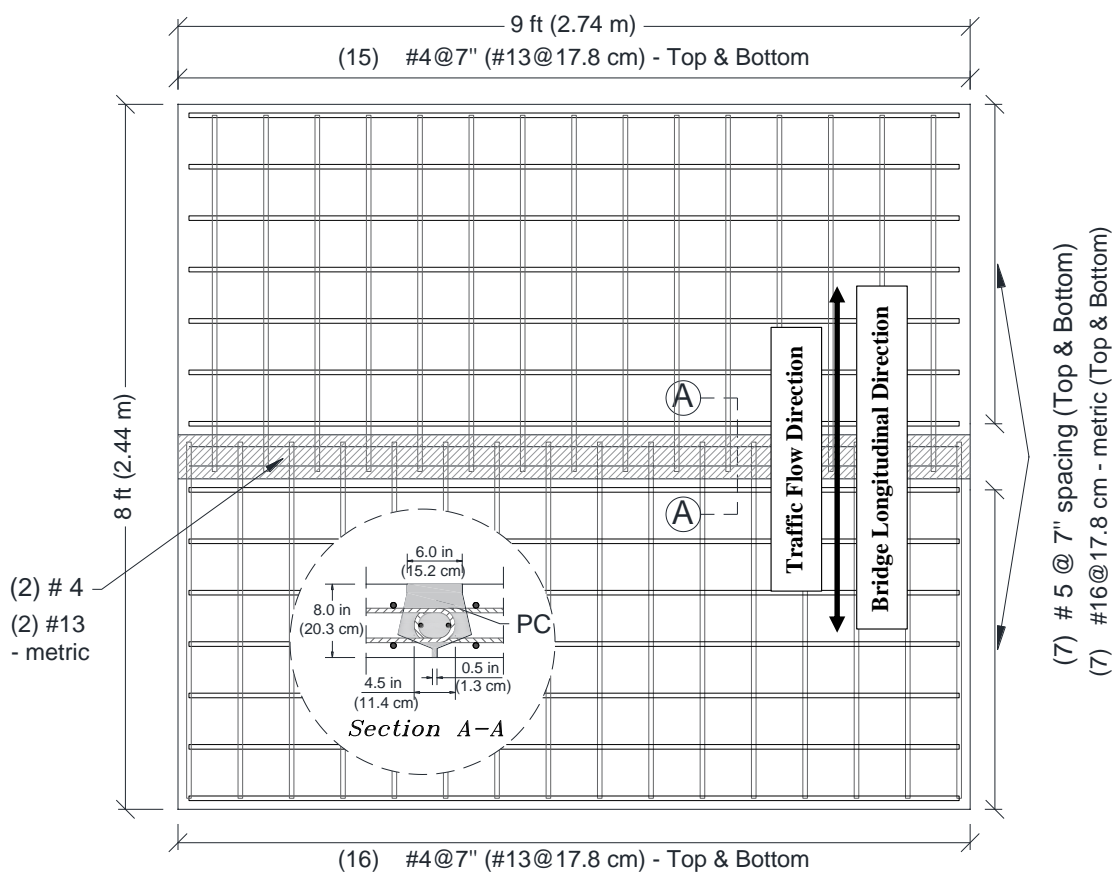


**Figure 2-3** Dimensions and design details of S3-PC-Loop specimen deck panels and field joint shear key

All the test specimens have general dimensions of 9 ft (2.74 m) length, 8 ft (2.44 m) width, and 8 in (20.3 cm) thickness with 6 in (15.2 cm) wide transverse joints at the middle of the specimens. While the test matrix of this study and the test variables of the three tested specimens are summarized in Table 2-1. Moreover, additional details on the joint design are provided. Using a U-bar splice can provide less splice length when compared to the straight splice. The U-bar splice could provide slightly better performance and force transfer between precast panels than the straight splice [8]. For #5 (#16 - metric) or smaller

reinforcing bars made of conventional steel, the minimum bend diameter should be six times the bar diameter of  $6 d_b$  as per ACI 318 requirements [31]. Because of the restricted deck slab thickness and the minimum required hook condition of  $6 d_b$ , #4 (#13 – metric) bars were used as the main reinforcement instead of #5 (#16 – metric) for specimen S3-PC-loop. The bend diameter used in this study was  $5.5 d_b$  which slightly varies from the standard  $6 d_b$  suggested value. It is noted that the suggested minimum bend diameter was established for two main reasons: feasibility of bending the reinforcement with minimizing the damage to the bars that would compromise their response and avoid possible crushing of concrete within the tight bend. A similar study that was conducted on precast deck panels using U-bar splice shows that it is feasible to use  $3 d_b$  as a minimum bend diameter [8]. One more advantage of using #4 (#13 – metric) bars is that the spacing between the reinforcement within the joint will be smaller which can provide more load resistance [6]. The choice of #5 (#16 – metric) bars for the longitudinal bottom reinforcement of specimens S1-UHPC and S2-PC was to provide wider spacing between reinforcement inside the joint and more clearance for the installation of the adjacent panels to account for the construction tolerances such as the accidental bar offsets. While the amount of the bottom longitudinal steel area is similar for all specimens as the #5@10 in (#16@25.4 cm) used for S1-UHPC and S2-PC is equivalent to the #4 @7 in (#13@17.8 cm) used for S3-PC-Loop. For specimens, S1-UHPC and S2-PC, the selected shear key dimensions and required lap splice length were based on the previous work at FHWA by Graybeal [1] on similar bridge deck slabs with UHPC field joints, which demonstrated good performance of this detail. Two reinforcing bars were added inside the connection for all three specimens and ran through the connection length, which is referred to as lacer bars. These bars provide confinement of concrete within the joint and serve as restraints for the U-bar splice in addition to allowing ductile failure to the U-bar splice transverse specimen [5].

**Table 2-1** Test matrix and specimen details (1 in = 2.54 cm, #4  $\approx$   $\Phi$ 13, & #5  $\approx$   $\Phi$ 16)

Specimen Name	Transverse Reinforcement		Longitudinal Reinforcement		Field joint material	Lap splice type	Lap splice length	Shear key shape
	Top	Bottom	Top	Bottom				
S1-UHPC	#5@7"	#5@7"	#4@15"	#5@10"	UHPC	Straight	5"	Diamond
S2-PC			#4@15"	#5@10"	PMMA-PC	Straight	5"	Diamond
S3-PC-Loop			#4@7"	#4@7"	PMMA-PC	Loop	4.5"	Modified Diamond

### 2.2.2 Test Setup and Instrumentation Plan

The experimental testing was conducted at the Earthquake Engineering Laboratory (EEL) at the University of Nevada, Reno (UNR). The test setup in this study was adopted to allow static testing of full-scale bridge deck subassemblies in three-point bending with a single point loading applied adjacent to the connection. Figure 2.4 shows a schematic drawing and a photograph of the test setup used in this study. The test setup assembly includes two seat beams aligned parallel to the longitudinal direction of the specimen, i.e. orthogonal to the transverse field joint direction. The specimens were supported over the full length of the seat beams. The spacing between the seat beams was adjusted to allow for an approximate centerline-to-centerline 8 ft (2.44 m) span which represented the assumed spacing between the inflection points of the deck slabs. A long strip of unreinforced 2-inch (5.1 cm) thick and 8-inch (20.3 cm) wide rubber pad was used between the specimen and seat beam to allow for rotation around the support axis. It is noted that precast bridge decks usually span across multiple girders, which provides negative moment regions over the girders and positive moment in the deck slabs almost halfway between the girders. This test setup was adopted to provide a simply supported deck slab with allowing some rotations at the ends only to represent positive moment case. The test setup did not consider any axial restraint, i.e. arching action, at the ends and ignored the associated contribution of this arching action to the load bearing capacity of the bridge deck. The applied mid-span vertical static load simulates the types of stresses usually imparted through the field



connections to provide continuity of load distribution between the precast panels. Flexure and shear are the main stresses that are usually required to be transferred through the connection. Thus, the point load position was determined to be in the mid-span and adjacent to the field connection as illustrated in Figure 2.4.

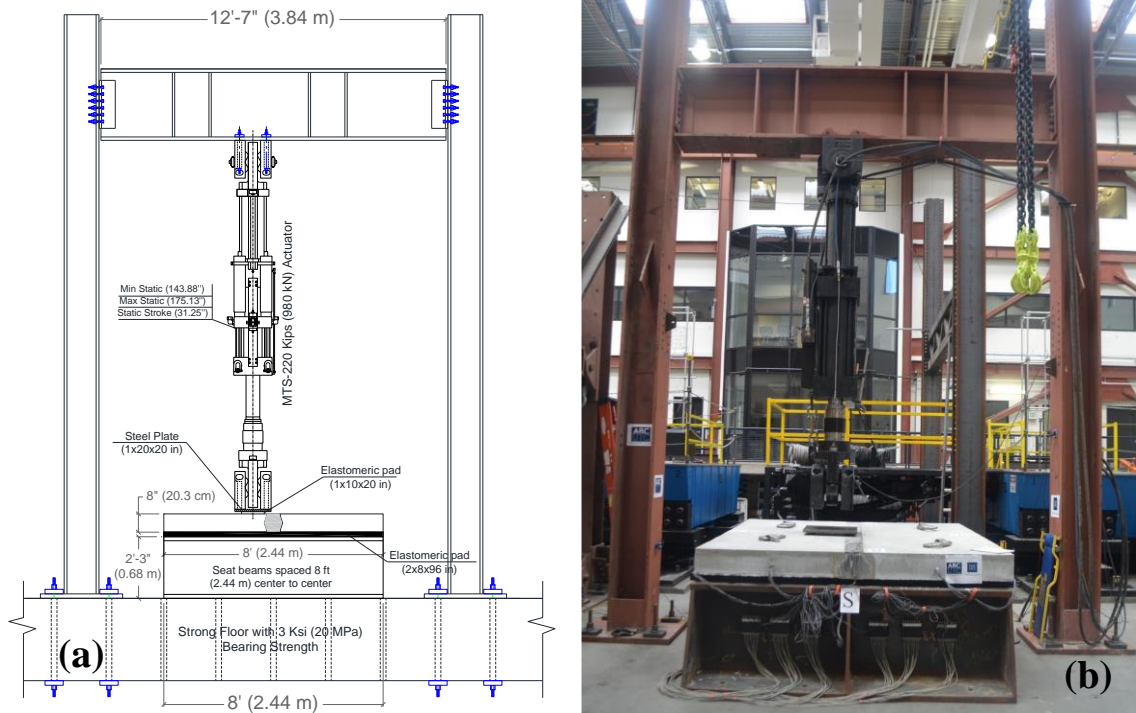


**Figure 2-4** (a) Schematic drawing of test setup, and (b) photograph of actual setup at UNR  
(1 in = 2.54 cm)

The load was applied using a 220-kip (980 kN) hydraulic actuator through a 1-inch (2.5 cm) thick elastomeric rubber pad of 20 in  $\times$  10 in (50.8  $\times$  25.4 cm) plan dimensions. The loading pad dimensions were determined based on the contact area of the typical AASHTO truck wheel. It is noted that the rubber pad was backed by a 1-inch (2.5 cm) thick steel plate for uniform distribution of the load. As previously mentioned, the objective of the test was to investigate the local flexural behavior of the interior transverse connections in a non-composite deck/girder bridge. The position of the interior transverse connections is located away from the main girder supports. The transverse connections over the girder supports (negative moment region) in a composite deck/girder bridge are mainly subjected to uniform tensile stresses throughout the depth of the connection. These types of stresses

along with any global flexural behavior experienced by composite deck/girder bridges were not investigated in this study.

The instrumentation plan for the first two identical specimens with a straight bar splice included a total of 44 strain gages for reinforcing bars distributed among the longitudinal and the transverse reinforcement, three concrete strain gages embedded within the joint, nine string potentiometers, and six LVDTs for displacement measurements. The third specimen with loop splice used 46 strain gages for reinforcing steel distributed among the longitudinal and the transverse reinforcement, three concrete strain gages embedded within the joint, nine string potentiometers, and three LVDTs for displacement measurements. Figure 2.5 shows the distribution of displacement measurements and locations of strain gages on the bottom reinforcement as a sample for all three specimens. The strain gages on the bottom transverse reinforcement were installed to capture the yielding of the bars due to the bending of the deck slabs and to monitor the load distribution between the connected precast panels. The strain gages distribution was denser close to the loading position due to the high local flexural stresses expected in this region. For the longitudinal reinforcement strain gages, each instrumented bar had two strain gages inside and just outside the joint region to interpret bar slip, if any. Moreover, the strain gages inside the connection were mainly installed to determine whether the bars yield within the joint and verify that the embedded length would satisfy the required development length within the field joint material. The displacement transducers were attached to the bottom of the deck slabs to measure the horizontal displacements between the precast deck panels and the field connection, i.e. monitor the opening of the bottom side of the connection. Several cameras were also used below the specimens to capture crack progress during testing.

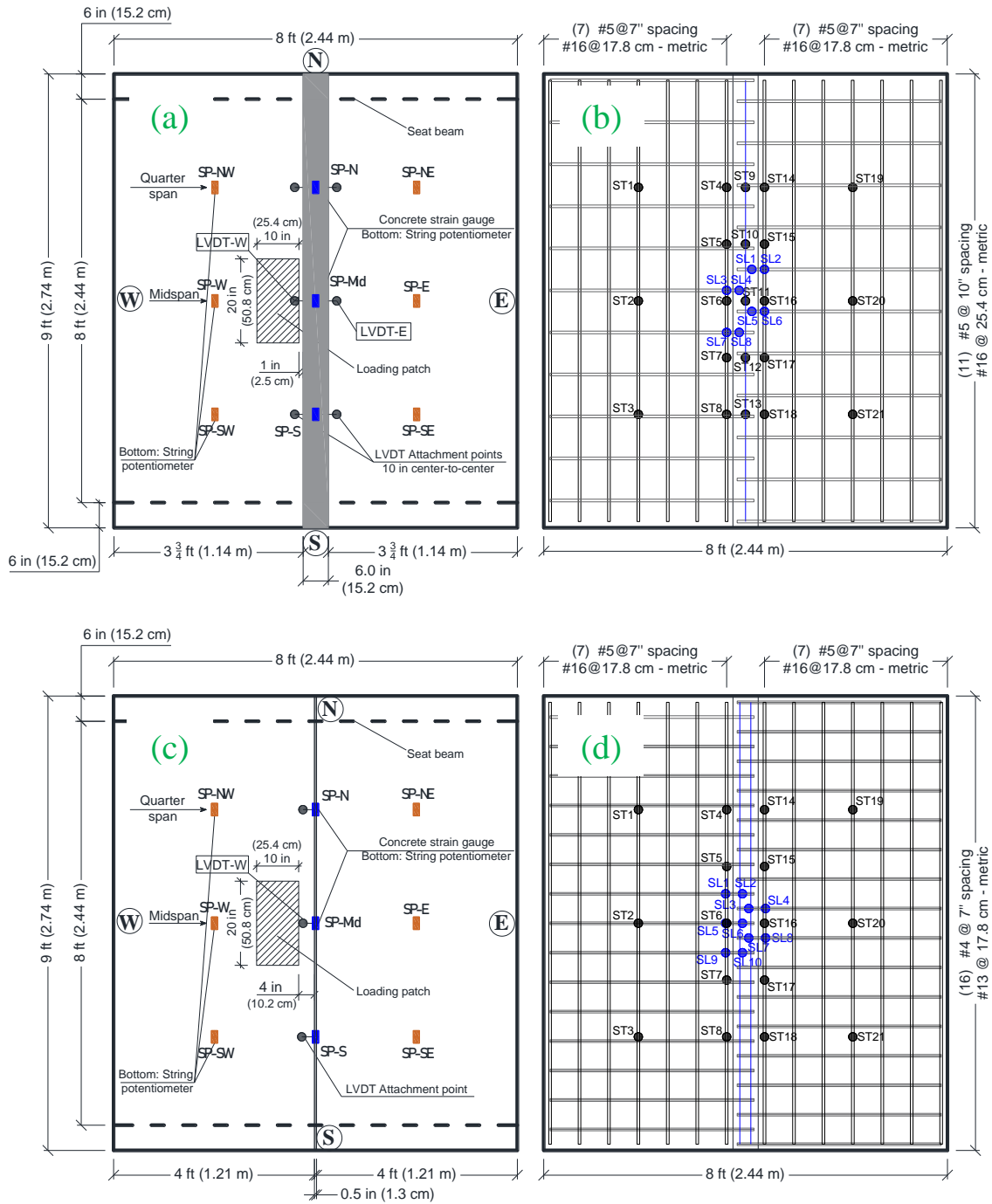


**Figure 2-5** Distribution of LVDTs and string potentiometers for displacement measurements for: (a) S1-UHPC/S2-PC, and (b) S3-PC-loop; locations of strain gages shown only for bottom reinforcement as a sample for: (c) S1-UHPC/S2-PC, and (d) S3-PC-loop

### 2.2.3 Loading Protocol

The loading protocol followed in this study included four cycles of loading and unloading, then a monotonic increased loading until failure as illustrated in Figure 2.6. The first two cycles included loading of the deck slabs to a certain load representing approximately the cracking load of the deck slabs then unloading. The second two cycles included loading of the deck slabs to a higher load limit which is slightly below the AASHTO ultimate load then unloading. The last cycle included the monotonic loading of the deck slabs until failure. The first four cycles were applied using force-control at a loading rate of 5 kips/min (22.2 kN/min). A similar rate was used for the unloading to avoid any sudden load drops or loss of contact at the loading pads. Next, displacement control was used for the monotonic loading of the last cycle to capture post-peak response through failure at the rate of 0.075 in/min (0.2 cm/min). The mid-span deflection of the specimen was used for the closed-loop displacement control applied for the last cycle. The reason for applying four cycles of loading and unloading was to investigate the behavior of the deck slab specimens under representative service loads, determine the crack pattern that would develop at earlier stages of loading, and estimate the average stiffness of the deck slabs from the obtained load versus mid-span displacement relationships.

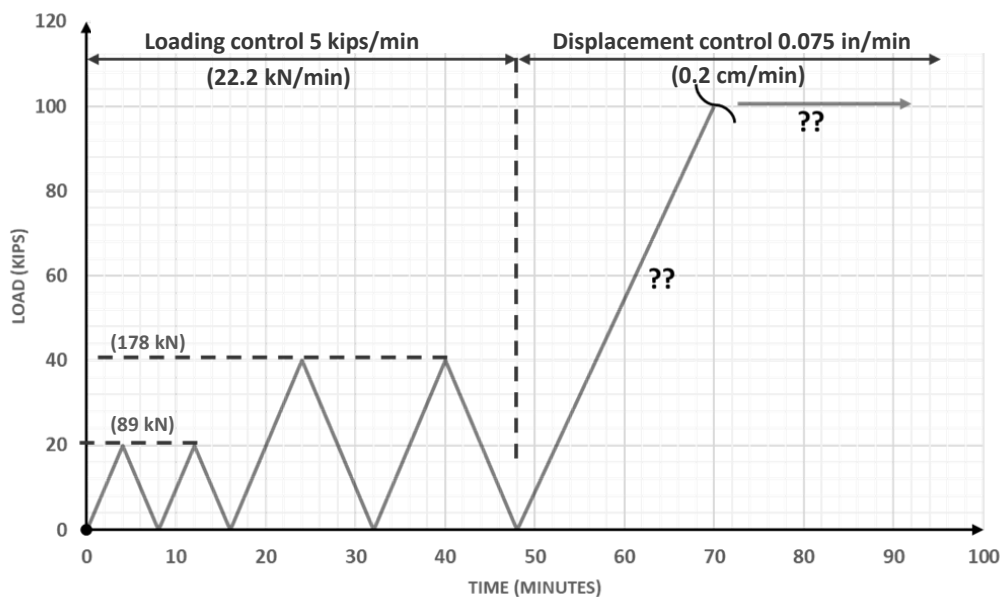


**Figure 2-6** Loading protocol for all tested specimens (1 kip = 4.448 kN)

#### ***2.2.4 Specimen Construction***

All the specimens were constructed at the fabrication yard of EEL at UNR. The construction was done over several phases as illustrated in Figure 2.7 and briefly explained below.

Fabrication of precast deck panels: The precast deck panels were constructed first. Each specimen consisted of two precast slab panels connected together with a field joint. The slab reinforcing bars were first instrumented then installed into the formwork. All precast panels were then cast using a single normal strength concrete batch from a ready-mix concrete truck.

Precast panels alignment: The precast slab panels were cured under normal conditions for approximately three weeks before the slabs were moved around for alignment. Each pair of two adjacent panels were aligned together with a gap of 6 in (15.2 cm) width to form the field joints.

Shear key preparation: This construction stage included the installation of the lacer rebars inside the joints, field joint side formwork, and the cleaning of the surface of the shear key using strong air pressure to remove dust and debris from the construction.

Pouring UHPC: Two UHPC batches were used in casting the field joint of specimen S1-UHPC. The shear key surface was sprinkled with water about half an hour before pouring the UHPC to prevent the old precast panels from absorbing the water out of the freshly mixed UHPC. The mixing process for UHPC was done using a high-shear mixer that is readily available at UNR. More information about the used commercial UHPC mix properties is provided in the next section.

Pouring PMMA-PC: The mixing process of PC was also done at the fabrication yard of EEL using a 1.5 ft<sup>3</sup> (0.0425 m<sup>3</sup>) rotary drum mixer. A primer liquid was initially applied to the shear key surfaces about 10 minutes before pouring the PC by using a brush to increase the adhesion between the PC and the old precast concrete panels.



**Figure 2-7** Photographs that illustrate the various construction stages and sequence of precast deck assemblies with UHPC and PC field joints

### 2.2.5 *Material Properties*

Different materials were used in this study as explained before. Normal strength concrete (NSC) with 5 ksi (35 MPa) specified 28-day compression strength was used for deck panels. For UHPC, the proprietary Ductal® JS1000 mix from LafargeHolcim was used because the research team has previous experience in mixing and testing this UHPC product [32]. For the PMMA-PC, the commercial product T-17 from Transpo Industries that has been recently used in the mechanical characterization and bond study of PMMA-PC [29] was also used in this study. Several material specimens were sampled, and several tests were conducted for the different materials as shown in Figure 2.8. For ASTM C39 compressive testing [33],  $6 \times 12$  in ( $15 \times 30$  cm) cylinders were used for NSC and  $3 \times 6$  ( $7.5 \times 15$  cm) cylinders were used for UHPC. For PMMA-PC testing, both  $3 \times 6$  ( $7.5 \times 15$  cm) cylinders and 2-inch (5.1 cm) cubes were used to conduct ASTM C469 [34] and C579 [35] tests, respectively, as shown in Figure 2.8. It is noted that the UHPC and PMMA-PC

cylinders were surface-prepared using a special grinding machine readily available at UNR (see Figure 2.8a) to get smooth flat and parallel surfaces for accurate strength evaluation.

A summary of the measured compressive strength of the conventional NSC, UHPC, and PMMA-PC at different ages is reported in Table 2-2. The reported material strengths are the average of a minimum of three samples tested for each concrete type at each testing date. Previous studies done by the authors showed that the PMMA-PC has a compression modulus of elasticity of 2,800 ksi (19,305 MPa), a tensile strength of approximately 0.7 ksi (4.8 MPa), and flexural strength of 2.9 ksi (20 MPa) [36, 37]. The flexural strength was expected to be higher than the tensile strength (i.e., almost 4 folds) as of many reasons. First, the uniaxial tensile test subjects the reduced cross section of the specimen to a uniform maximum tensile stresses. While the stress distribution over the cross-section of the bending prisms are different, where the maximum compressive and tensile stresses are expected only at the outer fibers of the specimens above and below the neutral axis, respectively. Second, there are no test standards or procedures for the direct tensile testing of the polymer concrete dog-bone specimens. Hence, the specimens shape and dimensions in addition to the loading rate may affect the results of the uniaxial tests or underestimates the actual tensile strength of the polymer concrete. As a result, the flexural tests should be more reliable in the determination and assessment of the tensile strength and behavior of the polymer concrete. These studies also include more information regarding the material mixing and mechanical behavior of the PMMA-PC. Moreover, reinforcing steel coupons were also tested to get the actual yield and ultimate tensile strength of the #5 (#16 – metric) A706 Grade 60 (420 MPa) reinforcing bars used in this study. The measured yield and ultimate tensile strength were determined to be 63.5 ksi (438 MPa) and 103 ksi (710 MPa), respectively. The measured yield and ultimate tensile strains are 0.278% and 20.08%, respectively.



**Figure 2-8** (a) Grinding of UHPC and PMMA-PC cylinders, and compression testing of: (b) 3×6 in (7.5×15 cm) UHPC cylinders, (c) 3×6 in (7.5×15 cm) PMMA-PC cylinders, (d) 2-inch (5.1 cm) PMMA-PC cubes, and (e) 6×12 in (15 × 30 cm) NSC cylinders

**Table 2-2** Summary of measured compressive strength of different materials used in this study

Type of Concrete	Standard Test	Specimen type and dimensions	Age	Average Strength, ksi, (MPa)
NSC	ASTM-C39 [33]	6 × 12 in cylinders (15 × 30 cm)	7 days	2.93 (20.2)
			28 days	4.32 (29.8)
			test day	5.20 (35.8)
UHPC	ASTM-C39 [33]	3 × 6 in cylinders (7.5 × 15 cm)	28 days	24.80 (171)
			test day	27.80 (191.7)
PMMA-PC	ASTM – C579/B [34]	2 × 2 × 2 in cubes (5.1 × 5.1 × 5.1 cm)	2 days	11.90 (82)
			7 days	12.10 (83.4)
			28 days	10.60 (73.1)
			test day	10.70 (73.8)
PMMA-PC	ASTM – C469 [35]	3 × 6 in cylinders (7.5 × 15 cm)	9 days	10.60 (73.1)
			28 days	8.56 (59)
			test day	9.03 (62.3)



## 2.3 Test Results and Discussion

The experimental results including global and local behavior of the tested specimens are presented in this section along with a comparative assessment of the structural performance of deck slabs with UHPC and PMMA-PC field joints. The results are presented in four sections that discuss damage progression and mode of failure, load-deflection relationships, reinforcement strains, and interface bonding, slippage, or opening.

### 2.3.1 Damage Progression and Mode of Failure

Before discussing the damage progression and mode of failure of the tested specimens, a brief summary of the key test results is provided in Table 2-3. The table includes the load capacity and deflection at peak load which provides a general idea about the comparative specimens' behavior at failure as discussed in this section. It is important to know that testing continued through failure only to understand the full structural behavior and different materials response and not to inform future design or so. That is because bridge decks are required to remain essentially elastic under code-compliant service and ultimate loads. Thus, other results such as the onset of yielding or the deflection at AASHTO service and ultimate loads as shown in Table 2-3 summary are used for assessing the deck systems design validity as discussed in the following sections.

**Table 2-3** Summary of key experimental test results

Specimen Name	Peak load, kips (kN)	Mid-span deflection at, in (cm)			Initial stiffness, kips/in (kN/cm)
		Peak load	Service load	Ultimate load	
S1-UHPC	117.9 (524.4)	2.33 (5.92)	0.175 (0.445)	0.384 (0.975)	240 (420.3)
S2-PC	113.2 (503.5)	2.53 (6.43)	0.205 (0.521)	0.460 (1.168)	190 (332.7)
S3-PC-Loop	122.5 (544.9)	2.63 (6.68)	0.177 (0.450)	0.397 (1.008)	220 (385.3)

#### 2.3.1.1 Specimen S1-UHPC

The peak load capacity of specimen S1-UHPC was 117.9 kips (524.4 kN) at which 2.33 in (5.92 cm) mid-span vertical displacement was measured. The observed mode of failure for

the UHPC transverse field joint specimen was yielding in the main reinforcement due to bending accompanied with crushing of the concrete at the top part of the loaded west side of the specimen. Deep and wide flexural cracks were observed at the bottom face of the precast slabs interrupted by two main localized cracks in the UHPC at the measured peak load. An interface crack at the top surface of the slab was observed between the unloaded east side and the UHPC connection at the peak load as shown in Figure 2.9a. The depth and length of this interface de-bonding were then increased as the applied displacements increased. After reaching the peak load, a series of drops in the force capacity was observed along with excessive flexural cracking at the bottom and crushing of the deck panels' concrete at the top (see Figures 2.9a and 2.9c). The test was stopped after a rebar popping sound was heard when the specimen was going through post-peak softening and strength degradation at approximately 80% of the peak load, which was found to indicate the rupture of one of the bottom transverse rebars inside the field connection.

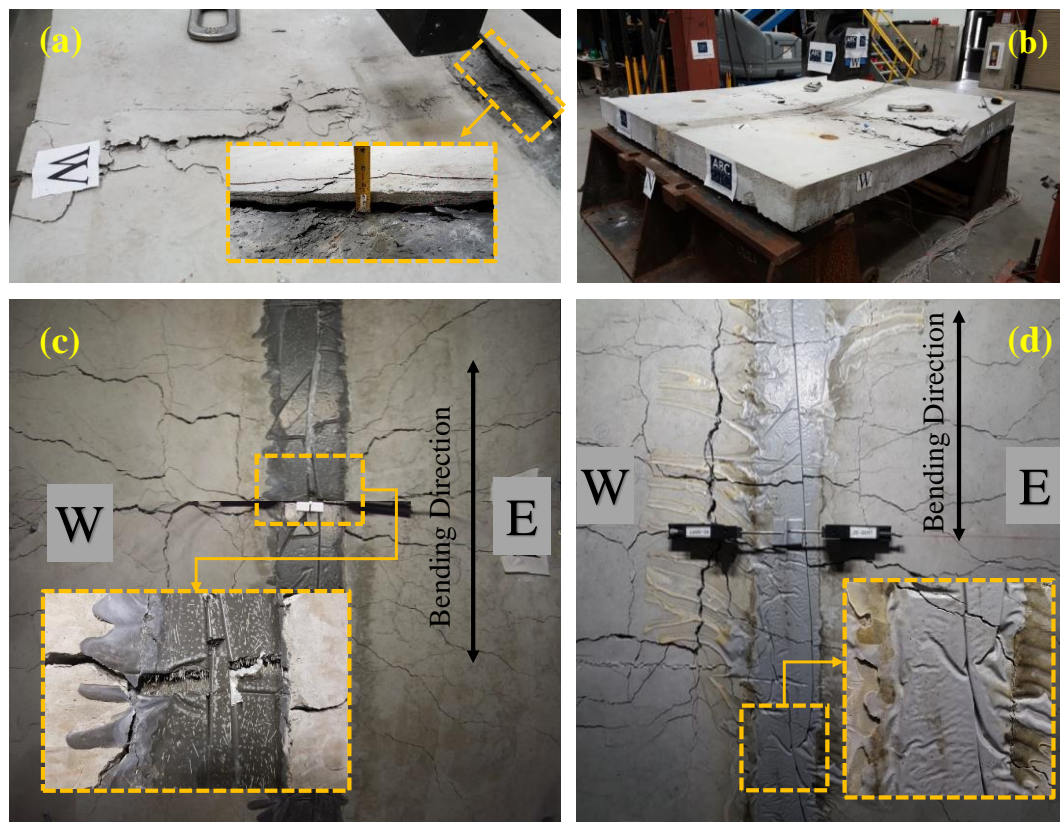


**Figure 2-9** Crack pattern, damage, and modes of failure at: (a) top side of S1-UHPC; (b) top side of S2-PC; (c) bottom side of S1-UHPC; and (d) bottom side of S2-PC.

### 2.3.1.2 Specimen S2-PC

The peak load of specimen S2-PC was determined to be 113.2 kips (503.5 kN) at 2.53 in (6.43 cm) mid-span vertical displacement. The observed mode of failure for the PMMA-PC transverse specimen was similar in the beginning to the UHPC case with yielding in the main reinforcement due to flexural bending. However, a rebar rupture was observed at the peak load of the specimen which caused a sudden drop in the ultimate load capacity of the specimen. Crushing of the concrete was then observed at the top surface of the loaded west side of the specimen and continued to propagate through the joint until reaching the unloaded east side. Deep and wide flexural cracks were observed at the bottom face of the precast slabs, these cracks continued to propagate through the joint when approaching the peak load. No interface cracking was observed at the top surface of the slab between the precast slab and the PMMA-PC connection at the peak load. However, a short-length interface cracking of approximately 5 in (12.7 cm) was observed at the bottom surface of the slab between the unloaded part and the PMMA-PC joint while approaching the end of the test as shown in Figure 2.9d. The test was again stopped after load capacity dropped to approximately 80% of the peak load. Figure 2.9b shows the overall damage and final status of specimen S2-PC after testing. Moreover, Figure 2.9d shows the crack pattern and damage at the bottom side of S2-PC, which is compared side-to-side with S1-UHPC shown in Figure 2.9b. Similar to UHPC, the PMMA-PC field joint reached the AASHTO ultimate load before any significant cracking was observed due to the high tensile properties of PMMA-PC which make the material suitable for deck field joints. Figure 2.10 shows and compares the crack pattern from the bottom side for all three specimens at the AASHTO ultimate load. The crack patterns in Figure 2.10 were marked and highlighted in the photographs to make them easier to inspect since the actual cracks at this load level were very narrow and tiny and hard to see.

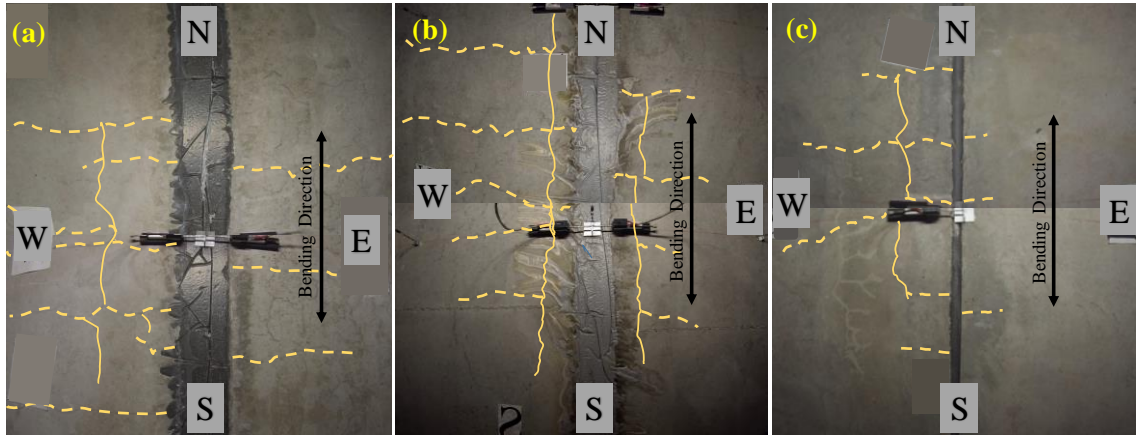


**Figure 2-10** Crack pattern at the AASHTO ultimate load level at the bottom side of: (a) S1-UHPC; (b) S2-PC; and (c) S3-PC-Loop.

### 2.3.1.3 Specimen S3-PC-Loop

The measured peak load of specimen S3-PC-Loop was 122.5 kips (544.9 kN) at 2.63 in (6.68 cm) mid-span vertical displacement. Similarly, the observed mode of failure for specimen S3-PC-Loop was yielding in the main reinforcement due to flexure accompanied with crushing of the concrete at the top of the loaded west side of the slab. After reaching the peak load, the concrete crushing started to propagate across the east and west sides of the slab with excessive crushing damage observed on the west side as shown in Figure 2.11a. Deep and wide flexural cracks were observed at the bottom face of the precast slabs, these cracks continued to propagate across the joint after reaching the peak load as shown in Figure 2.11b. No interface cracking was observed at the top surface of the slab between the precast slab and the PMMA-PC joint at the peak load. A series of drops in the force capacity was noticed beyond the peak load along with excessive flexural cracking at the bottom and crushing of the top deck panel concrete until the test was stopped at 80% of the peak load. It was observed that the early crack propagation of the S3-PC-Loop specimen was better than the other specimens due to the denser distribution of the bottom and top mesh reinforcement, i.e. #4@7" (#13@17.8 cm) instead of #5@10" (#16@25.4 cm) or #4@15" (#13@38.1 cm), resulted in better crack control. Also similar to S1 and S2, no significant flexural or interface cracks were observed in the field joints up to the AASHTO ultimate load level as shown in Figure 2.10 above.

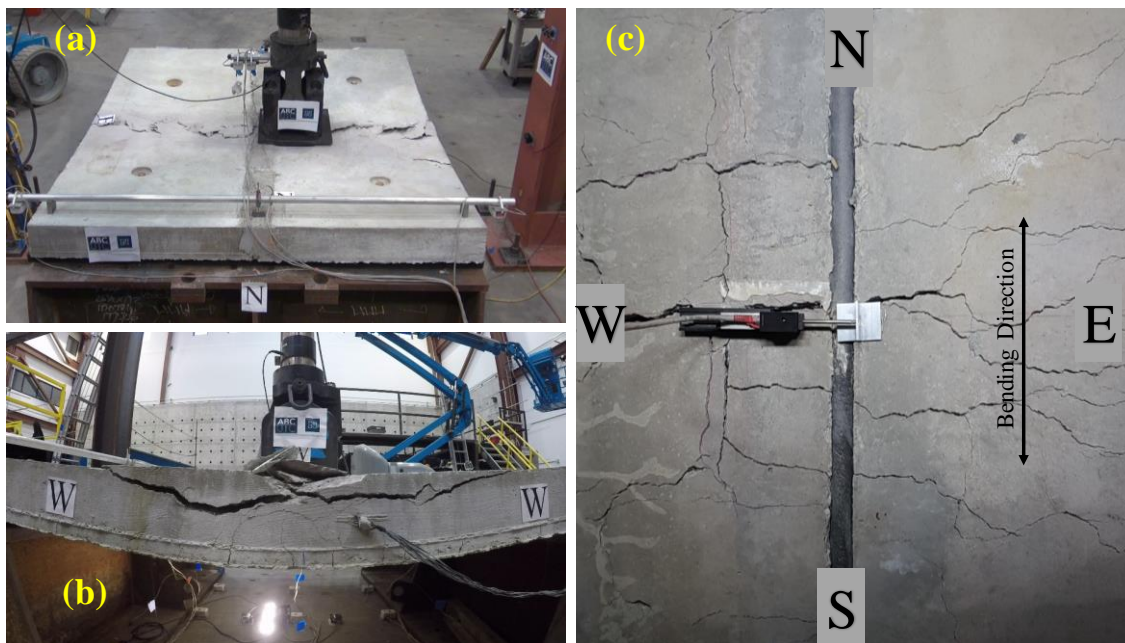


**Figure 2-11** Crack pattern, damage, and mode of failure of S3-PC-Loop as seen from: (a) top side; (b) west side; and (c) bottom side.

### 2.3.2 Load-Deflection Relationship

This section discusses the load and deflection response of the three specimens as evaluated at various loading levels. UHPC field joints are widely accepted and have been already employed in a large number of projects in the United States and worldwide and proved to provide a monolithic equivalent bridge deck behavior [38]. Thus, specimen S1-UHPC is considered to be the reference specimen against which the other two PMMA-PC specimens are compared and assessed. Subsequently, the load-deflection behavior is presented in two subsections for S1-UHPC versus S2-PC and S1-UHPC versus S3-PC-Loop comparisons.

#### 2.3.2.1 Specimen S1-UHPC versus S2-PC

The overall load versus the mid-span vertical displacement obtained from three different string potentiometers for S1-UHPC and S2-PC specimens is presented in Figure 2.12. It is noted that the data acquisition system had some signal noise during the third cycle of the specimen S2-PC test which slightly reduced the quality of the load-deflection curve for this part of the test. Two main observations can be drawn from Figure 2.12. The overall behavior of the two specimens with UHPC and PMMA-PC straight lap splice joints is very comparable, and the flexural capacity of both specimens well exceeded the ultimate limit

state specified in the AASHTO LRFD using the Equivalent strip method. This was expected because of many reasons such as the use of the nominal values for steel yielding strength and concrete compressive strength when calculating the AASHTO service and ultimate loads, the use of a reduction factor ( $\phi$ -factor) of 0.9 that magnifies the ultimate moment and consequently increases the required steel area, and neglecting the contribution of the top transverse reinforcement to the moment capacity while calculating the required area of the bottom transverse steel. Therefore, both UHPC and PC field connections are viable options for providing an ABC full-depth precast deck system that emulates conventional CIP decks in terms of strength requirements.

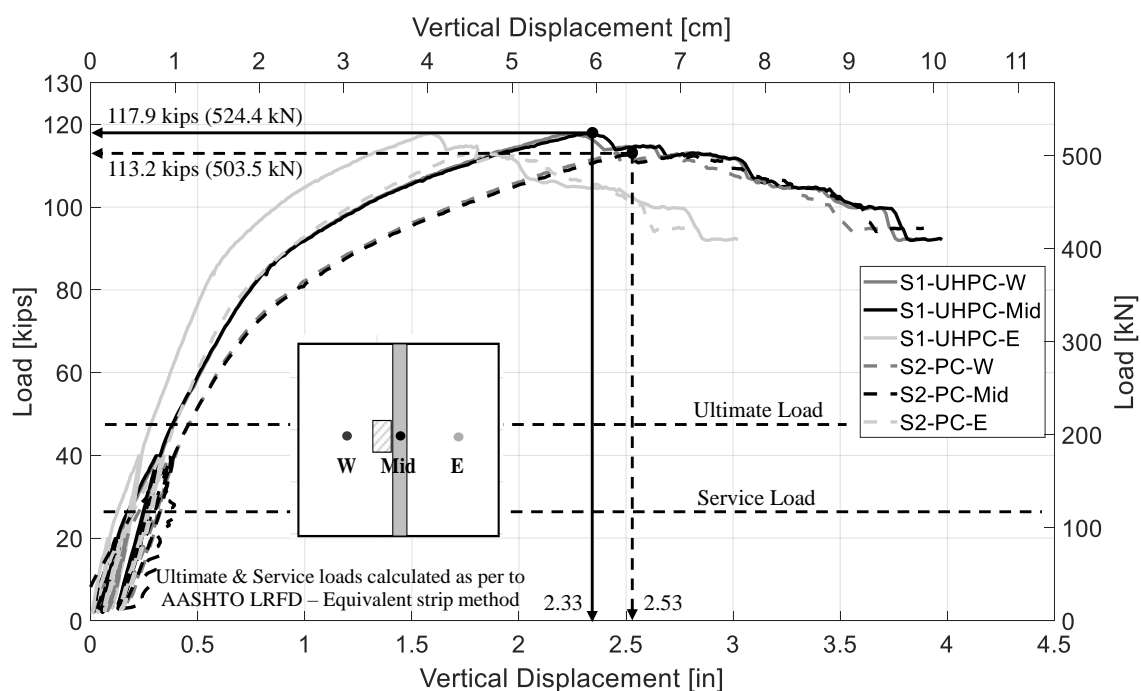


**Figure 2-12** Load-deflection relationship at mid-span of specimens S1-UHPC and S2-PC as measured at three different locations

The load-deflection curves shown in Figure 2.12 can be divided into four different regions of behavior. The first portion of the behavior represents the almost linear elastic behavior of the specimen when the applied load is approximately below 20 kips (88.9 kN). During this stage, only hair flexural cracks in the longitudinal direction were observed in the bottom face of the slab. A hair transverse crack located approximately 5 inches (12.7 cm) apart from the edge of the connection and ran parallel to the connection in the loaded west

side of the slab was also observed. No cracks were observed in the unloaded east side of the slab. No interface de-bonding or concrete crushing was observed during the “service” level loading of the behavior. No cracks were also observed in the field joints because of the higher tensile strength of the UHPC and PMMA-PC as compared to the conventional concrete. The second region in defining the load-deflection curve represents the essentially elastic behavior as the applied load exceeded the linear elastic load. This started in the third and fourth cycles of loading around the 40 kips (177.9 kN) vertical load where the flexural stiffness slightly decreased because of the concrete cracking and the residual displacement after unloading increased. The cracks at this level were still narrow and more importantly, the main reinforcement was not yet yielded. It is worth noting that no flexural or interface cracks were observed in the field connections up to the AASHTO specified ultimate load as previously shown in Figure 2.10.

The essentially elastic behavior continued as the load increased to approximately 85 kips (378.1 kN) and 75 kips (333.6 kN) for specimens S1-UHPC and S2-PC, respectively. As the load increased beyond this limit, the third region of the load-deflection curve can be defined by the significant reduction in stiffness where the specimens started softening due to yielding of the middle and west side transverse reinforcement in the bottom mesh. Hence, deep and wide flexural cracks were observed on the bottom side of the slab. No rebar slip was observed until reaching the peak load for both specimens. Following the peak load capacity, the fourth region can be defined by a global stiffness and strength degradation where the load capacity started to decrease with larger displacements observed. Again, it is noted that the goal of testing the specimens up to such high levels of loads and displacements beyond code-required limits was to have a better understanding of the mode of failure and check whether the different components of the deck system stay intact.

It can be also seen from Figure 2.12 that the UHPC specimen exhibited larger flexural stiffness than the PMMA-PC specimen because of the higher modulus of Elasticity as well as tensile and compressive strengths of UHPC. The initial flexural stiffness of the UHPC specimen was found to be 240 kips/in (420.3 kN/cm) versus 190 kips/in (332.7 kN/cm) for

the PMMA-PC specimen, i.e. the PC deck system stiffness was about 80% of the UHPC system. To further investigate the relative deflection between the two slab panels in a given specimen, the deflection was observed at three different locations in the middle of the specimen as illustrated in Figure 2.12. It is shown that the loaded west side of the slab and the field joint deflection were almost identical, which was the case for both specimens. However, the unloaded east side attained lower deflections which were expected because of the asymmetry of the specimen loading in the longitudinal direction, i.e. east-west direction. Another interpretation for this observation is that the field connection is not transferring the full applied loads between the two sides of the slab as there was a discontinuity in the reinforcement between both two sides. Moreover, this difference in deflections increased with the increase of the applied load due to the influence of the reduction in stiffness of the slabs after the propagation of excessive cracking. This is consistent with results from a previous analytical study that was part of the NCHRP 10-71 project [8] which showed that the shear and moment forces on the field joint are greatly reduced due to the stiffness reduction accompanied by cracking of the specimen.

#### 2.3.2.2 *Specimen S1-UHPC versus S3-PC-Loop*

The load versus the mid-span vertical displacement relationships obtained from three different string potentiometers for S1-UHPC and S3-PC-Loop specimens are presented in Figure 2.13. Similar to before, the overall behavior of both the UHPC with straight lap splice specimen and the PMMA-PC with loop splice specimen is comparable with a flexural capacity that exceeded the code limit state. However, the load capacity of specimen S3-PC-Loop is shown to have exceeded the other specimens. It is noted that main reinforcement (i.e., top and bottom transverse reinforcement) is set to be similar for all tested specimens, hence the increased capacity of the third specimen is attributed to the utilized loop splice. This confirms that also PC-Loop field connections provide a viable alternative for ABC precast deck systems that emulates or exceeds conventional CIP deck systems in terms of strength requirements. Moreover, the PMMA-PC connections with loop splice configuration enhanced the structural performance and increased the flexural stiffness of the deck slabs.



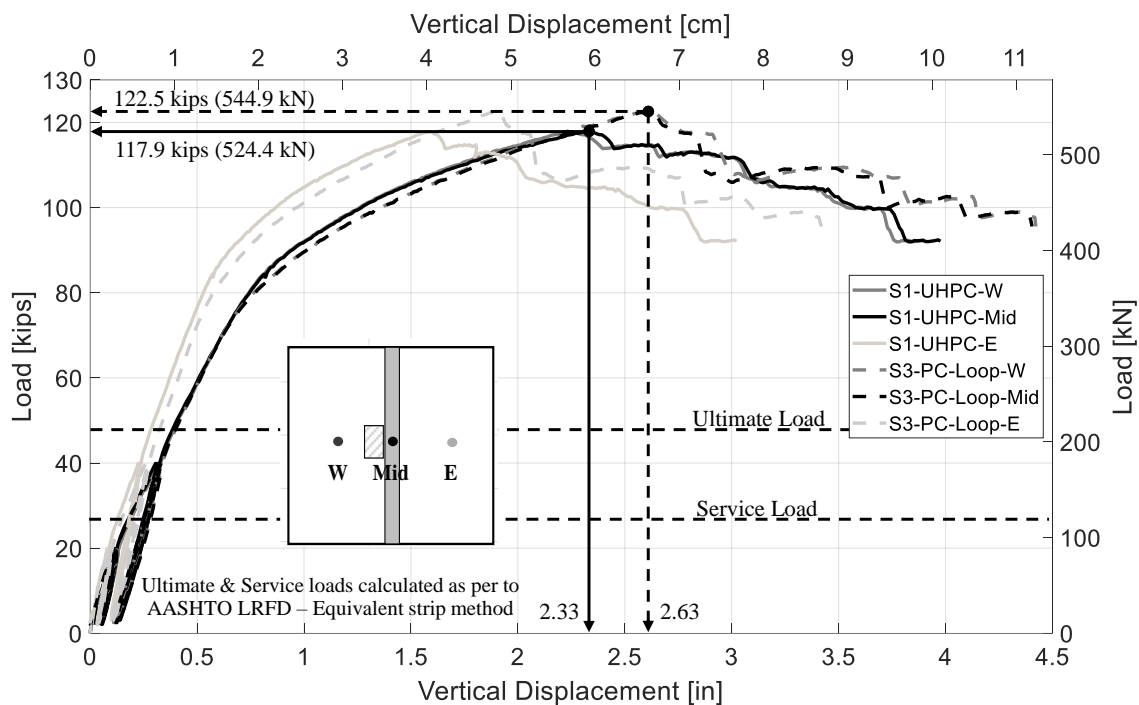


**Figure 2-13** Comparison of load-deflection relationship of specimens S1-UHPC and S3-PC-Loop as measured at the mid-span at three different locations.

The load-deflection relationship of specimen S3-PC-Loop shown in Figure 2.13 is quite similar in behavior to the other two transverse specimens in terms of the four main regions. Elastic behavior continued up to approximately 20 kips (88.9 kN) applied load with only hair flexural cracks observed at the bottom of the specimen. Then essentially elastic behavior was observed as the applied load exceeded the elastic load with no significance of interface debonding or cracking. Afterward, a significant reduction in the flexural stiffness due to yielding of the middle and west side transverse reinforcement in the bottom reinforcement mesh was observed after reaching approximately 80 kips (355.8 kN). Finally, both strength and stiffness degradation was observed after the 122.5-kip (544.9 kN) peak load capacity was reached with several load drops can be seen in the figure. It can be also inferred from Figures 2.12 and 2.13 that the PMMA-PC specimen with loop splice exhibited larger initial stiffness [ $\sim 220$  kips/in (385.3 kN/cm)] than the PMMA-PC specimen with straight splice, but still slightly less than that of the UHPC specimen. The load and mid-span deflection relationships of the three specimens are shown in Figure 2.14. As can be seen, the behavior of all the specimens is very comparable, however, specimen

S2-PC is shown to be softer than the other two specimens. While this did not severely affect the overall behavior and the load capacity of the specimen compared to the other specimens.

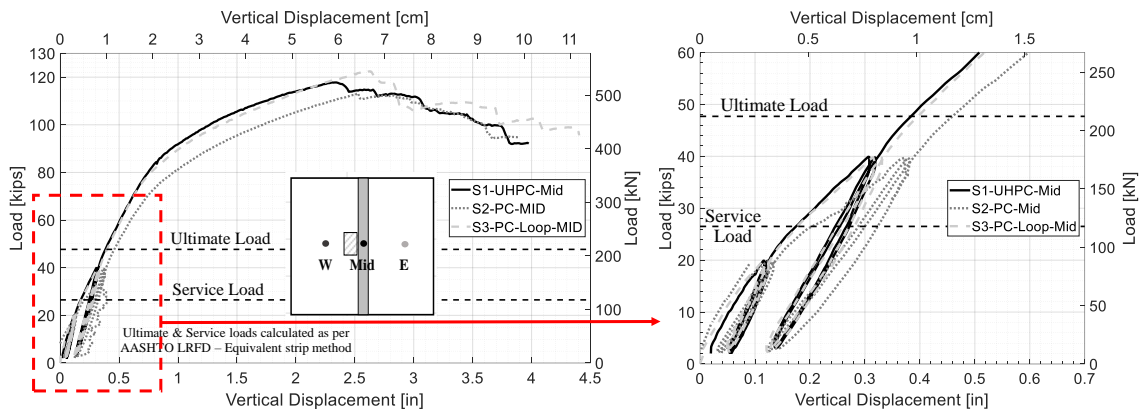


**Figure 2-14** Comparison of load and mid-span deflection relationship of specimens S1-UHPC, S2-PC, and S3-PC-Loop

All specimen deflections were measured at three different locations in the middle of the specimen as illustrated in Figures 2.12 and 2.13. The loaded west side of the slab and the field joint deflection were almost identical, and the unloaded east side attained lower deflections for all three specimens. As discussed earlier, this difference in deflections could happen out of two main reasons; asymmetry of the specimen loading in the longitudinal direction, and the capability of the field connection to transfer the full applied loads between the two sides of the slab. Figure 2.15 shows the difference between the mid-span vertical displacement and the east and west side displacements along with the applied vertical load of the slab. It can be seen that the difference in string potentiometer readings between the middle and the west sides of all three specimens was minimal, while the difference in deflection between the middle and east sides was relatively higher. The difference between the east and west side deflections at the measured peak loads of specimens S1-UHPC, S2-PC, and S3-PC-Loop is shown to be 0.75 (1.9 cm), 0.80 (2 cm), and 0.72 (1.8 cm) inches, respectively. The difference between the deflection of the middle and east unloaded side of the slab can give a good indication about the performance of the field joint and the ability to transfer the straining actions between both sides of the precast segments. The smaller the difference in deflection is, the better is the load distribution over

the slab and joint performance in transferring the loads. Hence, the PMMA-PC specimen with loop splice shows better load distribution than the other two specimens. It can be also seen from Figure 2.12 and Figure 2.13 that specimen S3-PC-Loop attained higher ultimate deflections and higher load capacity than the other two specimens. Therefore, the loop splice configuration and the denser reinforcement inside the field joint increase the flexural ductility of the deck slabs and enhances the load distribution across the precast panels.

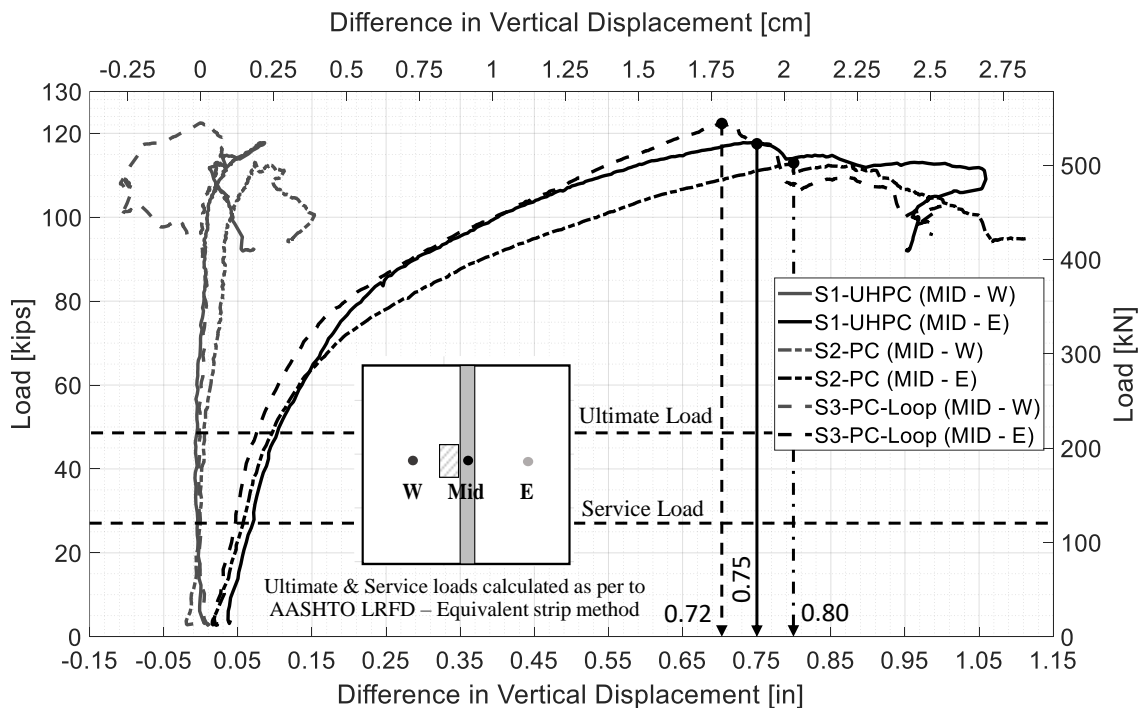


**Figure 2-15** Load versus difference between mid-span deflection under the field joint and the east and west sides under the deck panels

### 2.3.3 Reinforcement Strains

This section presents selected results from the measured strain data. The load versus strain readings of selected bottom transverse reinforcement at mid-span location are shown in Figure 2.16 and discussed here. It is noted that some of the strain gages were damaged during the test, especially at larger load levels. Figure 2.16 includes three sets of figures for all three specimens. Thus, the discussion is presented next in separate subsections for the three specimens for convenience.

### 2.3.3.1 Specimen S1-UHPC

Figure 2.16 shows that the largest strains were recorded in the middle rebars close to where the load was applied. The onset of yielding was observed in the rebar inside the joint at 65 kips (289.1 kN). This was followed by yielding in the rebars adjacent to the connection at almost 69 kips (306.9 kN) and 78 kips (347 kN) for the west and east sides, respectively. It is observed that the strain values at the same applied load level were different between the east and west sides of the slab. The west side showed higher values of strains than the east side. Most of the other rebars in the west side and the middle part of the slab yielded at approximately 78 kips (347 kN). After this limit, the load-deflection behavior of the slab significantly changed with large deflection increments corresponding to small force increments as previously shown in Figure 2.12. It can also be concluded that when yielding happened in the reinforcement of the west side while the east side reinforcement was still not yielded, the difference in deflections between the east and west side of the slab increased significantly. Rebar rupture was observed at the end of the test in the bottom transverse rebar that was located inside the UHPC joint as can be inferred from the strain readings. Finally, a key observation from the behavior depicted in Figure 2.16 for S1-UHPC is that none of the joint or slab transverse bottom reinforcement yielded before reaching the ultimate and service loads specified in AASHTO, i.e. the deck system remains elastic up to the code limits as required.

### 2.3.3.2 Specimen S2-PC

As mentioned before, the data acquisition readings in the third cycle of specimen S2-PC had some noise that partially affected the quality of plots. The onset of yielding was observed in the rebar inside the joint at 46 kips (204.6 kN). This was followed by yielding in the rebars adjacent to the connection at almost 60 kips (266.9 kN) and 68 kips (302.5 kN) for the west and east sides, respectively. Most of the rebars in the west side and the middle part of the slab yielded at approximately 68 kips (302.5 kN). The west side strains were higher than the east side until reaching the peak load and the bar rupture occurred. The east side strain then showed more strains due to the redistribution of forces as a result of this bar rupture. Moreover, and similar to S1-UHPC, the transverse bottom reinforcement inside the joint and the slab remained elastic up to the service and ultimate

loads specified in AASHTO, which further verifies the acceptable behavior of PMMA-PC for precast deck joints.

#### *2.3.3.3 Specimen S3-PC-Loop*

The onset of yielding was observed in the rebar adjacent to the connection on the west side at 67.5 kips (300.3 kN). This was followed by yielding in the rebar adjacent to the connection on the east side at 74 kips (329.2 kN). Most of the rebars in the west side and the middle part of the slab yielded at approximately 80 kips (355.9 kN). Again, it is observed that the strain values at the same applied load level were different between the east and west sides of the slab. In most of the cases, the west side showed higher values of strains than the east side. It is worth noting that the rebars inside the joint were not placed at the outermost surface of the slab as they were added inside the joint as lacer bars to provide some bearing forces for the loop splices inside the joint. Hence, the strain readings of these rebars were slightly lower than the adjacent rebars outside the joint. Moreover, and similar to the other specimens, the transverse bottom reinforcement inside the joint and slab remained elastic up to the service and ultimate loads specified in AASHTO, which further verifies the acceptable behavior of the PMMA-PC deck joints with loop splices.

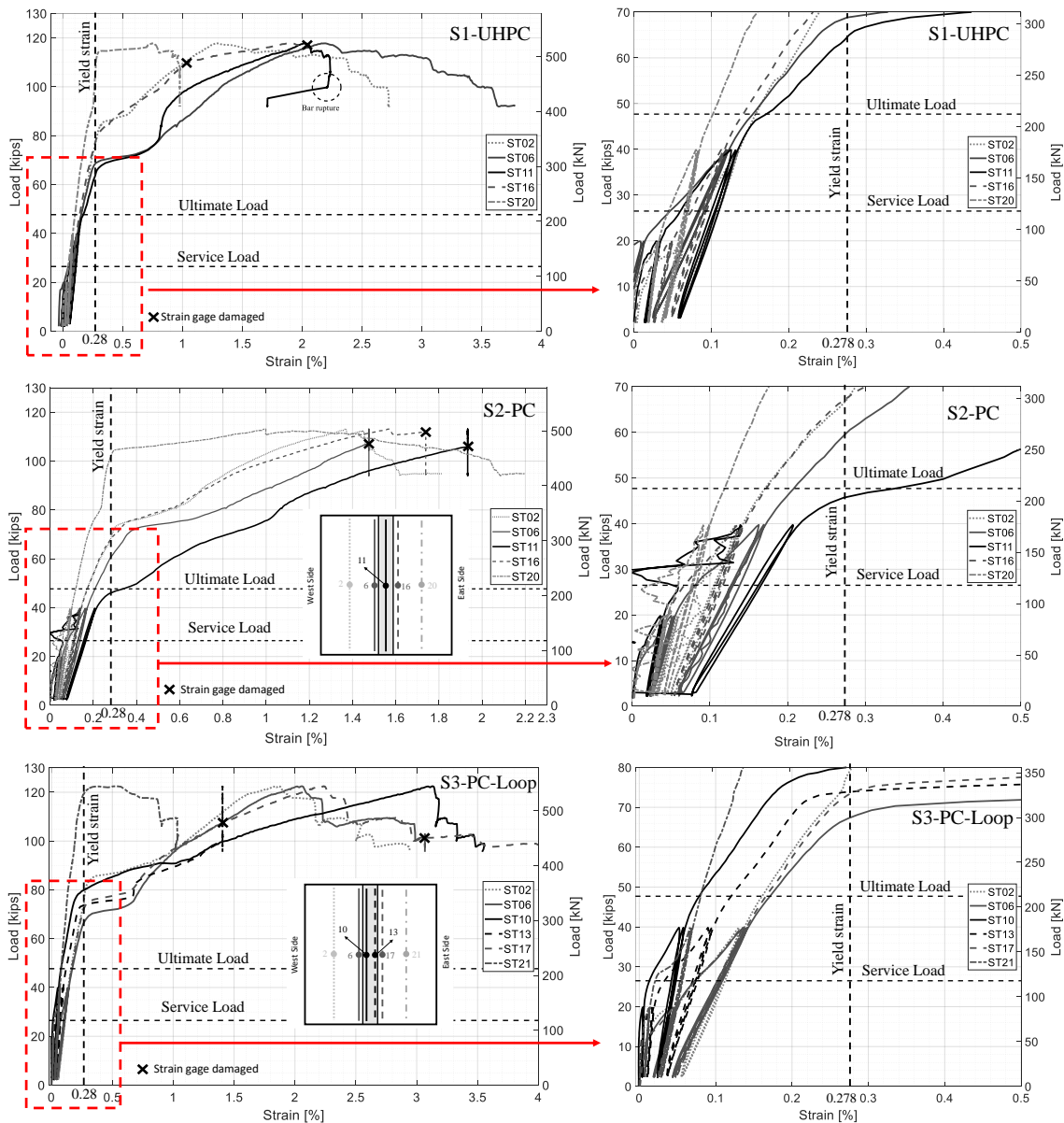


**Figure 2-16** Force versus strain measured at the mid-span location of the bottom transverse reinforcement

*2.3.3.4 Peak Strain Values*

The strain gage readings of the top and bottom transverse reinforcement at peak load are reported in the final report of this research project [37]. These strain values may serve as a reference for verification purposes of any further finite element or numerical studies that could be conducted in the future.

### 2.3.3.5 *Longitudinal Reinforcement Strains*

While Figure 2.16 focused on strains in bottom transverse reinforcement, the load versus strain readings of selected top longitudinal reinforcement at mid-span location is shown in Figure 2.17 for completeness. It can be seen that most of the strain values are typically below the measured yield strain of the reinforcement. However, the strain values of specimen S1-UHPC exceeded the yield limit and were extensively higher than the reported values in the other two specimens. The reason for this increase was probably due to the interface de-bonding that happened between the UHPC joint and the east side of the slab after reaching the peak load. It can also be seen that the recorded strain values of inside and outside the field joint were almost identical. This could be interpreted that no longitudinal rebar slippage took place up to the peak loads.

The strain values of specimen S3-PC-Loop were slightly less than that of specimen S2-PC due to the denser reinforcement distribution used in specimen S3-PC-Loop, i.e. #4@7" (#13@17.8 cm) instead of #5@10" (#16@25.4 cm) or #4@15" (#13@38.1 cm), and the continuity of the force transfer associated with using the loop splice. Hence, better load distribution is achieved by specimen S3-PC-Loop. The measured strain values of the longitudinal rebars inside and outside the joint at the ultimate and service loads were typically far below the yield strains. This could be informed that the demand in the field joints within the AASHTO design load limits does not even need the full development length of the rebars inside the joints. Hence, the lap splice length of the reinforcement that transversely connects two precast decks slabs does not need to be dominated by the required development length of the rebars inside the field joint.

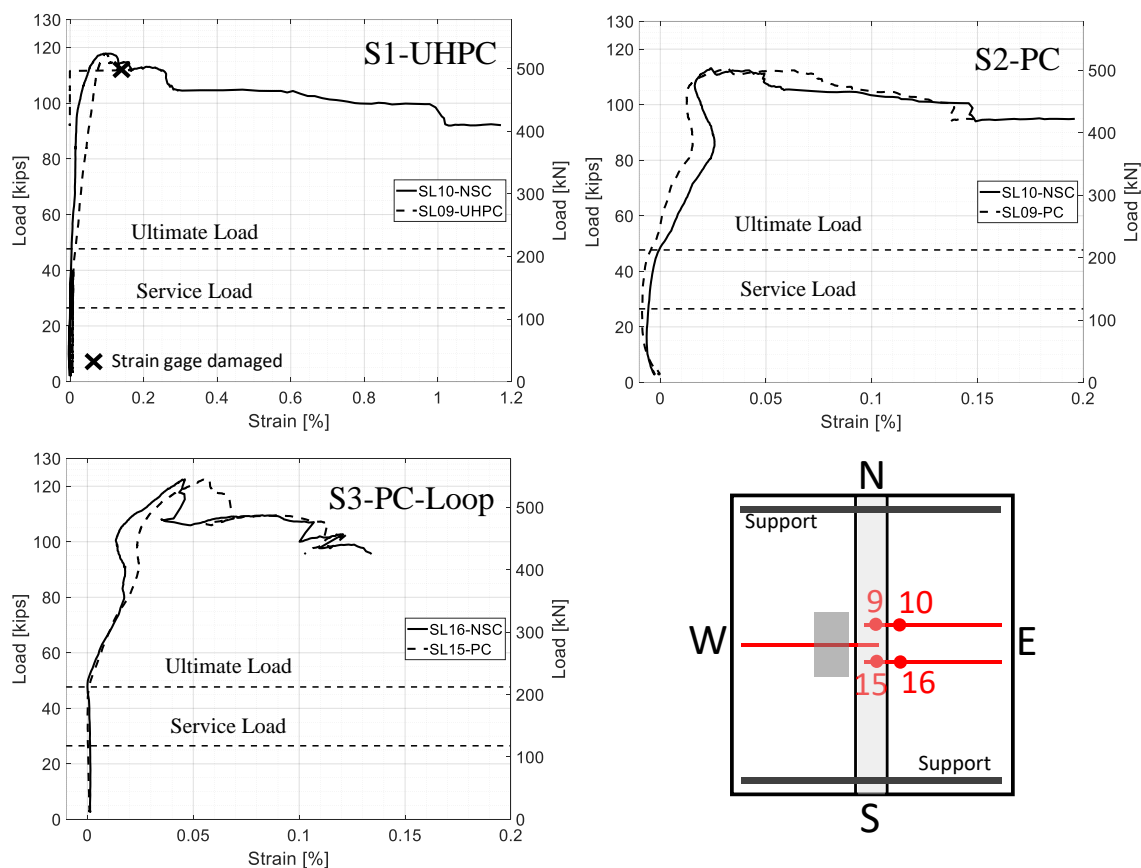


**Figure 2-17** Load versus strain measured at the middle top longitudinal rebars for all three specimens

### 2.3.4 Interface Opening

The lateral or horizontal interface opening width at the bottom face of the slab between the field connection and the precast parts was monitored through the test using six LVDTs. The interface opening width at service and ultimate loads for specimens S1-UHPC and S2-PC are reported in Table 2.5. The measurements from the LVDTs are discussed here to assess the bond performance between the field joint and the precast parts, and to compare the crack width with that of the maximum allowable limits specified in the AASHTO LRFD Article 5.6.7 [30]. The AASHTO LRFD specifies a maximum spacing between the rebars to control the flexural cracks. These maximum spacing limits were determined based on the maximum allowable crack width of 0.017 in (0.43 mm) for “class 1” exposure and 0.013 in (0.33 mm) for “class 2” exposure. The “class 2” exposure is typically used for situations in which the concrete is subjected to severe corrosion conditions. It can be seen from the table that interface opening at all different locations was less than the 0.013 in



(0.33 mm) limit except for one value which is explained in the following paragraph. The table also shows that the values of the crack opening at the west side are bigger than that of the east side and especially in the middle of the specimen where the maximum load is applied.

**Table 2-4** Interface opening width of specimens S1-UHPC and S2-PC at service and ultimate loads

LVDT Location (see Figure 5)	S1-UHPC				S2-PC			
	Service Load		Ultimate Load		Service Load		Ultimate Load	
	in ( $\times 10^{-3}$ )	mm	in ( $\times 10^{-3}$ )	mm	in ( $\times 10^{-3}$ )	mm	in ( $\times 10^{-3}$ )	mm
NW	2.8	0.071	6.2	0.157	1.0	0.025	12.5	0.317
NE	2.8	0.071	3.9	0.099	2.6	0.066	7.4	0.188
W	5.3	0.134	9.3	0.236	3.5	0.089	28.0	0.711
E	3.6	0.091	5.6	0.142	2.5	0.063	4.2	0.106
SW	6.3	0.160	10.4	0.264	5.3	0.134	1.2	0.030
SE	4.0	0.101	8.0	0.203	1.1	0.028	6.5	0.165

It was observed that specimen S1-UHPC reached the maximum allowable crack assuming a “class 2” exposure at approximately 60 kips (266.9 kN) of vertical load which is almost 1.25 and 2.25 times the specified AASHTO ultimate and service loads, respectively. This can confirm that the interface bond between the UHPC and the precast segments satisfied the design requirements and the code allowable limits. For S2-PC, it was observed that the crack width at the west side in mid-span is significantly higher than anywhere else along the joint. This could be attributed to the fact that the mid-span zone is subjected to the maximum applied load and maximum vertical deflection. Furthermore, the measurements of LVDT-W were significantly affected by the flexural cracks at the bottom of the specimen as they happened to be mounted over one of the wide flexural cracks that ran parallel to the joint in the transverse direction. The interface bonding for S2-PC was also investigated through the other LVDTs along the joint, i.e. LVDT-NW for instance. It was observed that the interface crack opening reached the maximum allowable crack assuming a “class 2” exposure at approximately 48 kips (213.5 kN) of vertical load which is less than

the UHPC case but still slightly higher than the ultimate load of the slab systems with PMMA-PC field joints. This observation, similar to UHPC, confirms that the interface bond between the PMMA-PC and the precast deck panels satisfied the design requirements and the code allowable limits.

### ***2.3.5 Comparative PC and UHPC application cost***

As mentioned earlier the material cost of the PMMA-PC is equal to half the cost of the commercial products of the UHPC. While the overall cost of the PMMA-PC including the mixing, placing, and finishing of the material is expected to be cheaper than the UHPC because of many reasons such as the ease of mixing and placing using the conventional mixers, less mixing time, and the speed of finishing using the traditional ways to maintain acceptable surface. Moreover, the PMMA-PC does not require any special treatment or curing regimes, unlike the UHPC that may require special heat curing in cold weather. A previous study by Mantawy et al. [29] has included a detailed design example and cost analysis of a practical precast bridge deck with PMMA-PC and UHPC field joints. The study considered the cost of one cubic yard of the PMMA-PC and UHPC per factory directions is \$2,000 and \$4,000, respectively. The study concluded that using the PMMA-PC instead of the commercial UHPC in the bridge deck field joints will ensure direct and indirect cost savings.

To provide more insight into the cost of applying PC and UHPC, the Caltrans Contract Cost Database [39] was checked for two recent projects that used PC and UHPC but for different applications. The average overall cost of two recently awarded bids for using polymer concrete for overlays and UHPC for deck joints were found to be \$2,790 and \$18,290 per cubic yard, respectively. This is not a direct comparison since the UHPC cost include some labor and material furnishing costs as well as quality control. However, it gives an idea about the higher cost of UHPC applications that is attributed to higher material cost in addition to the extra costs UHPC vendors charge for material mixing, furnishing, and quality control.

## 2.4 Concluding Remarks

This paper presents the structural performance of precast full-depth bridge deck panels connected using UHPC and PMMA-PC transverse field joints. Three simply-supported full-scale specimens were tested under vertical loading on one side of the joint at mid-span. The first two specimens considered transverse connection with diamond shear key shape and a non-contact straight lap splice of 5 inches (12.7 cm); a detail that has been demonstrated to properly transfer the flexure and shear stresses imparted through field joints and has been already implemented in recent ABC projects. For the third specimen, a new detail was proposed for the transverse connection with a modified diamond shear key shape, to eliminate the need for formwork erection, and a loop splice of 4.5 inches (11.4 cm) for using PMMA-PC for the field joint. The following observations and concluding remarks can be drawn from this comprehensive experimental study:

- Overall, the structural performance of full-depth precast deck systems with PMMA-PC field joints for transverse connections is demonstrated to be a viable alternative for ABC. The PMMA-PC field joints result in a very comparable behavior to the currently accepted practice of UHPC field joints in terms of service performance as well as load and deflection capacities.
- Both UHPC and PMMA-PC transverse field connections adequately satisfy the service and ultimate load requirements specified in the AASHTO LRFD, where deck systems remain elastic without any major flexural or interface cracking in the joint or any rebar slippage.
- No flexural cracks were observed in the UHPC or the PMMA-PC joints up to the AASHTO LRFD ultimate load level, which is attributed to the higher tensile properties of both used field joint materials compared to high strength grouts or conventional concrete.
- The initial stiffness of the deck system with UHPC joint was found to be higher than that of the system with PMMA-PC joint, which is attributed to the higher mechanical properties, mainly modulus of elasticity, of UHPC. However, the slightly lower stiffness from PC joints did not lead to any excessive deflections or deficiency in meeting code requirements,
- The proposed PMMA-PC field joint with a new shear key shape and shorter loop splice length was successfully validated as another viable alternative. This detail can provide

- more strength and ductility in addition to better load distribution across the precast panels than UHPC or PMMA-PC joints with straight lap splice. This could be a result of using a smaller bar size but denser reinforcement distribution inside the joint when compared to non-contact lap splices.
- Both UHPC and PMMA-PC systems showed adequate load distribution capabilities all the way through failure without any shear failure or significant interface debonding. However, the UHPC deck system exhibited two localized main cracks as opposed to several and multiple cracks in the PMMA-PC deck system at failure.

### **Acknowledgment**

This study is funded by the US DOT through the ABC-UTC (2016 cycle) headed at Florida International University. The authors would like to thank Transpo Industries for the T-17 polymer concrete material donation and Ductal® for the UHPC material donation. The authors also thank the laboratory staff at the Earthquake Engineering Laboratory at the University of Nevada, Reno for their assistance with the testing and experimental program.

### **References**

- [1] Graybeal, B. Behavior of Field-Cast Ultra-High Performance Concrete Bridge Deck Connections Under Cyclic and Static Structural Loading; Report No. FHWA-HRT-11-023; Federal Highway Administration, McLean, VA, 2010.
- [2] Hartwell, D. R. "Laboratory testing of Ultra High Performance Concrete deck joints for use in accelerated bridge construction" (2011). Graduate Theses and Dissertations. 10420.
- [3] Hwang H., Park S. Y. "A study on the flexural behavior of lap-spliced cast-in-place joints under static loading in ultra-high performance concrete bridge deck slabs" (2014). Canadian Journal of Civil Engineering, 41:615-623.
- [4] Vitek, J.L., Kolisko, J., Citek, D., Rehacek S., Coufal R. "UHPC connection of precast bridge deck" (2016). First International Interactive Symposium on UHPC.

- [5] Zhu P., Ma Z. J., Cao Q., French C. E. “Fatigue evaluation of transverse U-bar joint details for accelerated bridge construction” (2012). *Journal of Bridge Engineering*. Volume 17, No. 2, pp. 191-200
- [6] Li L., Jiang Z. “Flexural behavior and strut-and-tie model of joints with headed bar details connecting precast members” (2016). *Perspectives in Science*. Volume 7, pp. 253-260, ISSN 2213-0209.
- [7] Leboeuf S. V., Charron J. P., Massicotte B. “Design and behavior of UHPFRC field-cast transverse connections between precast bridge deck elements” (2017). *Journal of Bridge Engineering*.
- [8] National Cooperative Highway Research Program. *Cast-in-Place Concrete Connections for Precast Deck Systems*. NCHRP Report 10-71. Transportation Research Board, Washington DC, 2011.
- [9] Perry, V., Krisciunas, R., and Stofko, B. (2012). “Mackenzie River Twin Bridges—The largest field-cast UHPC connections project in North America.” *Proc., PCI—National Bridge Conf., Precast/Prestressed Concrete Institute, Chicago*.
- [10] Sritharan S., Aaleti S., Garder J., Bierwagen D., Abu-Hawash A. “Use of ultra-high performance concrete in bridge design” (2012).
- [11] ASTM. (2017). *Standard practice for fabricating and testing specimens of ultra-high performance concrete*. ASTM C1856/C1586-17.
- [12] Aboukifa, M., Moustafa, M. A., & Itani, A. M. (2020). *Comparative Structural Response of UHPC and Normal Strength Concrete Columns under Combined Axial and Lateral Cyclic Loading*. ACI SP 341. 71-96.
- [13] Aboukifa, M., & Moustafa, M. A. (2021). *Experimental seismic behavior of ultra-high performance concrete columns with high strength steel reinforcement*. *Engineering Structures*, 232, 111885.
- [14] Naeimi, N., & Moustafa, M. A. (2021). *Compressive behavior and stress–strain relationships of confined and unconfined UHPC*. *Construction and Building Materials*, 272, 121844.

- [15] Abokifa, M., & Moustafa, M. A. (2021). Full-scale testing of non-proprietary ultra-high performance concrete for deck bulb tee longitudinal field joints. *Engineering Structures*, 243, 112696.
- [16] Abokifa, M., & Moustafa, M. A. (2021). Mechanical Characterization and Material Variability Effects of Emerging Non Proprietary UHPC Mixes for Accelerated Bridge Construction Field Joints. *Construction and Building Materials*. (Under review)
- [17] Aboukifa, M., Moustafa, M. A., & Saiidi, M. S. (2021). Seismic response of precast bridge columns with composite non-proprietary UHPC filled ducts ABC connections. *Composite Structures*, 274, 114376.
- [18] Aboukifa, M., Moustafa, M. A., & Saiidi, M. S. (2020). SEISMIC RESPONSE OF PRECAST COLUMNS WITH NON-PROPRIETARY UHPC-FILLED DUCTS ABC CONNECTIONS.
- [19] ACI (American Concrete Institute). *Guide for the Use of Polymers in Concrete*; ACI 548.1R-09; ACI: Farmington Hills, MI, USA, 2009.
- [20] Ribeiro M., Tavares C., Ferreira A. “Chemical resistance of epoxy and polyester polymer concrete to acids and salts” (2011). *Journal of Polymer Engineering*, Volume 22, Issue 1, pp. 27-44.
- [21] Reis J.M.L., Ferreira A.J.M. “Fracture behavior of glass fiber reinforced polymer concrete” (2003). *Polymer Testing*, Volume 22, Issue 2, pp. 149-153, ISSN 0142-9418.
- [22] Fowler D. W., Paul D. R. “Polymer concrete for repair of bridge decks” (1978). *Proceedings, 2nd International Congress on Polymers in Concrete*, University of Texas, Austin, pp. 337-350.
- [23] Fontana J. J., Webster R., Kukacka L. E. “Rapid patching of deteriorated concrete using polymer concrete” (1978). *Proceedings, 2<sup>nd</sup> International Congress on Polymers in Concrete*, University of Texas, Austin, pp. 105-119.
- [24] Fowler D. W., Meyer A. H., Paul D. R. “Implementation manual for polymer concrete repair” (1983). *Research Report No. 246-4F*, Center for Transportation Research, University of Texas, Arlington.

- [25] Kukacka L. E., Fontana J. “Polymer concrete patching materials” (1977). Implementation Package No. 77-11, Volume 1 and 3, Federal Highway Administration, Washington, DC.
- [26] Whitney, D.P.; Fowler, D.W. New applications for polymer overlays. *Adv. Mater. Res.* 2015, 1129, 277–282.
- [27] Dinitz A. M., Ferri R. “Polymer Concrete (MMA) for Bridge Rehabilitation Applications” (1985). ACI SP-89-8, *Polymer Concrete: Uses, Materials, and Properties*, pp. 141-159.
- [28] Hsu M., Fowler D. W. “Creep and fatigue of polymer concrete” (1985). ACI, SP 89-17, pp. 323-343.
- [29] Mantawy, I.; Chennareddy, R.; Genedy, M.; Taha, M.R. Polymer Concrete for Bridge Deck Closure Joints in Accelerated Bridge Construction. *Infrastructures* 2019, 4, 31.
- [30] AASHTO (American Association of State Highway and Transportation Officials). *AAHSTO LRFD Bridge Design Specifications*, 7th ed.; American Association of State Highway and Transportation Officials: Washington, DC, USA, 2014.
- [31] ACI Committee. (2008). Building code requirements for structural concrete (ACI 318-08) and commentary. American Concrete Institute.
- [32] Aboukifa, M., Moustafa, M. A., Itani, A. M., & Naeimi, N. (2019). Durable UHPC Columns with High-Strength Steel (No. ABC-UTC-2013-C3-UNR02-Final). Accelerated Bridge Construction University Transportation Center (ABC-UTC).
- [33] ASTM C39. Standard Test Method for Compressive Strength of Cylindrical Concrete Specimens. American Society for Testing and Materials Standard Practice C39, Philadelphia, PA, 2001.
- [34] ASTM C469. Standard Test Method for Static Modulus of Elasticity and Poisson’s Ratio of Concrete in Compression. American Society for Testing and Materials Standard Practice C469, Philadelphia, PA, 2002.

- [35] ASTM C579-18. Standard Test Methods for Compressive Strength of Chemical-Resistant Mortars, Grouts, Monolithic Surfacing, and Polymer Concretes. West Conshohocken, PA; ASTM International, 2018.
- [36] Abokifa, M., & Moustafa, M. A. (2021). Experimental behavior of poly methyl methacrylate polymer concrete for bridge deck bulb tee girders longitudinal field joints. *Construction and Building Materials*, 270, 121840.
- [37] Abokifa, M., Moustafa, M. A., & Itani, A. M. (2021). More Choices for Connecting Prefabricated Bridge Deck Elements (No. ABC-UTC-2016-C1-UNR03-Final). Accelerated Bridge Construction University Transportation Center (ABC-UTC).
- [38] Graybeal, B. (2010). Field-cast UHPC connections for modular bridge deck elements (No. FHWA-HRT-11-022).  
California Department of Transportation (Caltrans). Caltrans Contract Cost Data, 2014. <https://sv08data.dot.ca.gov/contractcost/>. Accessed May 1, 2021.



### 3 EXPERIMENTAL BEHAVIOR OF POLY METHYL METHACRYLATE POLYMER CONCRETE FOR BRIDGE DECK BULB TEE GIRDERS LONGITUDINAL FIELD JOINTS

*This chapter is a standalone paper that has been published in the journal of Construction and Building Materials*

#### **Abstract**

As an emerging practice of accelerated bridge construction (ABC), top flanges of precast deck bulb tee girders (DBTs) can be longitudinally connected on-site using ultra-high performance concrete (UHPC) field joints. Robust UHPC mixes can be proprietary, expensive and might need special expertise to work with it. Thus, exploring viability of alternative materials for such field joints could be beneficial. Poly Methyl Methacrylate Polymer concrete (PMMA-PC) is another construction material with superior mechanical properties that have been used for overlays and can provide a potential alternative to UHPC for field joints. The objective of this study is to investigate the structural performance of PMMA-PC for DBTs longitudinal field joints and compare it to UHPC. An experimental investigation was conducted to test two full-scale specimens, with representative DBTs flanges/slabs, under vertical loading at the University of Nevada, Reno. The two specimens were identical except for field joint material (UHPC versus PMMA-PC). The structural response was evaluated for connection performance under the AASHTO service and ultimate loads, peak strength, damage progression and mode of failure, and local steel reinforcement strains. The results demonstrated that PMMA-PC can be successfully used for longitudinal field joints of the DBTs with comparable performance to UHPC field joints.

#### **3.1 Introduction**

Bridge decks are traditionally constructed using cast-in-place (CIP) normal strength concrete to create a monolithic deck slab that might be divided only using expansion joints. However, after many years of service, these CIP systems showed lack of durability compared to the emerging precast deck systems. Bridge decks are susceptible to rapid

degradation due to many factors such as structural loading and environmental conditions, the use of deicing chemicals in cold weather regions, and wearing due to high volumes of traffic, etc. Introduction of the precast systems in the construction of bridge decks has improved the quality and durability of bridge decks due to using of better materials and quality control used for precast elements. Nonetheless, the precast bridge decks has offered reduced construction time and cost savings, which makes it one of the most popular applications for accelerated bridge construction (ABC). Hence, many departments of transportation (DOTs) in different states or nations have implemented precast systems in both new construction or replacement of obsolete or deteriorated bridge superstructures with minimal traffic impact.

Deck bulb-tee (DBT) girders is one of the attractive superstructure systems that have been implemented by many state DOTs in the United States such as Washington and New York DOTs over the last few decades. The DBT girders provide fast erection for the bridge superstructure, less on-site activities, less traffic disruption, and more feasible option for bridge construction in rural areas. The I-shaped DBT girders have wide top flanges that establish the bridge deck. Such top flanges are connected together in the longitudinal direction to form a continuous deck surface as illustrated in Figure 3.1.

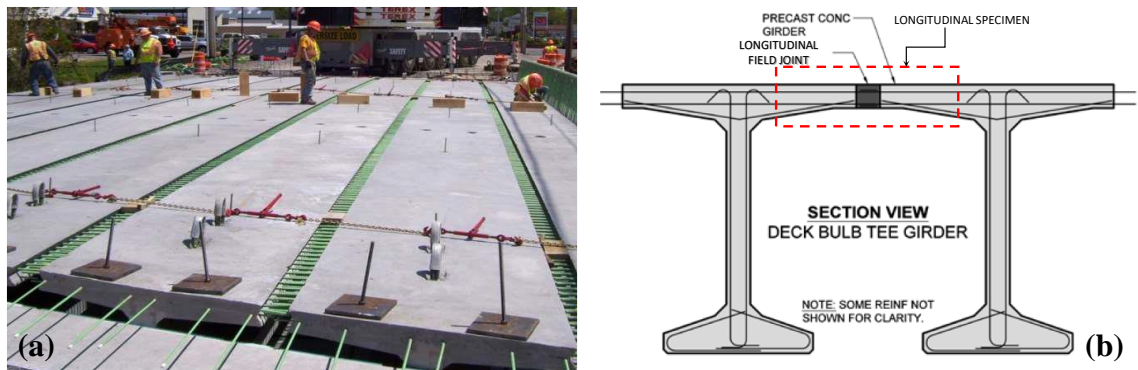


**Figure 3-1** Overview of precast DBT girders bridge deck system: (a) Construction of a DBT girders bridge of Route 31 Bridge in Lyons, New York (photo courtesy of NYSDOT [1]), and (b) schematic of field joints and test specimen adopted in this study (photo courtesy Peruchini et al. [2]).

Figure 3.1a shows an overall view of the DBT girders and the longitudinal field joints between the top flanges [1]. The study presented in this paper focuses on longitudinal joints between the top flanges of two adjacent DBTs. A schematic view of how the adopted test

specimens relate to the bridge superstructure is also illustrated in Figure 3.1b [2]. DBT girders are fabricated in a controlled environment at the fabrication facility and then shipped to the bridge location where they can be quickly assembled to form the bridge superstructure. However, this system requires on-site pouring of a longitudinal field joints between the top flanges of the girders to provide continuous load distribution along the transverse direction of the bridge. The longitudinal field joints of the DBTs have been traditionally constructed using a combination of welded clips and grouted joints. However, these connections showed lack of durability due to observance of interface cracking along the joint that may lead to leakage [3]. Therefore, using conventional construction techniques and materials for such joints can result in a relatively less durable connections when compared to the precast components or joined parts. Accordingly, many research studies focused on identifying and implementing durable materials for such joints which feature high early strength and high bond strength. The implementation of durable closure pour with superior mechanical properties in the precast deck field joints can simplify the connection details, enhance the connection durability, narrow down the width of the connections, save the time needed for formwork erection, and provide simpler reinforcement details inside the connections without requiring any post-tensioning.

For the past two decades, ultra-high performance concrete (UHPC) has become a popular solution for bridge deck field joints. UHPC is an advanced cementitious material with superior mechanical properties and durability resulting from the use of steel fibers (typically 2% of volume) and carefully packed materials. The increased implementation of UHPC field joints has been supported by large number of research studies that focused mostly on experimental testing and demonstration of the use of UHPC for various field joint types and configurations. Examples include the work done by Graybeal [4], Peruchini et al. [2], Hartwell et al. [5], Hwang and Park [6], and Coufal et al. [7], among others. Earlier research studies considered more common materials and focused on investigating the behavior of field joints with advanced grouts, high performance concrete (HPC), and HPC with fiber reinforcement [8-10]. However, many of these research efforts demonstrated the need for reinforcement post-tensioning inside the joint, or using mechanical splices and/or headed rebars, or adding of rebar confinement inside the joint,

or increase joint width to maintain the desired performance of the deck field joints. Many of these solutions are not viable for ABC where durable systems with less erection time, cost, and labor are desired.

In addition to exploring joint materials, other research studies considered different parameters of the field joints such as connections types, shear key shape, details of reinforcement, types of reinforcement, and tested the various connections details under different loading schemes. As a result of the large number of studies in this area, several reports were published through the national cooperative highway research program (NCHRP) to summarize and synthesize the state-of-the-art for prefabricated concrete components and deck connections and detailing. For example, NCHRP report 10-71 [11] focused on static and fatigue testing of both transverse and longitudinal field connections between precast concrete deck panels. Consequently, the synthesized practical and research projects converged on typical UHPC field joints that are 15 to 20 cm wide without post-tensioning and use simplified reinforcement configuration inside the joint with diamond shaped shear key type. This typical connection has been demonstrated to develop sufficient shear and bending capacities to link the precast deck components together [4, 12, 13]. Most of the aforementioned research efforts, in addition to field site investigations of actual bridge decks with UHPC field joints, showed that UHPC has acceptable performance and durability inside the field joints. However, some state DOTs found that the implementation of UHPC in such joints might be challenging because of bidding issues, since robust UHPC mixes are expensive, proprietary, and limited source, and also it requires special expertise to mix and place due to steel fibers. UHPC also exhibits high early shrinkage that requires more time and additional labor costs to have acceptable surface finish if no overlay is planned to be used.

For a more feasible solution and to avoid bidding issues, many state DOTs started to develop their own non-proprietary UHPC mixes with local and domestically available materials for the field joints closure materials [3]. A recent study sponsored by Washington DOT focused on experimental testing of a new developed non-proprietary UHPC in the longitudinal field joints of DBT girders [2]. This study tested a 0.6 m wide strips of the

deck representing the actual upper flanges of DBT girders under static bending. The study showed that there is no cracking happened to the body of the UHPC joint, however a significant cracking was observed at the cold joint interface between the UHPC and the conventional concrete part. This type of damage makes this system less desirable because the interface cracks usually allow the ingress of moisture and deicing chemicals that may lead to rapid corrosion of the reinforcement and deterioration of the bridge deck. There are many practical solutions that may provide enhancement to the interface bond between the field joint and the precast members such as using a female-female shear key shape and the use of surface preparation such as exposed aggregate. At the end, UHPC field joints are associated with many challenges, which can be mostly tackled, and the implications of these challenges may also be deemed insignificant when compared to the gained benefits from the UHPC unparalleled superior mechanical properties. Nonetheless, identifying other alternative materials that provide acceptable solutions, i.e. maintaining simpler reinforcement configurations and avoid post-tensioning for ABC and DBT field joints could be still very beneficial.

Poly Methyl Methacrylate (PMMA) polymer concrete (PC) is another advanced construction material that emerged over the past few decades and can provide a potential alternative to UHPC for bridge deck joints. PC features high bond strength, high early strength, high shear strength, adequate flowability, and high durability with respect to cycles of freezing and thawing [14, 15]. Furthermore, PC is corrosion resistant, fast curing, has very low permeability and superior cracking resistance [14-16]. The superior properties of PC make it a very attractive material for use in many industries and various structural engineering applications for more than four decades such as concrete patching and bridge repairs [17-20]. PC is also a popular material for use in bridge deck overlays [21]. Among the different types of PC, the PMMA-PC has been used for decades as bridge deck overlay and fast-permanent repair for runways and taxiways in many airports around the nation [22]. These specific applications have been promoted because of the enhanced fatigue strength of PMMA-PC relative to conventional Portland cement concrete [23]. A recent study [24] characterized the mechanical properties of the PMMA-PC to explore its future applicability for bridge field joints. That study focused on the development length and lap

splice length and demonstrated that the PMMA-PC could provide shorter development and lap splice lengths than typical UHPC with 2% steel fibers. The latter research among other applications of PC motivated this study to further investigate and demonstrate the structural behavior of PMMA-PC for DBT girders longitudinal field joints.

Based on the above summary, no former comprehensive work considered testing and validating other alternative emerging and advanced materials beyond UHPC for ABC connections and field joints. While PMMA-PC seems to be a viable candidate, none of the previous efforts considered large-scale testing and demonstration of using PMMA-PC for DBTs longitudinal field joints. The overall goal of this study is to investigate and validate the structural performance of PMMA-PC longitudinal field joints as compared to UHPC. There are two main objectives for this study. The first objective is to briefly characterize main mechanical properties of PMMA-PC to provide a better understanding of the material behavior that help interpret the large-scale application. The provided material characterization can also be used for future analytical studies and finite element modeling the extend the results of the test specimens presented herein. Thus, the second objective is to conduct full-scale experimental testing of deck assemblies of representative DBT girder flanges (slabs) with PMMA-PC and UHPC longitudinal field joints under static vertical loading. Two identical specimens that varied only in the field joint material, i.e. UHPC versus PMMA-PC, were tested and presented here. The paper comprises several sections that present the mechanical properties of PMMA-PC and details of the experimental program and tests results and discussions.

### **3.2 PMMA-PC Mechanical Properties**

PMMA-PC has physical and mechanical material properties that are arguably comparable to that of the high strength concrete and a gray color similar to cementitious concretes. However, PMMA-PC is not a cementitious material. PMMA-PC is created by mixing Methyl Methacrylate resin with a Benzoyl Peroxide initiator in addition to optional graded aggregate of 9.5 mm  $\times$  4.8 mm nominal maximum size. Adding of aggregate to the mix is only recommended for applications in which the thickness of the patch exceeds about 4 cm and a concrete should be used rather than a mortar. Examples of these applications are

bridge full-depth deck panels and DBT field joints. PMMA-PC without aggregate can be used for thin patches such as bridge deck overlays but thicker and larger patches should be mixed with the addition of aggregate. The utilized PMMA-PC has a specified compressive strength of 55-62 MPa after 24 hours, and specified tensile strength of 6.9-8.3 MPa. PMMA-PC is designed for use on new construction and rehabilitation of bridge decks, expansion joints, bearing pads, airport runways and other concrete structures due its fast setting, high bond strength and early strength. Unlike UHPC, different PMMA-PC products have been commonly used for decades around the nation as they are locally available and can be distributed to any place in North America for instance. Commercial PMMA-PC products are typically provided in pre-packed bags and pails. This section provides the mixing procedure and the basic mechanical properties of PMMA-PC under compression, flexure and direct tension. The test results reported in this section can be used for guidance and input for future finite element modeling as mentioned before in the study objectives.

### 3.2.1 Material Mixing

Commercial PMMA-PC is commonly packed as two different components. For PMMA-PC used in this study, the first is powder components packed in 22.7 kg bags and consists of a proprietary blend of sand, inert fillers, polymers, and initiators. The second component is liquid admixture that is packed in 3.8 liters pails and consists of a solvent free 100% reactive, low viscosity methyl methacrylate. The PMMA-PC is mixed using conventional rotary drum mixer. Figure 3.2 shows the two components of PMMA-PC and illustrates the mixing process. Moreover, Table 3.1 provides the mix components and quantities per cubic meter of the PMMA-PC.

**Table 3-1** PMMA-PC mixing proportions per cubic meter.

Ingredients	kg/m <sup>3</sup>	Percentage per weight (%)
Powder component	3,153	61.95
Liquid component	361	7.10
Aggregate (9.5 × 4.8) mm	1,577	30.95

The mixing procedure of PMMA-PC is divided into three main steps. First, PMMA-PC liquid component is added to the mixer. Next, PMMA-PC powder bags are added gradually over the course of half minute and then left to mix with the liquid for about three minutes until uniform consistency is reached to ensure appropriate PC paste. Finally, coarse aggregate, if needed, can be added gradually to the mix over the course of half minute and then left to mix for another one minute to ensure uniform distribution of the aggregate inside the concrete. Thus, the total mixing time of a PMMA-PC batch is about 5-6 minutes, which is compared to 25-30 minutes in case of UHPC with 2% steel fibers. It is worth noting that one of the advantages of the PMMC-PC, compared to UHPC, is the wide application temperature range  $-10$  to  $37.8$  °C. Special precautions are needed for mixing UHPC in extreme cold or hot weathers. UHPC needs more setting time in cold weathers and requires additional heat curing to speed up the strength gaining. In case of hot weather, the UHPC requires replacement of the mixing water with ice, which could limit the use of the UHPC in some cases. PC is a flowable material that does not need a vibrator for compaction, especially when coarse aggregate is used to avoid segregation. PC also does not require any special considerations for surface finishing beyond typical procedure for conventional concrete.



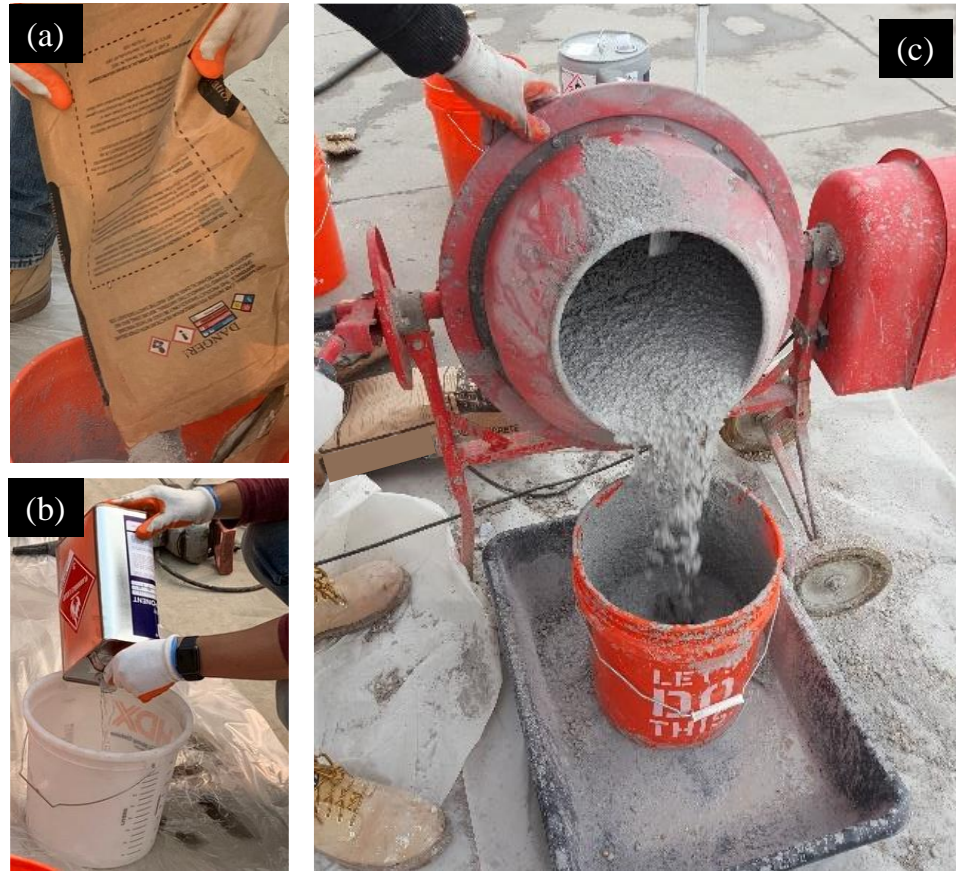


**Figure 3-2** Different components of commercial PMMA-PC used in this study: (a) powder bags, (b) liquid component pails, and (c) mixing process

### 3.2.2 Compressive Strength

To characterize the compressive strength of the PMMA-PC used in the experimental campaign,  $7.6 \times 15.2$  cm cylinders were prepared from the different PMMA-PC batches that were used inside the test specimens' longitudinal field joints. Prior to testing, both ends of PMMA-PC cylinders were smoothly grinded using a manually operated grinding machine to ensure a smooth and flat surface at both ends. A compression machine with maximum compression capacity of 2224 kN was used to test the PMMA-PC cylinders according to the ASTM standards C469 [25]. The cylinders were loaded first in two cycles up to approximately 40% of expected compressive strength. Then, the test cylinders were loaded to failure at a loading rate of approximately 1.11 kN/sec. The main aim of using this loading scheme was to get the full stress-strain curve and determine the static modulus of elasticity. The obtained stress-strain curve of the PMMA-PC cylinders at the day of testing of the

deck assembly specimen, i.e. at age of 70 days, is shown in Figure 3.3. The modulus of elasticity of the PMMA-PC was calculated based on the stress and strain values that correspond to 10% and 30% of the ultimate compressive strength. The average PMMA-PC elastic modulus was determined to be approximately 19,305 MPa. It can be seen from Figure 3.3 that the PMMA-PC has ultimate strain capacity that can be as high as 0.016, which is larger than typical ultimate strain capacity of conventional concrete and UHPC. The PMMA-PC can also sustain large strains and axial deformation after reaching the peak load, i.e. favorable post-peak behavior compared to other concretes.

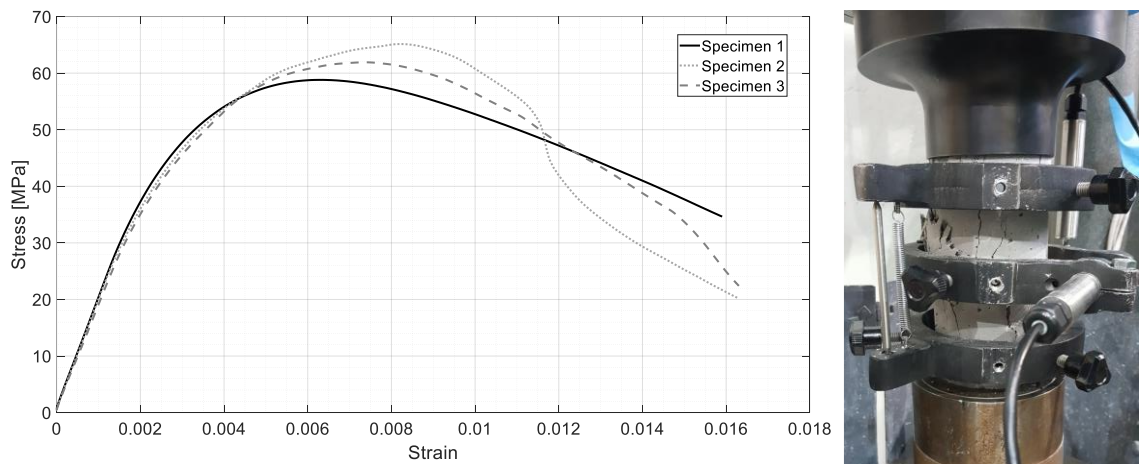


**Figure 3-3** Compressive stress-strain relationship of PMMA-PC cylinders (tested at 70 days)

### 3.2.3 Flexural Strength

For flexural strength and modulus of rupture characterization,  $7.6 \times 7.6 \times 30.5$  cm rectangular prisms were prepared from the PMMA-PC batches that were used inside the longitudinal field joint. A testing machine with maximum capacity of 250 kN was used to test the PMMA-PC prisms according to the ASTM standards C580 – method C [26]. The specimens were tested in flexure in a 3-point bending assembly with a vertical load applied at the middle of the specimen. The span between the two support points was 22.9 cm. The load was applied in the middle at a displacement rate 1.15 mm/min. The displacement rate was controlled by the speed of the machine cross head and was based on achieving a strain rate of 0.01 per minute at the top and bottom of the beam. The test specimens were loaded for one cycle till failure. The load and deflection relationships of the PMMA-PC specimens

at the same day of testing the bridge deck specimens are shown in Figure 3.4. It is noted that no dedicated displacement transducer was used to capture mid-span deflection of the prisms, as required by ASTM C580, because of the used setup limitation. Thus, the recorded displacements were based on the vertical movement of the machine cross head, and hence, are not representative of accurate specimen deflection.

The main purpose of the test was to get the flexural strength and determine the modulus of rupture of the PMMA-PC beams. Consequently, the accuracy of the measured displacements were not the main concern and they were measured and reported here for guidance only. The average flexural strength of the PMMA-PC test specimens at test day was determined to be 20 MPa. It can be implied from these tests that the flexural strength of PMMA-PC beams is higher than the conventional concrete and very comparable to UHPC. However, the failure of the PMMA-PC bending specimens was a brittle failure after the observance of the first crack, which is similar to conventional concrete but different from the steel fiber-enhanced UHPC behavior. With the assumption that there were no tension cracks happened before the failure of the specimens because of the linear relationship in Figure 3.4, the flexural elastic modulus of the PMMA-PC prisms is approximately equal the average between the tensile and compression elastic modulus reported in the previous and following sections. Hence, the average flexural elastic modulus is equal to 11,720 MPa. Therefore, the average flexural strain in which the PMMA-PC specimens were failed is equal to 0.17%.

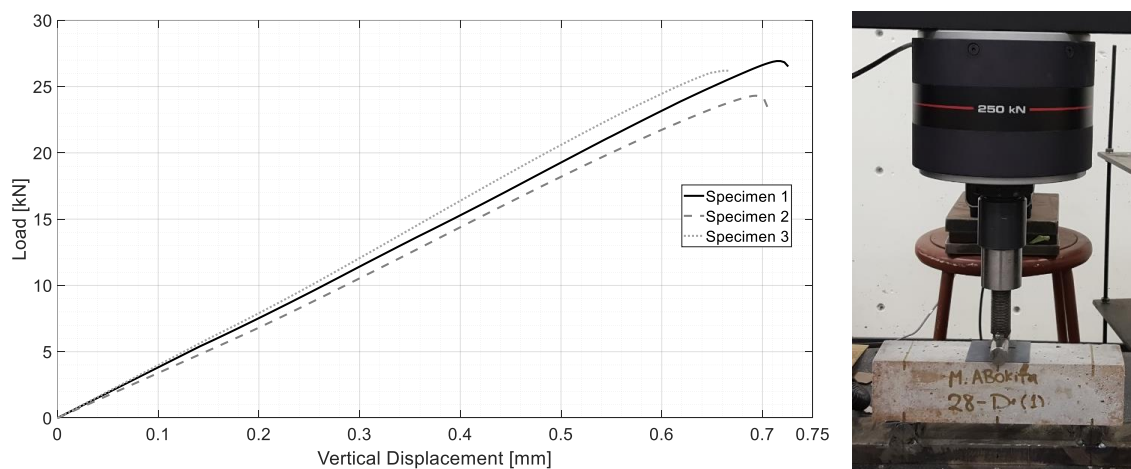


**Figure 3-4** Flexural load-deflection relationship of PMMA-PC beams at age of 70 days

### 3.2.4 *Direct Tension Strength*

The tension specimens had a dog-bone shape with a reduced section of a 2.5×2.5 cm cross-sectional dimensions at the middle of the specimen. Up to the time of the conducted material testing, there is no ASTM or similar standards for specimen preparation and direct tension testing of concrete materials. However, many studies were found in the literature focused on the direct tension testing of fiber reinforced concrete, and UHPC to study different fiber types and shapes, and variable amounts of fibers inside the mix [27-33]. The shape and dimensions of the tension specimens was proposed based on the best outcomes and recommendations reported in the literature. The selected length of the dog-bone specimen was 27.9 cm and wide parts of 3.8 cm at both ends to allow sufficient gripping area and to avoid any tension slippage. The tension specimens were cut by water jetting machine from a 1-inch thick PMMA-PC slab. The water jetting allowed for accurate specimen dimensions and better round edges. The testing machine with maximum capacity of 250 kN was also used to test the PMMA-PC dog bone specimens. A laser extensometer with two laser targets attached at the ends of the reduced section were used to measure the tensile strains and relate them to the corresponding tension stress calculated from the applied load at the machine load cell.

The tension load was applied through displacement control of the machine head with a speed of 0.00254 mm/sec, which is the rate selected based on the average values reported in literature. The gage length of the dog bone specimens was approximately 7.6 cm. The test specimens were loaded for one cycle till failure. The direct tensile stress-strain relationship of the PMMA-PC specimens at the same day of testing the bridge deck specimens (70 days age) are shown in Figure 3.5. The average tension strength of the PMMA-PC dog-bone specimens at test day is 4.7 MPa. It can be seen that the direct tensile strength of the PMMA-PC dog-bone specimens is almost double the typical conventional concrete values and slightly less than UHPC with 2% fiber. The failure of the PMMA-PC tension specimens was more likely a ductile failure as can be seen from Figure 3.5. The initiation of micro-cracking is expected to be approximately between 0.15% to 0.17% tensile strain as the tensile stress-strain curve started to soften with a noticeable decrease in stiffness.

Then, the PMMA-PC specimens had a sustained capacity with increasing tensile strains and good ductility until the failure happened between 0.35% to 0.45% ultimate tensile strain, which is important characteristic that need to be considered for PC modeling or analytical assessments.

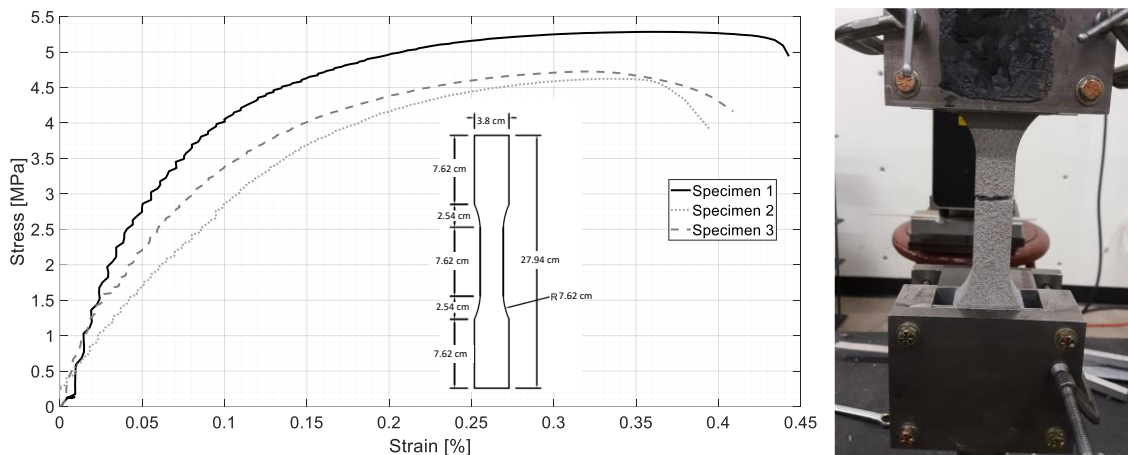


**Figure 3-5** Direct tension stress-strain relationship of PMMA-PC dog-bone specimens at age of 70 days

### 3.3 Experimental Program

This section provides the structural details of the test specimens, test setup and instrumentation plan, loading protocol, specimen fabrication, and other material properties.

#### 3.3.1 Specimens Design and Test Matrix

The experimental work presented in this paper is part of a major ongoing research project at the University of Nevada, Reno that aims at identifying and testing alternative materials for various ABC connections. The tests discussed here include two full-scale specimens that represent full-depth longitudinal field joints between two adjacent DBT girders. Both specimens were identical except for the field joint material, i.e. UHPC and PMMA-PC, which are designated as S1-UHPC and S2-PC, respectively. It is noted that not the full DBT girders were tested but only representative parts from the slabs as illustrated before in Figure 3.1. The design of the specimens was done according to the AASHTO LRFD Bridge Design Specification [34]. The design moments were determined based on the AASHTO Equivalent strip method. The moment values provided in this method takes into

account the largest values that could be experienced by the deck slabs with respect to different loading conditions. The thickness of the test specimens was determined based on the typical AASHTO/PCI standard DBTs top flange thickness, i.e. 15.24 cm [35].

Moreover, the design of the test specimens and the longitudinal field joints was done taking into account many practical considerations and previous research recommendations to speed up the construction process, enhance constructability, provide better structural performance, and increased durability of the field joints. (1) Top and bottom meshes of the DBT top flanges were spliced together inside the longitudinal field joints to provide continuity of moment and shear transfer across the transverse direction of the bridge. (2) Non-contact lap splice was used inside the joint. (3) The hypothetical DBT girders represented through the flanges/slabs were connected together through passive field joints without any reinforcement post-tensioning or welding of the reinforcement inside the joints. (4) Straight splices were used to provide simpler reinforcement details inside the joint. (5) Female-female diamond shaped shear key was used in this study given its previously demonstrated performance for transferring shear and bending and enhanced durability as compared to flat ends shear keys. (6) No protective coatings such as epoxy-coated reinforcement was used to maintain full bond and in turn, minimize the lap splice length and field joint width.

The test specimens had 2.54 cm bottom concrete cover and 5.08 cm top concrete cover that adequately satisfy the AASHTO code requirements for bridge decks with normal condition exposure in a non-corrosive environment. The deck slabs, i.e. DBT flanges, were designed based on class two exposure, which also controls the spacing between the bottom main reinforcement to avoid the positive flexural cracking under service limit state. For the test specimens, the transverse reinforcement was placed in the outer layers of the deck slabs to maximize the flexural capacity in the transverse direction and increase the demand in the joint. Grade 60 reinforcing steel as specified by ASTM A706 was used for all reinforcement components in this study. The precast panels that represents the top flanges of the DBT girders was constructed using normal strength concrete with 34.5 MPa specified compressive strength at 28 days.

In DBT girders, the moment distribution due to the vertical loading at the top flanges is negative moment at top of the girders and positive moment at the middle section in-between the adjacent girders. Hence, dimensions and boundary conditions of the test specimens were selected based on simulating the expected positive moment portion of the top DBT flanges only (see Figure 3.1 above). The effective span length of the test specimens was selected based on the expected distance between the flexural inflection points of the original deck slabs. Usually in the case of bridge decks, it is hard to determine the exact location of such bending inflection points because of the numerous loading conditions. Thus, the effective span of the test specimens was estimated based on dead loads for simplicity and was adjusted to be 1.83 m, which is approximated as two thirds of the DBT top flange width of 2.44 m. Since the effective span represents the positive flexural part of the slab and there is no negative moment in this part, the amount of negative reinforcement was taken as the same as the main positive reinforcement. The overall dimensions, reinforcement details, and the field connection details of the tested specimens are shown in Figure 3.6. Field connection of 15.24 cm width was used in this study as illustrated also in Figure 3.6. The selected shear key shape and dimensions in addition to the required lap splice length were adopted based on the previous work by Graybeal [4]. A similar joint shape and splice configuration demonstrated acceptable performance in similar bridge deck slabs with UHPC field joints. Two reinforcing bars were added inside the connection for the two specimens and ran through the connection length, which referred to as lacer bars. The general dimensions and test parameters of both specimens discussed above are summarized in Table 3.2 to present the test matrix for this study.

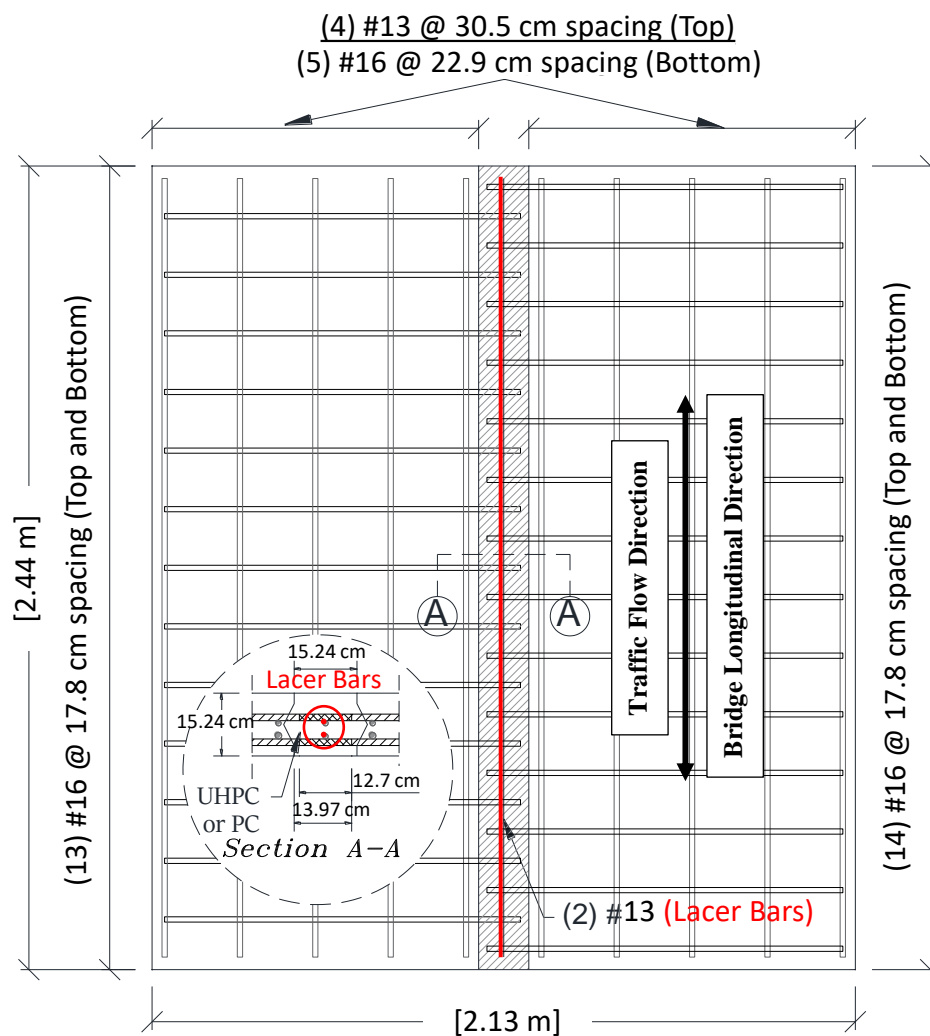


**Figure 3-6** Dimensions and design details of S1-UHPC and S2-PC specimens including two representative deck panels of DBT girders and a field joint shear key

**Table 3-2** Test matrix and specimen details.

Specimen Name	Joint Orientation	Overall specimen dimensions (L × W × thickness) m	Field joint material	Lap splice type	Joint width, cm	Lap splice length, cm
S1-UHPC	Longitudinal	2.44 × 2.13 × 0.15	UHPC	Straight	15.24	12.7
S2-PC	Longitudinal	2.44 × 2.13 × 0.15	PMMA-PC	Straight	15.24	12.7



### ***3.3.2 Test Setup and Instrumentation Plan***

The experimental testing of both specimens was conducted at the Earthquake Engineering Laboratory (EEL) at the University of Nevada, Reno (UNR). The assembly of the test setup was adopted to allow three point static bending of the tested specimens. The tested specimens were seated over two beams at the long edges, while a single point static load was applied adjacent to the connection. A photograph and a schematic drawing of the test setup are shown in Figure 3.7. The two seat beams were aligned in the equivalent longitudinal direction of the bridge, i.e. parallel to the longitudinal field connection. The specimens were supported over the entire 2.44 m length of the seat beams. The spacing between the seat beams was adjusted to be 1.83 m to represent the assumed effective span of the longitudinal specimens as previously mentioned. The 1.83 m spacing is approximately the distance between two adjacent inflection points in the transverse direction of the bridge. This test setup was adjusted to provide a simply supported deck slab with allowing some rotations at the ends only to represent positive moment case. Therefore, two long strips of unreinforced 5.1 cm thick and 20.3 cm wide rubber pads were placed over the seat beams to accommodate any rotations at the support axis.

The objective of the tests was to investigate the local flexural behavior of the longitudinal connections in DBT girder bridge without considering the action between the DBT flanges and the girders web parts. Only the local flexural behavior of the representative DBT deck portions was investigated through applying a patch load adjacent to the joint to investigate the performance of the longitudinal joint in transferring the shear and flexure stresses across two adjacent DBT girders. The test setup did not consider any axial restraint, i.e. arching action, at the ends and ignored the associated contribution of this arching action to the load bearing capacity of the bridge deck specimen. The static vertical load was applied using a 978.6 kN hydraulic actuator through a 2.54 cm thick elastomeric rubber pad of 50.8 cm × 25.4 cm plan dimensions. The loading pad dimensions were determined based on the contact area of the typical AASHTO truck wheel. It is noted that the rubber pad was backed by a 2.54 cm thick steel plate to allow for a uniform distribution of the applied load.

The instrumentation plan for both specimens was identical. The instrumentation included a total of 41 strain gages for reinforcing bars distributed among the transverse and longitudinal reinforcement, three concrete strain gages installed inside the joint concrete material, nine string potentiometers to measure the specimen deflection, and six LVDTs to monitor the interface crack opening between the joint and concrete panels. Figure 3.8 shows the distribution of different instrumentation devices and locations of strain gages on the bottom reinforcement as sample for both test specimens. The strain gages of the bottom transverse reinforcement were installed to capture the yielding of the bars due to the bending of the deck slabs and to monitor the load distribution between the connected slab portions. More strain gages were installed closer to the loading position because of the expected higher local flexural stresses in this region. Regarding the strain gages of the transverse bars, each instrumented bar had two strain gages at the interface between the joint and the precast panels. The strain gages were installed inside and just outside the joint region to interpret bar slip, if any. Moreover, the strain gages inside the joint were mainly installed to verify whether the bars will yield within the joint and to ensure that the embedded length will satisfy the required development length within the field joint material. The displacement transducers were attached to the bottom of the deck slabs to measure the horizontal displacements between the deck panels and the field joint, i.e. monitor the opening of the bottom side of the connection. Several cameras were also used below the specimens to capture the crack progress during testing.



### 3.3.3 Loading Protocol

The loading protocol followed in this experimental study included four cycles of loading and unloading then a monotonic increased loading till failure as illustrated in Figure 3.9. The first two cycles included loading up to a load that approximately represent the cracking load of the slabs (66.72 kN) then unloading . The third and fourth cycles included loading of the specimens to a higher load limit (133.45 kN) that is slightly below the AASHTO ultimate load then unloading . The last cycle included the monotonic increased loading of the test specimens till failure. For the first four cycles, the load was applied using force-control at a loading rate of 22.24 kN/min. Similar rate was used for the unloading to avoid any sudden load drops or loss of contact at the loading pad. Then, displacement control was used for the monotonic loading of the last cycle to capture post-peak response through failure at the rate of 1.9 mm/min.

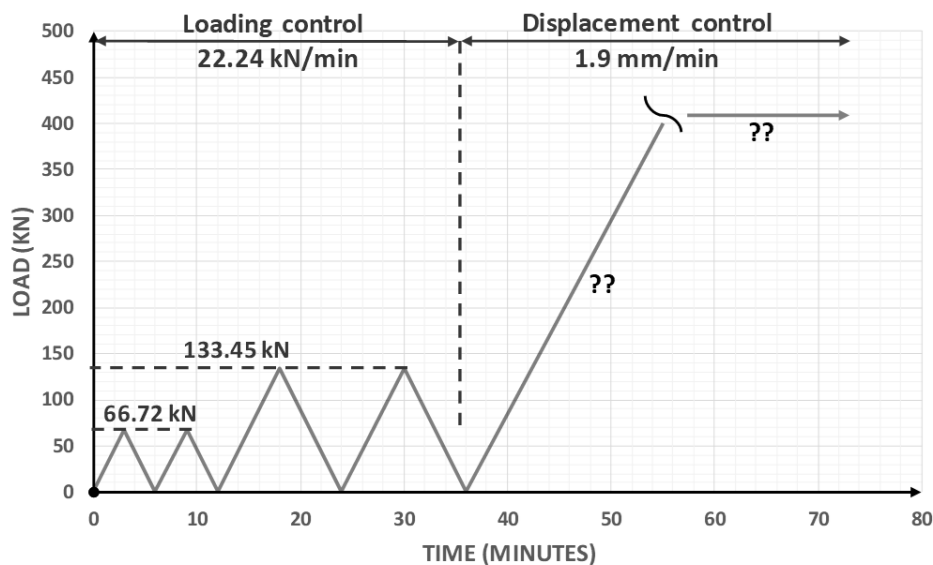


**Figure 3-9** Loading protocol for both tested specimens

The mid-span deflection of the specimen was used for the closed-loop displacement control applied for the last cycle. The reason for applying four cycles of loading and unloading was to study the flexural behavior of the test specimens in addition to the joint performance under representative service loads, observe the crack pattern that would develop at earlier stages of loading, and estimate the average flexural stiffness of the deck slabs from the obtained load versus mid-span displacement relationships.

### 3.3.4 Specimens Construction

Both specimens were fabricated at the fabrication yard of EEL at UNR. The construction process was divided into several phases as shown in Figure 3.10 and briefly discussed next.

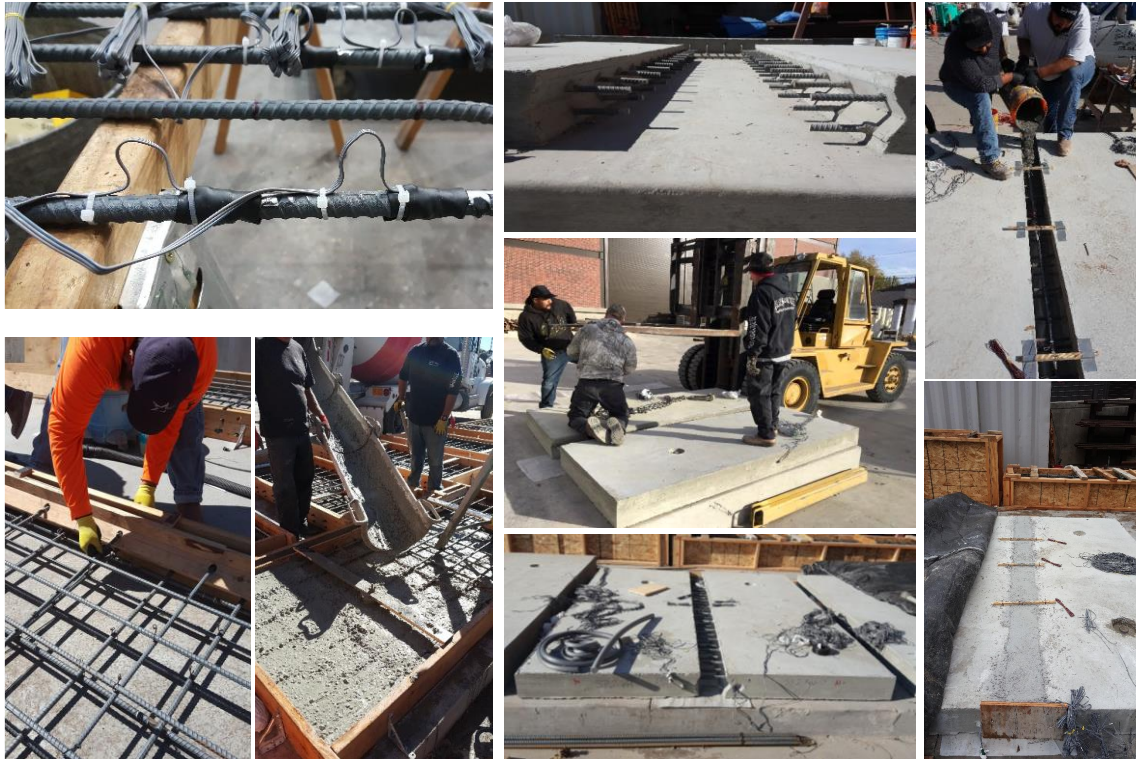


**Figure 3-10** Photographs to illustrate the various construction stages and sequence of representative DBT flanges/slab assemblies with UHPC and PC field joints

Construction of precast deck: Each specimen had two precast panels that represented the DBT girder flanges and were connected later with a field joint. Thus, precast panels were constructed first. This process included the installing strain gages of the bars then placing reinforcement into the formwork. This was followed up by pouring the specified 34.5 MPa normal strength concrete with using a single batch from a ready-mix concrete truck.

Alignment of precast panels: The precast panels were left on-site for approximately three weeks to gain strength before moving them closer to form the field joint. Each pair of two adjacent panels was aligned together with a 15.24 cm gap in-between to pour the field joint material later.

Shear key preparation: The shear key surface was prepared by the cleaning of the surface using strong air pressure followed by sprinkling of water to remove any dust or debris. Then, two longitudinal bars called “lacer bars” were added inside the joint as shown in Figure 3.6 to provide confinement to the reinforcement inside the joint and a side formwork were installed at the end of the joints.

Pouring UHPC: The mixing of UHPC was done on-site using a high-shear mixer that is readily available at UNR. More information about the commercial UHPC mix used in this study is presented in the next section. One UHPC batch was used to pour the field joint of specimen S1-UHPC. The shear key surface was sprinkled with water about half an hour before pouring UHPC to prevent the old precast panels from absorbing water from the freshly mixed UHPC. The mixing time of the UHPC batch was approximately 20 mins.

Pouring PMMA-PC: The mixing of PMMA-PC was also done on-site using an available rotary drum mixer of 0.05 cubic meter capacity. The mixing time of one batch of PMMA-PC required approximately 5 minutes as previously mentioned. A primer liquid was initially applied to the shear key surfaces about 10 minutes before pouring PMMA-PC using a brush to increase the adhesion between the PMMA-PC and the precast concrete panels.

### ***3.3.5 Material Properties***

Different materials were used in the fabrication of the test specimens as explained before. Normal strength or conventional concrete with 34.5 MPa specified 28-day compressive strength was used for deck panels. A proprietary UHPC was used inside the joint of specimen S1-UHPC. The research team has previous experience in mixing and testing this UHPC product [36-37]. The type of material that is used in specimen S2-PC is the same that has been recently used in the mechanical characterization and bond study of PMMA-PC [24]. Several material samples were prepared during the construction process, and several material tests were done for the different materials as shown in Figure 3.11. Detailed stress-strain characterization of the PMMA-PC is provided in previous section, and complementary material test results on PMMA-PC are presented here for completeness. For ASTM C39 compressive testing [38],  $15.2 \times 30.5$  cm cylinders were

used for normal strength concrete and  $7.6 \times 15.2$  cm cylinders were used for UHPC. For PMMA-PC testing, both  $7.6 \times 15.2$  cm cylinders and 5.1 cm cubes were used to conduct ASTM C469 [25] and C579 [39] tests, respectively, as shown in Figure 3.11. It is noted that the UHPC and PMMA-PC cylinders were surface-prepared using a special grinding machine readily available at UNR (see Figure 3.11a) to get smooth flat and parallel surfaces for accurate strength evaluation.

A summary of the measured compressive strength of the conventional concrete, UHPC, and PMMA-PC at different ages is reported in Table 3.3. The reported material strengths are the average of a minimum of at least three samples tested for each concrete type at each testing date. Moreover, reinforcing steel coupons were also tested under direct tension to get the actual yield and ultimate tensile strength of the  $\phi 16$  A706 Grade 60 reinforcing bars used in this study. The measured yield and ultimate tensile strength were determined to be 437.8 MPa and 710.2 MPa, respectively. The measured yield and ultimate tensile strains were 0.28% and 20.1%, respectively.



**Figure 3-11** (a) Grinding of UHPC and PMMA-PC cylinders; and compression testing of: (b)  $7.6 \times 15.2$  cm UHPC cylinders, (c)  $7.6 \times 15.2$  cm PMMA-PC cylinders, (d) 5.1 cm PMMA-PC cubes, and (e)  $15.2 \times 30.5$  cm conventional concrete cylinders

**Table 3-3** Summary of measured compressive strength of different materials used in this study

Type of Concrete	Standard Test	Specimen type and dimensions	Age	Average Strength, MPa
Conventional concrete	ASTM-C39 [38]	15.2 × 30.5 cm cylinders	7 days	20.2
			28 days	29.8
			test day	35.9
UHPC	ASTM-C39 [38]	7.6 × 15.2 cm cylinders	28 days	171
			test day	191.7
PMMA-PC	ASTM – C579/B [39]	5.1 cm cubes	2 days	82.0
			7 days	83.4
			28 days	73.1
			test day	73.8
PMMA-PC	ASTM – C469 [25]	7.6 × 15.2 cm cylinders	9 days	73.1
			28 days	59.0
			test day	62.3

### 3.4 Test Results and Discussion

The experimental test results including global and local behavior of the tested specimens are presented in this section along with comparative evaluation of the structural performance of deck assemblies with UHPC and PMMA-PC longitudinal field joints. The results are discussed in four sections that illustrate damage progression and mode of failure, load-deflection relationships, reinforcement strains, and interface bonding, slippage, or opening.

#### 3.4.1 Damage Progression and Mode of Failure

Brief summary of the key test results is provided first in Table 3.4. The table reports the load capacities of the two specimens in addition to the corresponding deflections at mid-span to provide an overall idea about the comparative specimens' behavior at failure, which is discussed in more details next. It is worth noting that the test continued through failure only to understand the full structural behavior and different materials response and not to inform future design or so. That is because bridge decks are required to remain essentially



elastic under code-compliant service and ultimate loads. Thus, other results such as onset of yielding or the deflection at AASHTO service and ultimate loads as shown in Table 3.4 summary are used for assessing the deck systems design validity as discussed in following sections.

**Table 3-4** Summary of key experimental test results

Specimen	Peak load, kN	Mid-span deflection			Initial stiffness, kN/cm
		@ peak load, cm	@ service load, cm	@ ultimate load, cm	
S1-UHPC	515.1	3.83	0.49	0.98	420.3
S2-PC	436.8	3.58	0.59	1.08	367.8

#### 3.4.1.1 Specimen S1-UHPC

The peak load capacity of specimen S1-UHPC was 515.1 kN at which 3.83 cm middle vertical displacement was measured. The observed mode of failure for the UHPC longitudinal field joint specimen was yielding in the main reinforcement due to bending associated with crushing of normal strength concrete at the top of the south precast panel around the loading pad location. Many flexural cracks were observed at the bottom side of the precast panels, these cracks becomes wider and deeper when approaching the middle of the specimen and especially under the loading pad position. It was observed that multiple flexural cracks in the precast panels were interrupted by three main localized cracks in the UHPC joint at the measured peak load. Crushing of concrete was initially triggered at the location of the loading pad at approximately 458.2 kN and then propagated through the east and west sides of the south precast panel as shown in Figure 3.12a. Signs of punching shear was also observed at the end of test under the loading rubber pad.

After reaching the peak load capacity, big chunk of conventional concrete popped up at the top surface due to the excessive concrete crushing that was simultaneous with the crack localization opening at the bottom of the UHPC joint that lead up to sudden drop in the load capacity of the specimen. The flexural cracks at the bottom face was mainly localized in the loaded (south) precast panel exactly under the location of the loading pad as shown in Figure 3.12b. However, limited flexural cracking was observed under the unloaded

(north) precast panel. The first flexural crack in the UHPC joint was observed at approximately 444.8 kN of vertical loading. Shear cracking was observed at the west side of the loaded panel, the crack propagated from the bearing pads till the UHPC joint in a diagonal formation as shown in Figure 3.12c. Long length and narrow width interface crack was observed at the end of the test at the bottom between the loaded south side and the UHPC joint as shown in Figure 3.12d. No bar rupture or bar slip was indicated during the test. The test was stopped when the specimen was going rough post-peak softening and strength degradation at approximately 80% of the peak load capacity.

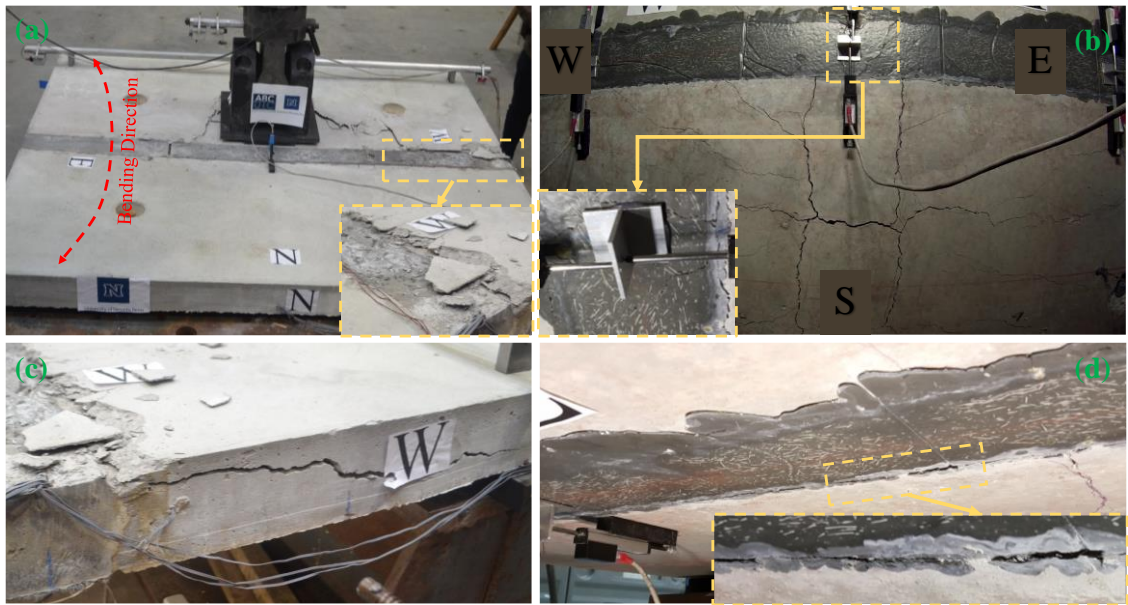


**Figure 3-12** Crack pattern, damage, and modes of failure at: (a) top side of S1-UHPC; (b) bottom side of S1-UHPC; (c) west side of S1-UHPC; and (d) interface crack of S1-UHPC

#### 3.4.1.2 Specimen S2-PC

The peak load capacity of specimen S2-PC was determined to be 436.8 kN at which 3.58 cm middle vertical displacement was measured. The observed mode of failure for the PMMA-PC longitudinal field joint specimen was yielding in the main reinforcement due to bending accompanied with interface cracking between the loaded south panel and the PC joint. This interface crack was initially observed at the bottom of the slab after reaching approximately 391.4 kN of the applied load. After reaching the peak load, crushing of normal strength concrete was observed at the top side of the loaded (south) precast panel, which led to a sudden drop in the load capacity of the specimen. At failure, deep and wide

flexural cracks were observed at the bottom of the precast panels with multiple transverse cracks also observed in the PC joint but with relatively narrow width compared to that in conventional concrete. Again, the flexural cracks at the bottom of the specimen was mainly localized in the south precast panel under the position of the loading pad as shown in Figure 3.13a. However, limited flexural cracking was only observed under the unloaded side of the slab. Crushing of concrete appeared around the rubber loading pad at the top of the south side following the observation of punching shear under the loading pad at approximately 418.1 kN. Afterwards, the top cracks in the south precast panel propagated through the east and west sides as shown in Figure 3.13b. It is noted that crushing of conventional concrete was observed in the post-peak behavior after the load capacity of the specimen started to drop. The first transverse crack in the PC field joint was observed at approximately 333.6 kN. The expected reason for failure was the interface cracking at mid-span between the loaded south side and the PC joint as shown in Figure 3.13a. Another interface crack was also observed at the east side, which was developed between the north side of the slab and the PC joint as shown in Figure 3.13c. No bar rupture or bar slip was indicated during the test. The test was again stopped after load capacity dropped to approximately 80% of the peak load.

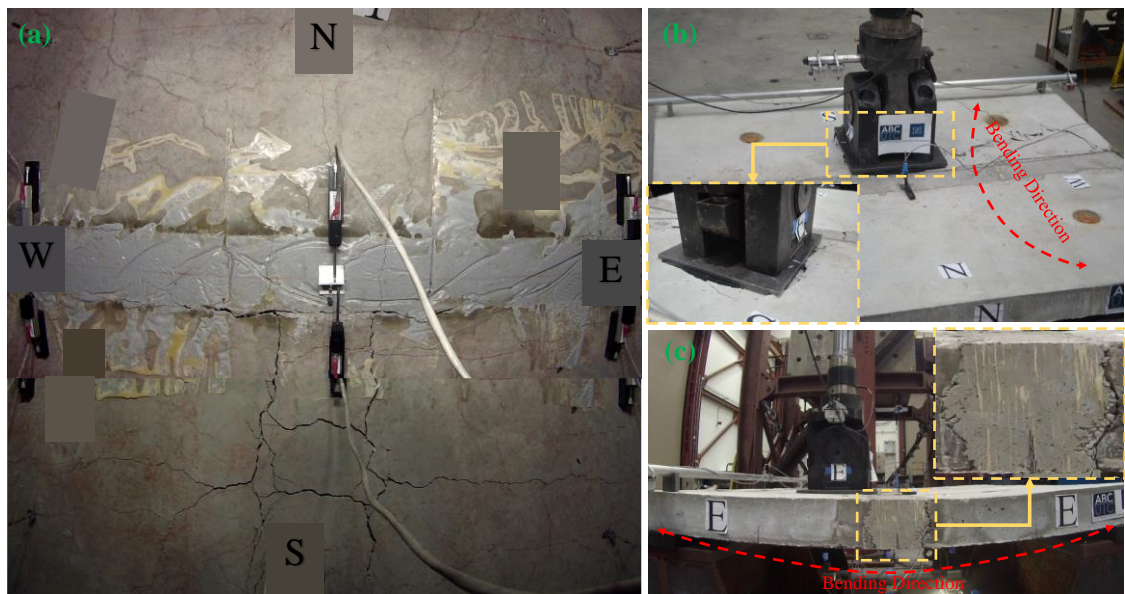


**Figure 3-13** Crack pattern, damage, and modes of failure at: (a) bottom side of S2-PC; (b) top side of S2-PC; and (c) east side of S2-PC

Similar to UHPC, the PMMA-PC field joint reached the AASHTO ultimate load before any significant cracking was observed due to the high tensile properties of PMMA-PC which make the material suitable for deck field joints. Figure 3.14 shows and compares the crack pattern from the bottom side for both specimens at the AASHTO ultimate load level. The crack patterns in Figure 3.14 were marked and highlighted in the photographs to make them easier to inspect since the actual cracks at this load level were very narrow, tiny, and hard to see. It can be seen that both specimens have almost the same crack pattern as they are mainly cracked under the loading pad. However, the PC specimen has more cracks closer to the field joint. Therefore, the early crack propagation of the UHPC specimen was better than the PC specimen due to the rigidity of the UHPC specimen.

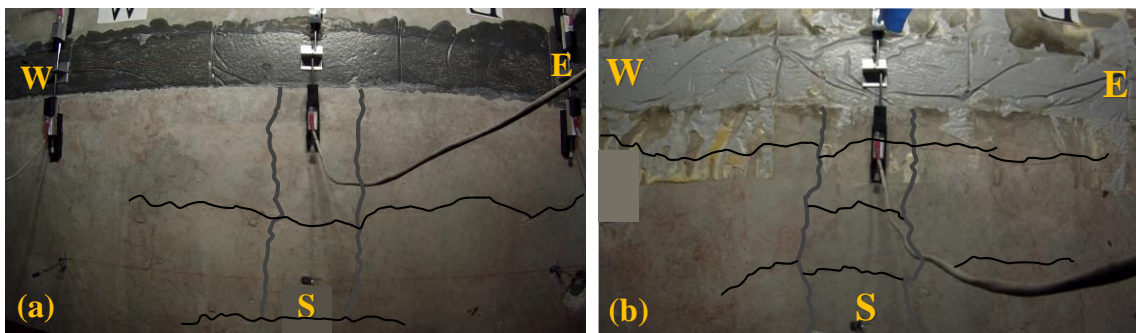


**Figure 3-14** Crack pattern at AASHTO ultimate load at the bottom side of (a) S1-UHPC and (b) S2-PC

### 3.4.2 Load-Deflection Relationship

This section illustrates the load and deflection behavior of the two tested specimens as evaluated at different loading levels. The load and deflection relationship of both specimens are presented in a comparative format to show the difference in behavior between both specimens and to establish a comparison in terms of flexure stiffness, peak load, peak vertical displacement, and uniformity of the load distribution. The applied load versus the measured mid-span vertical displacements at three different locations along the longitudinal joint for both specimens are presented in Figure 3.15. Three main observations can be drawn from Figure 3.15. First, the overall flexural response of the two specimens is very comparable however the load capacity of the UHPC specimen is comparably higher than that of the PC specimen. Second, the initial stiffness of the UHPC specimen is slightly

higher than that of the PC specimen due to the higher mechanical properties of the UHPC compared to the PC. Finally, the flexural capacity for both specimens surpassed the ultimate limit state specified in the AASHTO LRFD. Consequently, both UHPC and PC field joints are considered as viable solutions for use in precast bridge deck systems that can satisfy the target behavior of conventional CIP decks in terms of strength and load distribution requirements.

The load-deflection curves shown in Figure 3.15 can be divided into different regions of behavior. The first region represents the linear elastic flexural response of the specimens when the applied load is approximately below 66.7 kN. Through this linear response, no flexural cracks were observed at the bottom side of specimen S1-UHPC as the specimen did not yet reach its cracking moment. However, there was only one hair longitudinal crack in specimen S2-PC that was located approximately 12.7 cm apart from the edge of the joint and ran parallel to the joint in the south precast panel. Moreover, no interface debonding or concrete crushing was observed during the “service” level load. In addition, no cracks were also observed in the field joint because of the higher tensile properties of the UHPC and PMMA-PC as compared to normal strength concrete. The second region in defining the load-deflection curve represents the onset of the nonlinear behavior as the applied load exceeded the linear elastic load. This nonlinear behavior started through the loading of the third and fourth cycles around 133.4 kN where the flexural stiffness decreased and the residual displacement after unloading increased. A hair longitudinal crack was observed in specimen S1-UHPC which was located approximately 30.5 cm apart from the edge of the connection and ran parallel to the connection in the south precast panel. However, no flexural cracks were observed on the north precast panels for both specimens. The cracks at this level were still narrow and more importantly, the reinforcement was not yet yielded. It is worth noting that no flexural or interface cracks were observed in the UHPC or PC field joints up to the AASHTO ultimate load (indicated by dashed line in Figure 3.15).

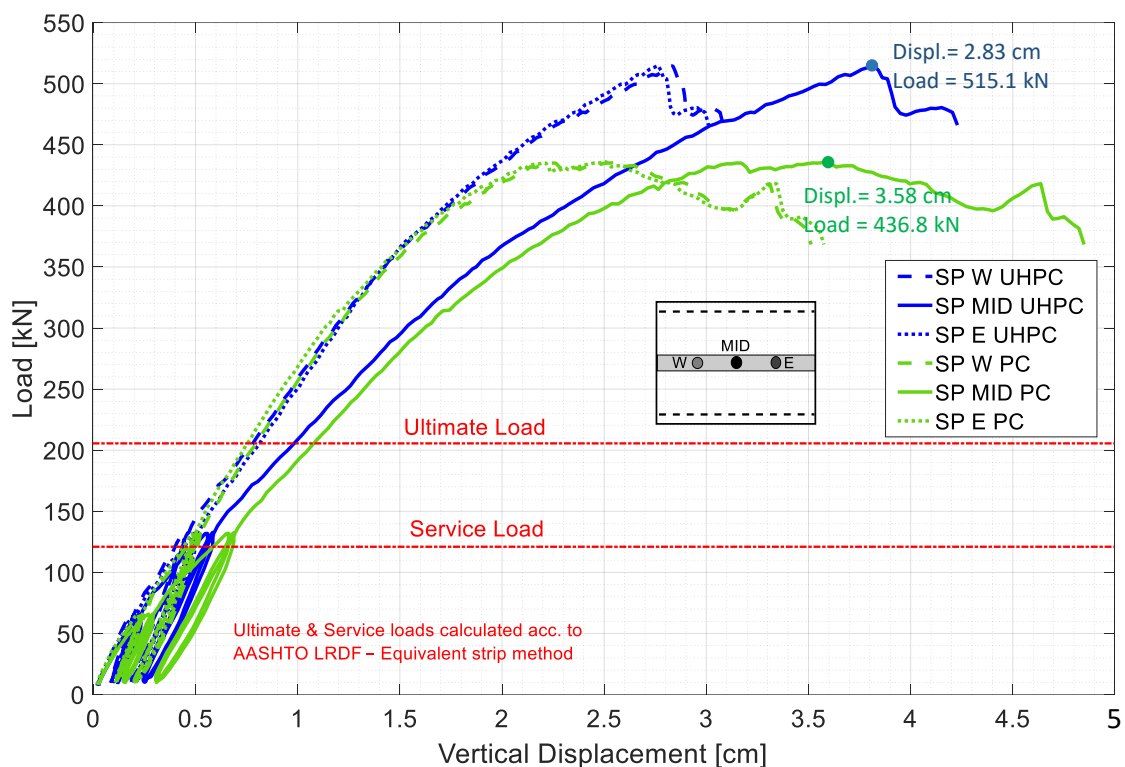


**Figure 3-15** Load-deflection relationship at mid-span of specimens S1-UHPC and S2-PC as measured at three different locations

The slightly nonlinear response persisted as the load increased to approximately 355.9 kN and 333.6 kN for specimens S1-UHPC and S2-PC, respectively. The reason for the nonlinear response was attributed to the yielding of several middle transverse bars at the bottom reinforcement of the south precast panel. As the load was further increased, the third region of the load-deflection curve can be defined by the significant reduction in stiffness where the specimens started softening due to yielding of most of the transverse reinforcement in the bottom mesh. This was associated with deep and wide flexural cracks that were observed in the bottom side of both specimens. No rebar slip was observed until reaching the peak load. Following the peak load capacity, the fourth region can be defined by a degradation in the load capacity of the specimens. For specimen S1-UHPC, there were sudden drops in the load capacity of the specimens due to the crack localization in the UHPC joint in addition to the excessive concrete crushing at the top surface of the south precast panel. While for specimen S2-PC, the failure was more ductile due to the excessive flexural cracking at the bottom of the specimen especially under the location of the loading pad. Then these cracks

were extended to the middle of the PC joint at approximately 333.6 kN that led to redistribution of the applied loads to the west and east sides of the specimen until finally interface de-bonding was observed. This load redistribution allowed more ductile failure of the PC specimen. It is noted again that the goal of loading the specimens up to such high levels of loads and displacements beyond code-required limits was to have better understanding of the modes of failure and check whether the different components of the deck system stay intact till the end of the test. It is worth noting that no rebar rupture was indicated throughout any of the tests.

Moreover, it can be seen from Figure 3.15 that the UHPC specimen had larger flexural stiffness than the PMMA-PC specimen because of the higher modulus of Elasticity as well as tensile and compressive strengths of UHPC. The initial flexural stiffness of the UHPC specimen was found to be 420.3 kN/cm versus 367.8 kN/cm for the PMMA-PC specimen, i.e. the PC deck system stiffness was about 88% of the UHPC system. It can also be seen from Figure 3.15 that the flexural behavior of the two specimens was very comparable till reaching approximately 400.3 kN where the PC specimen started to soften and lose stiffness due to the interface crack that happened between the PC joint and the south loaded side of the slab as mentioned before.

The west and east side deflections that was measured along the field joints of both specimens are almost identical due to the symmetry of loading in the longitudinal direction and the capability of both joints to uniformly distribute the applied load to both east and west sides till the end of the test despite the excessive flexural cracking of the specimen and the field joints. The difference between the middle deflections and the east or west side deflections of the PC joint is higher than that of the UHPC joint due to the difference in stiffness and rigidity between both joints. The UHPC joint has higher stiffness and act as a rigid beam in the longitudinal direction and consequently less difference in deflections between the middle and east or west sides and better load distribution in the longitudinal direction. It was also observed that the difference in deflections between middle and the east or west sides is increasing with the increase of the applied load. At the beginning, the loads were too small and there were only limited flexural cracks and hence this allowed

the slab to bend uniformly. However, with increasing the load, the flexural stiffness of the slab was decreased because of the extensive flexural cracking that lead to increase of the difference in deflections between the middle and the east or west sides. The load versus vertical displacement readings from the string potentiometers located at quarter spans in addition to the middle string potentiometer for both specimens are presented in Figure 3.16.

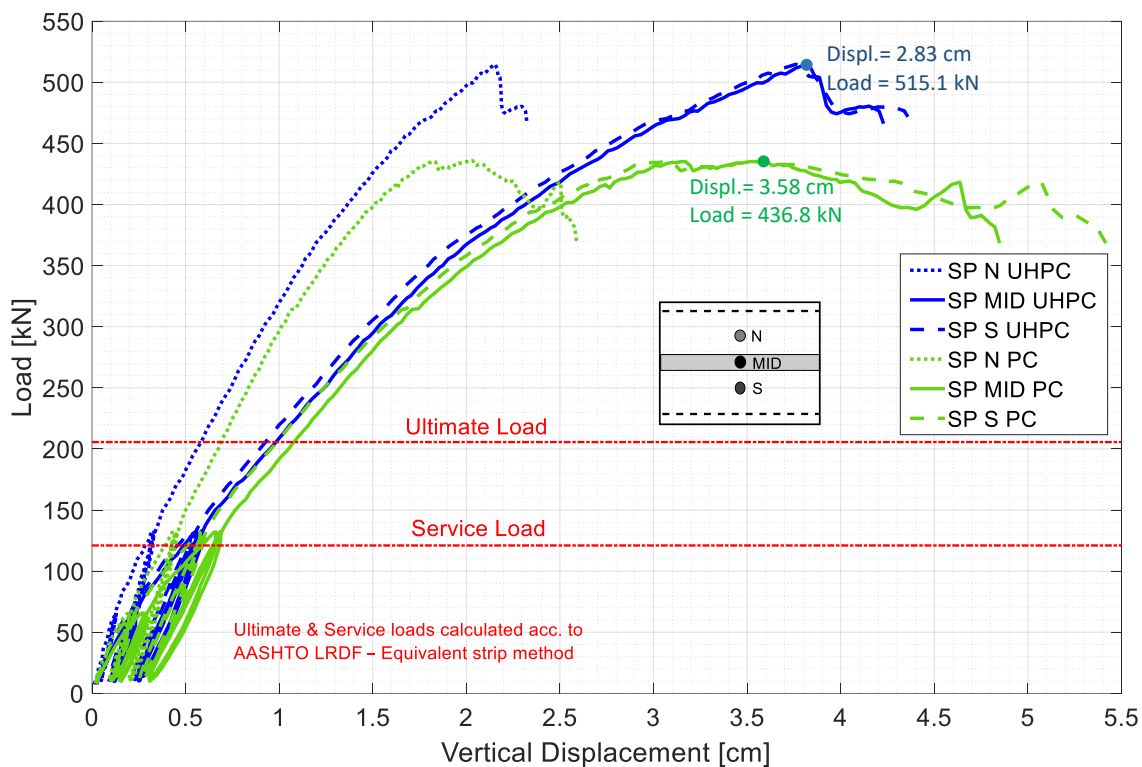


**Figure 3-16** Load-deflection relationship at quarter and mid span of specimens S1-UHPC and S2-PC

It can be seen from Figure 3.16 that the measured deflection at the south side of the specimen and the deflections at the middle of the field joint were almost identical. However, the unloaded side of the specimen (north side) attained lower deflections which was expected because of the asymmetry of the specimen loading in the transverse direction, i.e. north-south direction. Another interpretation for this observation is that the field joint is not transferring the full applied loads between the two sides of the slab as there is a discontinuity in the reinforcement between both sides. Moreover, this difference in deflections increased with the increase of the applied load due to the influence of the reduction in stiffness of the slabs after the propagation of the flexural excessive cracking.



This is consistent with results from a previous analytical study that was part of the NCHRP 10-71 project [11] which showed that the shear and moment forces on the field joint are greatly reduced due to the stiffness reduction accompanied with cracking of the specimen. Figure 3.17 shows the difference between the mid-span vertical displacement and the displacements of the north and south sides along with the applied vertical load of the specimens.

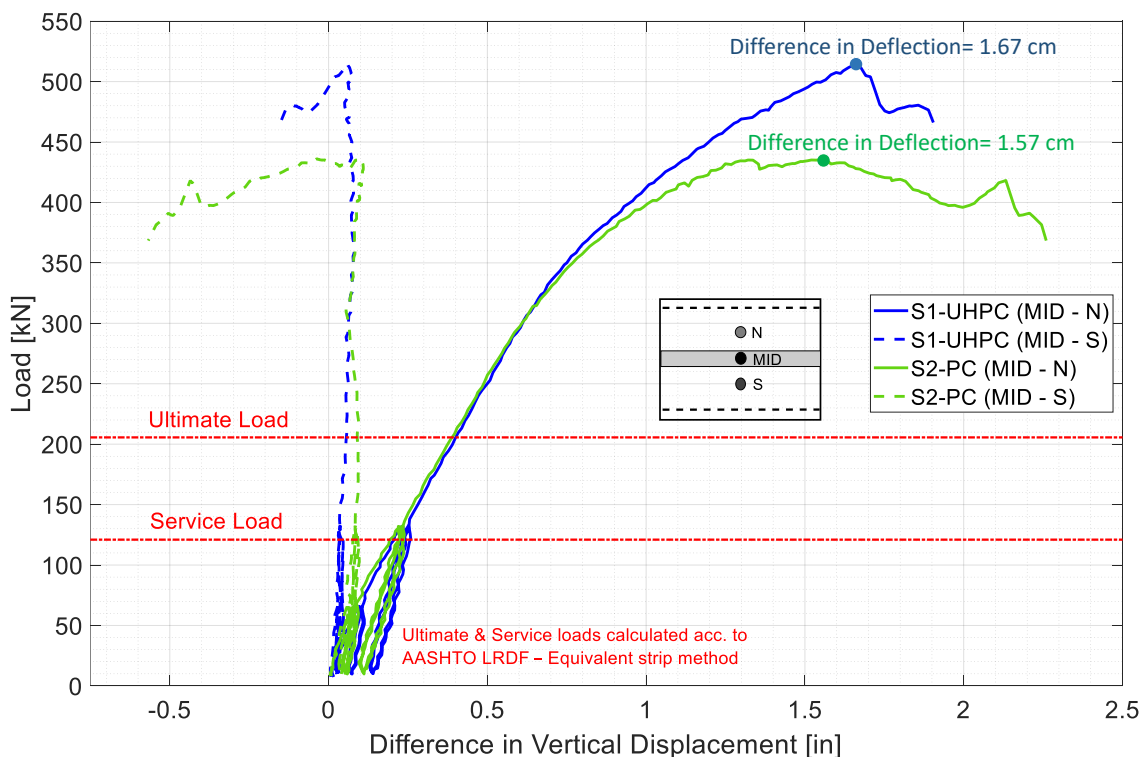


**Figure 3-17** Load versus difference between middle deflection and the deflections of north and south sides

It can be seen from Figure 3.17 that both specimens are very comparable in behavior as the difference between the middle deflections and the south deflections is minimal till reaching the peak loads for both specimens. The difference between the middle deflections and the north deflections are comparably higher and increased with the applied loads. The difference between the middle and north side deflections at the measured peak loads were 1.67 cm and 1.57 cm for specimens S1-UHPC and S2-PC, respectively. The differences between the middle and north deflections were almost identical for both specimens till reaching approximately 333.6 kN. After this load limit, the PC joint was cracked, and it

was subjected to stiffness degradation that resulted in the redistribution of the loads towards the east and west sides of the specimen. This change in behavior resulted in a significant increase in the difference in deflections between the middle and the north side of specimen S2-PC. This difference was also subjected to more increase because of the interface debonding that happened at 392.5 kN at the middle of the specimen between the south slab panel and PC field joint. The difference between the deflections of the middle and north unloaded side of the specimen can give a good indication about the performance of the field joint and the ability of transferring the straining actions between both sides of DBT slabs. As the difference in deflections decrease, this is an indication that the load distribution over the slab is better and the joint performance in transferring the loads is even better.

### ***3.4.3 Reinforcement Strains***

This section shows selected results from the measured strain data. The load versus strain readings of selected bottom transverse reinforcement at mid-span location are shown in Figures 3.18 and 3.19 for specimens S1-UHPC and S2-PC, respectively and discussed here. It is noted that some strain gages were damaged during the test especially at higher load levels that led to strain gages and wire damages associated with the excessive damage of concrete. The following subsections discuss the strain results for each specimen separately for convenience.

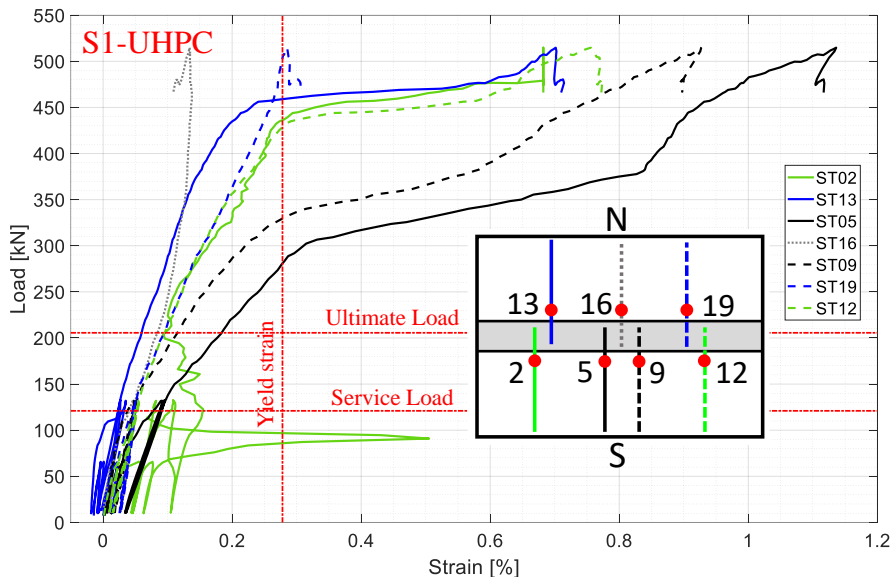


**Figure 3-18** Load versus strain measured near the mid-span location of the bottom transverse reinforcement of specimen S1-UHPC

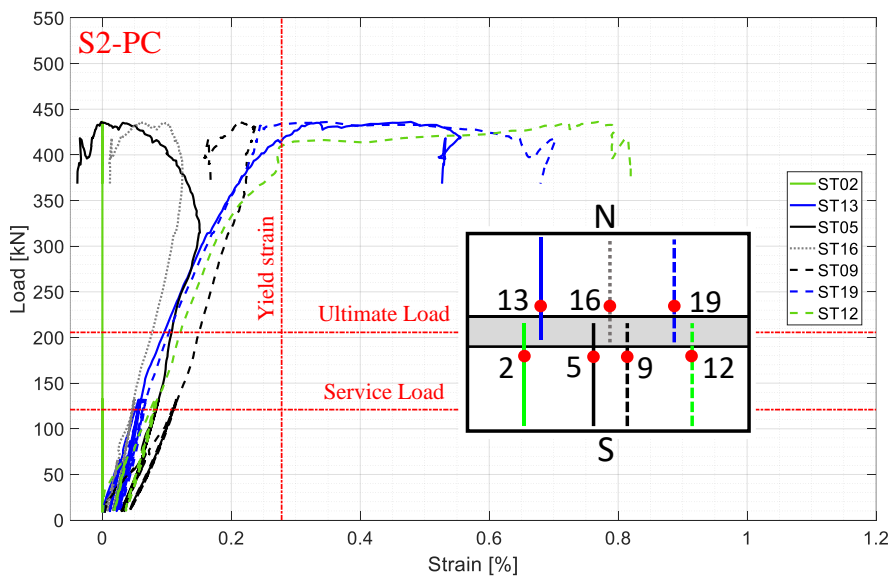


**Figure 3-19** Load versus strain measured near the mid-span location of the bottom transverse reinforcement of specimen S2-PC

### 3.4.3.1 Specimen S1-UHPC

It can be seen from Figure 3.18 that the largest strains were recorded in the two middle bars in the south precast panel close to where the load was applied. The onset of yielding was observed in one of the bars at the middle of the south precast panel at 284.7 kN. This was followed by yielding in the adjacent rebar at 311.4 kN. After this limit, the load deflection

behavior of the slab was significantly changed to global softening with large deflection increments corresponding to small applied load as previously shown in Figures 3.15 and 3.16. Most of the bottom transverse bars at both precast panels were yielded at approximately 444.8 kN, after then a concrete crushing was initiated at the top surface of the south precast panel. It was observed that the strains of the reinforcement in the south side was slightly higher than the values of strains at the north side. It is worth noting that there is no bar rupture was indicated throughout the test. Finally, a key observation from the behavior depicted in Figure 3.18 for S1-UHPC is that none of the transverse bottom reinforcement yielded before reaching the ultimate and service loads specified in the AASHTO, i.e. the deck system remains elastic up to the code limits as required.

#### 3.4.3.2 Specimen S2-PC

Similar to the observations of specimen S1-UHPC, the largest strains were recorded in the middle bars in the south precast panel close to where the load was applied in case of S2-PC. However, this observation has changed after reaching approximately 333.6 kN as the PC joint started to have cracks in the middle and the load was redistributed to the east and west sides. This was followed by release in the strains of the middle bars and increase of the strains at the west and east side bars. This was concluded by having significantly higher strains at the east and west sides by the end of the test. The onset of yielding was observed in one of the instrumented bars at the east of the south precast panel at 409.2 kN. However, after reviewing the test results, it was inferred that the onset of yielding happened around 333.6 kN but seems to have happened in one of the non-instrumented bars, i.e. one of the bars in the middle of the south precast panel and adjacent to the middle instrumented bars.

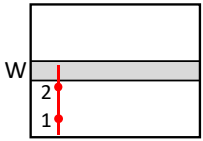
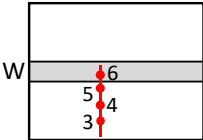
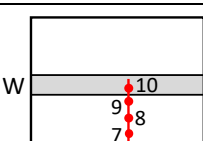
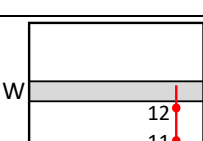
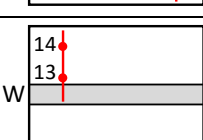
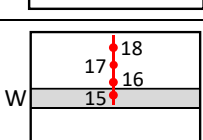
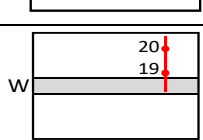
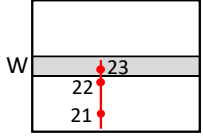
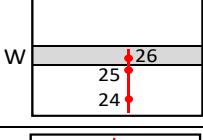
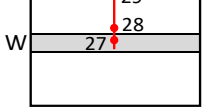
Most of the bottom transverse bars at both slab panels were yielded at approximately 435.9 kN, after then the load carrying capacity of the specimen started to decrease because of the interface cracking and the loss of stiffness that happened to the PC joint that was one of the main reasons for failure. Again, it was observed that the strains of the reinforcement in the south side was slightly higher than the values of strains at the north side. It is noted that there is no bar rupture was indicated throughout the test. Moreover, and similar to S1-UHPC, the transverse bottom reinforcement remained elastic up to the service and ultimate

loads specified in AASHTO, which further verifies the acceptable behavior of PMMA-PC for DBT girders longitudinal joints.

#### *3.4.3.3 Peak strain values*

The measured strain values of the top and bottom transverse reinforcement at peak loads for both tested specimens are reported in Table 3.5. These strain values were reported herein to serve as a reference for verification purposes of any future finite element or numerical studies. It can be seen that the strain values of the reinforcement inside the UHPC joint exceeded the yield strain. This is an indication that the UHPC joint with 15.24 cm width is considered sufficient to provide a proper development length for the bars inside the joint. Consequently, this will provide adequate load transfer between both precast panels. For specimen S2-PC, none of the strain gages that were installed inside the PC joint captured any yield strain because of the load redistribution that happened after the PC cracking as mentioned before. Consequently, it was hard to determine the adequacy of the joint width in terms of the required development length. However, it can be still concluded from the overall behavior that the PMMA-PC filled joint with 15.24 cm width can provide adequate development length that can transfer the applied load across different DBT slabs up to 333.6 kN, i.e. more than 1.5 times the required AASHTO ultimate load.

**Table 3-5** Summary of the measured reinforcement strain values at peak load.

Reinforcement	Strain Gage Location	SG #	S1-UHPC Strain (%)	S2-PC Strain (%)
Bottom Transverse Reinforcement		ST 1	0.25	0.32
		ST 2	N/A	N/A
		ST 3	N/A	N/A
		ST 4	N/A	0.10
		ST 5	1.14	0.02
		ST 6	0.51	N/A
		ST 7	N/A	N/A
		ST 8	N/A	0.21
		ST 9	0.93	0.21
		ST 10	0.86	N/A
		ST 11	0.27	0.79
		ST 12	0.76	0.77
		ST 13	0.70	0.48
		ST 14	0.14	N/A
		ST 15	0.14	N/A
		ST 16	0.14	0.06
		ST 17	0.16	0.09
		ST 18	0.01	0.02
		ST 19	0.29	0.35
		ST 20	0.15	N/A
Top Transverse Reinforcement		ST 21	0.14	0.31
		ST 22	0.15	0.36
		ST 23	0.13	0.13
		ST 24	0.12	0.13
		ST 25	0.18	0.13
		ST 26	-0.05	0.14
		ST 27	0.17	-0.02
		ST 28	0.06	N/A
		ST 29	-0.002	-0.004

### 3.4.3.4 Longitudinal reinforcement strains

While Figures 3.18 and 3.19 above focused on strains in the bottom transverse reinforcement, the load versus strain readings of selected longitudinal reinforcement at mid-span location is shown in Figure 3.20 for completeness. It can be seen that none of the joint or slab longitudinal reinforcement yielded before reaching the ultimate and service loads specified in the AASHTO, i.e. the deck system remains elastic up to the code limits as required. It was also observed that the strains of the longitudinal bars which are located inside the field joints and the south precast panel were comparably higher than the strains of the rebar on the north precast panel due to the asymmetry of loading in the transverse direction.

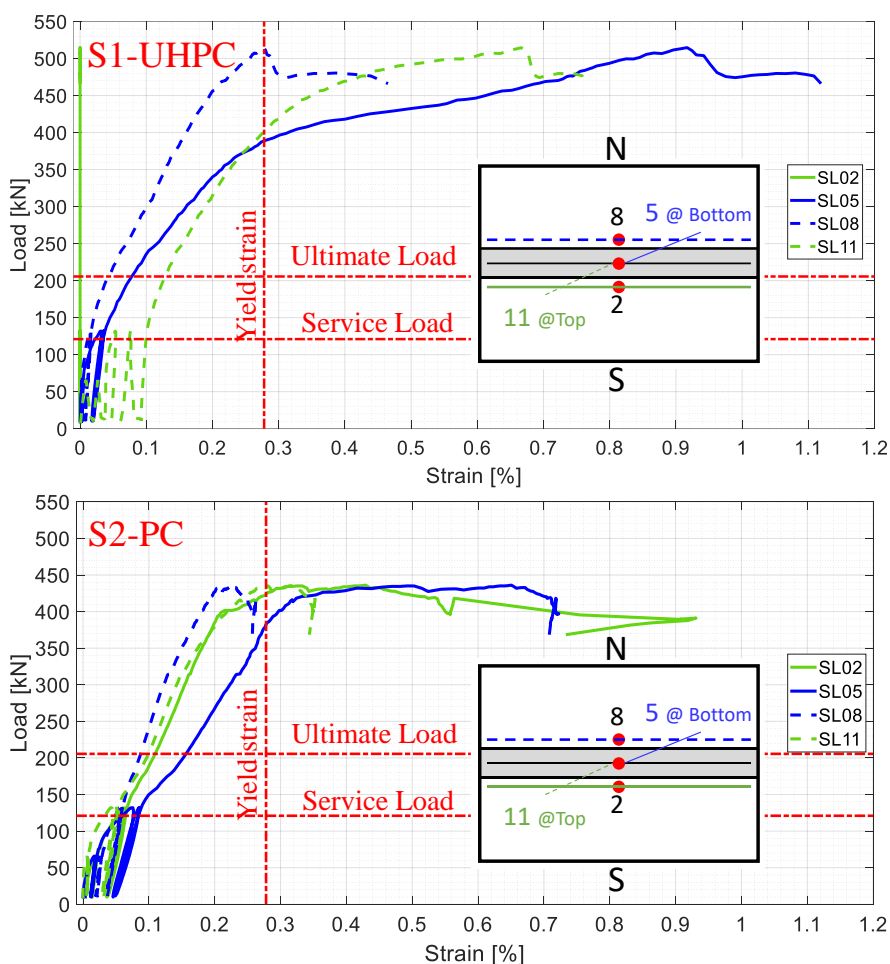


**Figure 3-20** Load versus strain measured at the middle longitudinal bars for both test specimens

### 3.4.4 Interface Opening

The lateral or horizontal interface opening width at the bottom face of the slab between the field joint and the precast panels was monitored through the test with using six LVDTs. The interface opening width at the AASHTO service and ultimate loads for both test specimens are reported in Table 3.6. The measurements from the LVDTs are discussed here to assess the interface bond performance between the field joint and the precast parts, and to compare the crack width with that of the maximum allowable limits specified in the AASHTO LRFD Article 5.6.7 [34]. The AASHTO LRFD specifies a maximum spacing between the rebars to control the flexural cracks. These maximum spacing limits were determined based on the maximum allowable crack width of 0.43 mm for “class 1” exposure and 0.33 mm for “class 2” exposure. The “class 2” exposure is typically used for situations in which the concrete is subjected to severe corrosion conditions.

**Table 3-6** Interface opening width of specimens S1-UHPC and S2-PC at service and ultimate loads

LVDT Location (see Figure 3.8)	S1-UHPC		S2-PC	
	Service Load, (mm)	Ultimate Load, (mm)	Service Load, (mm)	Ultimate Load, (mm)
NW	0.22	0.45	0.22	0.41
SW	0.17	0.29	0.28	0.44
N	0.22	0.47	0.26	0.49
S	0.19	0.45	0.28	0.42
NE	N/A	N/A	0.21	0.40
SE	0.19	0.31	0.18	0.30

At the early stages of the applied load where the vertical displacements were minimal, the results from the LVDTs were more accurate in representing the interface crack width. However, the LVDT measurements became non-representative of interface opening when approaching the failure load because of the excessive vertical displacements and severe flexural cracking in the slab. Thus, the measurements at higher load levels were not reported here. It can be seen from Table 3.6 that both specimen had very comparable values for the interface crack opening at the early behavior of the specimen up to the AASHTO ultimate load. It can be seen also from the table that interface opening at all different



locations at the AASHTO service loading was less than the 0.33 mm limit. It was observed that specimen S1-UHPC reached the maximum allowable crack assuming a “class 2” exposure at approximately 155.7 kN of vertical load which is higher than the specified AASHTO service load but still below the ultimate load. While for S2-PC, it was observed that it reached the maximum allowable crack assuming a “class 2” exposure at approximately 137.9 kN of vertical load. This can confirm that interface bond between the UHPC or PMMA-PC and the DBT slabs satisfied the design requirements and the code service load limits.

### **3.5 Summary and Conclusion**

This paper presented results from comprehensive experimental testing that demonstrated the use of alternative closure pour material for longitudinal field joints between DBT girders in bridge deck systems. This paper discussed the static structural performance of deck assemblies that consisted of representative DBT slab portions and longitudinal field joints filled with either UHPC or PMMA-PC. First, the main mechanical properties of the PMMA-PC were reported to provide a better understanding of the proposed field joint material. Next, two simply-supported full-scale specimens were tested under vertical loading on one-side of the joint at mid-span. Both specimens considered longitudinal connection with diamond shaped shear key and a non-contact straight lap splice of 12.7 cm. This paper discussed the test results in terms of the structural behavior and performance assessment of each specimen under the specified AASHTO service and ultimate loads. Moreover, a comparison between both specimens was established to verify the adequacy of using PMMA-PC inside DBTs field joints instead of UHPC. The following observations and concluding remarks can be drawn from this experimental investigation:

- From the conducted brief material characterization, PMMA-PC are shown to have larger compressive ultimate strain than conventional normal strength concrete and UHPC as well as enhanced post-peak behavior and strain deformation capacity. The flexural strength of PMMA-PC and corresponding modulus of rupture, as obtained from standard prisms, is higher than typical normal strength concrete values, and comparable to UHPC with 2% fibers. However, PMMA-PC prisms show brittle failure after first crack formation as in conventional concrete.

- Direct tensile strength of PMMA-PC, as obtained from dog-bone specimens, is almost double typical normal strength concrete values and only slightly less than typical values of UHPC with 2% fibers. Unlike UHPC, the failure of PMMA-PC in tension is brittle after the first crack is formed. However, the PMMA-PC still provides a sustained tensile capacity with increased strains and very adequate ductility up to the instant of main crack formation.
- Overall, the structural performance of DBT girder flanges/slabs with full-depth longitudinal PMMA-PC field joints is demonstrated to be a viable alternative for ABC. The PMMA-PC field joints results in a very comparable performance to the currently accepted practice of UHPC field joints in terms of service performance as well as load and deflection capacities.
- Both UHPC and PMMA-PC longitudinal field joints adequately satisfy the service and ultimate load requirements specified in the AASHTO LRFD, where deck systems should remain elastic without any major flexural or interface cracking in the joint or any rebar slippage. Moreover, no flexural cracks were observed in the UHPC or the PMMA-PC joints up to the AASHTO LRFD ultimate load level, which could be attributed to the higher tensile properties of both materials compared to high strength grouts or conventional concrete.
- Initial stiffness of the deck system with UHPC joint was found to be higher than that of the system with PMMA-PC joint, which is attributed to the higher mechanical properties, mainly modulus of elasticity, of UHPC. However, the slightly lower stiffness from PC joints did not lead to any excessive deflections or deficiency in meeting code requirements. Additionally, the flexural capacity of the UHPC specimen was found to be higher than the PMMA-PC specimen. Nonetheless, both specimens had comparable behavior in terms of loads, deflections, and field joint performance at the AASHTO ultimate load level, which is the more relevant limit state.
- PMMA-PC can be effectively used inside full-depth DBT girders field joints without any need for post-tensioning or mechanical splicing. This indirectly also confirms that the 15.24 cm field joint width, typically used for UHPC, is also sufficient for PMMA-PC to provide emulative, i.e. monolithic-equivalent, bridge deck systems in terms of load distribution.

## Acknowledgment

This study is funded by the US DOT through the ABC-UTC (2016 cycle) headed at Florida International University. The authors would like to thank Transpo Industries for the T-17 polymer concrete material donation and Ductal® for the UHPC material donation. The authors also thank the laboratory staff at the Earthquake Engineering Laboratory at the University of Nevada, Reno for their assistance with the testing and experimental program.

## References

- [1] Graybeal, B. (2014). Design and construction of field-cast UHPC connections (No. FHWA-HRT-14-084; HRDI-40/10-14 (750) E). United States. Federal Highway Administration.
- [2] Peruchini, T. J., Stanton, J., & Calvi, P. (2017). Investigation of Ultra-High Performance Concrete for Longitudinal Joints in Deck Bulb Tee Bridge Girders (No. WA-RD 869.2). Washington (State). Dept. of Transportation. Office of Research and Library Services
- [3] Qiao, P., Zhou, Z., & Allena, S. (2016). Developing Connections for Longitudinal Joints between Deck Bulb Tees-Development of UHPC Mixes with Local Materials (No. WA-RD 869.1). Washington (State). Department of Transportation.
- [4] Graybeal, B. A. (2010). Behavior of field-cast ultra-high performance concrete bridge deck connections under cyclic and static structural loading (No. FHWA-HRT-11-023). United States. Federal Highway Administration.
- [5] Hartwell, D. R. (2011). Laboratory testing of Ultra High Performance Concrete deck joints for use in accelerated bridge construction. Graduate Theses and Dissertations. 10420. <https://lib.dr.iastate.edu/etd/10420>.
- [6] Hwang, H., & Park, S. Y. (2014). A study on the flexural behavior of lap-spliced cast-in-place joints under static loading in ultra-high performance concrete bridge deck slabs. *Canadian Journal of Civil Engineering*, 41(7), 615-623.

- [7] Coufal, R., Vitek, J. L., Rehacek, S., Kolisko, J., & Citek, D. (2016, July). UHPC Connection of Precast Bridge Deck. In International Interactive Symposium on Ultra-High Performance Concrete (Vol. 1, No. 1). Iowa State University Digital Press.
- [8] Zhu, P., Ma, Z. J., Cao, Q., & French, C. E. (2012). Fatigue evaluation of transverse U-bar joint details for accelerated bridge construction. *Journal of Bridge Engineering*, 17(2), 191-200.
- [9] Li, L., & Jiang, Z. (2016). Flexural Behavior and Strut-and-tie Model of Joints with headed bar details Connecting Precast Members. *Perspectives in Science*, 7, 253-260.
- [10] Verger-Leboeuf, S., Charron, J. P., & Massicotte, B. (2017). Design and behavior of UHPFRC field-cast transverse connections between precast bridge deck elements. *Journal of Bridge Engineering*, 22(7), 04017031.
- [11] French, C. E., Shield, C. K., Klaseus, D., Smith, M., Eriksson, W., Ma, Z. J., ... & Chapman, C. E. (2011). Cast-in-place concrete connections for precast deck systems (No. NCHRP Project 10-71).
- [12] Perry, V., Krisciunas, R., & Stofko, B. (2014). Mackenzie River Twin Bridges: North America's Largest Field-Cast Ultra-High-Performance Concrete Connections Project. *PCI Journal*, 59(2).
- [13] Sritharan, S., Aaleti, S., Garder, J., Bierwagen, D., & Abu-Hawash, A. (2012). Use of ultra-high performance concrete in bridge design. US-Japan Cooperative Program in Natural Resources.
- [14] ACI Committee 548, Polymers in Concrete, & Fowler, D. W. (1992). Guide for the Use of Polymers in Concrete. American Concrete Institute.
- [15] Ribeiro, M. C. S., Tavares, C. M. L., & Ferreira, A. J. M. (2002). Chemical resistance of epoxy and polyester polymer concrete to acids and salts. *Journal of Polymer Engineering*, 22(1), 27-44.
- [16] Reis, J. M. L., & Ferreira, A. J. M. (2003). Fracture behavior of glass fiber reinforced polymer concrete. *Polymer testing*, 22(2), 149-153.

- [17] Fowler, D. W., & Paul, D. R. (1979). Polymer Concrete Repair of Bridge Decks (No. FHWA/TX-79-02+ 114-8 Intrm Rpt.). US Department of Commerce, National Technical Information Service.
- [18] Fontana, J. J., Webster, R., & Kukacka, L. E. (1978). Rapid patching of deteriorated concrete using polymer concrete (No. BNL-24217; CONF-781020-2). Brookhaven National Lab., Upton, NY (USA).
- [19] Fowler, D. W., Meyer, A. H., & Paul, D. R. (1983). Implementation manual for polymer concrete repair. Center for Transportation Research.
- [20] Kukacka, L. E., & Fontana, J. (1977). Polymer concrete patching materials (Vol. 77, No. 11). Department of Transportation, Federal Highway Administration, Office of Development, Implementation Division.
- [21] Whitney, D. P., & Fowler, D. W. (2015). New applications for polymer overlays. In *Advanced materials research* (Vol. 1129, pp. 277-282). Trans Tech Publications Ltd.
- [22] Dinitz, A. M., & Ferri, R. (1985). Polymer Concrete (MMA) for Bridge Rehabilitation Applications. Special Publication, 89, 141-160.
- [23] Hsu, M., & Fowler, D. W. (1985). Creep and fatigue of polymer concrete. Special Publication, 89, 323-342.
- [24] Mantawy, I., Chennareddy, R., Genedy, M., & Taha, M. R. (2019). Polymer concrete for bridge deck closure joints in accelerated bridge construction. *Infrastructures*, 4(2), 31.
- [25] ASTM. (2014). ASTM C469: Standard test method for static modulus of elasticity and poisson's ratio of concrete in compression. West Conshohocken, PA: American Society for Testing and Materials.
- [26] ASTM, C. C580 Standard Test Method for Flexural Strength and Modulus of Elasticity of Chemical-Resistant Mortars, Grouts, Monolithic Surfacing, and Polymer Concretes.

- [27] Naaman, A. E. (2007, December). High performance fiber reinforced cement composites: classification and applications. In CBM-CI international workshop, Karachi, Pakistan (pp. 389-401).
- [28] Wille, K., Naaman, A. E., El-Tawil, S., & Parra-Montesinos, G. J. (2012). Ultra-high performance concrete and fiber reinforced concrete: achieving strength and ductility without heat curing. *Materials and structures*, 45(3), 309-324.
- [29] Graybeal, B. A., & Baby, F. (2013). Development of Direct Tension Test Method for Ultra-High-Performance Fiber-Reinforced Concrete. *ACI Materials Journal*, 110(2).
- [30] Nguyen, D. L., Ryu, G. S., Koh, K. T., & Kim, D. J. (2014). Size and geometry dependent tensile behavior of ultra-high-performance fiber-reinforced concrete. *Composites Part B: Engineering*, 58, 279-292.
- [31] Pyo, S., Wille, K., El-Tawil, S., & Naaman, A. E. (2015). Strain rate dependent properties of ultra high performance fiber reinforced concrete (UHP-FRC) under tension. *Cement and Concrete Composites*, 56, 15-24.
- [32] Kim, J. J., & Reda Taha, M. (2014). Experimental and numerical evaluation of direct tension test for cylindrical concrete specimens. *Advances in civil engineering*, Vol. 2014, Article ID 156926. <https://doi.org/10.1155/2014/156926>
- [33] Zhou, Z., & Qiao, P. (2020). Direct Tension Test for Characterization of Tensile Behavior of Ultra-High Performance Concrete. *Journal of Testing and Evaluation*, 48(4).
- [34] AASHTO (American Association of State Highway and Transportation Officials). AASHTO LRFD Bridge Design Specifications, 7th ed.; American Association of State Highway and Transportation Officials: Washington, DC, USA, 2014.
- [35] PCI (Precast/Prestressed Concrete Institute) PCI Bridge Design Manual, 3rd ed.; First Release, 2011.
- [36] Aboukifa, M., Moustafa, M. A., Itani, A. M., & Naeimi, N. (2019). Durable UHPC Columns with High-Strength Steel (No. ABC-UTC-2013-C3-UNR02-Final). Accelerated Bridge Construction University Transportation Center (ABC-UTC).

- [37] Aboukifa, M., Moustafa, M. A., & Itani, A. M. (2020). Comparative Structural Response of UHPC and Normal Strength Concrete Columns under Combined Axial and Lateral Cyclic Loading. ACI SP 341. 71-96.
- [38] ASTM C39. Standard Test Method for Compressive Strength of Cylindrical Concrete Specimens. American Society for Testing and Materials Standard Practice C39, Philadelphia, PA, 2001.
- [39] ASTM C579-18. Standard Test Methods for Compressive Strength of Chemical-Resistant Mortars, Grouts, Monolithic Surfacing, and Polymer Concretes. West Conshohocken, PA; ASTM International, 2018.

## 4 MECHANICAL CHARACTERIZATION AND MATERIAL VARIABILITY EFFECTS OF EMERGING NON-PROPRIETARY UHPC MIXES FOR ACCELERATED BRIDGE CONSTRUCTION FIELD JOINTS

*This chapter is a standalone paper that has been published in the journal of Construction and Building Materials*

### **Abstract**

Accelerated bridge construction (ABC) field joints, e.g. precast deck panels joints, are among the common structural applications of ultra-high performance concrete (UHPC). The higher cost and limited availability of commercial UHPC products have motivated researchers to develop non-proprietary UHPC (NP-UHPC) using locally available materials. One of these efforts is the recent work by the ABC University Transportation Center (ABC-UTC) in the United States to develop NP-UHPC mixes for use in ABC field joints. This paper documents the ABC-UTC mix design and proportions and has two main objectives. First, provide a full material characterization of such mix to allow for future replication and use of this material for different bridge applications as well as modeling purposes. Second, investigate the effect of material sourcing and variability, such as fine aggregate types and particle gradation, on the main mechanical properties of the material. The material characterization tests included flowability, compression, flexure, and direct tensile tests of the NP-UHPC mixes. The results from these tests are then compared with various proposed equations from the literature to verify their validity for use with the considered NP-UHPC mixes.

### **4.1 Introduction**

Ultra-high performance concrete (UHPC) is a new class of advanced construction materials with enhanced mechanical and durability properties due to steel fiber reinforcement, low water to binder ratio, and optimized particle packing density [1-3]. UHPC typically consists of a well-graded mixture of Portland cement, silica fume, ground quartz, high-range water reducer (HRWR), fine sand, and discontinuous steel fiber reinforcement [4,5]. Typical compressive strength of UHPC may exceed 21.7 ksi (150 MPa) with a sustained post-



cracking tensile strength of at least 0.72 ksi (5 MPa) [6]. The unparalleled properties of UHPC have motivated the bridge engineering community to implement it in various applications, such as accelerated bridge construction (ABC) field joints, over the past two decades [7]. However, most of the current implementations of UHPC worldwide use mostly commercial proprietary UHPC products, and until a few years ago, there was even only one commercial product available in the United States [8]. The proprietary nature of UHPC along with the high cost and limited availability of the material have motivated transportation agencies along with academic and industrial research to find other alternative materials for ABC field joints [e.g. 9]. Some other research efforts focused on making UHPC more accessible and less expensive through the development of non-proprietary UHPC (NP-UHPC) mixes using locally available materials. Former studies [e.g. 10] demonstrated that it is possible to develop NP-UHPC with a compressive strength greater than 30 ksi (200 MPa) without requiring any special treatment conditions. Due to the high number of these research efforts, a FHWA report was published to summarize some of these research findings to accelerate the use of NP-UHPC and promote more resilient US transportation infrastructures [8].

Many state departments of transportation (DOTs) have funded research on developing and testing several NP-UHPC mixes using locally available materials in their states for use in different bridge applications [e.g. 11-13]. A recent contribution in this area is the multi-institutional collaboration in the US between five consortium universities within the ABC university transportation center (ABC-UTC), where the University of Oklahoma (OU) led the ABC-UTC NP-UHPC mix design [14-16]. In an earlier study by the authors [17], the ABC-UTC NP-UHPC was successfully implemented for full-scale bridge joints as illustrated in Figure 4.1. In that study [17], we compared the structural response of deck assemblies with commercial proprietary UHPC and ABC-UTC NP-UHPC field joints, and demonstrated that the developed NP-UHPC mixes can be efficiently used for such ABC connections. These results motivated this paper to provide a reference baseline comprehensive mechanical characterization of the ABC-UTC NP-UHPC.

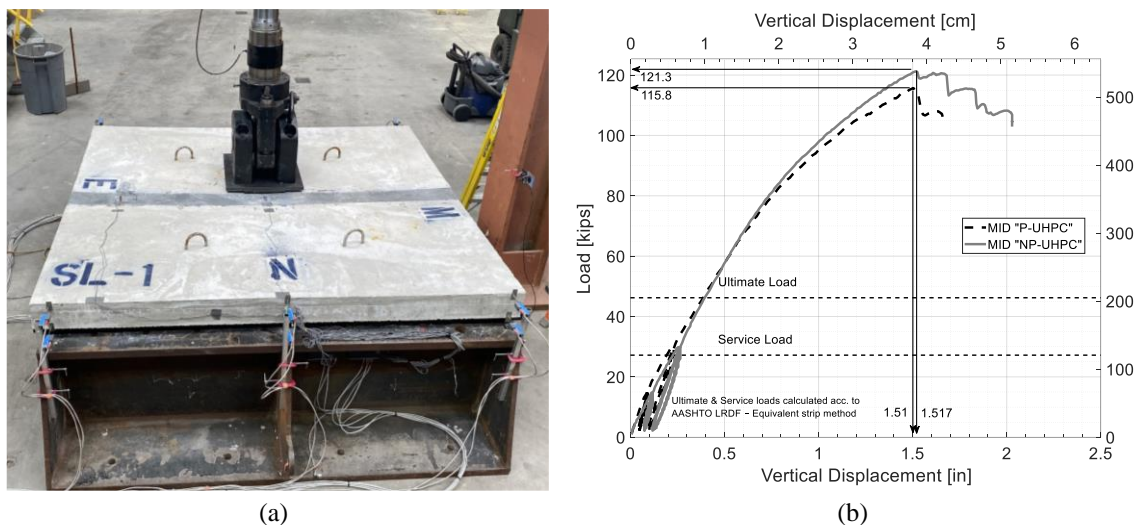


**Figure 4-1** (a) Test setup of precast deck assembly with longitudinal NP-UHPC field joint; (b) comparison of load-deflection relationships of specimens with proprietary UHPC and ABC-UTC NP-UHPC

The first goal of this study is to characterize the main physical and mechanical properties of the ABC-UTC NP-UHPC mix when produced using different materials from various regions of the US (mostly Western US). The documented work herein provides confidence in reproducing desired UHPC mix characteristics and mechanical behavior from different materials that vary from original development. Material characterization and mix repeatability is needed for expanding future implementation of NP-UHPC mixes for ABC applications and field joints. The main physical and mechanical characterization investigated in this study considered flow tests of the fresh mixes and compression, flexural, and direct tension tests of hardened UHPC at different ages. For full documentation, this paper delivers the necessary information on the mix design, sourcing of the material ingredients, and mixing procedure of the developed NP-UHPC mixes. The second goal of this study is to investigate the variability effects of using different materials and sources, i.e. using different fine aggregate (sand) types and particle grading, on the main mechanical properties of the developed NP-UHPC mixes. Results from the different tested NP-UHPC mixes are also used here to check the validity of existing mechanical behavior equations, which have been mostly developed using commercial UHPC mixes, for representing NP-UHPC.

## **4.2 Background on Developing Non-proprietary UHPC**

This section provides a brief literature review and background on the previous work by OU on the development of the ABC-UTC NP-UHPC mix in terms of mix design, proportioning, material constituents, and mixing methodologies.

### ***4.2.1 Mix Design***

Among the various recent NP-UHPC development efforts, researchers from OU developed a NP-UHPC mix for Oklahoma DOT using their local materials [16]. The final NP-UHPC mix design was developed after establishing a wide parametric study that included evaluation of the particle packing density of a large number of different mix designs and comparison with the optimum packing curve generated from the Modified Andreasen and Andersen particle packing equation [18]. The mix design process investigated the effect of using different mixing proportions and combinations of various material ingredients. The final mix design included the replacement of the high cement ratio with almost 30% cement slag by weight to reduce the overall NP-UHPC mix cost. Research at OU used the final mix design in precast bridge deck joints and demonstrated acceptable behavior when compared to commercial UHPC formulations [19]. The final NP-UHPC mix developed by OU was selected as the main candidate for the ABC-UTC NP-UHPC initiative. Figure 4.2 provides the mix design in the form of components and mixing proportions and more details can be found in [16, 19]. As part of the ABC-UTC collaborative effort, one task we undertook at the University of Nevada, Reno (UNR) is to reproduce the original OU mix using the locally-sourced Oklahoma set of materials, then identify and employ comparable materials from western US regions such as Nevada and California. This paper presents the several NP-UHPC mixes sampled and produced at UNR along with results from the selected mechanical tests for comparison and assessment purposes.

### ***4.2.2 Mixing Proportions***

The mixing proportions of the baseline NP-UHPC mix using 1% and 2% steel fibers by volume are shown in Figures 4.2a and 4.2b, respectively. As a reference to the developed mixes and for further comparisons, the composition of a typical commercial UHPC product

that incorporates 2% steel fibers by volume, as obtained from the FHWA report [4], is shown in Figure 4.2c. Figure 4.2d shows the range of the mixing proportions of the seven different NP-UHPC mix designs which were recommended by the FHWA for the Northeast, upper Midwest, and Northwest regions [8]. It is noted that the mixing proportions of these seven mixes were proposed without the addition of steel fibers, and in turn, should be adjusted when fibers are added. The volume percentage of steel fibers added to the mix should be replaced with the same volumetric amount of aggregate [8].

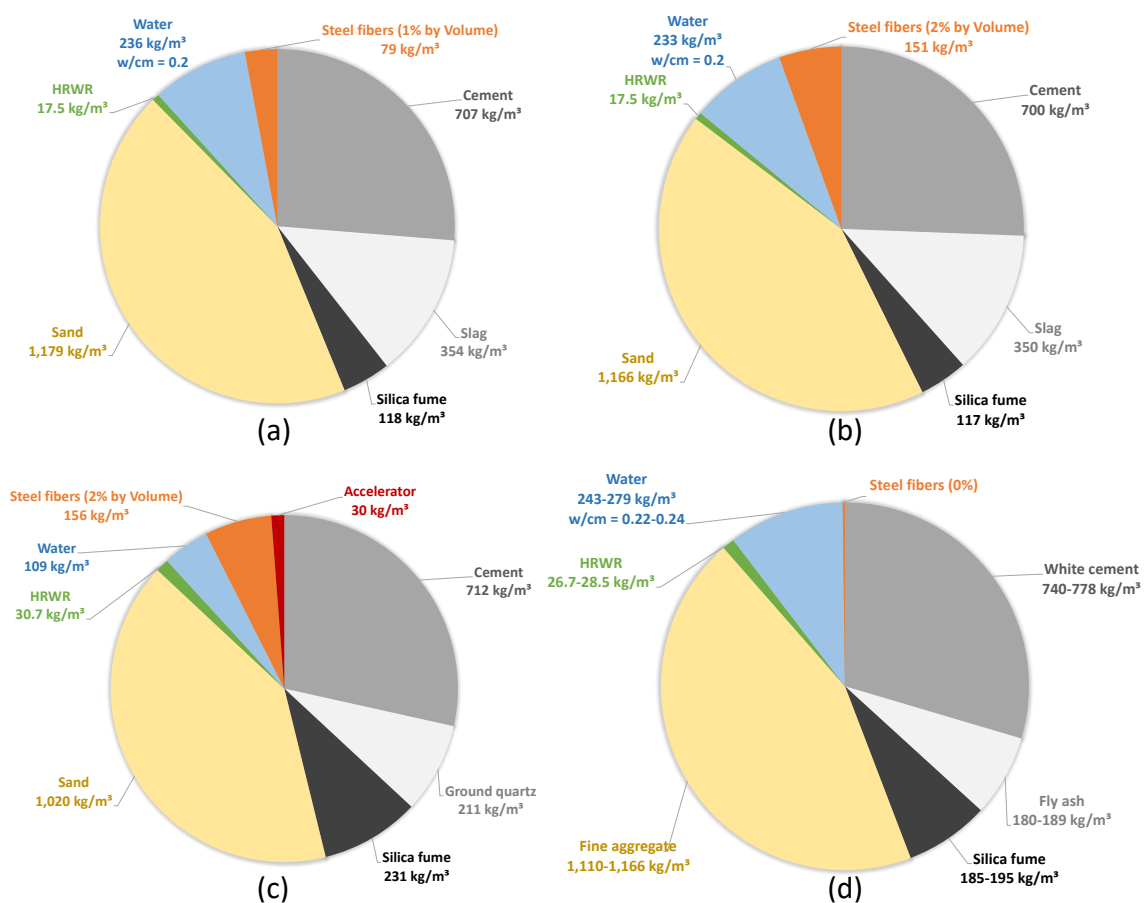


**Figure 4-2** Mixing proportions of: (a, b) ABC-UTC NP-UHPC baseline mix with 1% and 2% steel fibers, (c) typical commercial UHPC mix reported in [4], and (d) FHWA NP-UHPC mixes reported in [8]

### 4.2.3 Material Constituents

Most of the NP-UHPC mixes reported in the literature were developed through the mixing and proportioning of six or more main ingredients as briefly reviewed in this section.

Cement is a primary ingredient of any NP-UHPC mix as it acts as the main binder in the UHPC matrix. At least 20% of the total volume of UHPC is cement [20]. The typical volume of the cementitious paste in the UHPC mixes ranges from 50% to 75% [4,11,21]. Many previous studies investigated the effect of using different types of cement on the flow properties and compressive strength of the developed NP-UHPC mixes [8,21,22]. Most of the work recommended the use of type I/II Portland cement due to its low content of cement tricalcium aluminate ( $C_3A$ ) that can reduce the required amount of water, decrease the developed hydration heat, and provide better performance for UHPC [e.g. 23]. Because of the low water to cement ratios (w/c) in the typical UHPC mixes, the cement amount in the mix is not fully hydrated and the remaining un-hydrated cement particles act only as a filler material. Thus, many researchers have investigated the effect of replacing a percentage of cement with diverse supplementary cementitious materials (SCMs) such as silica fume, slag cement, fly ash, and quartz powder [20]. This study included 40% replacement of the cement with slag (30%) and silica fume (10%) to reduce cost and increase particle packing density.

Silica fume is one of the byproducts of the production of the Ferrum-silicon alloy and it is a common SCM used in UHPC. Due to the very fine particle size of the silica fume, which usually has a mean average of 0.1-0.3 micrometer, it is used in the UHPC mixtures as a micro filling material to physically fill the gaps between the mixture particles and generally improve the packing density of the mixture. Many researchers have investigated the effect of varying the percentage of silica fume on the flow properties and strength of the NP-UHPC mixes. In various NP-UHPC mix design guidelines, the content of silica fume ranges from 21% to 50% of cement weight [e.g. 4,11,12]. However, in some of the cases, the high content of silica fume has resulted in more entrapped air voids because of the lower flowability [20]. Consequently, research efforts have optimized silica fume dosage to only 14% [20] and 20%-30% [21] by cement weight. The silica fume content used in the present study is approximately 17% of the cement mass.

Slag cement is another SCM that is a byproduct of the steel industry and is known as ground granulated blast furnace slag (GGBS). Slag cement in the UHPC mixture undergoes

pozzolanic reactions that result in a denser UHPC matrix, enhanced workability, reduced permeability and carbon footprint [24]. However, other studies [25, 26] showed that slag replacement could reduce compressive strength of UHPC if half the cement is partially substituted by slag cement or result in a less flowable fresh mix. Due to its wide range of effects, some studies focused on optimizing the dosage of slag cement and recommended it to be somewhere between 20% [26] and 30% [20]. The ABC-UTC NP-UHPC uses a 30% replacement of the used cement with slag cement.

A key component of UHPC that is responsible for various aspects of the unparalleled mechanical properties such as higher tensile strength and ductility, is steel fibers. Straight steel fibers with 0.2 mm diameter and 13 mm length are the most frequently used type in UHPC as they could provide the best performance [8]. Since the steel fibers are the most expensive component of UHPC mixes, their dosage should be carefully controlled and optimized to provide attractive and less expensive alternative NP-UHPC mixes. The ABC-UTC NP-UHPC has implemented the usage of both 1% and 2% steel fibers by volume as two alternative NP-UHPC mix solutions.

HRWR is a chemical admixture that is added to UHPC mixes to enhance workability and is also known as a superplasticizer. HRWR is mainly added to account for the significantly less water content typically used in the UHPC formulations to ensure adequate flow properties and self-consolidation of the fresh mix. The most common type of HRWR reported in the literature [e.g. 12, 20, 27] in the development of NP-UHPC and used herein, is the polycarboxylate ether-based HRWR. The required amount of HRWR is usually adjusted based on the w/c to provide the desired workability of the fresh mix. For example, it is recommended to use 1% by cement weight polycarboxylate ether-based HRWR when combined with a 0.22 w/c ratio [27]. It is noted that the state-of-the-art FHWA reports [4, 8] recommended to use this w/c ratio of 0.22 for developing UHPC but use less water amount for NP-UHPC matrices with coarse aggregate than the ones with fine aggregates. It is also noted that many studies have recommended partial or full replacement of water with crushed ice in case of mixing UHPC at temperatures that exceeded 25°C [e.g. 28]. For

the ABC-UTC NP-UHPC, a 1.5% by cement weight HRWR is used in combination with a 0.20 w/c ratio.

The last major component of UHPC is aggregate. Most of the developed NP-UHPC mixes use a high percentage of fine aggregates or coarse aggregates [e.g 29]. Natural fine sand is the most commonly reported type of UHPC fine aggregate in the literature. The optimum binder to the aggregate ratio for the typical NP-UHPC mixes found in the literature is 1.0 or 1.1 [8, 30]. These optimal values were suggested to reduce the shrinkage of the developed NP-UHPC mixes [30] and provide adequate volume and cost-effective NP-UHPC mixes. A binder to the aggregate ratio of 1.0 is adopted for the ABC-UTC NP-UHPC in the present study.

#### ***4.2.4 Mixing Methodology***

The mixing and placing procedures of UHPC can affect its mechanical properties and must be appropriately coordinated to achieve consistency of the developed mixes. The mixing of UHPC usually requires a time-specific procedure to maintain the uniformity of the mixed constituents in the UHPC mix. The over-mixing or under-mixing of the UHPC should be avoided. The mixing methodology adopted in this study for the ABC-UTC NP-UHPC includes the initial mixing of all the dry components, i.e. cement, sand, silica fume, and slag, for 10 minutes. Afterward, the required amount of water is mixed with half the superplasticizer amount and gradually added to the mix over the course of two minutes and mixing continues for another minute. Next, the other half amount of the superplasticizer is added over the course of one minute and mixing continues for an additional 5-10 minutes until the mix turns flowable and more like a paste. Finally, the steel fibers are gradually added over the course of two minutes and mixing continues for another two minutes before the NP-UHPC batch is ready for casting. For this study, all the NP-UHPC mixing was done at UNR using a high shear mixer (Imer Mortarman 360).

#### **4.3 Variability Study**

As mentioned earlier, one of the main objectives of the present experimental work is to reproduce and understand the variation in the ABC-UTC NP-UHPC mechanical properties

when using different materials. The sought variability had two components: (1) material sourcing variability associated with utilizing different material sources from different regions of the country, and (2) aggregate type and grading variability through the using of fine masonry sand or sieved and non-sieved crushed aggregate sand in the NP-UHPC mixes. Accordingly, five different NP-UHPC mixes were produced and used in this study. More details on the two components of the variability along with a summary of the five different mixes utilized herein are provided in this section.

#### ***4.3.1 Material Sources Variability***

Different sets of materials for the ABC-UTC NP-UHPC mix were acquired using the locally available materials in the Midwest/South region (as provided by our collaborators from OU) versus what we identified and procured in the Western region. All mixing proportions followed the same baseline AB-UTC NP-UHPC mix (see Figure 4.2 above). The main objective of this part of the study again is two-fold. The first part is to verify the repeatability of baseline mix and mechanical characteristics if independently produced by a different team using different equipment and in a different setting. The second part is investigating the reproducibility of the baseline mix using a whole different set of materials locally supplied in the NV and CA regions. Verifying repeatability or reproducibility was established by relating and comparing various mechanical properties as discussed in the next section. Table 4.1 shows a list of the material suppliers and material types used in for both reproducibility and repeatability of the ABC-UTC NP-UHPC using materials from Western US (acquired by UNR) and Midwest/South US (provided by OU), respectively.

#### ***4.3.2 Aggregate Types and Grading Variability***

For most of the NP-UHPC constituents, these are commercial products that satisfy respective ASTM standards and follow rigorous quality control through production. However, for sand and fine aggregates, there are thousands of types available in the US market and their properties differ from one region to another. Hence, there are high levels of uncertainty associated with the random particle size gradation and variation of sand or aggregate types, which could significantly affect the characteristics of a certain NP-UHPC



mix. Thus, the objective of this part of the study is to investigate whether the characteristics of the ABC-UTC NP-UHPC, originally designed using fine masonry sand for fine aggregate, can be reproduced using other locally available types of sand in the west, especially in NV. If successful, this investigation will provide a foundation for the wide future implementation of NP-UHPC mixes across different regions of the country using different sand types and gradation. The type of sand acquired by UNR is a blend of well-graded small-size crushed aggregates added to fine and medium sand. The maximum size of the crushed aggregates is less than 4.76 mm. The crushed aggregate sand is locally known as concrete sand as it is usually used in the production of conventional concrete.

**Table 4-1** Material constituents and local suppliers of the NP-UHPC mixes used in this study.

Material	Acquired by UNR		Provided by OU	
	Type/Name	Supplier	Type/Name	Supplier
Cement	Type I/II	Nevada Cement, Reno-NV	Type I	Ash Grove, Chanute-KS
Silica Fume	MasterLife® SF100	BASF	Norchem	Norchem, Marietta-OH
Slag	Slag Cement	Lehigh Hanson, Sacramento-CA	Lafarge Slag	LafargeHolcim, South Chicago-IL
Steel Fibers	Dramix® OL 13/0.2	Bekaert	Dramix® OL 13/0.2	Bekaert
HRWR	MasterGlenium®79 20	BASF	MasterGlenium®7920	BASF
Aggregate	Crushed Aggregate Sand	Martin Marietta, Sparks-NV	Fine Masonry Sand	Metro Materials, Norman-OK
Water	Potable Water	N/A	Potable Water	N/A

In the literature, many types of sand and aggregates have been used in the development of local NP-UHPC mixes such as masonry sand, river sand, silica sand, quartz sand, basalt, limestone, and volcanic rock as mentioned before. In general, fine sand has been the most common type. However, using coarse aggregate or a mix of various aggregate sizes in NP-UHPC mixes has been widely considered to study its effect on strength. The FHWA study [8] showed that the NP-UHPC matrices with fine aggregated exhibit a slightly higher compressive strength than the coarse NP-UHPC matrices, but yet, allows the use of fine and coarse aggregates up to a maximum particle size of 9.5 mm [8]. Collepardi et al. [29]

showed that an equal volume replacement of fine ground quartz with a natural coarse aggregate with a maximum size of 8 mm did not affect the compressive strength. Another study by Arora et al. [31] showed that it is possible to achieve a higher packing density and high compressive and flexural strengths for the NP-UHPC mixes using a combination of three different coarse aggregate sizes (6.25 mm, 4.75 mm, and 2.36 mm) and two fine aggregate sizes (0.6 mm and 0.2 mm). Nevertheless, the large number of studies in the literature reported sizes between #8 (2.36 mm) and #18 (1 mm), which guided our selection at UNR. It is noted that the crushed aggregate sand used in the present study was also used in a former study at UNR to develop a NP-UHPC mix for seismic ABC connections for California DOT (Caltrans) [32, 33].

Careful sieving of crushed aggregate sand could be beneficial for enhancing the NP-UHPC mix strength, but it is also time- and labor-consuming and may prohibit scalability for large-scale applications. Thus, one other motivation of this study is to explore the use of raw crushed aggregate sand and establish a comparison between NP-UHPC mixes with and without the sieving procedure noted above. Accordingly, three types of sand were used in this study (see Figure 4.3) as follows: (1) Type A denotes non-sieved crushed aggregate sand acquired by UNR; (2) Type B denotes sieved crushed aggregate sand acquired and processed by UNR; and (3) Type C denotes the fine masonry sand provided by OU. Before any mixing, all sand types were carefully dried in a controlled oven temperature of 250°C for 24 hours then left to cool down on-site for at least 48 hours. Sieve analysis according to ASTM C136 [34] was also done for the three sand types to evaluate and report the sand particle size distribution to allow for the future replication of the NP-UHPC mixes using similar sand types from other local sources. Figure 4.3 provides the particle size distribution curves of the three sand types used in this study.

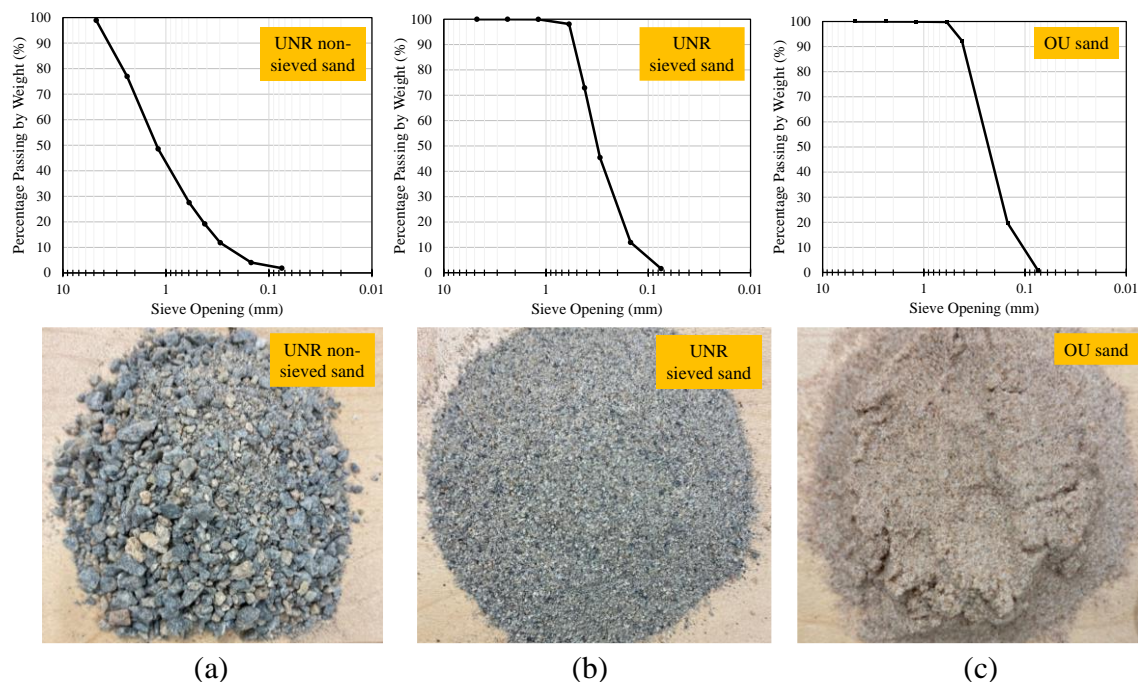


**Figure 4-3** Different sand types used in the various NP-UHPC mixes in this study: (a) UNR non-sieved crushed aggregate sand, (b) UNR sieved crushed aggregate sand, and (c) OU fine masonry sand.

### 4.3.3 NP-UHPC Mixes Summary

Based on the material and aggregate variability explained above, five NP-UHPC mixes were considered and experimentally tested through this study as shown in Table 4.2. It is noted that the steel fiber content was also considered as an additional variable.

**Table 4-2** Summary of five different NP-UHPC mixes used in this study

Notion	Prescriptive Batch ID*	Local materials acquired by	Steel fiber content (% by volume)	Sand type (as per Figure 4.3)
B1	B1 – UNR – 2% – NS	UNR	2 %	Type A
B2	B2 – UNR – 2% – S	UNR	2 %	Type B
B3	B3 – UNR – 1% – NS	UNR	1 %	Type A
B4	B4 – UNR – 1% – S	UNR	1 %	Type B
B5	B5 – OU – 2% – NS	OU	2 %	Type C

\*“NS” denotes non-sieved sand or raw sand, and “S” denotes sieved sand

## 4.4 Test Results and Discussion

This section provides the material and mechanical characterization test results of all five studied NP-UHPC mixes. For verifying repeatability, respective results from OU selected tests are used. Four types of tests were conducted and discussed here: flow tests, compression tests, flexural tests, and direct tension tests. The section also provides a detailed assessment of how the NP-UHPC test results relate to strength prediction equations available in the literature, which have been mostly developed based on commercially available proprietary UHPC mixes.

### 4.4.1 Flow Tests

UHPC is a highly flowable material that does not require special considerations such as tamping or vibration during placing or casting processes. Thus, the assessment of the flow properties of fresh mixes is one of the important criteria in developing NP-UHPC mixes with optimized particle packing density. The optimization of the mixture paste is usually associated with adequate flowability of the fresh mix and high compressive strength, which makes these two main properties the basic qualifiers for NP-UHPC mix development. The FHWA study [8] evaluates the efficiency of the newly developed NP-UHPC mixes based on a unitless efficiency parameter  $E$ , which is calculated based on the flowability, compressive strength, and material cost of the mixes. The flow of the freshly mixed UHPC has been frequently assessed in the literature using the test methods in ASTM C1856, C1437, and C230 [35-37], which are the methods adopted in this study. For typical flow tests, a sample of the fresh NP-UHPC mix was taken immediately after mixing, then poured into the flow cone mold to the full capacity. The cone was then removed gently upward one minute after the mixing completion to allow the paste to flow over the 255 mm diameter table. Then, the mortar was left to spread over the table for two minutes according to the ASTM C1856 standards [35] or until the flow become steady to measure the static flow of the mix. Finally, the flow table was dropped 25 times in 15 sec to measure the dynamic flow. The static and dynamic flows of the NP-UHPC were calculated based on the average of maximum and minimum diameters [35].

The ASTM C1856 specifies a flow limit between 200 and 250 mm, while different state DOTs and the FHWA require a flow of 179 to 250 mm [20]. However, based on the work at OU [19], it was found that a flow target of 250 mm can lead to steel fibers segregation as the fibers would not stay suspended at the flow, and hence, the study recommended a target flow value of 175 to 195 mm for the developed NP-UHPC mixes. Based on the above values, the assessment criteria followed here considers the mix appropriate if the static flow diameter is between 190 to 225 mm and the dynamic flow diameter is around 250 mm. It is noted that the flow of the NP-UHPC mixes can be greatly affected by the type and degree of fineness of sand. Thus, it is recommended to always test the flow properties of future mixes replication to ensure consistency and validity. If needed, a slight modification in the dosage of the HRWR based on the different sand types is also permitted to ensure that the flow of the NP-UHPC mixes is satisfying the recommended values.

The static and dynamic flow values of the five considered NP-UHPC mixes are shown in Figure 4.4. Photos of the static flow of the fresh NP-UHPC mixes are shown in Figure 4.5. The average of both static and dynamic flow measurements of the fresh NP-UHPC mixes falls within the specified flow requirements of the FHWA and ASTM C1856. It is noted that some of the mixes required slight adjustments to the HRWR to ensure consistent flow properties. The applied adjustments varied between  $-15\%$  to  $+10\%$  of the actual doses (see Figure 2) of the HRWR specified weights.

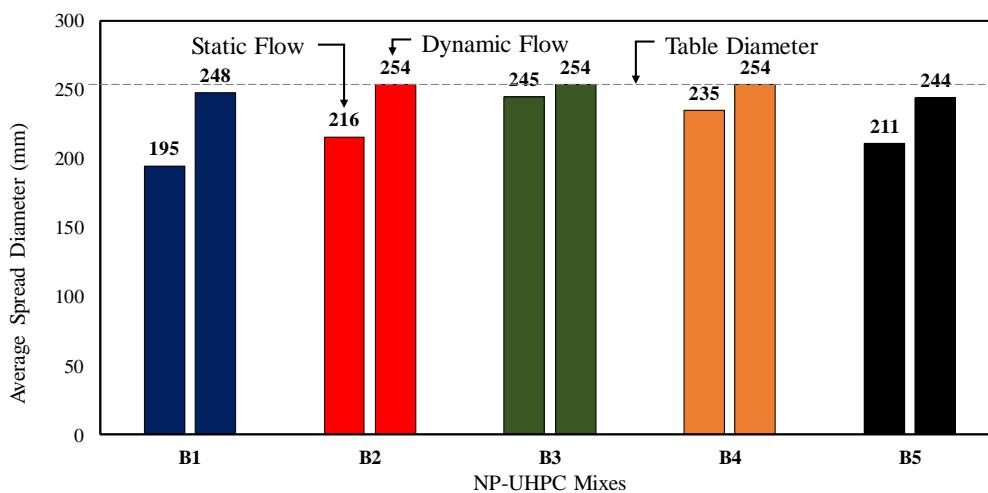


**Figure 4-4** Static and dynamic flow table measurements of the five different fresh NP-UHPC mixes.

The static flow measurements were typically within the 190-225 mm recommended flow limits, except for B3 and B4. All the dynamic flow measurements were around the recommended value of 250 mm. The photos in Figure 4.5 show that the fresh mixes with fine sands had a consistent steel fibers distribution over the flow spread. Oppositely, the fresh mixes with non-sieved sand (i.e. B1 and B3) are shown to have an accumulation of the steel fibers around the bigger particle sizes of the crushed aggregates in the mix. This accumulation is very clear in the B1 with the 2% steel fiber amount, while it is negligible in B3 with the 1% steel fiber amount.



**Figure 4-5** Static flow of the fresh NP-UHPC mixes.

#### **4.4.2** *Compression Tests*

UHPC is known for its superior compressive strength which is almost 5-6 times that of the conventional concrete. Research studies, reports by FHWA, and different state DOTs, and ASTM commonly specify minimum compressive strength values to categorize a material as UHPC. For example, ASTM C1856 [35] and FHWA [8] specify a minimum 28-day compressive strength of 117 and 150 MPa, respectively to define UHPC. However, for emerging NP-UHPC mix development, more economic mixes based on the application might not require a very high compressive strength. For the ABC-UTC NP-UHPC mix, the main goal is to provide a robust material for ABC field joints. Thus, a target compressive strength of about 120 MPa was set for such development. Meanwhile, it is also important to keep in mind that for ABC applications, emerging guidelines [e.g. 38] do not recommend opening the bridge for traffic or removing formwork unless the UHPC reaches a minimum compressive strength of 97 MPa.

#### 4.4.2.1 Test procedure and specimens preparation

According to the test standards ASTM C1856 [37], it is recommended to use a modified version of the ASTM C39 [39] to determine the compressive strength of the UHPC. The modification includes testing of 3×6 in (7.6×15.2 cm) cylinders under a rate of loading of 1 MPa/s. Note that increasing the loading rate has a negligible effect on the measured strength [40]. Moreover, the test cylinders should be prepared by grinding the ends to a certain tolerance in lieu of capping or other sample preparation methods. In this study, previous expertise among the research team and dedicated equipment [28, 41] have been leveraged to carefully prepare and use cylinders for compressive testing as explained later. The compressive strength of the various NP-UHPC mixes was determined at different ages including 3, 7, 28, and 56 or 230 days (a consequence of COVID-19 full shut down in April 2020). Three 3×6 in (7.6×15.2 cm) UHPC cylinders were prepared and tested at each age from each NP-UHPC mix. A satec compression machine with a loading capacity of 500 kips (2220 kN) was used at a rate of approximately 150 psi/s (1 MPa/s) for all tests (see Figure 4.6 a).



**Figure 4-6** Compression testing of NP-UHPC cylinders: (a) test setup; (b) grinding machine for cylinder preparation; and (c) views of typical NP-UHPC cylinder through preparation sequence.

Previous studies [e.g. 4] have investigated the effect of various curing conditions such as steam curing at elevated temperatures, high moisture conditions, and ambient-cured

conditions on the compressive strength of UHPC. Special curing like steam curing is not always practical for real bridge applications and the ambient curing conditions are more feasible and appropriate for many applications [42]. Thus, in the present study, all test cylinders were left in the fabrication yard for one day after mixing before transferring them to a temperature-controlled room with normal humidity and room temperature of about 73 °F (~ 23 °C). The test specimens were continuously subjected to the described curing conditions up to approximately two hours before compression testing to allow some time for cylinders preparation. Cylinders preparation aimed at removing the weak top layer, which could lead to underestimating the compressive strength of UHPC cylinders if not removed, then grinding the two ends as per ASTM C1856 [35] provisions to ensure perpendicularity and planeness. A saw cutting machine was used to remove the top weak crust of the UHPC cylinders and a special hydraulic grinding machine was used for end grinding as shown in Figure 4.6b. The test cylinders had a final length to diameter ratio after preparation between 1.86 and 1.93. Figure 4.6c shows photos of the NP-UHPC cylinder ends following the previously mentioned sequence.

#### 4.4.2.2 *Compressive strength gain*

The measured compressive strength versus age of the NP-UHPC mixes is plotted in Figure 4.7. Each data point in the curves represents the average measured compressive strength obtained from three test cylinders at a certain age. Many efforts in the literature have investigated the compressive strength gain of commercial UHPC products, and they recommended equations to predict the strength of UHPC cured at laboratory temperature 73 °F (~ 23 °C) based on the age of concrete [5,42]. These equations are yet to be verified for emerging NP-UHPC mixes such as the ones presented in this study. Two equations proposed by Graybeal [5, 42] were selected for assessment and plotted in comparison with the measured strength of the NP-UHPC mixes in Figure 4.7. The first equation (Equation 4-1 below) was initially proposed by Graybeal [5] based on regression analysis of the compression test results of commercial UHPC cured under standard laboratory conditions for any time after 0.9 days. Graybeal [42] then revised the equation with a focus on readily available UHPC for ABC field connections. The updated equation (Equation 4-2) can be used for UHPC cured at three different temperature conditions, i.e. 105 °F (~ 40 °C), 73 °F



(~ 23 °C), and 50 °F (~ 10 °C), and provides a relationship between the compressive strength, curing temperature, and age. For such, Equation 4-3 can be used to determine the time to initiation of the strength gain.

$$f'_{c,t} = f'_c \left[ 1 - \exp \left( - \left( \frac{t - 0.9}{3} \right)^{0.6} \right) \right] \quad (4-1)$$

$$f'_{c,t} = f'_c \left[ 1 - \exp \left( - \left( \frac{t - t_{start}}{a} \right)^b \right) \right] \quad (4-2)$$

$$t_{start} = 2.8 / \sqrt{T} \quad (4-3)$$

where,  $f'_{c,t}$  is compressive strength at age “ $t$ ” days after mix initiation;  $t$  is time after casting in days;  $f'_c$  is UHPC compressive strength at 28 days;  $t_{start}$  is time of initiation of strength gain in days;  $T$  is the curing temperature in degrees Celsius;  $a$  is a fitting parameter in days (for 23 °C,  $a = 1.0$  day); and  $b$  is a dimensionless fitting parameter (for 23 °C,  $b = 0.3$ ).

Figure 4.8 shows the results of the compressive strength gain of the NP-UHPC mixes along with its comparison against two other commercial UHPC mixes reported in the literature [40,42]. As mentioned earlier, each data point on the curve represents the average result of three test specimens. Hence, error bars were added to Figure 4.8 to show the upper and lower bound deviations of the specimen's results from the average plotted values. Generally, most of the data points have deviations less than 5 MPa which is typically below 5% of the average compressive strength value. Both mixes represented the commercial product Ductal JS1100RS (rapid strengthening UHPC) but the premix materials had different ages at the time of casting. Both mixes had steel fibers of 2% by volume and added accelerator admixture and were cured at 73 °F. From the figures, it is observed that all the NP-UHPC mixes satisfied the minimum compressive strength of 117 MPa, which was specified by the ASTM C1856. Most of the mixes also reached the 97 MPa compressive strength limit after approximately 7 days; the threshold recommended for opening bridges for traffic or removing formwork. Both equations were able to closely predict the compressive strength gain of the developed mixes at the early ages and up to

around 56 days. It is clearly shown that Equation 4-3 slightly overestimates the strength of the NP-UHPC during the first week as this equation is mainly developed for the UHPC mixes that use accelerator admixtures or agents in their mixtures.

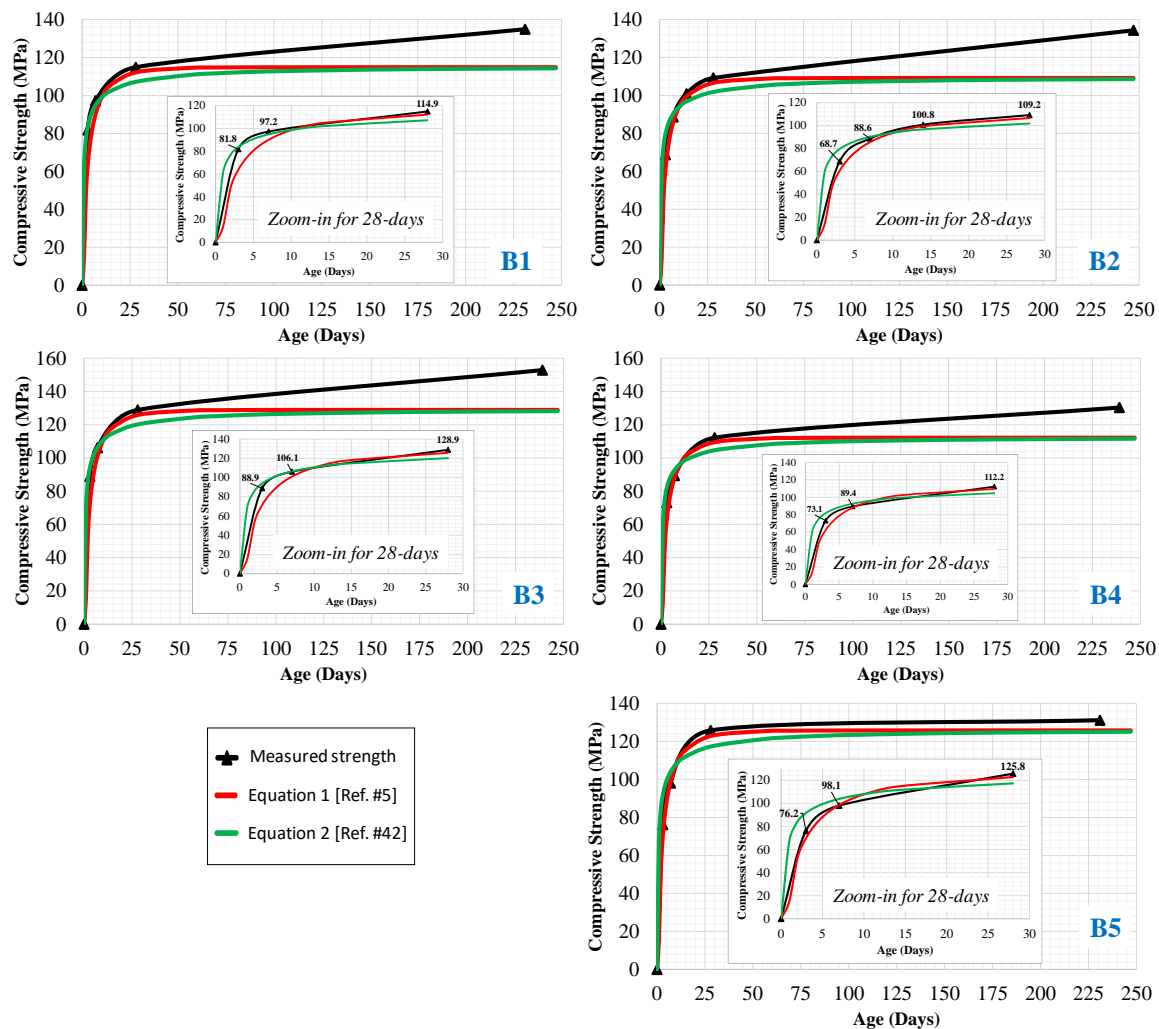


**Figure 4-7** Compressive strength gain of NP-UHPC mixes in comparison with prediction equations [5, 42].

The NP-UHPC mixes with 2% steel fibers have very comparable compressive strength and strength gain over time, while the mixes with 1% steel fibers are more scattered with around 20 MPa difference. This concludes that the compressive strength of the mixes with 2% steel fibers is less sensitive to the variability in the aggregate type or the source of the materials. While the compressive strength of the mixes with 1% steel fibers is more dependent on the type of aggregate used in the mix. The NP-UHPC mixes with local

materials sourced by UNR and non-sieved sand (i.e. B1 and B3) have a higher compressive strength and more rapid early strength gain. B3 has the highest compressive strength among all the developed NP-UHPC mixes, hence it is recommended for future implementation in large-scale applications.

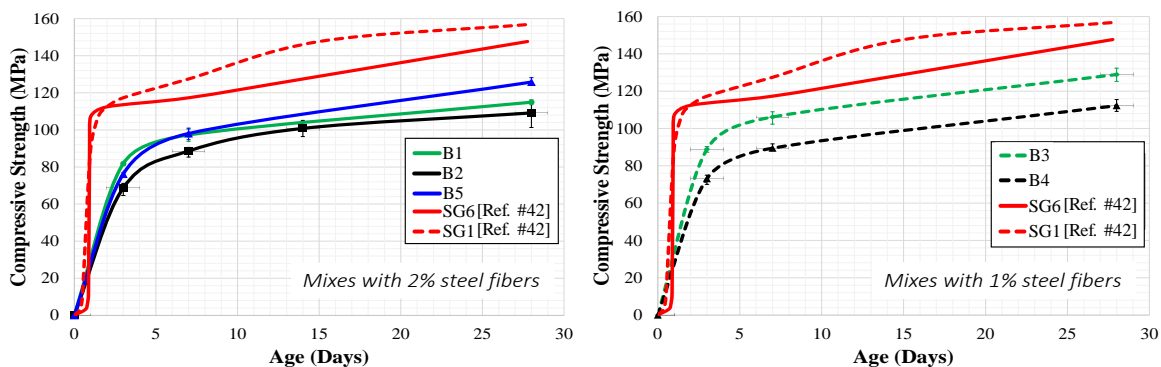


**Figure 4-8** Compressive strength versus time for mixes with 2% (left) and 1% (right) steel fibers.

#### 4.4.2.3 Full compression stress-strain behavior

The full compressive stress-strain behavior and elastic modulus of the NP-UHPC cylinders were determined according to the ASTM standards C469 [43] along with ASTM C1856 [35]. It is noted that only a few studies have reported full stress-strain curves for commercial UHPC [e.g. 41], and much less even considered NP-UHPC. Thus, this paper also fills a knowledge gap in this area by providing sufficient information about the full compression and tension behavior of NP-UHPC, which is crucial for modeling [e.g. 44-46] and future expansion of UHPC use. The curing and preparation of the test samples followed the same procedure used before for the compressive strength testing. The test samples were tested at ages between 231 and 247 days. These specimens were initially prepared to be tested after 56 days while the tests were delayed because of the COVID-19 related laboratory shut down and operation resumption. The test specimens were fully instrumented using three displacement transducers (LVDTs) to determine the full stress-strain relationship of the different mixes Figure 4.9 shows the test setup and instrumentation. The same loading rate of approximately 1 MPa/s was applied throughout all the tests.

Figure 4.10 shows the average compressive stress-strain response of the developed NP-UHPC mixes in comparison to the previously proposed constitutive stress-strain equations (Equations 4-4 to 4-6 below) reported in the literature [47, 48]. The constitutive stress-strain relationship of the UHPC is determined based on the deviation from the linear elastic response as shown in Equation 4-4 [47].

$$f_c = \varepsilon_c E (1 - \alpha) \quad (4-4)$$

$$\alpha = a e^{\frac{\varepsilon_c E}{b f_c}} - a \quad (4-5)$$

$$\alpha = a \left( \frac{\varepsilon_c E}{f_c} \right)^b \quad (4-6)$$

where  $f_c$  is compressive stress;  $\varepsilon_c$  is compressive strain;  $E$  is the actual measured modulus of elasticity based on the experimental results; and  $\alpha$  is linearity deviation parameter that is determined based on Equations 4-5 [47] or 6 [48]. The linearity deviation parameter  $\alpha$  usually varies depending on the different types of UHPC and different curing regimes and is calculated based on the fitting parameters (i.e.  $a$  and  $b$ ). Based on [47], the values for  $a$  and  $b$  for untreated regime are 0.011 and 0.44, respectively. However, Haber et al. [48] suggested Equation 6 for calculating  $\alpha$  with values for  $a$  and  $b$  are 0.106 and 2.754 at 23 °C, respectively, which was based on data from six different commercial UHPC products.

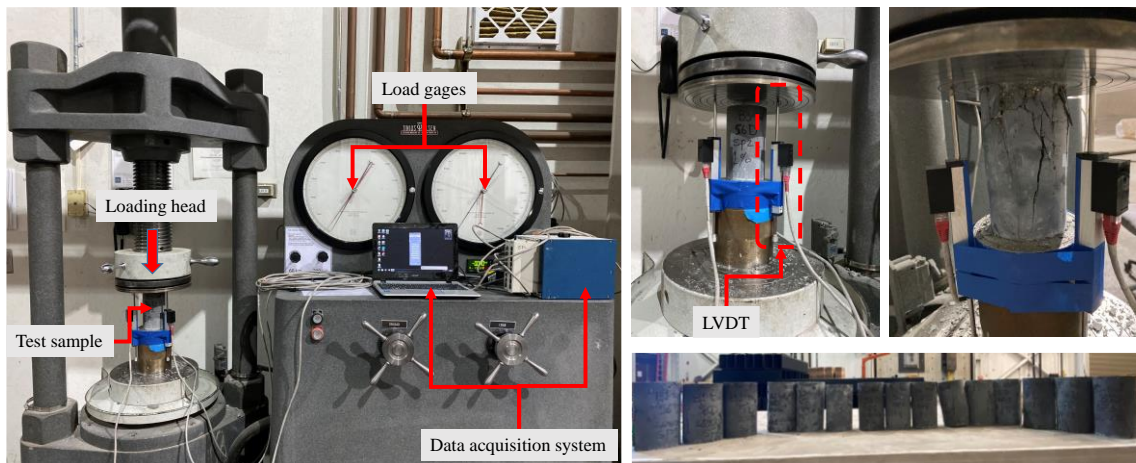


**Figure 4-9** Test setup of the compressive stress-strain behavior test.

As seen in Figure 4-10, the compressive stress-strain behavior of the developed mixes is almost linear up to approximately 50% of the maximum stress. A minor nonlinear response was observed when approaching the failure of the specimens, which is consistent with FHWA previous studies [47]. Moreover, the results from both equations are closely matching with the average response of the tested NP-UHPC mixes with a slight underestimation of compressive strength prior to failure.

Figure 4-11 shows the average compressive strains measured at the peak stress of the NP-UHPC mixes. The measured strains at the peak of all the developed mixes are very comparable as they ranged from 0.00432 (B5) to 0.00512 (B3). It was also observed that the strains of B3 and B4 with 1% steel fibers were slightly higher than the rest of the mixes with 2% steel fibers. It is noted that the reported strains in Figure 4-11 are comparable to the range of the strains reported in the literature. For example, the strains at peak compressive stress for the six commercial UHPC products tested by Haber et al. [48] ranged between 0.00274 and 0.00524.

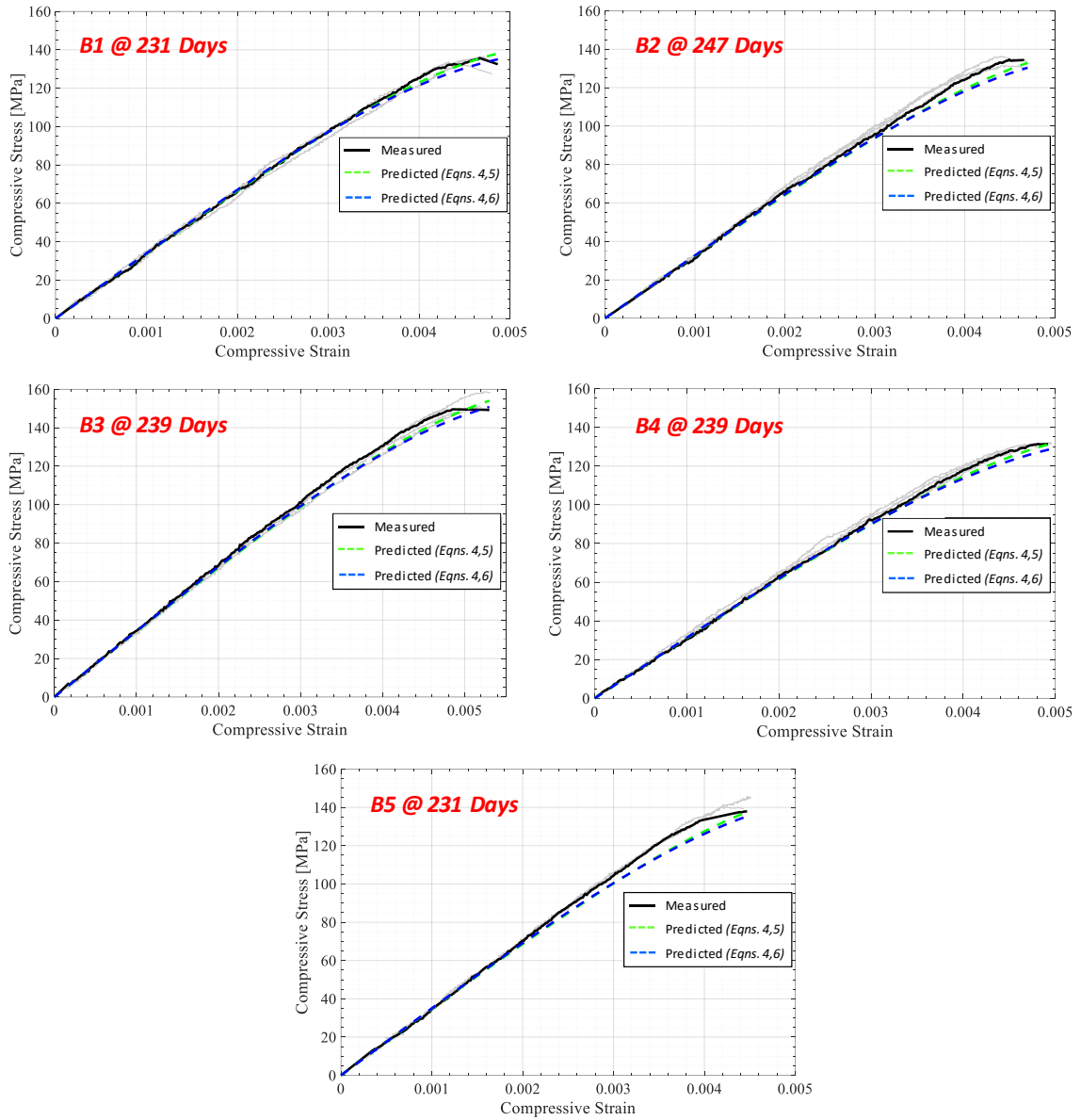


**Figure 4-10** Compressive stress-strain relationships of the five tested NP-UHPC mixes.

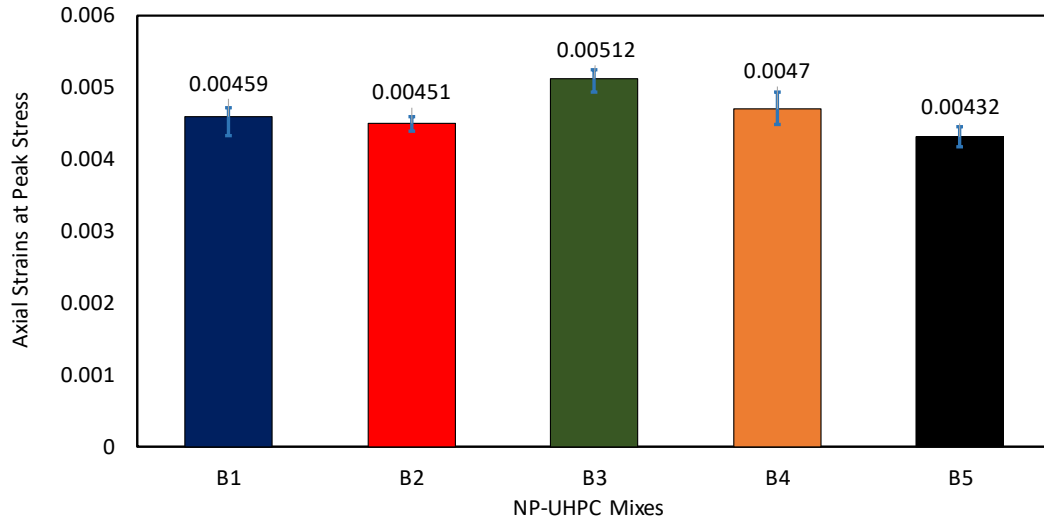


**Figure 4-11** Average axial strains measured at peak compressive stresses.

#### 4.4.2.4 Modulus of elasticity ( $E_c$ )

The compressive elastic modulus was calculated based on the linear best-fit approximation of the stress-strain relationship between 10% and 40% of the peak compressive stress. The relationship between the compressive strength and the elastic modulus of the UHPC has been previously investigated by many researchers and consistently reported as a multiplier of the square root of the compressive strength  $f'_c$ . Graybeal [47] proposed a multiplier of 3,840 (when  $f'_c$  under the root is in MPa) based on results of commercial UHPC products. He also proposed another multiplier of 4,070 based on the results of a commercial rapid strengthening UHPC product [42]. More recent work at the FHWA [48] provides a multiplier of 3,760 based on the results of six commercial UHPC products. It is noted that all these equations were developed for commercial UHPC products. Thus, it is of interest to check the validity of these equations for predicting the modulus of elasticity of the tested NP-UHPC mixes. Figure 4.12 shows the comparison between predictions based on the various aforementioned equations, i.e.  $E_c = 3840\sqrt{f'_c}$  or  $4070\sqrt{f'_c}$  or  $3760\sqrt{f'_c}$  and the measured experimental values. The comparison shows that all previously developed equations extensively overestimate the modulus of elasticity of the NP-UHPC mixes. Hence, a new equation is proposed herein to better estimate the modulus of elasticity of

NP-UHPC as  $E_c = 2,860\sqrt{f'_c}$  (for  $f'_c$  in MPa). The results from the new proposed equation are also listed in Figure 4.12 for comparison.

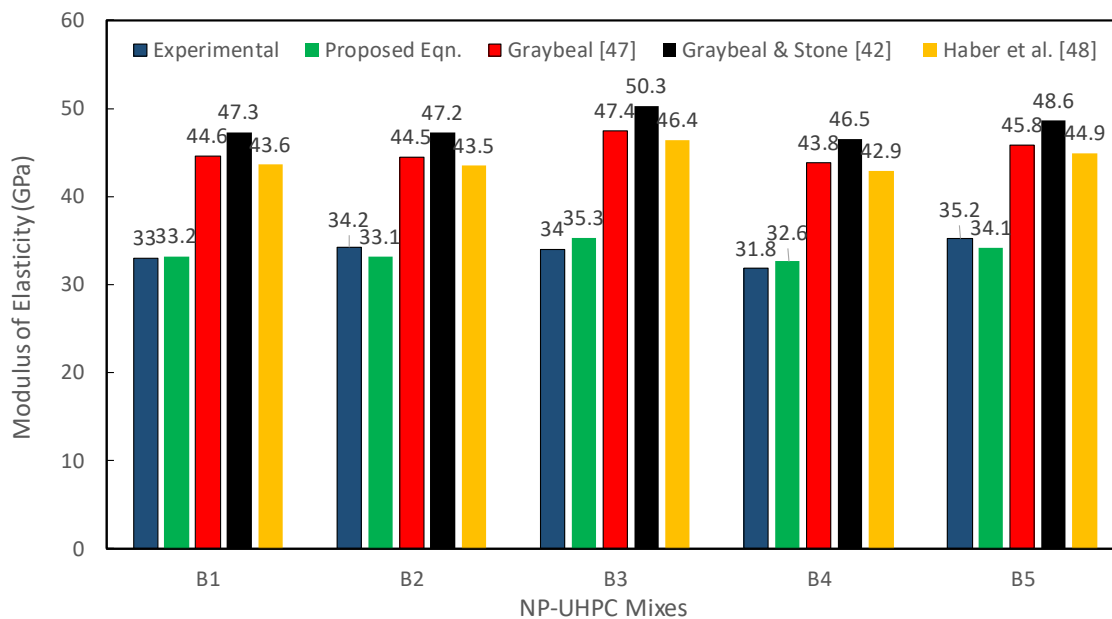


**Figure 4-12** Measured modulus of elasticity for the various NP-UHPC mixes and comparison against different predictions using selected equations from the literature and a new proposed equation.

#### 4.4.3 Flexure Tests

Due to the importance of characterizing the UHPC tensile behavior, several methods have been used such as flexure tests, splitting tension tests, and direct tension tests. Ongoing research efforts in the US are aiming at developing a future standard direct tension test exclusive for UHPC. However, until such test methodology is established, standard flexure tests along with non-standard direct tension tests are commonly considered for UHPC, which were both done in this study and reported in this section and the next one, respectively. The ASTM C1856 [35] recommends testing UHPC prisms according to ASTM C1609 [49] to determine flexural strength.

##### 4.4.3.1 Test procedure and specimens preparation

Flexural strength tests were conducted on  $76 \times 76 \times 280$  mm prisms with a 229 mm simple span. The loads were applied at third points according to ASTM C1609 [49] along with



ASTM C1856 [35]. An Instron testing machine with a maximum capacity of 250 kN was used to test the NP-UHPC samples at age of 7 and 28 days as well as other later ages dictated by COVID-19 related laboratory shut down and operation resumption. A sampling rate of 10 Hz was used to collect data from the tests. The load was controlled by the mid-span displacement of the specimen. A displacement rate of 0.076 mm/min was used up to 0.254 mm mid-span vertical displacement, then the rate was increased to 0.127 mm/min until the end of a given test. The mid-span deflection of the beams was measured using a laser extensometer device. The laser extensometer reads the extension between two fixed laser targets as one target was attached at the middle of the beam and the other was attached at a fixed point over the bending table as shown in Figure 4.13. The curing of the test specimens followed the same procedure used for the compression cylinders where the prisms were covered with plastic sheets and left in the fabrication site for one day after casting. Then, the samples were demolded on the second day and left to cure on 73 °F (~ 23 °C) up to the testing day. The bending prisms do not require special preparation or grinding as the prisms were aligned on their flat sides during the flexure testing.

#### 4.4.3.2 Flexural strength

The flexural strength measured at different ages for the NP-UHPC mixes is shown in Figure 4.14. The flexural strength of the specimens was calculated based on the maximum bending moment and the final beam dimensions after testing assuming a linear-elastic behavior. The results of the flexural strength confirm that the NP-UHPC mixes with 2% steel fibers have higher flexural strengths than that of the mixes with 1% steel fibers as expected. The use of half the amount of steel fibers (i.e. 1% versus 2%) has led to a reduction of the 28-day flexural strength of about 12% and 31% for the NP-UHPC mixes with sieved and non-sieved sand, respectively. As seen in Figure 4.14, the flexural strength of B5 is very comparable to that of B1 and B2 and the difference between all the results is within 15% only. Hence, it can be concluded that the flexural strength of the proposed NP-UHPC mixes with 2% steel fibers is only slightly affected by the change in material sources. B1 with non-sieved sand had a higher early flexural strength compared to B2, while the flexural strength of B2 exceeded that of B1 at later ages. This was anticipated because the NP-UHPC mixes with fine particle gradation usually require more time for the hydration process to gain strength compared to the mixes

with coarse sand. B3 had a lower flexural strength than B4. Thus, it can be concluded that using coarse sand may slightly decrease the flexural strength of the NP-UHPC mixes because of the less homogeneity of the fibers as they may accumulate around the bigger sand particles as previously shown in the flow test photos in Figure 4.5. The flexural strength of the NP-UHPC mixes reached approximately 90% of the 28-days strength after one week and then slightly increased by only 10% between 28 and about 235 days age.

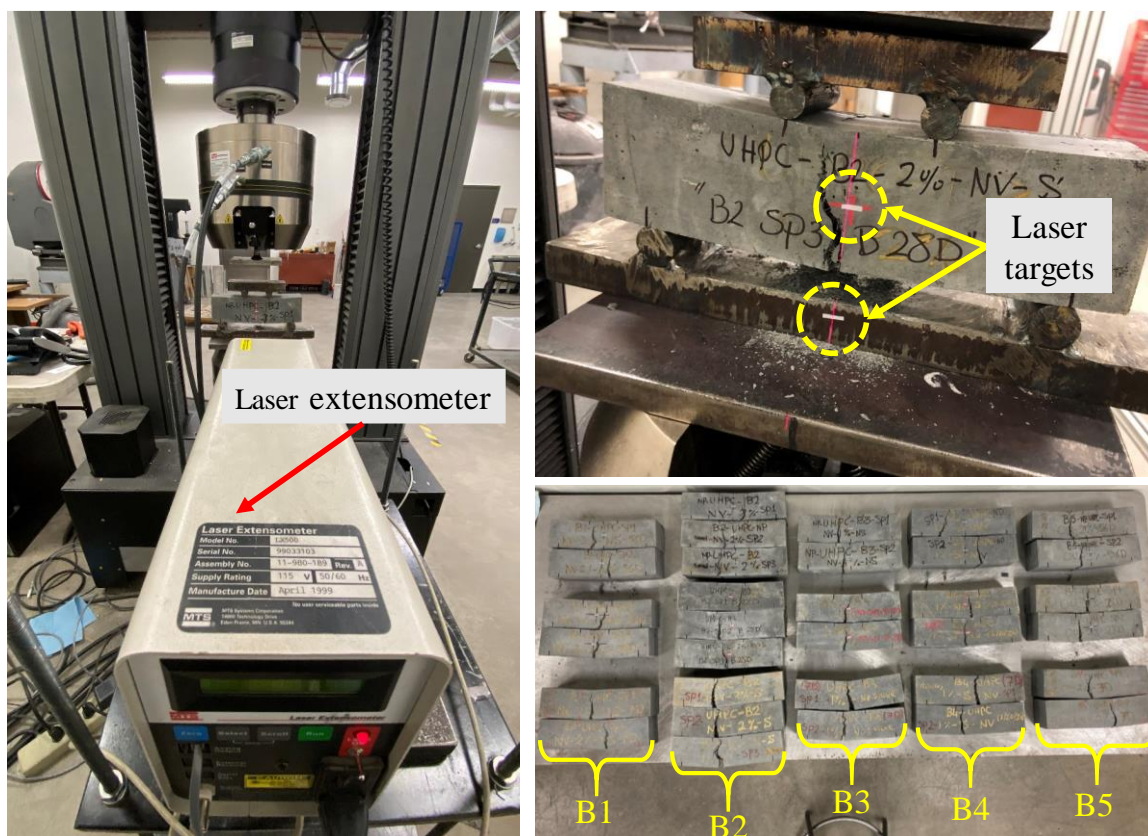


**Figure 4-13** Flexural testing and instrumentation of the NP-UHPC prisms.

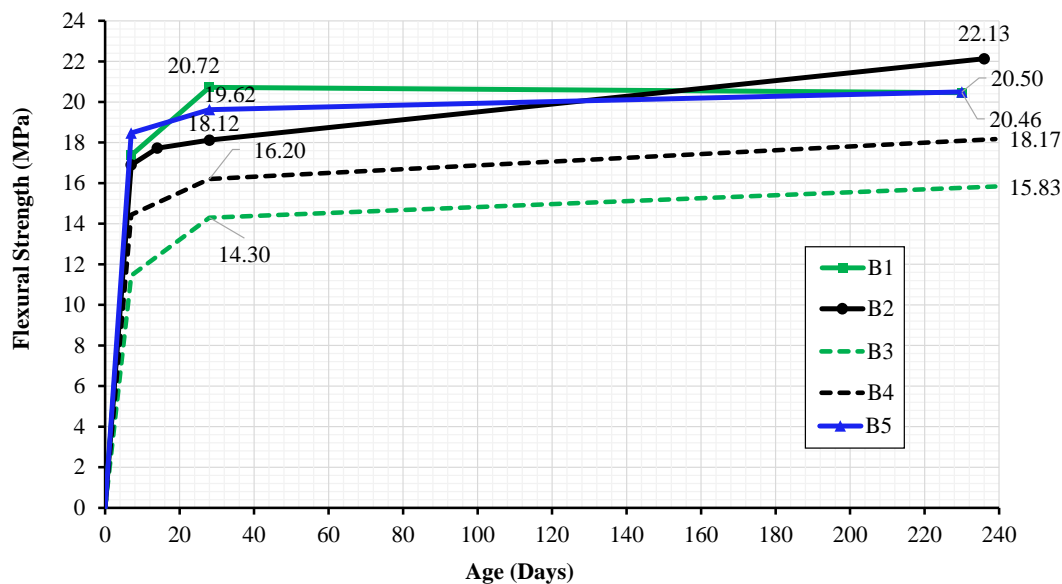


**Figure 4-14** Flexural strength versus time for the NP-UHPC mixes

#### 4.4.3.3 Flexural behavior

The average relationships between the flexural stress and the middle deflection of the NP-UHPC prisms are shown in Figure 4.15 for the different ages. Figure 4.15 also provides the individual figures of the specimens from B2 to show samples of the typical variation in the results of the bending tests. The flexural behavior of NP-UHPC beams was linearly elastic up to the initiation of the first crack at approximately 50% of the flexural strength. Then, more micro-cracking took place leading to a slight inelastic behavior. During this stage, the composite action of the steel fibers that bridge across the cracks has led to sustained strain hardening and more ductile behavior through failure. The NP-UHPC prisms reached their peak strength after the propagation of significant cracking across the highly stressed and weakest section at the middle third of the beam (i.e., between the two loading points). Afterwards, a gradual decline in strength was observed due to the pullout of the steel fibers. The flexural behavior of all the NP-UHPC mixes is very comparable and they all feature sustained strain hardening without brittle or sudden failure. This indicates that the use of sieved or non-sieved sand does not affect the full range of flexural behavior. It is also noted that as the age increases, the flexural strength increases and the rate of the decline in strength through failure would slightly increase.

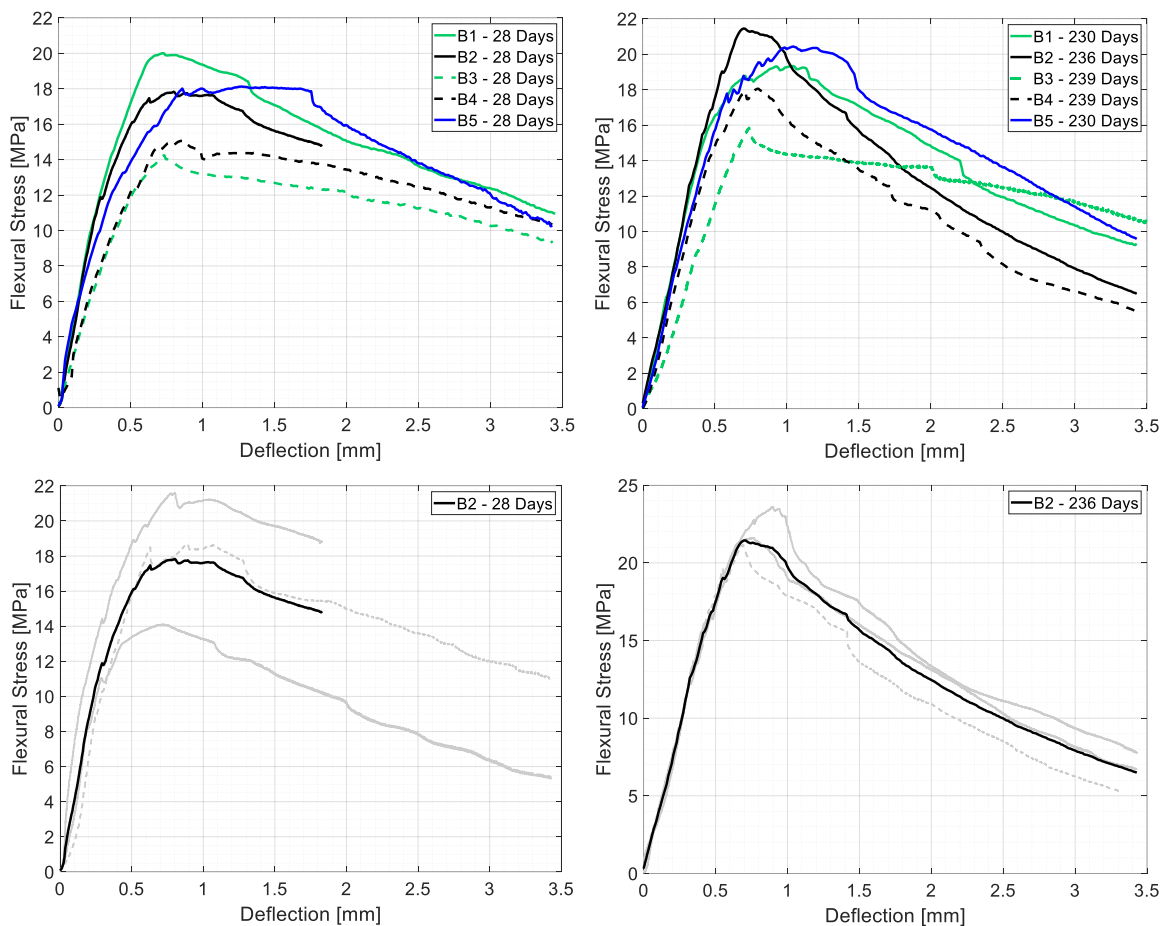


**Figure 4-15** Average flexural stress versus middle deflection relationships for the NP-UHPC prisms tested at different ages.

#### 4.4.4 Direct Tension Test

Although flexure tests are more convenient, they still overestimate the actual tensile strength of UHPC because of the non-uniform stress distribution across the beam and the dependence on boundary conditions or prism dimensions. Hence, it is more essential to determine the exact tensile strength of UHPC in general, and the NP-UHPC for this study as well, using direct tension testing. Dog-bone shape specimens have been commonly used for direct tension tests with varying dimensions and sizes. The tensile stress distribution over the reduced cross-section of the dog-bone specimen is more uniform compared to the flexural prisms. The direct tensile strength and full stress-strain behavior of the NP-UHPC mixes were investigated and reported in this section. Because of the lack of standard test procedures for the direct tensile testing of UHPC, many studies in the literature have

recommended testing of different specimen shapes and sizes under different loading procedures to capture the post-cracking tensile behavior of the UHPC. However, due to the convenience of simpler tests like flexure, other studies have established correlations between the flexural and tensile behavior of UHPC such as a recent FHWA study [50].

#### *4.4.4.1 Test procedure*

The direct tensile strength of the NP-UHPC mixes was determined based on testing of dog-bone shaped samples with a nominal cross-section at the reduced section of 2.54 cm × 2.54 cm dimensions. The length of a typical specimen is 28 cm with a gauge length of 6.35 cm. An Instron testing machine was used to test the samples at 7 and 28 days. A sampling rate of 50 Hz was used to collect the data of the test. A displacement-controlled loading rate of 0.127 mm/min was used throughout most of the test up to the post-peak drop to 90% of the observed peak load, then the displacement rate was increased to 1.27 mm/min until the test was terminated. The tensile strains were captured during the test using a laser extensometer device that typically reads the extension between two shiny targets attached at the end of the reduced section of the dog-bone specimen. Figure 4.16 shows the direct tension test setup for one of the dog-bone specimens tested at UNR. Note that all dog-bone specimens were fabricated using plastic molds and cured following the same procedure as flexural and compression test specimens.

#### *4.4.4.2 Tensile strength*

The relationships between the direct tensile strength versus the age for the different NP-UHPC mixes are shown in Figure 4.17. Again, error bars were added to the figure to show the upper and lower bound deviations of the specimen's results from the average plotted values. Most data points have deviations less than 1 MPa which is typically between 10-20% of the average compressive strength value. The large deviation values were expected because of the small dimensions of the test specimens which makes their direct tensile strength more vulnerable to the effect of the uniformity of the steel fibers distribution. The results show that B2 has the highest tensile strength while B3 has the lowest tensile strength among all the proposed mixes. The use of 1% steel fiber amount in B3 instead of the 2% used in B1 has resulted in a decrease in the 28-days tensile strength by approximately 15%.

B4 also had 28% less 28-day tensile strength than that of B2. It is also noted that the change in the material sources between mixes B2 and B5 has resulted in a slight increase in the 28-days tensile strength of about 10%. Hence, it is possible to replicate the mixes using different material sources without severely affecting the tensile strength of the material. At 28 days, it is indicated that the use of non-sieved sand instead of the fine sieved sand has resulted in less tensile strength of the mixes for both 1% and 2% steel fiber cases. This behavior is consistent with the results from the flexural tests and attributed to the homogeneity and dispersion of the steel fibers across the cross-section.

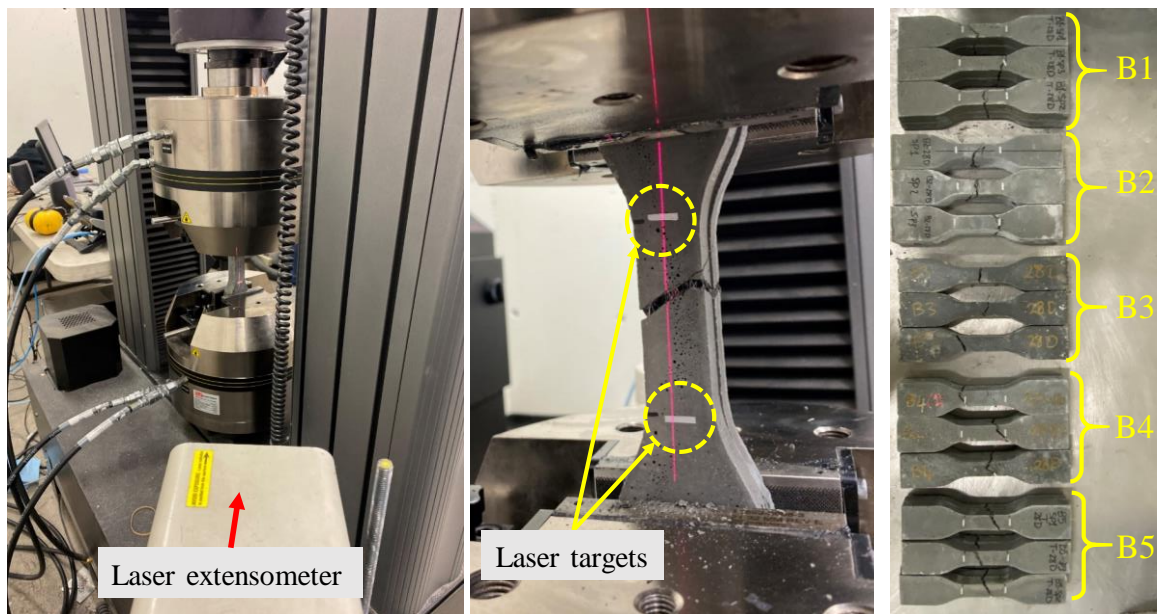


**Figure 4-16** Direct tension testing of NP-UHPC dog-bone specimens.

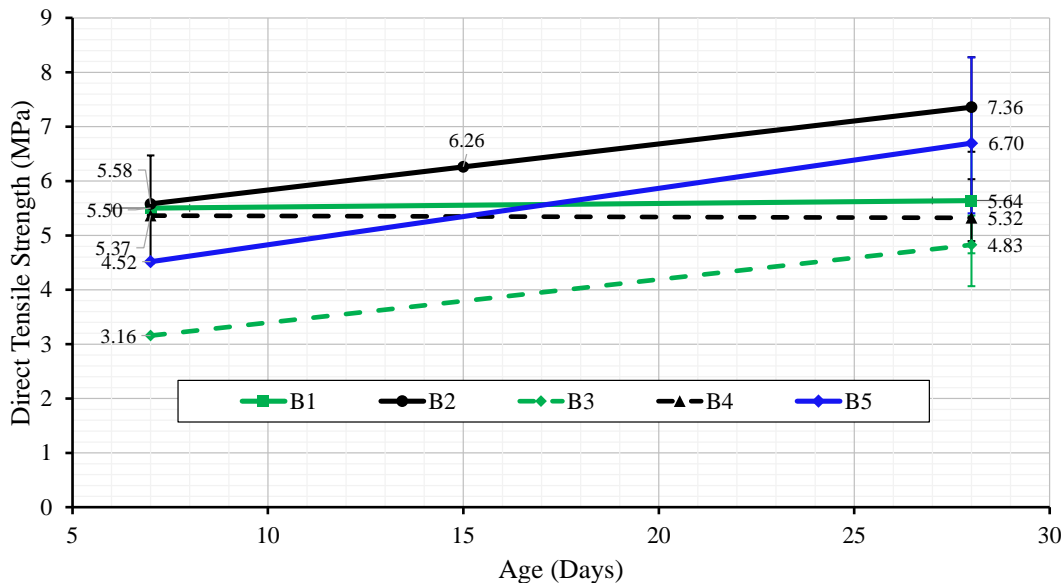


**Figure 4-17** Direct tensile strength versus time of the NP-UHPC mixes.

#### 4.4.4.3 Tensile behavior

Robust UHPC mixes exhibit a high tensile capacity and sustained post-cracking strength, which is desired to verify the emerging NP-UHPC mixes used in this study. Many research efforts that focused on the tensile behavior of UHPC [e.g. 50] suggest that the tensile behavior of UHPC can be idealized and divided into four regions of behavior. The first region is the linear elastic behavior before the initial cracking. The second region indicates the initiation of non-linearity through the multi-cracking. The third region is the crack straining which includes the engagement of steel fibers in carrying the internal tensile forces between the cracks and this behavior is usually called bridging action. The last region is mainly the failure or the crack localization and this is usually associated with the pullout of the steel fibers. The tensile stress-strain relationships for the NP-UHPC mixes at 7 and 28 days are shown in Figure 4.18. The results indicate that all the NP-UHPC mixes exhibited the desired prolonged and ductile behavior through failure. The 28-days tensile behavior of B2 and B5 are very comparable, which indicates that the tensile behavior of the NP-UHPC mixes in this study was not dependent on the variation of the material sources. This observation should be more investigated in future studies through conducting

experimental testing of different NP-UHPC mixes with more variation in the material sources to be able to get a general conclusion of this behavior.

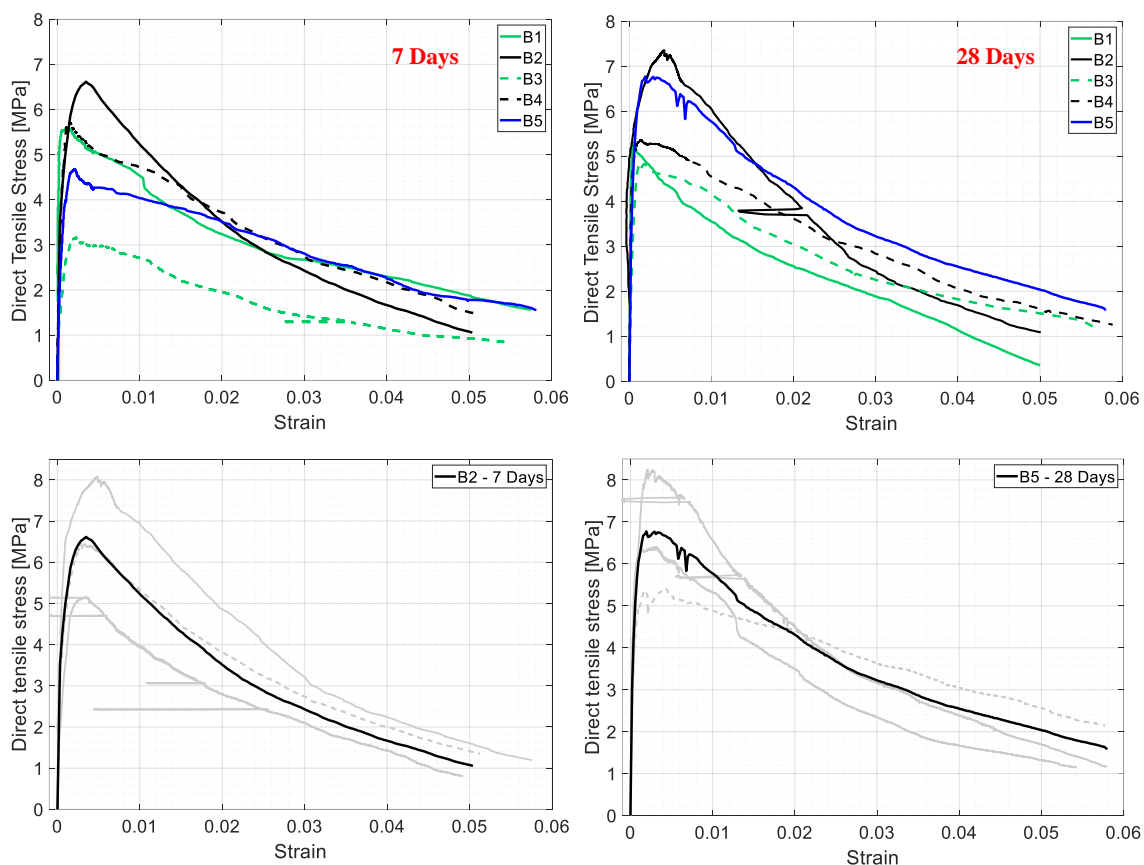


**Figure 4-18** Direct tension stress-strain relationships of all NP-UHPC mixes tested at 7 and 28 days.

#### 4.5 Summary and Concluding Remarks

This research study presents the implementation of an emerging class of NP-UHPC for ABC field joints. The ABC-UTC NP-UHPC mix has been designed at OU and this study investigated the repeatability and reproducibility of a baseline mix using local materials from the Western US. The NP-UHPC mixes using Western US materials have been successfully tested in transverse and longitudinal bridge deck joints, which motivated this study to provide mechanical characterization and behavior relationships that can be used for future modeling and larger applications. A total of five NP-UHPC mixes have been considered to investigate the effect of varying material sources as well as aggregate types



and nominal sizes on the main mechanical properties. The flow properties of the developed mixes were tested and compared with the recommended flow values. Moreover, different sets of testing were conducted on the developed mixes to test the compressive, flexural, and direct tensile strength and full behavior of the different NP-UHPC mixes. The results reported in this paper provide guidance for bridge and field engineers and researchers to further replicate the proposed NP-UHPC mixes by establishing the baseline mechanical properties for assessment and modeling. Several observations and conclusions could be drawn from this experimental study as follows:

- The basic characteristics of the ABC-UTC NP-UHPC mix originally designed at OU based on materials from the Midwest and South US regions can be successfully replicated using a full independent set of materials and different aggregate types from the Western US.
- Overall, the flow properties of all different NP-UHPC mixes are acceptable according to the flow requirements specified by ASTM C1856 or emerging FHWA reports. However, the fresh mixes with non-sieved sand (i.e. B1 and B3 in this study) are shown to have less uniform steel fiber dispersion because of the accumulation of the steel fibers around bigger sand particles.
- The developed NP-UHPC mixes with sieved and non-sieved sand both meet the minimum compressive strength requirements specified by ASTM C1856 (117 MPa). The equations for predicting UHPC compressive strength gain over time are validated for use for NP-UHPC mixes up to 56 days, but underestimate the strength at higher ages. Moreover, other proposed equations from literature (Equations 4-4 to 4-6) for predicting compressive stress-strain behavior of UHPC [47,48] are also validated for NP-UHPC.
- The compressive strength of NP-UHPC with 2% steel fibers is less sensitive than the ones with 1% fibers to the variability in aggregate types or material sources. Meanwhile, NP-UHPC mixes with local materials from the Western US and non-sieved sand (i.e. B1 and B3) have higher compressive strength and more rapid early strength gain compared to other mixes.

- The various equations proposed in the literature for estimating UHPC modulus of elasticity are shown to inaccurately overestimate that for the NP-UHPC mixes. Thus, based on the conducted test results, the following equation is proposed to use for estimating the ABC-UTC NP-UHPC modulus of elasticity:  $E_c = 2,860\sqrt{f'_c}$  (for  $f'_c$  in MPa), but more future testing is still needed.
- The flexural behavior and tensile behavior of the different NP-UHPC mixes are very comparable and they all have sustained strain hardening without brittle or sudden failure. Moreover, using 1% steel fibers by volume instead of the more common 2% is shown to reduce both flexural and direct tensile strengths only by about 15% and 30% for NP-UHPC mixes with sieved sand and non-sieved sand, respectively.
- Based on all the tests, comparisons, and assessments conducted in this study, the ABC-UTC NP-UHPC mix with 1% steel fiber and non-sieved sand (i.e. B3) strikes the best balance between acceptable mechanical properties and cost (less fibers, less work for sieving, etc.). Therefore, this mix provides a reasonable NP-UHPC candidate and hence, is recommended for future implementation and large-scale ABC applications.
- Finally, this study also enriches the literature by providing full tensile and compressive stress-strain relationships for NP-UHPC which can be readily used for defining constitutive laws and future modeling to further explore more applications of NP-UHPC.

### **Acknowledgments**

This study is funded by the US DOT through the ABC-UTC (2016 cycle) headed at Florida International University. The authors would like to thank Lehigh Southwest Cement Co. for the cement slag donation, Martin Marietta Inc. for the crushed aggregate sand donation.

### **References**

- [1] Holschemacher, K., & Weiße, D. (2005). Economic mix design ultra high-strength concrete. Special Publication, 228, 1133-1144.
- [2] De Larrard, F., & Sedran, T. (1994). Optimization of ultra-high-performance concrete by the use of a packing model. Cement and concrete research, 24(6), 997-1009.

- [3] Resplendino, J. (2011). Introduction: What is a UHPFRC?. *Designing and Building with UHPFRC*, 3-14.
- [4] Russell, H. G., Graybeal, B. A.. (2013). Ultra-high performance concrete: A state-of-the-art report for the bridge community. FHWA-HRT-13-060, Office of Infrastructure Research and Development.
- [5] Graybeal, B. A. (2006). Material property characterization of ultra-high performance concrete. FHWA-HRT-06-103. United States, FHWA Office of Infrastructure Research and Development.
- [6] Graybeal, B. (2011). Ultra-high performance concrete (No. FHWA-HRT-11-038).
- [7] Wang, D., Shi, C., Wu, Z., Xiao, J., Huang, Z., & Fang, Z. (2015). A review on ultra high performance concrete: Part II. Hydration, microstructure and properties. *Construction and Building Materials*, 96, 368-377.
- [8] Graybeal, B. A. (2013). Development of Non-Proprietary Ultra-High Performance Concrete for Use in the Highway Bridge Sector: TechBrief (No. FHWA-HRT-13-100). United States. Federal Highway Administration.
- [9] Abokifa, M., & Moustafa, M. A. Experimental behavior of poly methyl methacrylate polymer concrete for bridge deck bulb tee girders longitudinal field joints. *Construction and Building Materials*, 270, 121840.
- [10] Wille, K., Naaman, A. E., & Parra-Montesinos, G. J. (2011). Ultra-High Performance Concrete with Compressive Strength Exceeding 150 MPa (22 ksi): A Simpler Way. *ACI materials journal*, 108(1).
- [11] El-Tawil, S., Alkaysi, M., Naaman, A. E., Hansen, W., & Liu, Z. (2016). Development, characterization and applications of a non proprietary ultra high performance concrete for highway bridges (No. RC-1637). Michigan. Dept. of Transportation.
- [12] Berry, M., Snidarich, R., & Wood, C. (2017). Development of non-proprietary ultra-high performance concrete (No. FHWA/MT-17-010/8237-001). Montana. Dept. of Transportation. Research Programs.
- [13] Hernandez, J. A. A. (2016). Development and laboratory testing of Ultra High Performance Concrete (Doctoral dissertation).
- [14] Abokifa, M., & Moustafa, M. A. (2021). Development of Non-Proprietary UHPC Mix: Application to Deck Panel Joints. Quarterly Progress Report.
- [15] Shahrokhinasab, E., & Garber, D. (2021). Development of “ABC-UTC Non-Proprietary UHPC” Mix, Final Report # ABC-UTC-2016-C2-FIU01-Final, ABC-UTC, Miami, FL.

- [16] Looney, T., McDaniel, A., Volz, J., & Floyd, R. (2019). Development and characterization of ultra-high performance concrete with slag cement for use as bridge joint material. *Development*, 1(02).
- [17] Abokifa, M., & Moustafa, M. A. (2021). Full-Scale testing of Non-Proprietary UHPC for Deck Bulb Tee Longitudinal Field Joints. *Engineering Structures*, 243, 112696.
- [18] Funk, J. E., & Dinger, D. R. (2013). Predictive process control of crowded particulate suspensions: applied to ceramic manufacturing. Springer Science & Business Media.
- [19] Looney, T., Coleman, R., Funderburg, C., Volz, J., & Floyd, R. (2021). Concrete Bond and Behavior of Non-proprietary Ultra high-Performance Concrete Bridge Slab Joints. *Journal of Bridge Engineering*, 26(2), 04020128.
- [20] Mendonca, F., El-Khier, M. A., Morcous, G., & Hu, J. (2020). Feasibility Study of Development of Ultra-High Performance Concrete (UHPC) for Highway Bridge Applications in Nebraska (No. SPR-P1 (18) M072). Nebraska Department of Transportation.
- [21] Park, J. J., Kang, S. T., Koh, K. T., & Kim, S. W. (2008). Influence of the ingredients on the compressive strength of UHPC as a fundamental study to optimize the mixing proportion. In *Proceedings of the second international symposium on ultra high performance concrete* (pp. 105-112). Kassel Germany.
- [22] Alkaysi, M., El-Tawil, S., Liu, Z., & Hansen, W. (2016). Effects of silica powder and cement type on durability of ultra high performance concrete (UHPC). *Cement and Concrete Composites*, 66, 47-56.
- [23] Shi, C., Wu, Z., Xiao, J., Wang, D., Huang, Z., & Fang, Z. (2015). A review on ultra high performance concrete: Part I. Raw materials and mixture design. *Construction and Building Materials*, 101, 741-751.
- [24] ACI Committee 233. (2011). Slag Cement in Concrete and Mortar. American Concrete Institute (233R-03). American Concrete Institute.
- [25] Kim, H., Koh, T., & Pyo, S. (2016). Enhancing flowability and sustainability of ultra high performance concrete incorporating high replacement levels of industrial slags. *Construction and Building Materials*, 123, 153-160.
- [26] Yazıcı, H., Yardımcı, M. Y., Yiğiter, H., Aydın, S., & Türkel, S. (2010). Mechanical properties of reactive powder concrete containing high volumes of ground granulated blast furnace slag. *Cement and Concrete Composites*, 32(8), 639-648.

- [27] Schröfl, C., Gruber, M., & Plank, J. (2008). Structure performance relationship of polycarboxylate superplasticizers based on methacrylic acid esters in ultra high performance concrete. In *Second International Symposium on Ultra High Performance Concrete* (pp. 383-390).
- [28] Aboukifa, M., Moustafa, M. A., Itani, A. M., & Naeimi, N. (2019). Durable UHPC Columns with High-Strength Steel (No. ABC-UTC-2013-C3-UNR02-Final). Accelerated Bridge Construction University Transportation Center (ABC-UTC).
- [29] Collepardi, S., Coppola, L., Troli, R., & Collepardi, M. (1997). Mechanical properties of modified reactive powder concrete. *ACI SPECIAL PUBLICATIONS*, 173, 1-22.
- [30] Xie, T., Fang, C., Ali, M. M., & Visintin, P. (2018). Characterizations of autogenous and drying shrinkage of ultra-high performance concrete (UHPC): An experimental study. *Cement and Concrete Composites*, 91, 156-173.
- [31] Arora, A., Almujaiddi, A., Kianmofrad, F., Mobasher, B., & Neithalath, N. (2019). Material design of economical ultra-high performance concrete (UHPC) and evaluation of their properties. *Cement and Concrete Composites*, 104, 103346.
- [32] Aboukifa, M., Moustafa, M. A., & Saiidi, M. S. (2021). Seismic response of precast bridge columns with composite non-proprietary UHPC filled ducts ABC connections. *Composite Structures*, 274, 114376.
- [33] Subedi, D., M. A. Moustafa, M. S. Saiidi, (2019). "Non-Proprietary UHPC for Anchorage of Large Diameter Column Bars in Grouted Ducts," Report No. CCEER-19-03, May 2019.
- [34] ASTM C136/C136M-14 (2014) "Standard Test Method for Sieve Analysis of Fine and Coarse Aggregates, ASTM International", West Conshohocken, PA.
- [35] ASTM C1856/C1856M-17. (2017). Standard practice for fabricating and testing specimens of ultra-high performance concrete. ASTM International", West Conshohocken, PA.
- [36] ASTM C1437. (1999). Standard Test Method for Flow of Hydraulic Cement Mortar, Document Number: ASTM C1437-01, ASTM International.
- [37] ASTM, A. (2014). Standard specification for flow table for use in tests of hydraulic cement. ASTM Int., 1-6.
- [38] California Department of Transportation, Notice to Bidders and Special Provision. Contract No. 06-0K4604, Project ID 0612000105, 2015.
- [39] Standard Test Method for Compressive Strength of Cylindrical Concrete Specimens, ASTM C39, ASTM International, Volume 04.02, West Conshohocken, PA, 2012.

- [40] Graybeal, B. A. (2015). Compression testing of ultra-high-performance concrete. *Advances in Civil Engineering Materials*, 4(2), 102-112.
- [41] Naeimi, N., & Moustafa, M. A. (2021). Compressive behavior and stress–strain relationships of confined and unconfined UHPC. *Construction and Building Materials*, 272, 121844.
- [42] Graybeal, B. A., & Stone, B. (2012). Compression response of a rapid-strengthening ultra-high performance concrete formulation (No. FHWA-HRT-12-065). United States. Federal Highway Administration. Office of Infrastructure Research and Development.
- [43] ASTM C469/C469M-14. Standard Test Method for Static Modulus of Elasticity and Poisson's Ratio of Concrete in Compression. American Society of Testing and Materials (2014).
- [44] Joe CD, Moustafa MA. Cost and ecological feasibility of using UHPC in bridge piers. In first international interactive symposium on UHPC; 2016. p. 18-20.
- [45] Naeimi, N., & Moustafa, M. A. (2020). Numerical modeling and design sensitivity of structural and seismic behavior of UHPC bridge piers. *Engineering Structures*, 219, 110792.
- [46] Dhakal, S., & Moustafa, M. A. (2019). MC-BAM: Moment–curvature analysis for beams with advanced materials. *SoftwareX*, 9, 175-182.
- [47] Graybeal, B. A. (2007). Compressive behavior of ultra-high-performance fiber-reinforced concrete. *ACI materials journal*, 104(2), 146.
- [48] Haber, Z. B., De la Varga, I., Graybeal, B. A., Nakashoji, B., & El-Helou, R. (2018). Properties and behavior of UHPC-class materials (No. FHWA-HRT-18-036). United States. Federal Highway Administration. Office of Infrastructure Research and Development.
- [49] ASTM C1609/C1609M-07. Standard test method for flexural performance of fiber-reinforced concrete (using beam with third-point loading). American Society of Testing and Materials (2007).
- [50] Graybeal, B. A., & Baby, F. (2019). Tension testing of ultra-high performance concrete (No. FHWA-HRT-17-053). United States. Federal Highway Administration. Office of Infrastructure Research and Development.

## 5 EXPERIMENTAL BEHAVIOR OF PRECAST BRIDGE DECK SYSTEMS WITH NON-PROPRIETARY UHPC TRANSVERSE FIELD JOINTS

*This chapter is a standalone paper that has been published in the journal of Materials, MDPI*

### **Abstract**

Full-depth precast bridge decks are widely used to expedite bridge construction and enhance durability. These deck systems face the challenge that their durability and performance are usually dictated by the effectiveness of their field joints and closure joint materials. Hence, commercial UHPC products have gained popularity for use in such joints because of their superior mechanical properties. However, the proprietary and relatively expensive nature of the robust UHPC mixes may pose some limitations on their future implementation. For these reasons, many research agencies along with state departments of transportation sought their way to develop cheaper non-proprietary UHPC (NP-UHPC) mixes using locally supplied materials. The objective of this study is to demonstrate the full-scale application of the recently developed NP-UHPC mixes at the ABC-UTC in transverse field joints of precast bridge decks. This study included experimental testing of three full-scale precast bridge deck subassemblies with transverse NP-UHPC field joints under static vertical loading. The test parameters included NP-UHPC mixes with different steel fibers amount, different joint splice details, and joint widths. The results of this study were compared with the results of a similar proprietary UHPC reference specimen. The structural behavior of the test specimens was evaluated in terms of the load versus deflection, reinforcement and concrete strains, and full assessment of the field joint performance. The study showed that the proposed NP-UHPC mixes and field joint details can be efficiently used in the transverse deck field joints with comparable behavior to the proprietary UHPC joints. The study concluded that the proposed systems remained elastic under the target design service and ultimate loads. In addition, the study showed that the use of reinforcement loop splices enhanced the load distribution across the specimen's cross-section.

## 5.1 Introduction

Cast-in-place (CIP) construction techniques have been widely used for many years in the construction of bridge decks around the nation. The reason for the wide implementation of these CIP systems is the relatively cheaper costs relative to other systems and easier construction. However, these systems showed a lack of performance, degradation in strength and less durability after spending many years in service. As a result, nearly 56,000 US bridges are considered structurally deficient based on the records of the American Road and Transportation Builders Association (ARTBA) [1]. While bridge decks deteriorate faster than the other bridge components, more than \$ 8 billion are spent annually on repairing or replacing these deteriorated decks [1]. Approximately 85% of the US daily commuters travel on state-owned bridges, which makes it more difficult to use the traditional construction techniques or CIP methods in the replacement or rehabilitation of the deteriorated decks. This has paved the way for a wider implementation of prefabricated construction techniques to accelerate the deck erection. Prefabricated bridge decks (PBES), which is one of the accelerated bridge construction (ABC) applications, can enhance constructability issues, offer higher quality, provide accelerated and safer construction, and minimize traffic disruption. On the other hand, the prefabricated bridge deck elements usually require to be connected on the field through field joints that could form a weak link that affects the overall system performance. These field joints can be classified into two main types. Transverse joints that run perpendicular to the traffic flow direction and longitudinal joints that run along the longitudinal axis of the bridge, i.e., parallel to the traffic direction. Figure 5.1 shows both field joint types in a typical precast bridge deck system. The use of traditional joint closure materials like conventional concrete and non-shrink grouts for such joints has resulted in either relatively wide joints because of the required longer development length, or narrow joints with mechanical splicing of reinforcement or post tensioning. Moreover, these types of joints require longer time and effort to fabricate than using advanced materials like UHPC, hence, they are not adequate as ABC techniques. Nonetheless, interface cracking under service and ultimate design load levels has been one of the main issues associated with the use of traditional materials in field joints. With the recent introduction of advanced materials to the bridge community,



many researchers have explored many types of these advanced construction materials for use as a bridge deck field joint filler material. Some researchers focused on the experimental investigation and demonstration of the bridge decks with field joints filled with advanced grouts [2–4], high-performance concrete (HPC) [2,5], and HPC with fiber reinforcement [5]. However, many of these research efforts included special considerations for the reinforcement splices inside the joint, such as rebar post-tensioning, using of mechanical splices, using of headed bars, or adding rebar confinement inside the joint to decrease the required splice length.

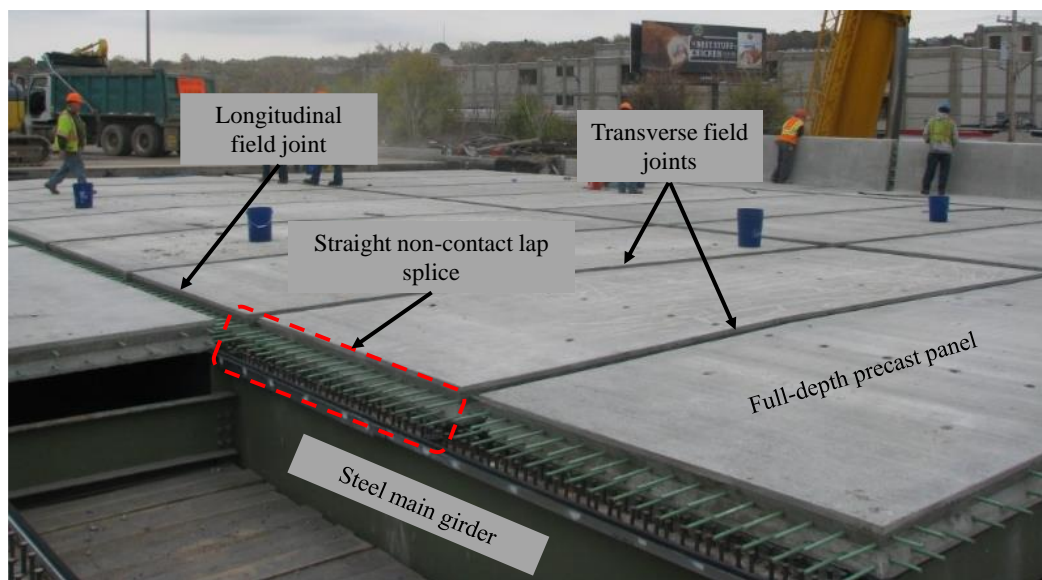


**Figure 5-1** Types of field joints in a typical prefabricated bridge deck system.

Currently, ultra-high performance concrete (UHPC) has gained a great significance and reputation as a bridge deck joint material. Many research studies demonstrated that the ideal UHPC field joint has a diamond-shaped shear key, 15.2–20.3 cm joint width, and traditional straight or loop splices. These typical joint details are sufficient in transferring shear and bending across the prefabricated deck elements [6–9]. However, the use of UHPC comes with several challenges. First, the commercial UHPC products are costly and the material can be 15 to 20 times more expensive than conventional concrete. Moreover, commercial UHPC is proprietary and only supplied by a limited number of vendors. This often limits state DOTs that are trying to avoid sole-sourcing among other bidding issues to use UHPC. Hence, there is a growing interest from various state DOTs and research

agencies in developing non-proprietary UHPC (NP-UHPC) mixes to be used for different bridge applications. These research efforts aimed at making UHPC more accessible and less expensive through using locally available materials in the NP-UHPC mixtures [10–16]. The NP-UHPC is much cheaper than the P-UHPC as the typical P-UHPC and NP-UHPC costs are estimated to be around \$ 3300 and \$ 1300 per cubic meter, respectively [17,18]. However, there are still some limitations on the large-scale production of UHPC because of the long mixing time and the relatively small batch size. This has motivated researchers and precast concrete plants to explore different ways of mixing UHPC in large quantities [19,20]. A recent literature study showed that it is applicable to mix NP-UHPC mixtures in large quantities to fabricate a full UHPC pi girder bridge using the conventional ready mix-trucks [19]. One major contribution to this field of study is the recent research work done by the five consortium universities within the ABC university transportation center (ABC-UTC) in the US [20,21]. The University of Oklahoma has led this project by developing the mix design and material testing of the baseline NP-UHPC mix [22]. The information regarding the baseline mix design was shared with the other universities to examine the viability of using this NP-UHPC mix in various ABC applications. The experimental work covered in this paper, which was part of this wider collaboration project, was conducted by the University of Nevada, Reno (UNR). The main role for UNR in this project was to first extend the use of the NP-UHPC mix design to develop NP-UHPC mixes using locally available materials in Nevada (NV) and California (CA). Next, we conducted experimental testing of full-scale precast bridge deck panel systems with transverse and longitudinal field joints that were filled with the developed NP-UHPC mixes. This paper covers the experimental results of the transverse joint specimens only to provide a detailed discussion of the structural behavior and analysis of the joint performance.

The overall objective of this study is to investigate the structural performance of the prefabricated deck elements with NP-UHPC transverse filed joints. Moreover, the study aimed at validating the use of the NP-UHPC as a closure joint material in comparison with a robust commercial UHPC product. Other objectives of this study included engineering and optimization of the NP-UHPC mixes and joint details to provide efficiently equivalent systems at a cheaper cost. The engineering solutions used in this study included the

optimization of the amount of steel fibers in the NP-UHPC mixes, varying the joint width, using different joint splices, and varying the distribution of the overlapped reinforcement. Three full-scale specimens were experimentally tested in this study under static vertical loading. The paper includes several sections that present a discussion of the development of the mix, results from a similar precedent study with commercial UHPC to use for reference, details of the experimental program, test results/discussion, and conclusions.

## **5.2 Background**

This section provides detailed information about the development, composition and material characterization of the NP-UHPC mix utilized in this study. Moreover, this section also highlights the experimental test results of a similar bridge deck specimen with a proprietary UHPC (P-UHPC) transverse field joint previously tested by the authors [23,24]. The main test results obtained from that reference P-UHPC specimen are shown in this section to allow for comparisons with the NP-UHPC specimens tested in this study.

### **5.2.1 NP-UHPC Mix**

Many state DOTs have commissioned university research teams to develop NP-UHPC mixes using locally sourced materials. In fact, this has resulted in the development of cheaper UHPC mixes with comparable mechanical characteristics to commercial UHPC mixes. One of these research efforts is the work done by the University of Oklahoma (OU) [22]. They developed an NP-UHPC mix with a 30% cement slag replacement by weight to reduce the overall cost of the material. This NP-UHPC mix was selected by the ABC university transportation center (ABC-UTC) for further experimental testing in different ABC applications, such as the bridge deck field joints. UNR was part of this wide research project and our role was to experimentally test the same NP-UHPC mix using locally available materials in the NV and CA states in the bridge deck field joints. Our work at UNR comprised three main parts which included first the development and material testing of different NP-UHPC mixes to engineer and optimize the materials and the amount of the steel fibers needed inside the mix [25]. As a result of this preliminary assessment, two NP-UHPC mixes were proposed and selected for further experimental testing and implementation in deck field joints. The large-scale experimental testing of the NP-UHPC

field joints was divided into two parts. The first part included full-scale testing of portions of deck bulb tee (DBT) girders with NP-UHPC longitudinal field joints [26]. The second part, which was presented in this paper, included full-scale testing of precast bridge deck assemblies with transverse NP-UHPC field joints. The last part of this project is what we present in detail in this paper. Two typical NP-UHPC mixes were used in this study that differed only in the percentage of the steel fibers included in the mix (i.e., 1% versus 2% by volume, which corresponds to 3% versus 6% by weight). The dimensions of the steel fibers are 13 mm in length and 0.2 mm in diameter with a nominal tensile strength of 2750 MPa. The mixing proportions and the material sources of both mixes are shown in Table 5.1.

As mentioned earlier, the main aim of the first step in this project was to determine the main mechanical properties of the developed NP-UHPC mixes. Hence, this paper does not present material characterization but provides an overview of the main mechanical properties of the NP-UHPC mixes used herein. For more details, the reader is referred to the additional information and test results and discussion reported in [25,26]. Table 5.2 shows the results of the 28-day compressive strength, flexural strength and direct tensile strength for both mixes. It is noted that both mixes reached the 97 MPa compressive strength limit after 7 Days, which is the threshold recommended by FHWA to open the bridges for traffic or to strip off the formwork [27].

**Table 5-1** Mixing Proportions and Material Sources of the NP-UHPC Mixes.

Material	1% steel fiber mix Quantity, kg/m <sup>3</sup>	2% steel fiber mix Quantity, kg/m <sup>3</sup>	Material Supplier
Cement	707	700	Type I/II Nevada Cement, Reno
Slag	354	350	Lehigh, Sacramento
Silica Fumes	118	117	BASF (Master Life SF 100)
Water	236	233	Potable Water
w/b	0.2	0.2	
Sand	1179	1166	Crushed Aggregate Sand, Martin Marietta Sparks, NV
Steel Fibers	79	151	Bekaert (Dramix OL 13/0.2)
Superplasticizer	13.5	13.5	BASF (Glenium 7920)

**Table 5-2** Main Mechanical Properties Tested at 28 days for the NP-UHPC Mixes.

Property	1% Steel Fibers Mix	2% Steel Fibers Mix	Standard Test Method
Compressive Strength, MPa	128.9	114.9	Modified ASTM C39 [28]
Flexural Strength, MPa	14.3	20.7	ASTM C1609 [29]
Direct Tensile Strength, MPa	4.83	5.64	N/A

### 5.2.2 Reference Specimen with P-UHPC Joint

As mentioned above, the experimental results of a reference specimen with a P-UHPC transverse joint are presented briefly in this section for completeness. This specimen was tested as a part of a comprehensive experimental study which included testing of five large-scale bridge deck specimens with transverse and longitudinal field joints. The main aim of that precedent study was to compare and investigate the structural performance of bridge deck specimens with polymer concrete and P-UHPC field joints [23,24]. The reference specimen had overall planar dimensions of 2.44 m  $\times$  2.74 m and a thickness of 20.3 cm. The P-UHPC transverse field joint had a width of 15.24 cm and a diamond-shaped shear key and was located in the middle of the specimen. The details of the P-UHPC joint were proposed based on real bridge practical implementations and the results of many research projects. These typical joint details have been demonstrated to develop sufficient shear and bending capacities to provide integrity between the joined deck panels. The design details of this reference specimen are typical of that of the first specimen which is tested in this study. The specimen was simply supported and loaded at mid-span with a static vertical load. The results of the load versus mid-span deflection relationship of the reference specimen are shown in Figure 5.2a. Moreover, Figure 5.2b shows the load versus the reinforcement strain readings of the bottom transverse bars (i.e., main reinforcement) of the P-UHPC specimen. The results shown here are used later for the comparison and assessment of similar specimens with the proposed NP-UHPC transverse joints. The mixing proportions of the P-UHPC mix in comparison with the NP-UHPC mix with 2% steel fibers are shown in Table 5.3. It is noted that the weight of the dry premix of the NP-

UHPC mix represents the sum of the weights of all the dry components including the cement, slag, silica fumes, and sand.

The peak load capacity of the reference specimen was 524.5 kN at which 5.92 cm mid-span vertical displacement was measured. The failure of the specimen was dominated by flexure as it included yielding of the main reinforcement followed by the crushing of concrete at the top of the precast panels. It was observed that no interface cracks or bond slippage had happened up to the peak load capacity of the specimen. Moreover, the specimen had remained essentially elastic in which no reinforcing bars had yielded up to the AASHTO LRFD ultimate load level as shown in Figure 5.2b.

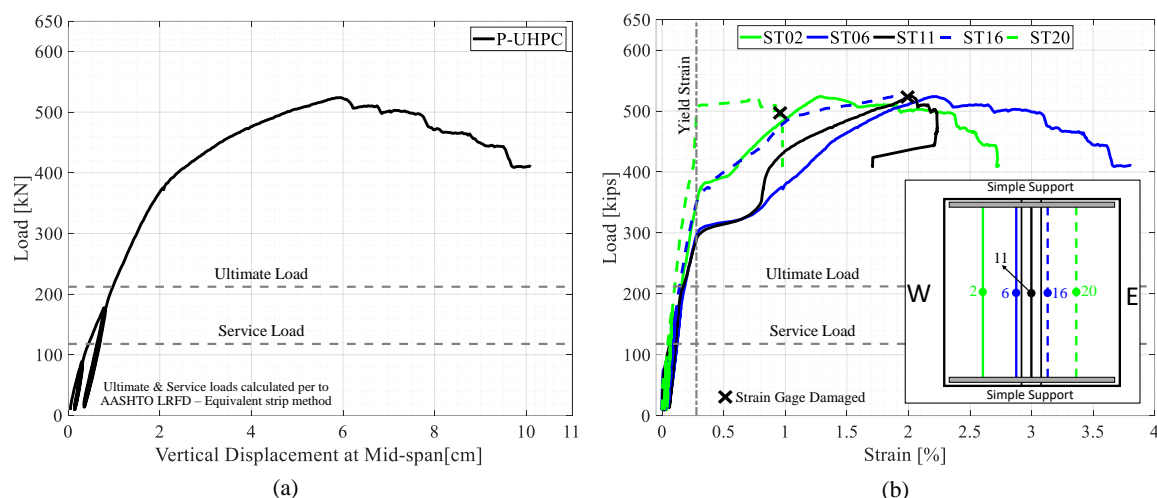


**Figure 5-2** Experimental test results of the reference P-UHPC specimen: (a) Load versus mid-span deflection; (b) Load versus tensile strains at the middle of the bottom transverse reinforcement.

**Table 5-3** Mixing Proportions of the P-UHPC and NP-UHPC Components.

Material	P-UHPC Weight (kg/m <sup>3</sup> )	Percentage by Weight (%)	NP-UHPC Weight (kg/m <sup>3</sup> )	Percentage by Weight (%)
Dry premix	2195	87.6	2333	85.5
Water or ice	130	5.0	233	8.5
Superplasticizer	30	1.2	13.5	0.5
Steel fibers (2% by volume)	156	6.2	151	5.5

### 5.3 Experimental Program

This section provides information regarding the design and structural details of the specimens, fabrication process, experimental test setup, loading methodology, and instrumentation plan.

#### 5.3.1 Specimens Design and Test Matrix

The experimental program presented in this study included testing three full-scale bridge deck specimens with transverse NP-UHPC field joints. The structural design details of all test specimens are shown in Figure 5.3. Each specimen consists of two precast deck panels which were cast using conventional concrete with a specified compressive strength of 34.5 MPa. The precast panels were joined together in the transverse direction of the bridge (i.e., perpendicular to the direction of motion of traffic as illustrated in Figure 5.1 above) using NP-UHPC full-depth field joints. Each panel had a protruded longitudinal reinforcement which was spliced at the field joint location to provide continuity of load transfer across the panels. The experimental program included testing of different parameters, such as different types of reinforcement splices, splice lengths, joint materials, and reinforcement configurations. All specimens had the same overall dimensions and top and bottom transverse reinforcement (i.e., main reinforcement). Non-contact lap-splices were utilized in this study, but they varied in their length and type. Table 5.4 shows the test matrix and test variables of three tested specimens in addition to the P-UHPC reference specimen which is referred to as “S0”.

**Table 5-4** Experimental Test Matrix and Specimen Design Details (Dimensions are in cm).

Specimen Name	Transverse Reinforcement		Longitudinal Reinforcement		Field Joint Material	Lap Splice type	Lap Splice Length
	Top	Bottom	Top	Bottom			
S0 (reference)	#16 @ 17.8	#16 @ 17.8	#13 @ 38.1	#16 @ 25.4	P-UHPC 2%	Straight	12.7
S1-Str-2%			#13 @ 29.6	#16 @ 25.4	NP-UHPC 2%	Straight	12.7
S2-Lop-2%			#13 @ 17.8	#13 @ 17.8	NP-UHPC 2%	Loop	11.4
S3-Str-1%			#13 @ 29.6	#13 @ 17.8	NP-UHPC 1%	Straight	17.8

Abbreviations; Str: Straight splice, Lop: Loop splice.

The first specimen “S1-Str-2%” had a straight splice with 12.7 cm length, while the second specimen had a loop splice with 11.4 cm length. The loop splice can provide less splice length compared to the straight splice because of the bearing effects at the bend. The use of loop splices inside the field joints was shown to provide better joint performance and better load transfer across the precast panels [24]. A smaller bar diameter (i.e., #13 versus #16) was selected for the longitudinal reinforcement of specimen “S2-Lop-2%” to accommodate the bend diameter requirements in the ACI 318 provisions [30]. The NP-UHPC mixes, which were used in both specimens, have a 2% by volume steel fibers amount.



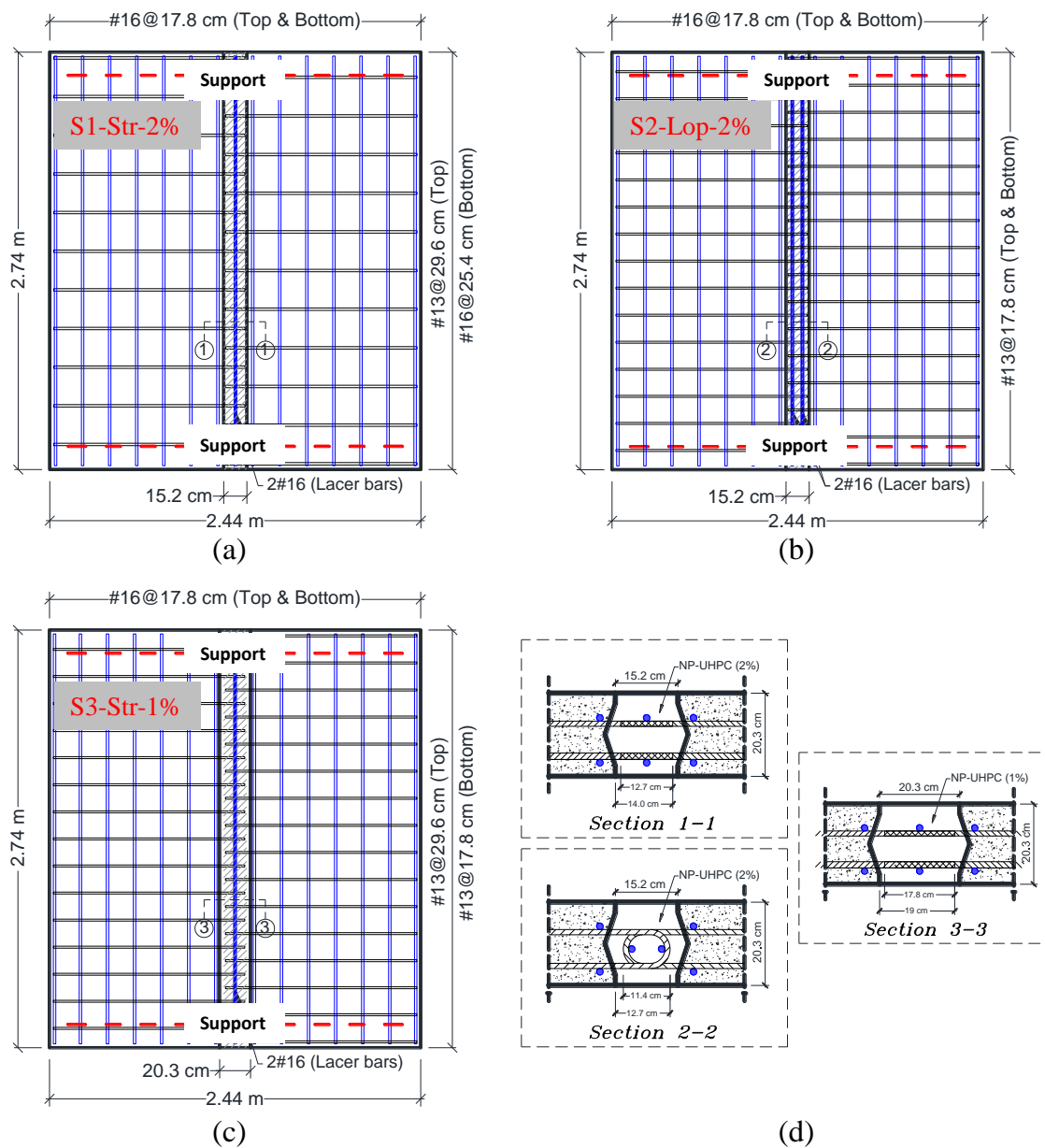


**Figure 5-3** Overall dimensions and structural design details of specimens (a) S1-Str-2%; (b) S2-Lop-2%; (c) S3-Str-1%; (d) close-up view of the field joint details.

As mentioned earlier, one of the objectives of this study was to engineer and optimize the materials in the field joints. Hence, an NP-UHPC mix with only half the amount of steel fibers (i.e., 1% by volume) was used for the third specimen “S3-Str-1%”. This was mainly sought to reduce the cost of the material as the steel fibers are the most expensive component in the NP-UHPC composition. Along with that, the authors proposed an

increase of the lap splice length of this specimen by 40% to be 17.8 cm. This increase in the splice length was suggested to compensate for the expected lower performance of the NP-UHPC with 1% steel fibers compared to that of the 2% steel fibers which may require a slightly longer development length. The bottom longitudinal reinforcement of specimen “S1-Str-2%” includes #16 bars which were spaced at 25.4 cm. The authors have also suggested using the same amount of steel for the bottom longitudinal reinforcement of the third specimen while using #13 bars at 17.8 cm spacing. The choice of using a smaller bar diameter resulted in narrower spacing between the reinforcement inside the joint which was proved to enhance the field joint performance and overall load distribution over the specimen [24]. In summary, the joint material of the third specimen was optimized to include only half the steel fibers amount. However, the splice length was increased and the spacing of the bottom longitudinal reinforcement was decreased to compensate for the slightly lesser strength of the NP-UHPC.

The design of the specimens followed the same design provisions of CIP bridge decks in the AASHTO LRFD Bridge Design Specification [31]. This design procedure does not account for the deck discontinuity and the field joint effects. The moment demands were calculated based on the AASHTO equivalent strip method. This method takes into account the largest moment values imposed on the bridge decks from the numerous live loading conditions. The cross-section of the bridge example used to design the test specimens has five steel girders spaced at 3.65 m on the center and a 20.3 cm thick concrete deck slab. Grade 60 reinforcing steel has been used for the reinforcement of the test specimens. The precast deck panels had 2.54 cm and 5.08 cm bottom and top concrete covers, respectively. To facilitate the bridge deck erection and casting of the joints, non-contact lap splices, which were arranged in a staggered formation, were used inside the joint. No adhesive coatings or surface preparation have been used for the surface of the diamond-shaped shear keys. This was done mainly to examine the weakest possible interface between the joint and the panels and to minimize the time and labor required for this task in the real field implementations. All specimens had general outside concrete dimensions of 2.74 m  $\times$  2.44 m  $\times$  20.3 cm.

### 5.3.2 *Test Setup and Instrumentations*

The experimental testing of the test specimens was done at the Earthquake Engineering Laboratory (EEL) at UNR. The test specimens were simply supported over two seat beams and loaded with a vertical static loading from a 980 kN hydraulic actuator at the middle. This led to a three-point bending configuration. The load was applied adjacent to the field joint to produce the highest shear stresses at the interface between the field joint and the precast panel. The typical mode of failure for these types of joints during the service life of bridges are the interface cracks, hence it is essential to investigate the efficiency of the interface bond between the joint and the precast members at the service and ultimate loads. Elastomeric rubber bearings were used on the top of the steel seat beams to allow a zero moment or free rotation at supports. The test setup was not designed to provide fixity at the ends to mimic the real bridge deck case scenario. Thus, the span length of the specimens was set up based on the estimated distance between the bending inflection points. As mentioned earlier, the bridge example had 3.65 m spacing between the main beams. For ideal uniform load distribution over the bridge deck, negative moments were expected near the main beam locations while a positive moment was expected at the middle. The distance between the seat beams was adopted to represent the effective span length or the distance between the bending inflection points where the bending span length was adopted to be 2.44 m. This distance represents almost two-thirds of the 3.65 m main beams spacing from the utilized bridge example. The mid-span vertical load was applied at the edge of the field joint to test the largest possible shear stresses at the interface between the joint and the precast panels.

Figure 5.4 shows a schematic drawing and a photograph of the test setup used in this study. Several types of instrumentation devices were used to monitor deflections, concrete cracks, and reinforcement and concrete strains at different locations of the specimens and throughout the test. Figure 5.5 shows some of the instrumentation devices used in this study. Figure 5.5 also shows the locations of the string potentiometers which were used to measure the deflections of the test specimens.

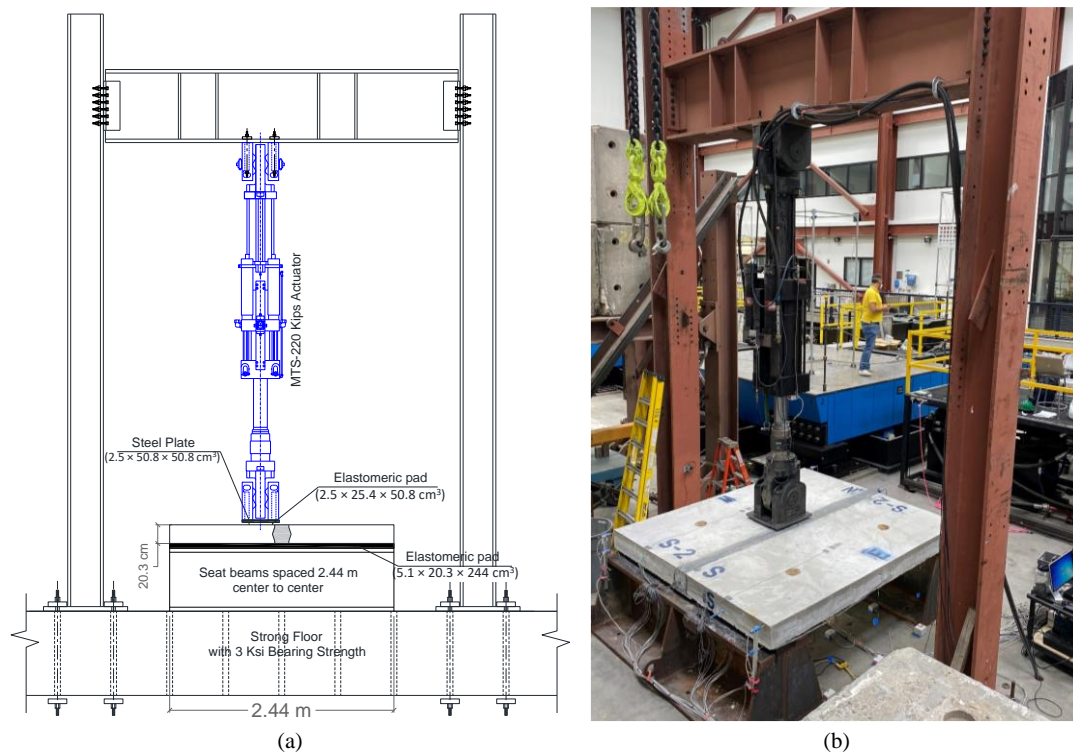


**Figure 5-4** Experimental test setup (a) schematic drawing of the test setup; (b) photograph of the actual test setup at UNR.

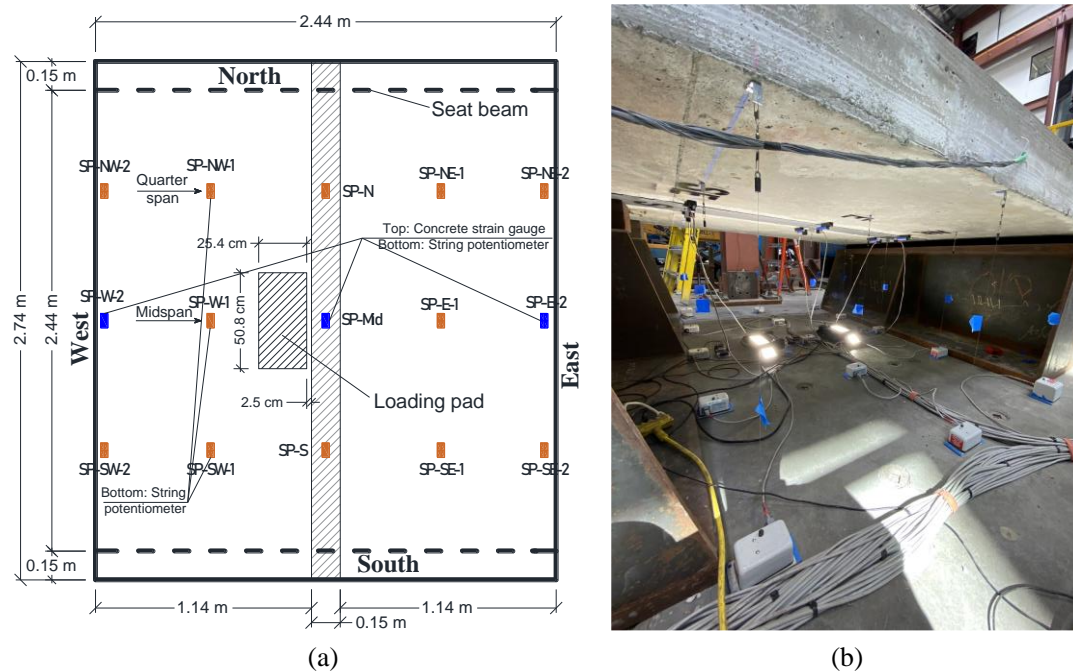


**Figure 5-5** Instrumentation plan (a) plan view for the locations of the string potentiometers; (b) photograph of the instrumentations.

### ***5.3.3 Loading Protocol***

The loading procedure used in the present study, which was also used to test the reference specimen with P-UHPC, i.e., S0, consisted of four cycles of loading and unloading at small load levels. These cycles were followed by a static monotonic loading up to the failure of the specimen. The purpose of establishing these initial cycles was to study the performance of the test specimens under representative service loads. The initial cycles included two 89 kN cycles, then two other 178 kN cycles. Loading and unloading rates of 22.24 kN/min were used during the first four cycles, while the last cycle was controlled by the mid-span deflection at a rate of 1.9 mm/min up to failure.

### ***5.3.4 Fabrication of Test Specimens***

The construction of the test specimens followed three main phases as illustrated in Figure 5.6. First, two precast panels were fabricated for each specimen using conventional concrete from a single ready-mix batch. The conventional concrete had a compressive strength of 27.5 MPa at 15 days and 52.4 Mpa at test days. After two weeks, every two panels were aligned together leaving a middle gap to pour the field joints. Finally, the field joints were poured using the NP-UHPC mixes with 2% and 1% steel fibers. The measured compressive strengths at test days of the 2% and 1% NP-UHPC mixes were 146.4 Mpa and 125.7 Mpa, respectively. The P-UHPC reference specimen was fabricated using conventional concrete with 35.8 Mpa compressive strength measured on the day of the test, and the P-UHPC had a compressive strength of 191.7 Mpa on the day of the test.

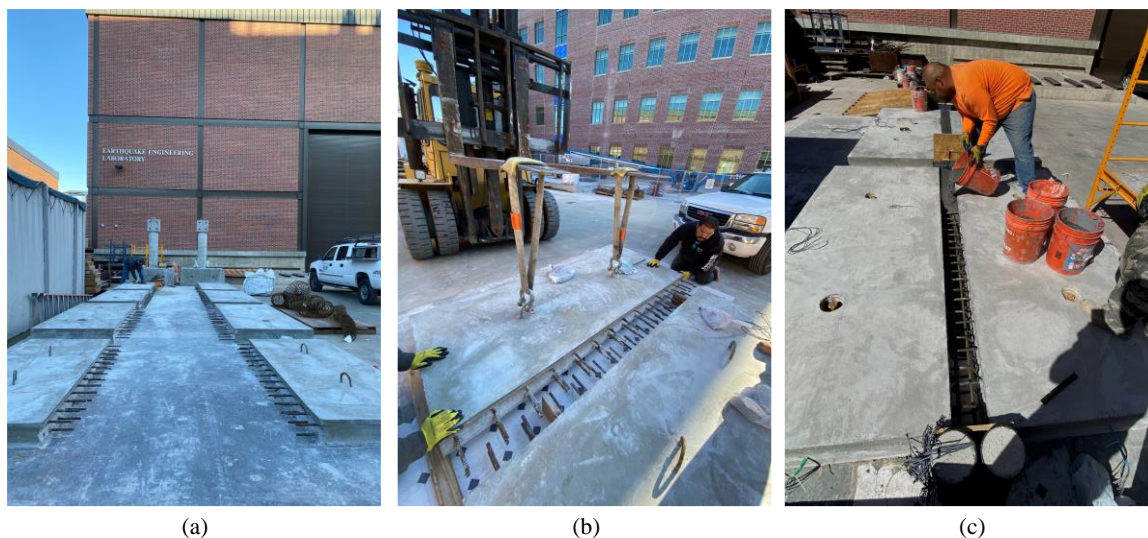


**Figure 5-6** Construction of the test specimens (a) fabrication of the deck panels; (b) alignment of the deck panels; (c) pouring the NP-UHPC inside the field joints.

## 5.4 Test Results and Discussion

This section shows the experimental test results of the three tested specimens and provides a discussion of the global behavior of the tested specimens in terms of damage progression, modes of failure, and load-deflection relationships. Furthermore, the local behavior of the tested specimens is also reported herein in terms of the load versus the reinforcement and concrete strains. In addition, this section provides evaluation and comparisons of the proposed NP-UHPC systems with the reference P-UHPC specimen to validate the use of the new material for future applications.

### 5.4.1 Key Results

A brief summary of the key test results is provided in Table 5.5. The table shows the initial stiffness, load capacities, load at which the reinforcement started to yield and middle deflections of the three NP-UHPC specimens in comparison with the results of the reference P-UHPC specimen. It is known that the bridge decks are designed to remain essentially elastic under the code specified service and ultimate loads. However, the testing of the specimens continued up to failure in order to understand the structural behavior and joint performance at such higher loads and to determine whether the whole system remains intact or the field joint or the joint interface would be the weakest links.

The table shows that the peak load capacities and initial stiffness of the NP-UHPC specimens are higher than that of the reference specimen with P-UHPC. This behavior is attributed to the higher compressive strength of the precast panels of the NP-UHPC specimens, i.e., 52.4 MPa compared to 35.8 MPa for specimen S0. The three NP-UHPC specimens had very comparable behaviors. However, specimen S3-Str-1% had slightly less initial stiffness and load capacity because of the lower strength of the NP-UHPC with 1% steel fibers. This resulted in larger deflections at the AASHTO service and ultimate loads. To be able to compare the results of specimen S1-Str-2% with the reference specimen S0, the compressive strength of both specimens was normalized since there is a difference between the compressive strength of the precast panels and the field joints of both specimens. Each specimen was fabricated from two different components (i.e., concrete panels and UHPC joints). The weighted compressive strength of specimen S0, depending on the width and compressive strength of the two components, is 45.54 MPa. Meanwhile, specimen S1-Str-2% had a weighted compressive strength of 58.27 MPa. Hence, specimen S1-Str-2% had a 28% higher compressive strength than specimen S0. The 28% higher compressive strength resulted in a 21% increase in the initial stiffness and only a 12% increase in the load capacity of specimen S1-Str-2%.

**Table 5-5** Summary of Key Experimental Test Results.

Specimen Name	Peak Load (kN)	Load @ 1 <sup>st</sup> Yield (kN)	Load @ 1 <sup>st</sup> Interface Crack (kN)	Mid-span Deflection (cm)			Initial Stiffness, (kN/cm)
				Peak Load	Service Load	Ultimate Load	
S0	524.5	≈ 290	520	5.920	0.444	0.975	420.3
S1-Str-2%	592.0	≈ 320	335	6.217	0.349	0.811	510.6
S2-Lop-2%	598.1	≈ 298	445	6.697	0.345	0.805	545.3
S3-Str-1%	581.0	≈ 281	400	6.183	0.437	0.992	460.1

#### 5.4.2 Global Behavior of Specimens

The global behavior of the tested specimens was evaluated herein in terms of the damage progression, modes of failure and load versus deflection relationships.

#### 5.4.2.1 *Damage Progression and Mode of Failure*

The observed modes of failure of the test specimens were almost similar, as such flexural members are usually designed to be tension controlled. In this case, the cross-section of the deck specimens is under-reinforced which forces the main reinforcement to yield before the concrete crushing. Hence, the common observed mode of failure for all test specimens is yielding of the bottom transverse reinforcement due to bending followed by crushing of the conventional concrete at the top of the precast panels. Figure 5.7 shows the damage schemes at the bottom and top sides of the test specimens.

The crushing of concrete was initially observed near the applied load location just before the failure of the specimens at approximately 570 kN. Then, the crushing propagated across the width of the west and east precast panels. It was observed that specimen S1-Str-2% had crushing at the west precast panel only. This was due to the interface crack (see Figure 5.7a) that happened at the top and bottom of the specimen between the east precast panel and the field joint. This interface crack was the main reason for the interruption of the load transfer path from the loaded west panel to the east panel that resulted in crushing of the west panel only. This damage is similar to the damage of the reference specimen and unlike that of the other two NP-UHPC specimens as there were no interface cracks observed. It is noted that specimens S2-Lop-2% and S3-Str-1% had a denser longitudinal reinforcement which was overlapped inside the joint compared to specimen S1-Str-2%. This denser reinforcement inside the joint may enhance the interface and prevent interface separation between the joint and the precast panels. This note suggests that it is better to use more overlapped reinforcement inside the field joint to avoid interface cracking and to ensure better load distribution across the precast panels.

Bridge decks are mainly designed to elastically sustain the AASHTO service and ultimate load levels. Thus, it is important to evaluate the damage of the specimens at these specified load levels. At the AASHTO ultimate load, only limited and narrow flexural cracks were observed at the bottom of the precast panels. No flexural or interface cracks were observed on any of the joints at this load level because of the high tensile strength of the NP-UHPC and its higher bond strength with the precast panels. The field joints of specimens S1-Str-



2% and S2-Lop-2% were cracked at around 335 kN. The field joint of specimen S3-Str-1% was cracked at earlier loads (i.e., 260 kN) because of the lower tensile strength of the NP-UHPC with 1% steel fibers compared to the 2% steel fibers. On the other hand, the first interface crack was observed at 335, 445, and 400 kN for specimens S1-Str-2%, S2-Lop-2%, and S3-Str-1%, respectively. These interface cracks were located mainly at the middle bottom of the specimens between the field joint and the east precast panel as shown in Figure 5.7. More importantly, the effect of these cracks was minor and they did not dominate the failure of the specimens as all specimens failed in pure flexural behavior. One more key observation for the tested specimens is that there was no bar slip observed for the lap splices within the joints throughout the test. This means that the proposed lap lengths were adequate to transfer the forces between both precast panels up to failure loads. The test was stopped when a specimen lose 20% of the observed peak load capacity.

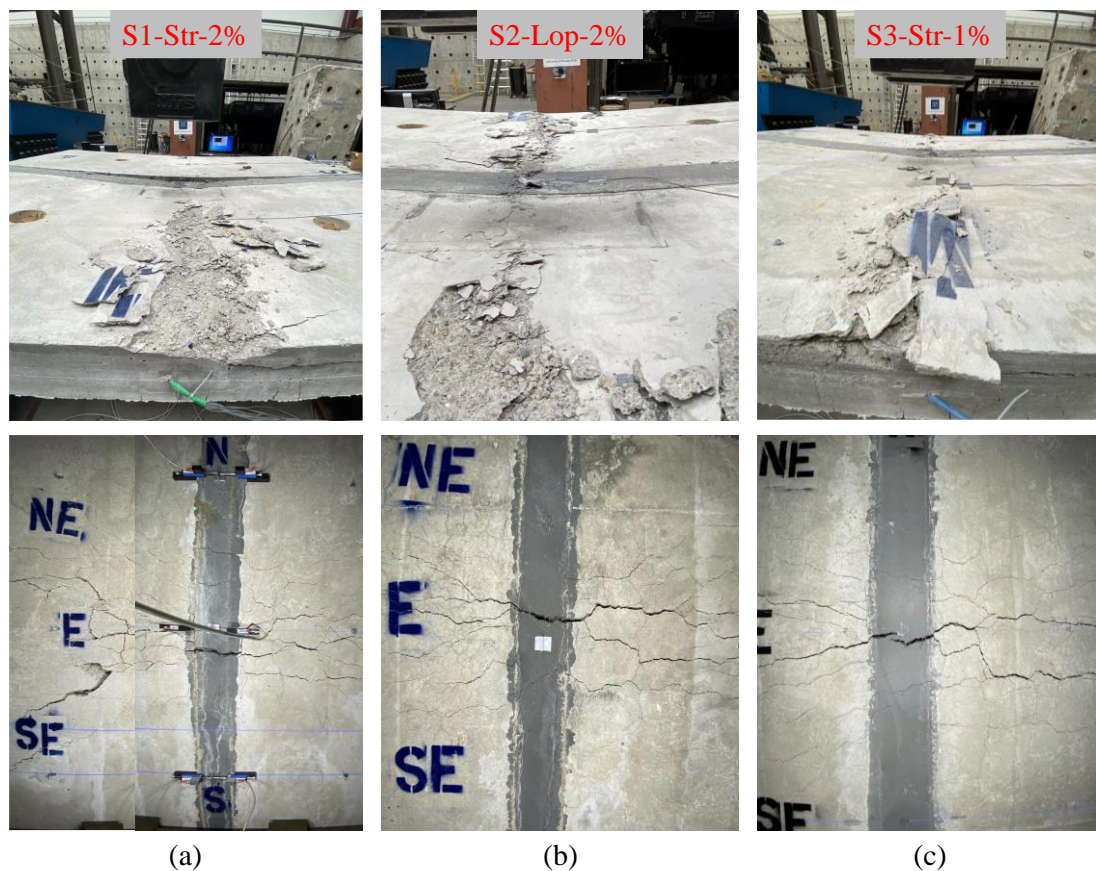


**Figure 5-7** Crack pattern, damage and modes of failure at the top and bottom of specimens (a) S1-Str-2%; (b) S2-Lop-2%; (c) S3-Str-1%.

#### 5.4.2.2 Load-deflection relationship

The global behavior of the test specimens was also evaluated based on the load versus middle deflection relationships. In this section, the load versus deflection relationships of the three test specimens are compared together. The main aim of this section is to investigate the effect of varying the test parameters on the flexural behavior of the specimens. Nonetheless, the overall behavior of the NP-UHPC specimens was also compared with that of the reference P-UHPC, which was provided in section 5.2.2. Figure 5.8a shows the load versus mid-span deflection relationships of the three test specimens. Figure 5.8b illustrates the different stages of behavior on the load versus deflection relationship of specimen S1-Str-2%. The flexural behavior of the tested specimens is almost similar if not identical. Hence, only the stages of the flexural behavior of specimen S1-Str-2% are shown here as a sample. The AASHTO LRFD limit states, shown in Figure 5.8, were calculated using the equivalent strip method. This method takes into account the largest possible moment values of the deck slabs with respect to the different loading conditions.

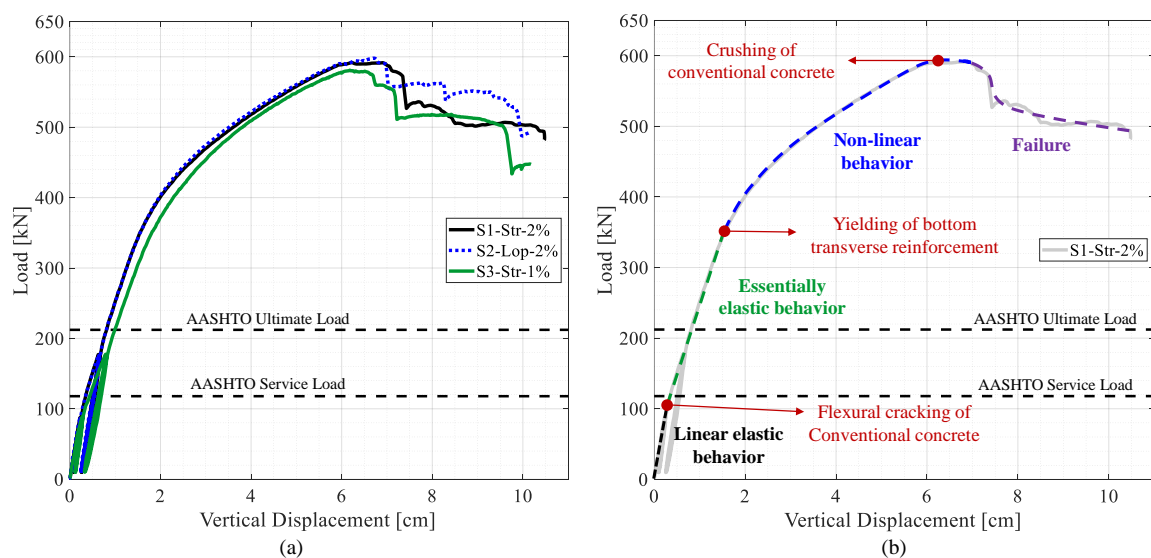


**Figure 5-8** Global Behavior of the NP-UHPC specimens: (a) Load versus mid-span deflection relationships of the tested specimens; (b) Stages of the flexural behavior of specimen S1-Str-2%.

In general, the flexural behavior of the test specimens was very comparable no matter the variation of the test parameters. However, it is shown that specimen S3-Str-1% had slightly

softer behavior due to the reduction in stiffness associated with the use of an NP-UHPC mix with only 1% steel fibers. The flexural capacity of the tested specimens had far exceeded the specified AASHTO LRFD ultimate limit state. There are many reasons for this large difference or factor of safety in this case. One reason is that the limit states were calculated based on the nominal steel yielding value of 410 MPa and nominal concrete compressive strength of 35 MPa. In reality, the actual steel yielding value was 480 MPa and the actual compressive strength was 52.4 MPa. Moreover, at the design stage of the test specimens, a moment reduction factor of 0.9 was used to magnify the moment demand and increase the required bottom transverse reinforcement. Nonetheless, the AASHTO LRFD design procedure does not count for the contribution of the top layer of reinforcement that usually yields to the more required bottom reinforcement.

The behavior of the tested specimens was similar to that of the P-UHPC specimen and the failure was dominated by flexure of the deck slabs without any major joint or joint interface failure or slippage of rebar lap splices inside the joints. Therefore, the NP-UHPC mixes used in this study with the proposed joint details can be considered as viable solutions for the transverse bridge deck field joints. The proposed NP-UHPC solutions can fulfill the target behavior of the conventional CIP bridge decks in terms of strength and flexure-dominated failure.

The typical flexural behavior of the tested specimens, as shown in Figure 5.8b, is divided into four main regions. The flexural behavior started with a linear elastic response up to approximately 100 kN in which the applied load was less than the cracking load of the specimens. The second region is defined by the essential elastic behavior in which the conventional concrete was cracked in tension while the reinforcement was not yet yielded. The concrete cracking resulted in a slight decrease in the flexure stiffness compared to the initial stiffness reported in Table 5.4. The initiation of yielding of the bottom transverse reinforcement was observed at the end of this stage which was associated with flexural and in some cases interface cracking of the field joints. This resulted in a non-linear flexural response of the specimens in which a significant reduction of stiffness was observed. This reduction in flexural stiffness was mainly due to a combination of factors including the

aggressive tensile cracking of the concrete, continued yielding of reinforcement, and, to less extent, the interface cracking of the joints. Finally, the failure of the specimens was observed after the crushing of the conventional concrete at the applied load location. This resulted in a global stiffness degradation in which the load capacity of the specimens decreases with increasing the applied vertical displacements.

### 5.4.3 Local Behavior of Specimens

The local behavior of the tested specimens was evaluated in this section in terms of the load versus the tensile strains of the transverse and longitudinal reinforcement in addition to the load versus the concrete compressive strains. Table 5.6 shows a summary of the largest recorded tensile strains of the transverse bottom reinforcement (i.e., main reinforcement), in addition to the maximum concrete compressive strains at the AASHTO LRFD service and ultimate loads. The following sections provide more details and discussion about these key results.

**Table 5-6** Summary of the Maximum Tensile Reinforcement Strains and Concrete Compressive Strains at the AASHTO LRFD Service and Ultimate Loads.

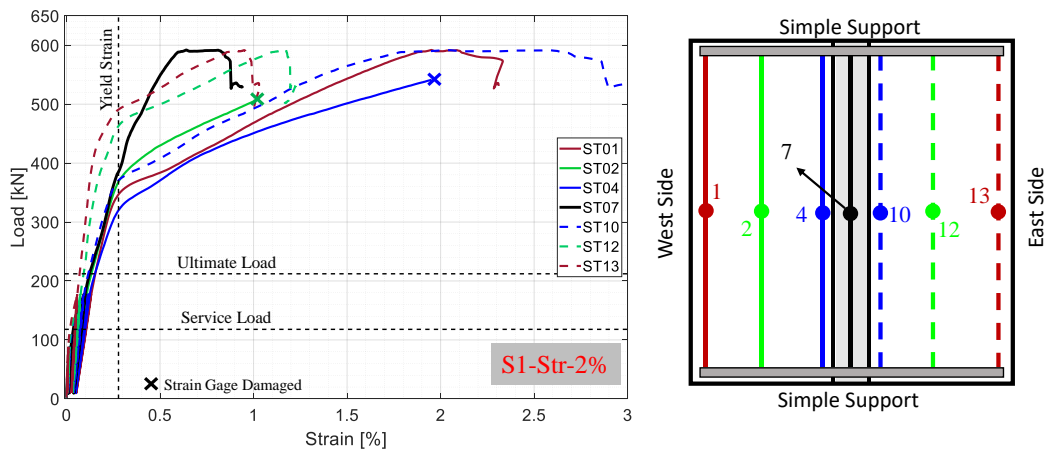
Specimen Name	Maximum Tensile Strain @ Bottom Transverse Reinforcement (%)		Maximum Concrete Compressive Strains ( $\times 10^{-3}$ )			
	Service Load	Ultimate Load	Precast Panels		NP-UHPC Joint	
			Service Load	Ultimate Load	Service Load	Ultimate Load
S1-Str-2%	0.068	0.154	0.30	0.65	0.29	0.72
S2-Lop-2%	0.069	0.174	0.38	0.73	0.39	0.88
S3-Str-1%	0.083	0.183	0.36	0.64	0.49	0.86

#### 5.4.3.1 Transverse Reinforcement Strains

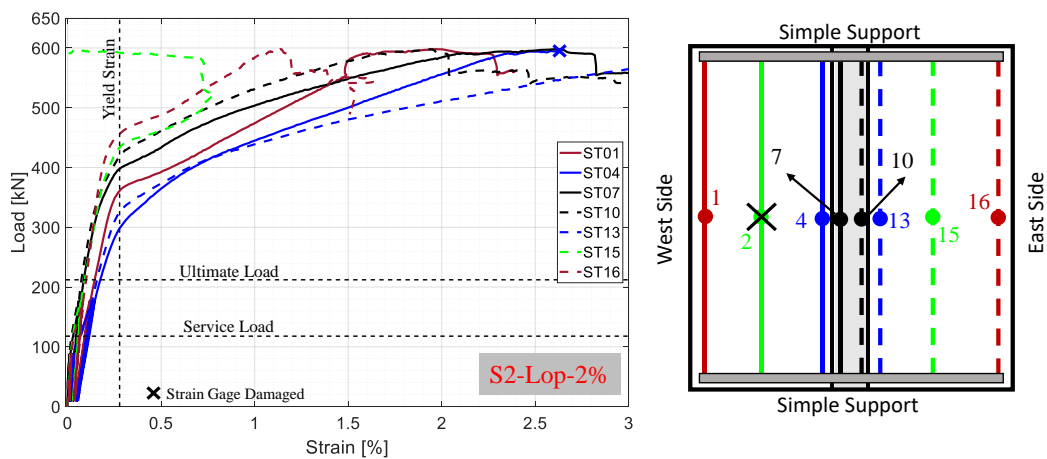
The load versus the measured tensile strains of the bottom transverse reinforcement at mid-span (i.e., maximum moment location) are shown in Figure 5.9. The figure also includes schematic drawings of the test specimens to show the location of the instrumented reinforcing bars and locations of the installed strain gages. It is noted that some of the strain gages were damaged, especially at larger strain levels as expected in typical destructive

testing. The damaged strain gages were noted in Figure 5.9. The main observation in Figure 5.9 is that the main reinforcing bars have not yielded before reaching the AASHTO LRFD ultimate load. This observation supports the fact that the specimens remained essentially elastic up to and slightly beyond the code allowable limit. This behavior was desirable to confirm that actual behavior exceeds nominal-based calculations, i.e., using the nominal values of 35 MPa for concrete compressive strength and 400 MPa for steel yielding strength of 400 MPa to calculate the AASHTO ultimate load. The actual strength values usually surpass these nominal values. Another reason for confirming the factor of safety belongs to the use of a reduction factor of 0.9 during the design stage, which increases the moment demand on the cross-section and consequently increases the required reinforcement. Nevertheless, the observed behavior verifies the acceptable performance of the NP-UHPC mixes as closure joint materials for the field joints of precast bridge decks.

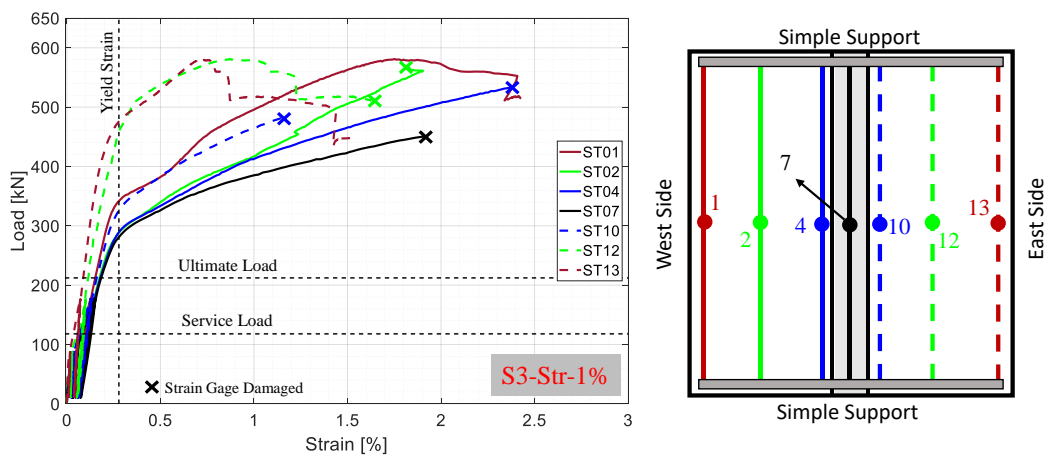
The yielding was initially observed either in the reinforcing bars which were located inside the field joints or adjacent to the west side of the joints. The first yield in the main reinforcing bars was observed at approximately 320, 298, and 281 kN for specimens S1-Str-2%, S2-Lop-2% and S3-Str-1%, respectively. The onset of yielding was followed by a sequence of yielding of the adjacent bottom transverse reinforcement. The excessive yielding of reinforcement resulted in global softening of specimens and consequently change of the flexural behavior to the non-linear response (see Figure 5.8b). It is also noted that the reinforcing bars which were located on the west precast panel were more stressed than the bars on the east side panel. This is attributed to the eccentricity of loading in the east-west direction as the load was applied on the west side of the field joint (see Figure 5.4). The two middle bars which were located inside the field joint of specimen S2-Lop-2% are usually called lacer bars. These bars are usually used to connect the inner tip of the loop splices (see Figure 5.3) to enhance the bearing reactions of the splices and increase ductility. As a result of the location of these lacer bars which were not located at the outermost surface of the joint, the tensile strains of these bars were found to be slightly lower than the other adjacent bars outside the joint.



(a)



(b)



(c)

**Figure 5-9** Load versus tensile strains of the bottom transverse reinforcement measured at mid-span of specimens (a) S1-Str-2%; (b) S2-Lop-2%; (c) S3-Str-1%.

#### 5.4.3.2 *Longitudinal Reinforcement Strains*

The previous section covered the tensile strains of the bottom transverse reinforcement (i.e., main flexural reinforcement). Thus, this complementary section focuses on the tensile strains of the longitudinal reinforcement (i.e., secondary flexural reinforcement) which were overlapped inside the joints. The strain gages were attached to the longitudinal bars near the two sides of the interface between the field joint and the precast panels as shown in Figure 5.10. The location of the strain gages was chosen based on two main reasons. First, the strain readings from both strain gages were intended to be compared together to anticipate if there is slippage of the reinforcement splices inside the joint. Second, the strain readings of the strain gages which were installed inside the joints (marked in red in Figure 5.10) were intended to be verified with the yield strain to determine if the development length was sufficient to yield the bars inside the joint. The two ways of verification may indicate if the proposed joint details and the utilized NP-UHPC mixes are sufficient to transfer the load from the west to the east precast panels. In this case, the proposed multi-component deck system can be considered equivalent to the monolithic CIP bridge decks. Figure 5.10 shows the results of the load versus the tensile strains of selected bottom longitudinal reinforcement. Figure 5.10 shows the maximum strain values of the longitudinal bars. It is noted that many of the strain gages were damaged during the construction of the specimens and field joints. Hence, the maximum strain results of the longitudinal bars of specimen S3-Str-1% were not shown in Figure 5.10.

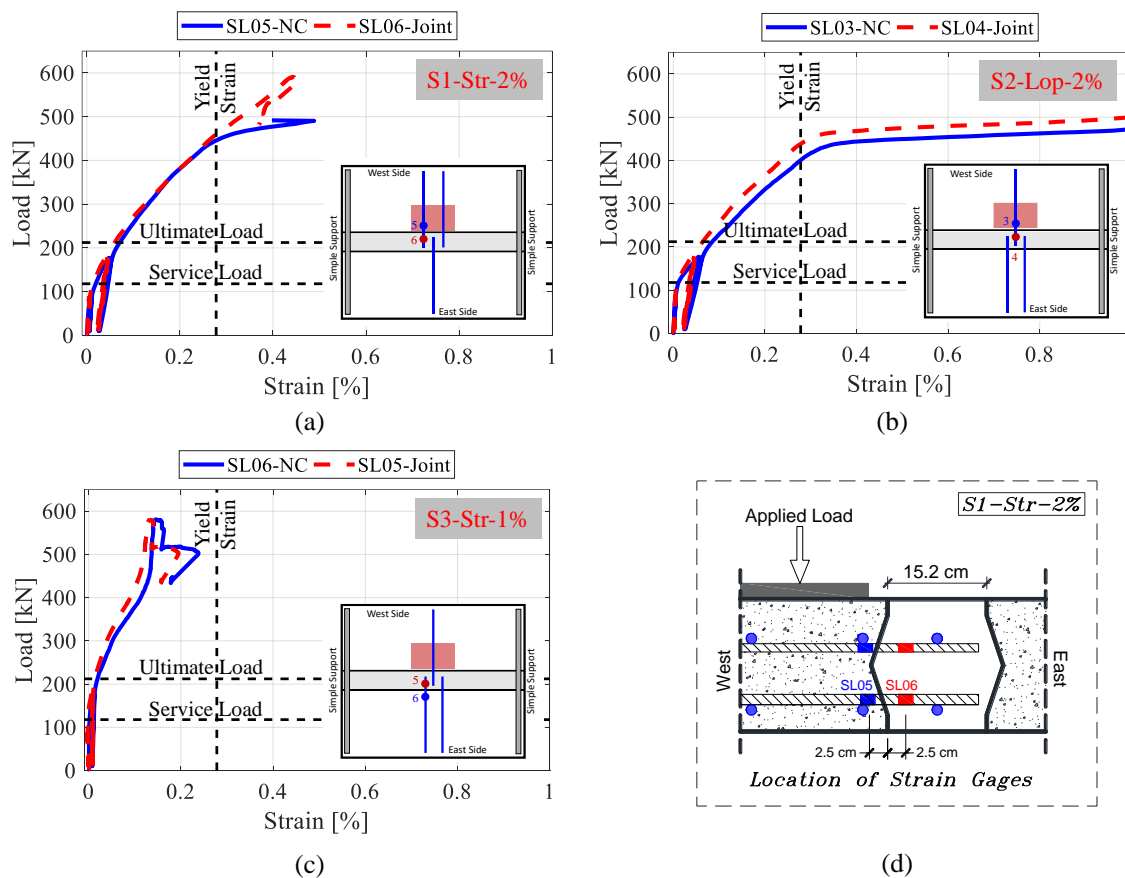


**Figure 5-10** Load versus tensile strains of selected bottom longitudinal reinforcement of specimens (a) S1-Str-2%; (b) S2-Lop-2%; and (c) S3-Str-1%.; (d) close-up view for the locations of the strain gages.

It was observed that the measured tensile strains of inside and outside the field joint were almost typical with no signs of bar slippage occurring up to the peak load. Nonetheless, the measured strain values of the longitudinal bars inside the joint for specimens S1-Str-2% and S2-Lop-2% exceeded the yield strain of reinforcement. This confirms that the proposed overlap length was sufficient to develop the yielding of reinforcement inside the joints. At the AASHTO ultimate load, the measured tensile strain values were typically far below the yield strain. This suggests that the demand on the field joints within the AASHTO design loads does not dictate the need for the full development length of the bars inside the joints. However, the use of the full development length may be required if the deck slabs were to be subjected to more demand loads than the specified AASHTO ultimate loads.



#### 5.4.3.3 Concrete Compressive Strains

The previous section focused on the tensile strains of the transverse and longitudinal reinforcement. Nonetheless, the load versus compressive strain readings of the conventional concrete and NP-UHPC are presented in this section (see Figure 5.11) for completeness. The concrete strain gages were placed at mid-span (maximum moment location) to measure the maximum compressive strength at the extreme concrete compression fibers of the precast panels and the field joint. The measured strain values were compared with the strains at which crushing of the conventional concrete and NP-UHPC were expected to happen. The crushing of the unconfined conventional concrete and NP-UHPC were expected to happen at compressive strains of approximately 0.003 and 0.005, respectively as per previous studies [26,30,31]. Hence, Figure 5.11 includes shaded areas, highlighted in blue color, to show the boundaries of the concrete crushing strain values. It is noted that some of the concrete strain gages were damaged during the test, especially at higher load values. Figure 5.11 shows when the concrete strain gages were damaged.

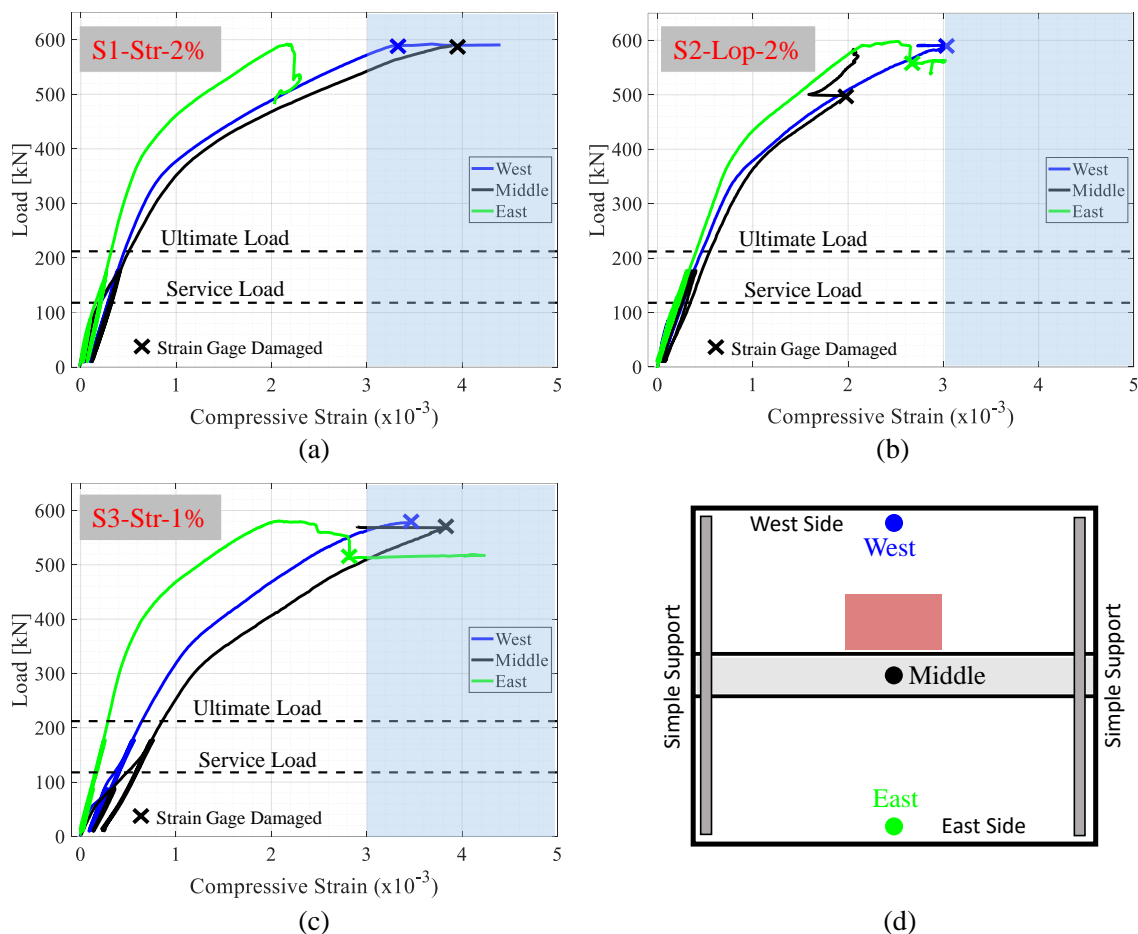


**Figure 5-11** Load versus concrete compressive strain measured at mid-span of specimens (a) S1-Str-2%; (b) S2-Lop-2%; and (c) S3-Str-1%.; (d) sketch of the test specimens with the locations of the concrete strain gages.

As mentioned earlier, crushing of concrete was observed slightly before the failure of the test specimens. The same observation can also be confirmed from the results shown in Figure 5.11. In the figure, the compressive strain readings indicated that most of the concrete strains are slightly more than 0.003 at the peak loads of the test specimens. The crushing of concrete was observed on the east and west precast panels, and similarly on the field joints. This behavior was slightly different from that of specimen S1-Str-2% as no crushing was observed in the east precast panel. The compressive strain values of specimen S1-Str-2%, which were measured at the east precast panel, were smaller than the crushing strain values. This is attributed to the interface crack between the field joint and the east precast panel that was the main reason for interrupting the load path from the applied load

location to the east panel. The concrete compressive strains of the east precast panel are slightly lower than the strains measured at the west panel and the field joint. This was expected because of the eccentricity of loading in the east-west direction. It was observed that specimen S2-Lop-2% has a slightly better strain distribution over the cross-section when compared to the other specimens. This indicates that the use of a loop splice instead of the straight lap splice enhanced the load distribution over the specimen cross-section. On the other hand, the dispersion of the concrete strains values of specimen S3-Str-1% may indicate a less favorable load distribution across the precast panels because of the use of an NP-UHPC mix with only 1% steel fibers.

## **5.5 Conclusions**

This paper summarizes the main results of the comprehensive full-scale experimental testing of representative precast bridge deck panels with NP-UHPC transverse field joints. The presented scope of work was part of a bigger research project that aims at developing and promoting NP-UHPC mixes and demonstrating their viability for various ABC applications, such as field joints of precast bridge decks. In this study, two NP-UHPC mixes with ingredients sourced from the western states (Nevada and California) were used as a closure joint material. The paper provides a brief discussion about the mix design and main mechanical properties of the utilized NP-UHPC mixes for completeness along with results of a similar specimen with P-UHPC transverse field joints for comparison purposes. The experimental program included testing three full-scale bridge deck specimens with transverse NP-UHPC joints. The test parameters included different joint splice details, joint widths, closure joint materials, and longitudinal reinforcement configurations. With the detailed discussion of the structural performance of the test specimens in terms of both global and local behaviors and comparison with reference P-UHPC specimen, the following observations and conclusions can be drawn:

- In general, the structural behavior and joint performance of the precast bridge decks with full-depth transverse NP-UHPC field joints are proof-tested and demonstrated to be acceptable and viable for ABC. As the proposed field joints adequately maintained

the load distribution capabilities along the specimen's cross-section up to the AASHTO ultimate loading without any major cracking or interface failure.

- The global and local behaviors of the test specimens with transverse NP-UHPC are shown to be very comparable to that of representative specimens of the readily implemented and acceptable practice of using commercial or proprietary UHPC mixes.
- All the test specimens had flexure-dominated failures in which yielding of reinforcement was observed before the concrete crushing and failure. As the yielding of the bottom transverse bars was observed at approximately 300 kN, while the crushing of concrete was observed approximately at 580 kN. In all tests, the NP-UHPC joints were confirmed to remain intact up to the full structural system failure level, i.e., NP-UHPC joints are not the weakest links in integrated deck systems.
- The initial stiffness and load capacities of the deck systems with NP-UHPC, which use a 2% by volume steel fibers amount, are slightly greater than that of the deck systems with NP-UHPC joints with only 1% steel fibers. For example, the peak load and initial stiffness of specimen S1-Str-2% were 592 kN and 510.6 kN/cm, respectively compared to 581 kN and 460.1 kN/cm for specimen S3-Str-1%. However, this slight reduction in stiffness does not have any implications for meeting the desired code limit states.
- The proposed deck systems with NP-UHPC transverse joints are able to fulfill the AASHTO LRFD service and ultimate load requirements without any major damage, splice slippage or interface cracking. In the conducted tests, only some interface cracks were observed at later loading stages which did not affect the failure of the specimens.
- The test specimens remained essentially elastic up to the AASHTO LRFD ultimate load in which no yielding of reinforcement was observed. The initiation of yielding was observed at the bottom transverse reinforcement at approximately 300 kN. The tensile strains of the longitudinal splices inside the joint indicated that the proposed overlap lengths were sufficient to yield the reinforcement inside the joint.
- The compressive strength of the conventional concrete and NP-UHPC showed that concrete crushing took place just before the failure of the specimens and after the yielding of the reinforcement (i.e., tension-controlled behavior is confirmed). The measured concrete strains indicate that the loop splices enhanced the load distribution

across the specimen's cross-section. Only the use of an NP-UHPC mix with 1% steel fibers would have a slightly less favorable load distribution, but with no adverse effects on meeting design requirements.

- Overall, the proposed NP-UHPC mixes with 1% and 2% steel fibers can be effectively used as closure joint materials for transverse field joints in precast bridge decks as they were able to provide full development for the reinforcement inside the joint and the provided adequate interface bond up to the AASHTO LRFD ultimate load.
- The performance of this material in field joints is very comparable to commercial/proprietary UHPC mixes as the peak load capacity of the NP-UHPC specimen was 592 kN compared to 524.5 kN for a similar P-UHPC reference specimen. Meanwhile, the NP-UHPC is cheaper than the P-UHPC where the typical P-UHPC and NP-UHPC material cost is estimated to be around \$ 3300 and \$ 1300 per cubic meter, respectively.
- The proposed transverse joint details and NP-UHPC materials are also able to provide equivalent behavior to monolithic CIP deck system as rendered from the observed failure mode, load distribution, or strain demands as the specimens remained elastic up to the AASHTO LRFD ultimate loads and the failure mode was mainly dominated by flexure of the specimens.

### **Acknowledgment**

The authors thank our partner at the ABC-UTC, Dr. Royce Floyd at the University of Oklahoma, for providing the mix design used in the ABC-UTC NP-UHPC initiative. We also thank the Laboratory staff at the University of Nevada, Reno for facilitating and helping with the large scale testing presented herein.

### **References**

- [1] American Road and Transportation Builders Association (ARTBA). *2020 Bridge Report*; ARTBA: Washington, DC, USA, 2020.

- [2] Zhu, P.; Ma, Z.J.; Cao, Q.; French, C.E. Fatigue Evaluation of Transverse U-Bar Joint Details for Accelerated Bridge Construction. *J. Bridg. Eng.* **2012**, *17*, 191–200, [https://doi.org/10.1061/\(asce\)be.1943-5592.0000257](https://doi.org/10.1061/(asce)be.1943-5592.0000257).
- [3] Li, L.; Jiang, Z. Flexural Behavior and Strut-and-tie Model of Joints with headed bar details Connecting Precast Members. *Perspect. Sci.* **2016**, *7*, 253–260, <https://doi.org/10.1016/j.pisc.2015.11.041>.
- [4] Badie, S.S.; Tadros, M.K. Full-depth precast concrete bridge deck panel systems. *Transp. Res. Board* **2008**, *584*, 115.
- [5] Verger-Leboeuf, S.; Charron, J.-P.; Massicotte, B. Design and Behavior of UHPFRC Field-Cast Transverse Connections between Precast Bridge Deck Elements. *J. Bridg. Eng.* **2017**, *22*, 04017031, [https://doi.org/10.1061/\(asce\)be.1943-5592.0001064](https://doi.org/10.1061/(asce)be.1943-5592.0001064).
- [6] Graybeal, B.A. *Behavior of Field-Cast Ultra-High Performance Concrete Bridge Deck Connections under Cyclic and Static Structural Loading*; No. FHWA-HRT-11-023; Federal Highway Administration: Washington, DC, USA, 2010.
- [7] French, C.E.; Shield, C.K.; Klaseus, D.; Smith, M.; Eriksson, W.; Ma, Z.J.; Zhu, P.; Lewis, S.; Chapman, C.E. *Cast-in-Place Concrete Connections for Precast Deck Systems*; No. NCHRP Project 10-71; The National Academies Press: Washington, DC, USA, 2011.
- [8] Perry, V.; Krisciunas, R.; Stofko, B. Mackenzie River twin bridges: North America's largest field-cast ultra-high performance concrete connections project. *PCI J.* **2014**, *59*, 40–48, <https://doi.org/10.15554/pcij.03012014.40.48>.
- [9] Sritharan, S.; Aaleti, S.; Garder, J.; Bierwagen, D.; Abu-Hawash, A. *Use of Ultra-High Performance Concrete in Bridge Design*; US-Japan Cooperative Program in Natural Resources, PWRI: Minamihara, Tsukuba, Ibraki, Japan, 2012.
- [10] Qiao, P.; Zhou, Z.; Allena, S. *Developing Connections for Longitudinal Joints between Deck Bulb Tees-Development of UHPC Mixes with Local Materials*; No. WA-RD 869.1; Department of Transportation: Washington, DC, USA, 2016.

- [11] Graybeal, B. *Development of Non-Proprietary Ultra-High Performance Concrete for Use in the Highway Bridge Sector*; FHWA Publication No. FHWA-HRT-13-100; Federal Highway Administration: Washington, DC, USA, 2013.
- [12] Aboukifa, M.; Moustafa, M.A.; Saiidi, M.S. *Seismic Response of Precast Columns with Non-Proprietary UHPC-Filled Ducts ABC Connections*; Report No. CCEER-20-08; Center for Civil Engineering Earthquake Research: Reno, NV, USA, 2020.
- [13] Aboukifa, M.; Moustafa, M.A.; Saiidi, M.S. Seismic response of precast bridge columns with composite non-proprietary UHPC filled ducts ABC connections. *Compos. Struct.* **2021**, *274*, 114376, <https://doi.org/10.1016/j.compstruct.2021.114376>.
- [14] Berry M, Snidarich R, Wood C. *Development of Non-Proprietary Ultra-High Performance Concrete*; No. FHWA/MT-17-010/8237-001; Montana. Dept. of Transportation. Research Programs: Helena, MT, USA, 2017.
- [15] Alsalman, A.; Dang, C.; Hale, W.M. Development of ultra-high performance concrete with locally available materials. *Constr. Build. Mater.* **2017**, *133*, 135–145, <https://doi.org/10.1016/j.conbuildmat.2016.12.040>.
- [16] Wille, K.; Naaman, A.E.; Parra-Montesinos, G.J. Ultra-High Performance Concrete with Compressive Strength Exceeding 150 MPa (22 ksi): A Simpler Way. *ACI Mater. J.* **2011**, *108*, 46–54.
- [17] Subedi, D.; Moustafa, M.A.; Saiidi, M.S. *Non-Proprietary UHPC for Anchorage of Large Diameter Column Bars in Grouted Ducts*; Report No. CCEER-19-03; Center for Civil Engineering Earthquake Research: Reno, NV, USA, 2019.
- [18] Tadros, M.K.; Gee, D.; Asaad, M.; Lawler, J. Ultra-High-Performance Concrete: A Game Changer in the Precast Concrete Industry. *PCI J.* **2020**, *65*, <https://doi.org/10.15554/pcij65.3-06>.
- [19] Kim, H.; Moon, B.; Hu, X.; Lee, H.; Ryu, G.-S.; Koh, K.-T.; Joh, C.; Kim, B.-S.; Keierleber, B. Construction and Performance Monitoring of Innovative Ultra-High-

- Performance Concrete Bridge. *Infrastructures* **2021**, *6*, 121, <https://doi.org/10.3390/infrastructures6090121>.
- [20] Abokifa, M.; Moustafa, M.A. *Development of Non-Proprietary UHPC Mix: Application to Deck Panel Joints*; Quarterly Progress Report; 2021, 1–10.
- [21] Shahrokhinasab, E.; Garber, D. *Development of “ABC-UTC Non-Proprietary UHPC” Mix, Final Report # ABC-UTC-2016-C2-FIU01-Final*; ABC-UTC: Miami, FL, USA, 2021.
- [22] Looney, T., McDaniel, A., Volz, J., Floyd, R. Development and characterization of ultra-high performance concrete with slag cement for use as bridge joint material. *BJCAE*, London, UK, **2019**, *1*.
- [23] Abokifa, M.; Moustafa, M.A. Experimental behavior of poly methyl methacrylate polymer concrete for bridge deck bulb tee girders longitudinal field joints. *Constr. Build. Mater.* **2020**, *270*, 121840, <https://doi.org/10.1016/j.conbuildmat.2020.121840>.
- [24] Abokifa, M., Moustafa, M.A., Itani, A.M. *More Choices for Connecting Prefabricated Bridge Deck Elements (No. ABC-UTC-2016-C1-UNR03-Final)*; Accelerated Bridge Construction University Transportation Center (ABC-UTC): Miami, FL, USA, 2020.
- [25] Abokifa, M.; Moustafa, M.A. Mechanical characterization and material variability effects of emerging non-proprietary UHPC mixes for accelerated bridge construction field joints. *Constr. Build. Mater.* **2021**, *308*, 125064, <https://doi.org/10.1016/j.conbuildmat.2021.125064>.
- [26] Abokifa, M.; Moustafa, M.A. Full-scale testing of non-proprietary ultra-high performance concrete for deck bulb tee longitudinal field joints. *Eng. Struct.* **2021**, *243*, 112696, <https://doi.org/10.1016/j.engstruct.2021.112696>.
- [27] California Department of Transportation. *Notice to Bidders and Special Provision*; Contract No. 06-0K4604, Project ID 0612000105; California Department of Transportation: Sacramento, CA, USA, 2015.



- [28] ASTM International. *Standard Test Method for Compressive Strength of Cylindrical Concrete Specimens, ASTM C39*; ASTM International: West Conshohocken, PA, USA, 2012; Volume 04.02.
- [29] American Society of Testing and Materials. ASTM C1609/C1609M-07. In *Standard Test Method for Flexural Performance of Fiber-Reinforced Concrete (Using Beam with Third-Point Loading)*; American Society of Testing and Materials: West Conshohocken, PA, USA, 2007.
- [30] ACI Committee. *Building Code Requirements for Structural Concrete (ACI 318-08) and Commentary*; American Concrete Institute: Farmington Hills, MI, USA, 2008
- [31] AASHTO (American Association of State Highway and Transportation Officials). *AAHSTO LRFD Bridge Design Specifications*, 7th ed.; American Association of State Highway and Transportation Officials: Washington, DC, USA, 2014.

## 6 FULL-SCALE TESTING OF NON-PROPRIETARY ULTRA-HIGH PERFORMANCE CONCRETE FOR DECK BULB TEE LONGITUDINAL FIELD JOINTS

*This chapter is a standalone paper that has been published in the journal of Engineering Structures*

### **Abstract**

Using deck bulb tee girders (DBTs) is one of the most popular and reliable solutions nowadays for accelerated bridge construction (ABC). DBTs usually require to be longitudinally connected on-site using robust materials such as ultra-high performance concrete (UHPC) for the field joints. The unparalleled mechanical properties of UHPC mixes have gained material popularity for ABC connections. However, the proprietary and relatively expensive nature of robust UHPC mixes pose some limitations, which motivated many researchers along with state departments of transportation to develop less expensive and non-proprietary UHPC mixes. The objective of this study is to leverage a readily developed non-proprietary UHPC mix, but using local materials available in the western United States, and to proof-test it in DBTs full-depth longitudinal field joints. An experimental investigation was conducted to test two full-scale specimens of a representative DBT top flange section with longitudinal field joints under static vertical loading. The specimens varied in the field joint material where one specimen used the developed non-proprietary UHPC and the other used a robust commercial UHPC mix. The structural behavior of both specimens was evaluated in terms of load and deflection capacities as well as the field joint performance. The results demonstrated that the developed non-proprietary UHPC mix can be efficiently used for longitudinal DBT field joints with comparable performance to proprietary UHPC joints.

### **6.1 Introduction**

As of April 2020, more than 46,000 bridges across the United States are considered structurally deficient [1]. Most of these bridges need bridge deck replacement or rehabilitation. The reason for this behavior is that bridge decks are usually susceptible to rapid degradation in their structural performance because of harsh environments where

they are more vulnerable to mechanical wear and tear effects. Moreover, the use of dicing salts in very cold weathers has resulted in a rapid reduction in the bridge deck lifetime because of the corrosion of reinforcement. The Accelerated Bridge Construction (ABC) techniques have paved the way to offer viable and rapid solutions for bridge deck replacements. The use of full-depth precast deck panels is one of these rapid solutions that can provide improved quality and durability. Moreover, the use of Deck-Bulb-Tee (DBT) girders has become a more popular application for bridge superstructure replacements especially in remote and rural areas where limited on-site activities are strongly required. DBT girders are prefabricated and shipped to the bridge site where they can be quickly assembled. Therefore, DBT girders can provide fast erection for bridge superstructures and hence less traffic disruption.

DBT girders can provide an integrated system that combines the typical I-section prestressed concrete girders with the top bridge deck layer. The integral DBT girders have top wide flanges that are connected on-site using longitudinal field joints as shown in Figure 6.1 [2]. Connecting the adjacent top flanges of the DBTs can provide a continuous multi-span bridge deck layer across the width of the bridge. Such DBTs longitudinal field connections between the top flanges of adjacent girders are the focus of this paper. Despite the major benefits of using the DBT systems, some state departments of transportation (DOTs) have limited their use because of the inadequate construction methods of the longitudinal field joints which were used in the past. In the past, welded clips and grouted joints were used in the longitudinal joints, which resulted in less durable joints due to the observance of interface cracking along the joint that may lead to leakage [3]. Thus, emerging research efforts investigated the applicability of using modern advanced materials such as ultra-high performance concrete (UHPC) for such joints to maintain simpler joint configurations in addition to increased durability [4].

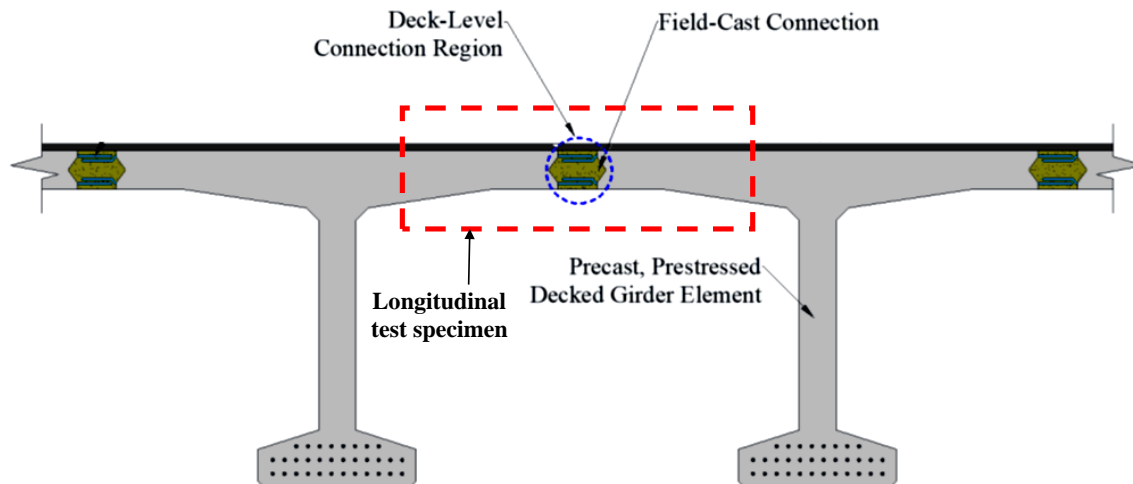


**Figure 6-1** DBT girders with full-depth longitudinal field joints [2].

UHPC is an advanced construction material that was developed in the late 20<sup>th</sup> century. It is a cementitious material with steel fibers and a low water-to-cement (w/c) ratio. The compressive strength of UHPC is typically 4-6 times higher than the normal strength concrete (NSC) in addition to other superior mechanical properties. Accordingly, many researchers examined the use of UHPC in many structural applications especially the use of UHPC in bridge field joints to connect different precast members. Examples of the research studies that focused on the use of UHPC in bridge deck field joints include, but are not limited to, the work done by Graybeal [4], Peruchini et al. [5], Hartwell et al. [6], Hwang and Park [7], Coufal et al. [8], Abokifa et al. [9], and Abokifa and Moustafa [10]. The earlier research studies examined the use of conventional construction materials for such joints as advanced grouts, high-performance concrete (HPC), and HPC with steel fibers [11-13]. However, special reinforcement requirements such as mechanical splices and post-tensioning along with relatively wider joints have been associated with the use of these conventional materials inside the field joints. Many of these previously provided solutions require more on-site work in addition to higher labor costs that are not viable for ABC.

When using UHPC, several research studies reported a typical UHPC field joint that has a diamond-shaped shear key and a 6 to 8 in (15.2 to 20.3 cm) width without reinforcement post-tensioning and with traditional straight or loop splices. These typical details of the

UHPC field joint demonstrated acceptable structural performance in transferring shear and bending across different precast panels in addition to significantly providing higher durability under cyclic loading [4, 14-16]. Nonetheless, UHPC is associated with practical challenges as it requires special expertise to mix and place due to steel fibers and has a long mixing time. However, these problems could be easily tackled by increasing the number of research studies that focus on developing large UHPC batches. Additionally, these problems could be solved by having more technical reports that provide better practices for mixing and placing UHPC along with the other solutions for the technical issues reported in various projects. Another major drawback of using UHPC that is also attracting more interest to resolve is the expensive and proprietary nature of robust UHPC mixes. This usually causes bidding issues among state DOTs that are trying to limit the sole sourcing of materials.

Same state DOTs sponsored research to develop their own non-proprietary UHPC (NP-UHPC) mixes with implementing locally and domestically available materials to avoid the cost and bidding issues associated with the proprietary UHPC [e.g. 3, 17-21]. But only very limited research studies focused on large-scale applications and experimental testing of newly developed and emerging NP-UHPC mixes when used in bridge deck field joints. A recent research project, which was funded by Washington DOT, aimed at developing NP-UHPC using locally available materials and tested the new mix in a hypothetical DBT longitudinal field joints setting [5]. However, this study tested only a small section of the deck representing actual DBT girders with a width of 2 ft [0.6 m] under static bending to determine the required joint width and splice length. The experimental results showed that a UHPC joint width of 7.11 in [18 cm] and a splice length of 5.11 in [13 cm] are considered sufficient to fracture the bars inside the joint. Moreover, the study concluded that the body of the UHPC joint did not suffer any cracking, while there was a significant interface crack at the cold joint between the UHPC and the adjacent precast members owing to the unprepared flat joint surface. These interface cracks usually allow the ingress of moisture and deicing chemicals that may lead to rapid corrosion of the reinforcement and deterioration of the bridge deck. Hence, it is strongly recommended from some literature studies to use female-female shear keys for such connections instead of the ordinary flat

surfaces to facilitate the compression strut transfer of applied loads, instead of relying on dowel action of reinforcing bars [22]. Looney et al. have also tested representative full-scale bridge deck specimens with proprietary and NP-UHPC longitudinal field joints [23]. The purpose of this study was to evaluate the behavior of a NP-UHPC mix, which was developed using locally available materials in the state of Oklahoma, as a bridge deck joint material [24]. The NP-UHPC mix design used in the present study follows the same mix design used in this literature study, but with using different material sources. The study concluded that the NP-UHPC mix performed comparably to the proprietary UHPC. This study has motivated the authors to further replicate the same mix design using local materials available in the western states. However, this study has also used the undesirable flat shear key shape with a relatively wider joint of 11.8 in width and a straight contact lap splice with adding splicing bars. Yuan and Graybeal have recommended the use of non-contact lap splices as they can exhibit higher bond strengths than the contact lap splice inside the UHPC [25].

To further resolve bidding and sole-source issues, some research efforts also considered identifying other alternative closure materials that can provide the same acceptable performance as proprietary UHPC in bridge deck field joints. For example, in recent work conducted by the authors [9, 10], poly-methyl methacrylate polymer concrete (PMMA-PC) was identified as a potential alternative to the UHPC for deck field joints. In a parallel ongoing research project, the authors tested three full-scale specimens with transverse field joints in addition to two other specimens with longitudinal field joints. The study established a direct “apples-to-apples” comparison between the specimens with robust proprietary/commercial UHPC mix and PMMA-PC field joints. We concluded that the PMMA-PC joints can provide the same structural performance as the UHPC joints without any interface cracking or bar slippage [9, 10]. The reason that project is considered a parallel effort is that the experimental work reported herein leverages and complements the recently completed work through using similar specimen designs and testing setup.

As mentioned above, there are only limited experimental validations for NP-UHPC field joints behavior and implementation. Some of these experimental efforts provided guidance

for the potential use of different NP-UHPC mixes in the field joints. However, the tested specimens in these studies have relatively smaller dimensions than the full-scale specimens or un-recommended shear key shapes and joint splices. . Hence, this paper aims at filling this important knowledge gap and providing a good understanding of the experimental behavior of the commonly used longitudinal field joints in DBT girders. The focus here is on extending the use of a NP-UHPC mix, readily developed through multi-institutional collaboration among the accelerated bridge construction university transportation center (ABC-UTC), by using locally available materials in Nevada and California and large-scale implementation. The NP-UHPC mix was considered as a closure pour material for both transverse and longitudinal full-depth deck joints. However, only experimental results for the longitudinal joint specimens are covered in this paper to provide a detailed presentation and analysis of test results and thorough discussion of the structural behavior of NP-UHPC longitudinal field joints. The overall objective of this paper is to investigate and validate the structural performance of NP-UHPC longitudinal field joints as compared to robust proprietary/commercial UHPC joints. The paper presents results from two full-scale experimental tests of deck assemblies of representative DBT girder flanges with proprietary and NP-UHPC longitudinal field joints under static vertical loading. The paper includes several sections that present a discussion on the developed mix and material characterization, details of the conducted experimental program, test results comparisons and discussions, and concluding remarks.

## **6.2 Non-Proprietary UHPC Mix Design And Characterization**

This study is part of a larger multi-institutional collaboration between all five ABC-UTC consortium universities. The University of Oklahoma (OU) led the development of the new NP-UHPC mix and have conducted most of the material, bond, and durability testing of the developed mix using materials locally available in the state of Oklahoma [24]. The final mix design has been shared among other ABC-UTC universities to establish the large-scale implementation of the mix using different material sources around the nation. For example, the University of Nevada, Reno (UNR) has investigated the use of the final shared mix design using local materials on the west coast inside the bridge deck field joints. One of

the side objectives of the ongoing efforts was to compare and assess some of the main mechanical properties of the developed NP-UHPC mix when assembled from different sources, then mixed and tested by different teams at various universities. Hence, several trial batches were mixed and tested at UNR before extending large-scale experimental testing of the new material inside the field joints. In this section, we compare the main physical and mechanical properties such as slump, compressive strength, and flexural strength of the NP-UHPC when assembled from different material sources at different ages. These tests were selected to be representative of the main mechanical properties of the new material and could be a useful tool for verifying the variations in the mechanical properties that may arise from using different material sources while using the same mix design.

Again, the research team at UNR was mainly responsible for the large-scale implementation and experimental testing and investigation of the new UHPC material inside the bridge full-depth deck joints. This task was divided into many steps starting from locating the local material suppliers in the Nevada and California states who can easily provide and ship the materials in large and small quantities. Then, mixing of trial batches that use the locally sourced materials and conduct material testing to validate the material properties and compare them with the reference UHPC mix developed and tested at OU. Once satisfactory results were obtained from the comparison of the material properties, the new UHPC mix sourced and mixed at UNR was extended and tested inside the deck field joints. This section provides a discussion of the mix development and characterization.

### ***6.2.1 Non-proprietary UHPC mixing proportions and procedure***

The baseline mix design that has been proposed by OU and utilized in this study is reported in Table 6.1. The table also shows the material suppliers for both UHPC mixes that were developed at OU and UNR. The commercially available proprietary UHPC products are usually composed of three different pre-packed components including a proprietary mix of dry components, liquid admixtures, and steel fibers. In this effort, the NP-UHPC was developed from mixing and proportioning of seven different components as illustrated in Table 6.1 and shown in Figure 6.2a.



**Table 6-1** Baseline non-proprietary UHPC mix design as developed by OU [24].

Material	Quantity, lb/yd <sup>3</sup>	Quantity, kg/m <sup>3</sup>	OU Supplier	UNR Supplier
Cement Type	1179.6	700	Type I, Ash Grove Chanute, Kansas	Type I/II Nevada Cement, Reno
Slag	589.8	350	Holcim, South Chicago	Lehigh, Sacramento
Silica Fume	196.6	116.6	Norchem Ohio	BASF (Master Life SF 100)
Water	393.2	233.3	Potable Water	Potable Water
<i>w/cm</i>	0.2	0.2		
Fine Masonry Sand	1966	1166.4	Metro Materials Norman, OK	Crushed Aggregate Sand, Martin Marietta Sparks, NV
Steel Fibers	255.2 (2% by volume)	151.4 (2% by volume)	Bekaert (Dramix <sup>®</sup> OL 13/0.2)	Bekaert (Dramix <sup>®</sup> OL 13/0.2)
Superplasticizer	22.2	13.2	BASF (Glenium 7920)	BASF (Glenium 7920)

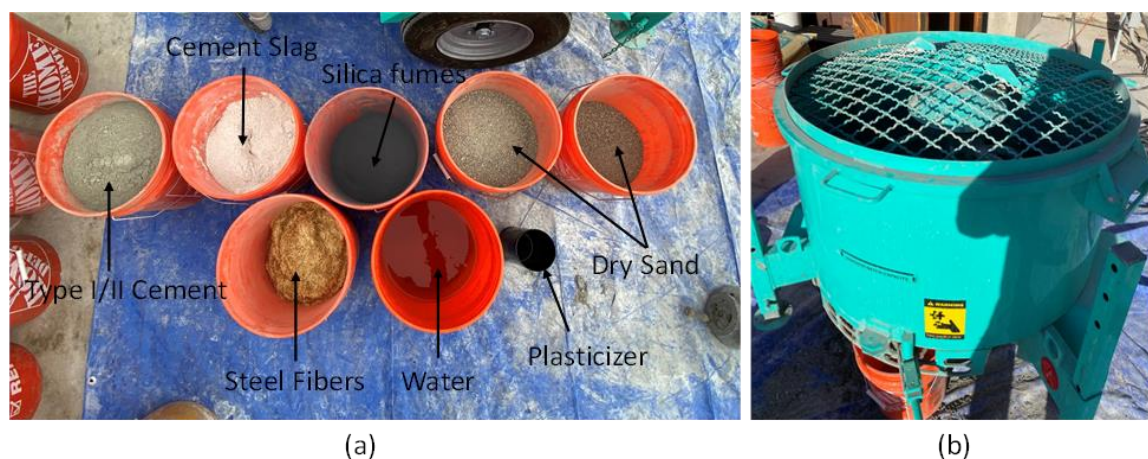


**Figure 6-2** NP-UHPC mixing at UNR: (a) UHPC mix components; (b) UHPC high shear mixer

The NP-UHPC was mixed at the fabrication yard of the Earthquake Engineering Laboratory (EEL) building at UNR using a high shear mixer that is readily available at UNR (see Figure 6.2b). The type of high shear mixer used in this study is “Imer 750”, which has a total capacity of 5.12 ft<sup>3</sup> (0.145 m<sup>3</sup>). Only half of the mixer capacity was utilized at a time for all the developed UHPC batches to ensure the consistency of the

batches and to better control the quality of the mixes. It is worth noting that the sand used in the material trials and eventually the large-scale implementation was left in trays inside a furnace to dry for 24 hours before mixing.

The mixing procedure of UHPC is divided into many steps while the average total mixing time of one UHPC batch is typically around 25-30 minutes. First, all dry components were added to the mixer and left to blend for 10 minutes. Then, the whole amount of water mixed with half the required amount of plasticizer was added gradually to the dry mixture over the course of 2 minutes. After one minute, the second half of the plasticizer was then gradually added to the mix over the course of one minute. Next, the components were left to mix for around 7-10 minutes until the mix turned to be flowable. Finally, steel fibers were added gradually to the UHPC paste over the course of 2 minutes and then left for 1-2 minutes to ensure a uniform distribution of the fibers inside the mix. It is strictly recommended to use 100% ice instead of the required quantity of water if the daytime temperature exceeded 25°C (77°F). This water replacement is mainly done to ensure that the mix will have sufficient working time for mixing, placing, and forming.

### ***6.2.2 Non-Proprietary UHPC Material Testing***

As mentioned earlier, the trial NP-UHPC batch made from the Nevada and California local materials was mixed and tested before using inside the field deck joint. This was done to ensure that the target mechanical properties of the trial mix conform to the properties of the baseline mix developed at OU. Different sets of material tests were conducted on the trial batch at different concrete ages. These tests included slump testing of the fresh NP-UHPC, and compression and flexural tests of the hardened NP-UHPC, as shown in Figure 6.3. The obtained test results were compared to the results from OU to verify the consistency of the results and validate the future use of our mix in large-scale testing and implementation.

The flowability properties of the mix were measured using a spread cone mold in accordance with ASTM C 1437/230 (see Figure 6.3a) [26, 27]. The spread of the flow diameter of the NP-UHPC, which was measured from the static flow test, was approximately 8 in (20.3 cm). While the flow diameter measured from the dynamic flow

test was greater than or equal to 10 in (25.4 cm). The compressive strength was measured using 3×6 in cylinders that were initially prepared through the surface grinding of both cylinders ends (see Figure 6.3b). The surface grinding was done, as recommended by the ASTM C1856 [28], to achieve appropriate flat and smooth surfaces at both cylinder ends. The compression testing followed was done in accordance with the ASTM C1856 along with ASTM C39 [29], where the specimens were preloaded to approximately 50% of the expected failure load, then the specimens were loaded to failure at a rate of 150 psi/sec [1034 kPa/sec]. The compression testing was conducted at several ages, i.e. 3, 7, and 28 days. Table 6.2 shows the compression test results of the mix developed at UNR compared to the results from the OU baseline mix.

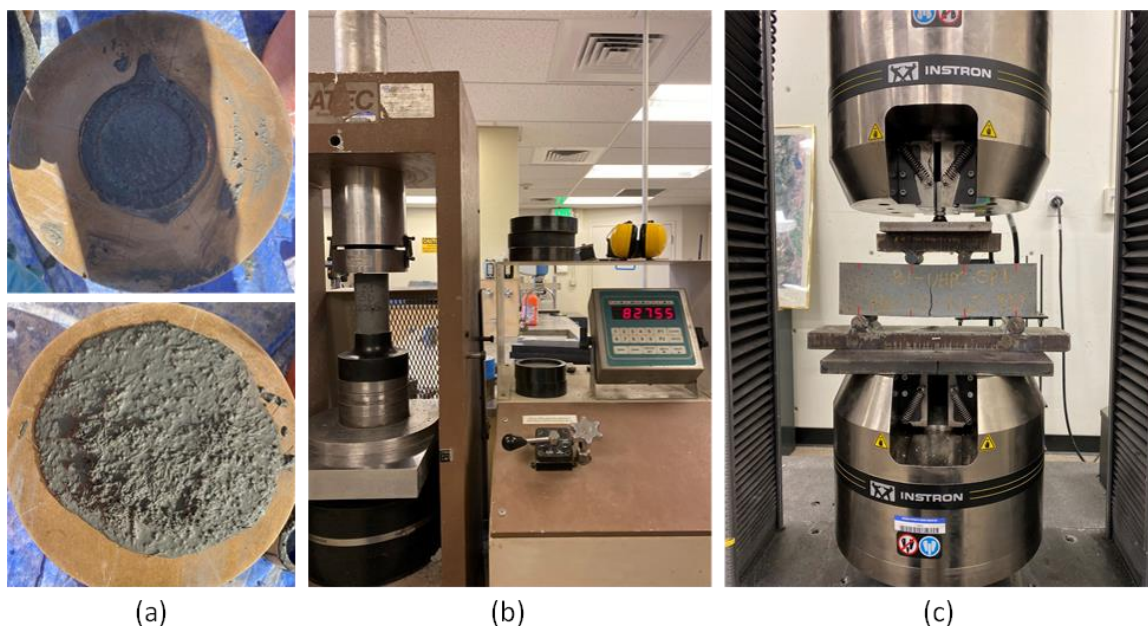


**Figure 6-3** NP-UHPC material testing at UNR: (a) slump test; (b) compression test; (c) flexure test.

For the flexural strength and modulus of rupture characterization, 3×3×12 in rectangular prisms were prepared from the trial NP-UHPC batch and tested according to the ASTM C1856 along with ASTM C1609 [30] (see Figure 6.3c). The rectangular prisms had a span of 9 in (22.9 cm) and loading was applied at two points in the middle third of the prism. The displacement rate at the beginning of the test was 0.003 in/min (0.076 mm/min) up to 0.01 in (0.254 mm) mid-span deflection, then the rate was increased to 0.005 in/min

(0.127 mm/min) until the end of the test. The flexure testing was done at 7 and 28 days. Table 6.3 shows the flexural test results of the NP-UHPC mix developed at UNR compared to the results of the OU baseline mix.

**Table 6-2** Compressive strength results [psi (MPa)] of the UNR and the OU NP-UHPC mixes

Batch Name	3 Days	7 Days	28 Days
UNR mix	11,860 (81.8)	14,100 (97.2)	16,660 (114.9)
OU mix	12,540 (86.5)	14,480 (99.8)	17,220 (118.7)

**Table 6-3** Flexural strength results of the UNR and the OU NP-UHPC mixes.

Batch Name	7 Days [psi (MPa)]	28 Days [psi (MPa)]
UNR mix	2,520 (17.4)	3,005 (20.7)
OU mix	N.A.	2,570 (17.7)

From the previous material characterization test results, it can be concluded that the main mechanical properties of the mixes developed by UNR and OU are very comparable. As a result, the trial mix developed at UNR was then replicated and used inside the longitudinal field joint to investigate the structural performance of the new material for such joints and compare its performance with that of the proprietary UHPC.

### 6.3 Experimental Program

This section provides information regarding the structural design, details, and construction of the test specimens along with the test setup, instrumentation plan, and loading protocol used in this study.

#### 6.3.1 Design and Fabrication of the Test Specimen

The design of the specimens was done according to the provisions of the AASHTO LRFD Bridge Design Specification [31]. The design procedure assumes a monolithic behavior of the bridge deck without accounting for the deck discontinuity and field joints effects. The bending and shear demands were calculated based on the AASHTO Equivalent strip method that considers the maximum moment and shear values experienced by a bridge deck from infinite loading conditions. The general dimensions of the test specimens were

determined based on the dimensions of the top flange of the standard and typical precast DBT girder in addition to the typical test specimens reported in previous research studies. The thickness of the top flange of the typical AASHTO/PCI standard DBTs is 6 in (15.2 cm) [32]. In literature, many researchers have conducted experimental testing of narrow strips of the top DBT girder flanges with a middle longitudinal field joint. For example, Haber and Graybeal have tested 6-in (15.2-cm) thick panels with general plan dimensions of 28 in (71.1 cm) width and 107 in (271.8 cm) length and a bending span of 90 in (228.6 cm) [2]. Peruchini et al. [5] have tested panels with a width of 24 in (61 cm) and a bending span of 90 in (228.6 cm). The minimum and maximum centerline to centerline spacing between the DBT girders as specified by WSDOT is 60 in (152.4 cm) and 96 in (243.8 cm), respectively and it has a typical 6 in (15.24 cm) thick top flanges [5]. However, other researchers have conducted large scale testing of relatively bigger test specimens with plan dimensions that range between 72-96 in (183-244 cm) width and 72-84 in (183-213 cm) length with a bending span of 72 in (183 cm) [e.g. 4, 14]. Hence, the general dimensions of the test specimens, as shown in Figure 6.4, were selected to be within the range of dimensions as reported in the previously mentioned literature studies.

As illustrated previously in Figure 6.1, the test specimens represent only a portion of the connected top flanges of the DBT with a longitudinal field joint at the middle of the specimen. The width of this portion was determined based on the likely representative distance between the bending inflection points so that the specimen would see just the expected positive moment part. Since it is hard to determine the exact locations of these inflection points, because of the large number of the expected loading conditions, the width of the specimen was taken as 7 ft (2.13 m) to allow for a 6 ft (1.83 m) positive bending span which is approximately 75% of the maximum centerline to centerline distance between DBT girders.

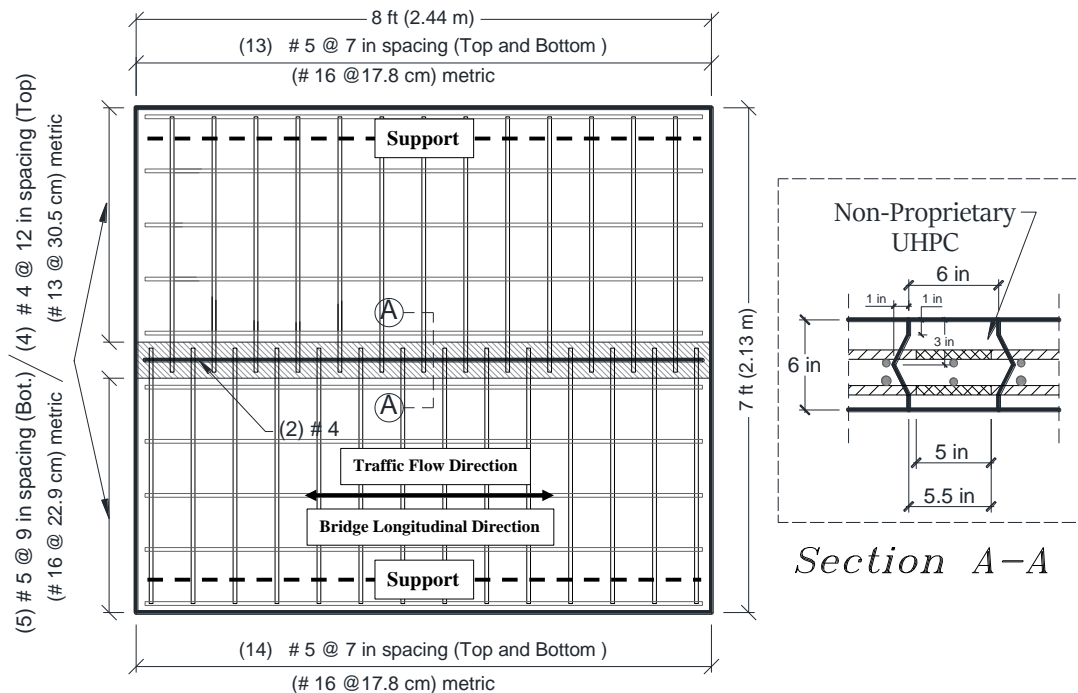


**Figure 6-4** General Dimensions and structural details of the test specimens and a cross sectional view of the longitudinal field joint (1 in = 2.54 cm, 1 ft = 30.48 cm).

Many practical considerations were taken into account during the choice of the longitudinal field joint details in order to enhance constructability and decrease the onsite activities. Hence, a non-contact lap splice was used to facilitate the assembly of the precast deck panels. A literature study concluded that Moreover, the use of advanced UHPC materials in such joints has eliminated the need for reinforcement post-tensioning [22,33,34], mechanical splicing [35], or splice confinement requirements [36] which were previously required to connect the precast elements. A diamond-shaped shear key was used for the longitudinal joint interface to enhance durability and decrease the likelihood of having interface cracks between the joint and the precast elements. The 6 in (15.24 cm) width of the longitudinal field joint (see Figure 6.4) was determine based on the bond tests developed by OU on the baseline NP-UHPC mix in addition to recommendations of previous research studies [4,9,10]. The transverse bars have a 5.5 in embedment length inside the field joints, which satisfied the minimum development length requirements of 8 times the diameter of the bar ( $8d_b$ ) as recommended by the FHWA [22].

The top and bottom concrete covers of the test specimen were selected based on the AASHTO code provisions for bridge decks with normal condition exposure in a non-corrosive environment. Thus, the test specimens had a 2 in (5 cm) top cover and a 1 in (2.5 cm) bottom cover. The transverse reinforcement was considered as the main reinforcement of the top DBT flanges and hence they were placed as the outermost layers to increase the moment capacity of the specimen that will consequently subject the field joint to higher load demands. All reinforcement used in this study was of Grade 60 steel that conforms to the ASTM A706 specification. The precast panels, which represent parts of the DBT top flanges, were fabricated using a normal strength concrete with a minimum specified compressive strength of 5 ksi (34.5 MPa) after 28 days.

The fabrication process of the test specimens is divided into several phases that mimic the way the DBT girders and longitudinal field joints are typically constructed in real field applications. However, it is noted that both specimens were constructed separately at two different times since the proprietary UHPC specimen was previously constructed as part of another precedent research project as previously mentioned. The fabrication process was done at the fabrication yard of the EEL at UNR as shown in Figure 6.5 and summarized in the following section. The DBT girders are usually fabricated away from the bridge site location and then left on the fabrication facility to cure in a controlled environment before shipping them to the field and connecting them using longitudinal field joints. Hence, for each specimen, two precast deck panels which represent a portion of the top flanges of the DBT girders were constructed first. Then, they were left to cure on-site under the normal ambient air conditions for more than 28 Days to gain full strength. Then, both precast panels were reassembled next to each other to form the 6 in (15.24 cm) field joint. Finally, the closure pour material (e.g. NP-UHPC) was then mixed and poured inside the joints and left to cure on-site before moving the specimens to the laboratory for experimental testing.



**Figure 6-5** Photographs from the fabrication process and illustration of the sequence of constructing test specimens.

### **6.3.2 Test Setup and Loading Protocol**

The experimental testing of the test specimens was done at the EEL at UNR. The test setup was adopted to investigate the local flexural behavior of the representative DBT flange portions and field joint performance under the typical AASHTO truck wheel patch size. However, other minor load effects were not considered in the utilized experimental test setup such as the action between the flanges and DBT girder web parts and the resulting forces due to adjusting the differential cambers in DBT girder bridges. Moreover, the test setup did not account for the axial restraint at both specimen ends and the associated contribution to the load-bearing capacity of the specimen as the test specimen only represents the distance between two adjacent bending inflection points in the bridge transverse direction. Hence, rubber bearing pads were used at both ends of the test specimen to allow for rotation at support locations. Wheel loads or live loads are typically considered the main demands while designing bridge decks and deck field joints, and in



turn, other load effects were eliminated to allow for the simplicity of the test setup. A photograph and a schematic drawing of the test setup showing the seat beams and applied load locations are shown in Figure 6.6.

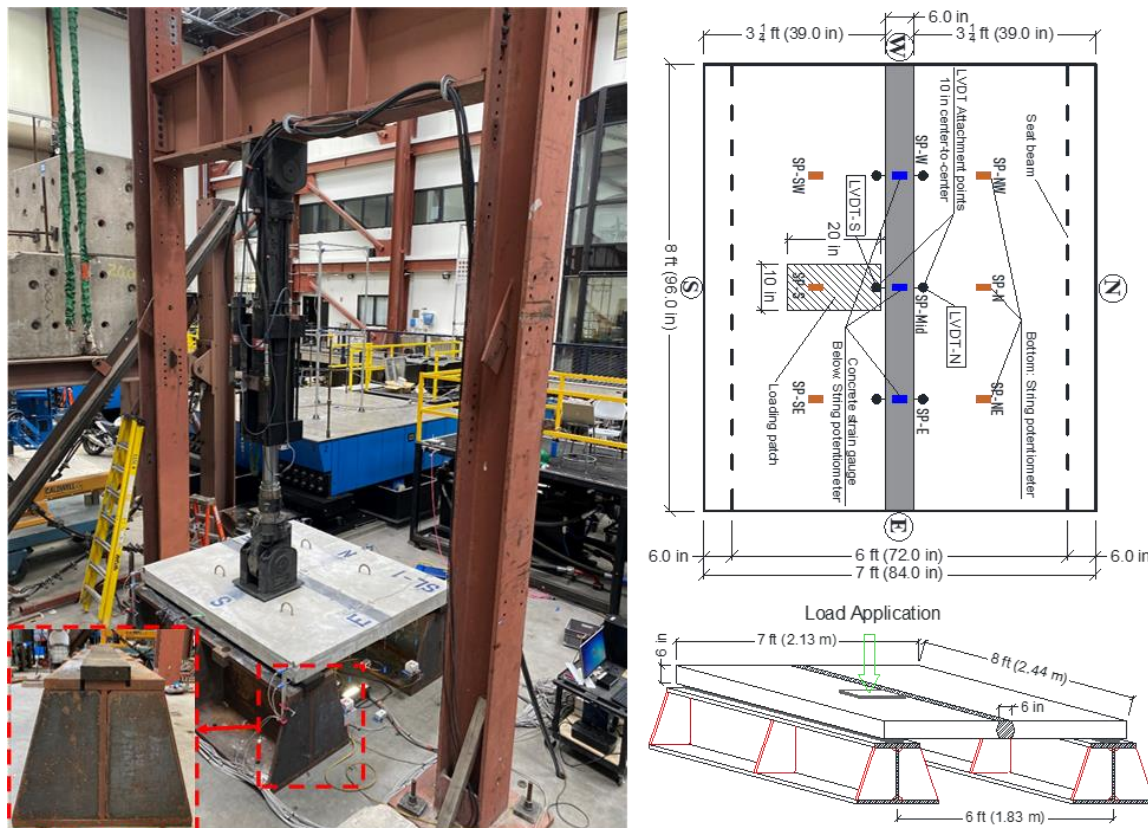


**Figure 6-6** Photograph and schematic drawing of the test setup (1 in = 2.54 cm, 1 ft = 30.48 cm).

The test specimens were simply supported over two seat beams that were aligned parallel to the longitudinal field joint. The test specimens were loaded using a hydraulic actuator (with up to 220-kip (978.6 kN) capacity) through a rubber pad of 20 in  $\times$  10 in (50.8 cm  $\times$  25.4 cm) footprint dimensions. The load was applied at the mid-span of the longitudinal direction of the test specimen and adjacent to the field joint to impose shear forces at the interface surface between the field joint and the precast deck panel. The loading procedure used in this study consisted of four cycles of loading and unloading at small load levels to investigate the performances of the field joints at representative service load conditions and to estimate the average early flexural stiffness of the test specimens. The first two cycles included loading of the specimen up to 15 kips (66.72 kN) and then unloading. The

second two cycles included loading of the specimen up to 30 kips (133.44 kN) and then unloading. The loading and unloading of the first four cycles were applied using a force control method with a rate of 5 kips/min (22.24 kN/min). Finally, displacement-control monotonic loading at a rate of 0.075 in/min (1.9 mm/min) was applied until failure to determine the peak load capacity in addition to assessing the post-peak response and determine the modes of failure of the test specimens.

### 6.3.3 Instrumentation Plan

The instrumentation plan for the test specimens, as shown in Figure 6.7, consisted of 35 reinforcement strain gauges that were installed to measure the strains of the transverse and longitudinal bars and monitor the load level at which the yielding occurs. Moreover, 15 string potentiometers were attached at the bottom of the specimen in a mesh configuration to measure the vertical deflection of the specimen. Finally, the instrumentation plan also included six linear variable displacement transducers (LVDTs) installed horizontally across the interface between the joint and the precast panels to measure the width of the interface crack that could happen through the test. Three cameras were also used below the specimen to monitor the progression of the crack through the test. A photograph of some of the instrumentation devices used in this study is shown in Figure 6.8.

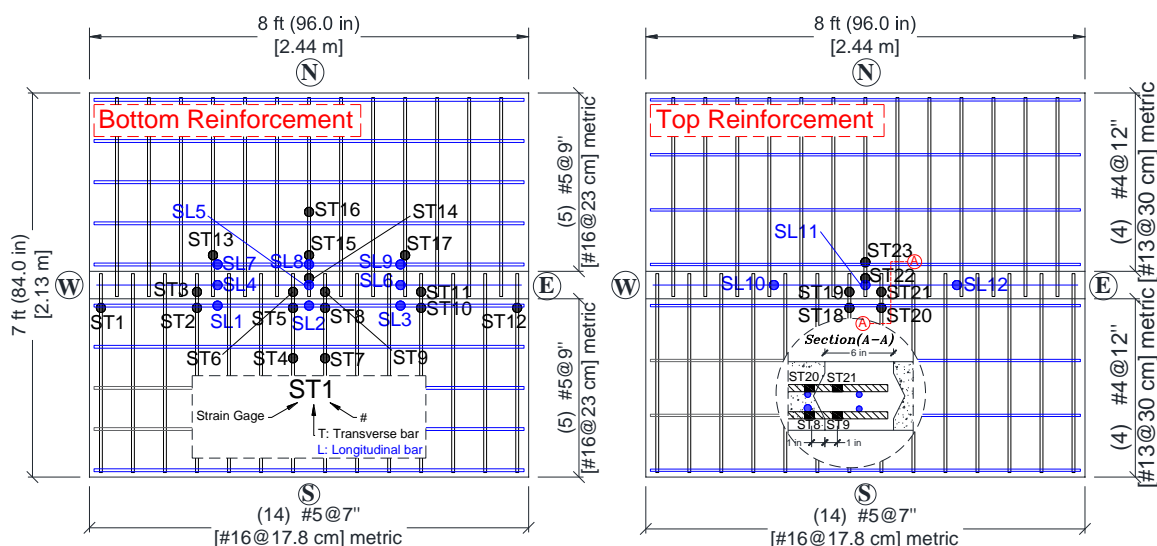


**Figure 6-7** Reinforcement strain gages distribution for the bottom and top reinforcement of S1-NP-UHPC.

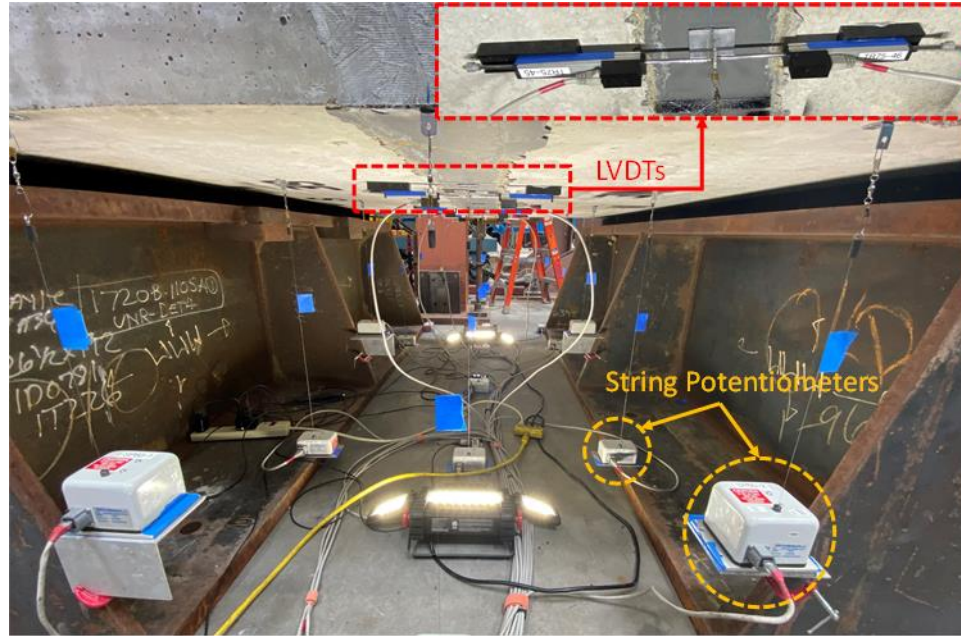


**Figure 6-8** Photograph of some of the instrumentation devices used in this study.

#### 6.4 Test Results and Comparative Behavior

The discussion of the global and local behaviors of both tested specimens is provided in this section and distributed among several subsections. As mentioned earlier, the experimental program included testing of two specimens. The first specimen used a NP-UHPC longitudinal field joint is denoted by “S1-NP-UHPC” throughout the rest of the discussion. The second specimen used a proprietary UHPC joint is denoted by “S2-P-UHPC”. The proprietary UHPC product used in the joint of specimen S2-P-UHPC is the commercially available Ductal® JS1000 mix from LafargeHolcim. The research team has previous experience in mixing and testing this robust commercial Ductal UHPC product [37, 38].

For completeness and consistency, the compressive strength of 3 in × 6 in cylinders of both proprietary and NP-UHPC used in this study were prepared and tested at different ages in accordance with the ASTM C1856 [28] along with ASTM C39 [29]. The compressive strength results were 24.8 ksi (171 MPa) and 27.8 ksi (191.7 MPa) for the Ductal UHPC at 28 days and the day of the test, respectively. The compressive strength of the NP-UHPC used in the test specimen was 13.86 ksi (95.6 MPa) and 22.52 ksi (155.3 MPa) at 7 days

and test day, respectively. The test results are mostly presented herein in the form of a detailed comparison between both specimens to validate the use of the developed NP-UHPC for longitudinal field joints. The structural performance of both tested specimens is presented and discussed in the following four subsections, which include the damage progression, load and deflection behavior, strains of the transverse and longitudinal reinforcing bars, and bonding at the joints interface.

#### ***6.4.1 Global Behavior of Specimens***

The global behavior of the tested specimens is assessed by studying the flexural response of both specimens as represented by load-deflection relationships in addition to a detailed discussion of the damage progression, crack patterns, and modes of failure.

##### ***6.4.1.1 Damage Progression***

A summary and overview of key experimental test results are provided first in Table 6.4 for both tested specimens. The table shows the peak load capacities in comparison to the calculated peak load values of both specimens in addition to the vertical deflections at the center of the specimens reported at the peak load and the AASHTO service and ultimate loads. It is worth noting that the theoretical or the calculated peak load values, as shown in Table 6.4, were calculated based on the moment-curvature analysis of the slab cross-section using the actual material properties. The table also shows the initial flexural stiffness of both specimens. The table provides an overall idea of the behavior of both specimens up to failure in a comparative way, before providing a detailed discussion of the global flexural behavior of the specimens later in this section. It is worth noting that the test continued until failure to investigate whether the whole precast system with field joint will remain intact with no significant interface cracking or slippage of reinforcement within the joint. This is mostly an academic point and not expected to represent a real-life scenario as bridge decks are usually designed to remain within the linear elastic range under code limits of service and ultimate loads. For the latter purpose, the reinforcement strains will be verified later in the following sections to determine the loads at which the onset of yielding occurs and compare it with the service and ultimate loads.

**Table 6-4** Summary of main experimental test results

Specimen	Peak Load, Kips (kN)	Middle Deflection at, in (cm)			Initial Stiffness kip/in (kN/cm)
		Peak Load	Service Load	Ultimate Load	
S1-NP-UHPC	121.3 (539.6)	1.517 (3.85)	0.223 (0.57)	0.391 (0.99)	215 (376.5)
S2-P-UHPC	115.8 (515.1)	1.510 (3.83)	0.193 (0.49)	0.387 (0.98)	240 (420.3)

Several conclusions can be quickly deduced from the previous table as both specimens have very comparable behavior in terms of load-carrying capabilities and corresponding deflections. However, it can be seen that specimen S1-NP-UHPC has a higher flexural capacity than specimen S2-P-UHPC. This higher capacity is attributed to the higher compressive strength of the precast panels of specimen S1-NP-UHPC, i.e. 7.5 ksi at the test day, compared to 5.2 ksi for specimen S2-P-UHPC panels. It can be seen that the peak load values of both specimens exceeded the calculated load values assuming the continuity of the deck specimen or in other words monolithic deck systems. From the calculated and measured peak load values, the over the strength of specimen S1-NP-UHPC is less than that of specimen S2-P-UHPC, i.e. 16.6 % and 24.5 %, respectively, as a result of the higher mechanical properties of the proprietary UHPC compared to the NP-UHPC. Moreover, the initial stiffness of specimen S2-P-UHPC is first shown to be slightly higher than the other specimen because of the higher mechanical strength of the proprietary UHPC compared to the developed NP-UHPC. However, the flexural behavior of both tested specimens was almost similar, as such flexural members are commonly designed to be tension-controlled, i.e. under reinforced sections, which allows the main steel to yield before the crushing of concrete happens. Hence, the observed mode of failure for both specimens was yielding in the bottom transverse reinforcement followed by crushing of the normal strength concrete around the loading position in the south precast panel. When the applied load exceeded the code service and ultimate loads, the flexural cracks at the bottom of the specimens become more obvious and aggressively propagated until reaching the peak load capacity of the specimen where extremely wide cracks were observed in the precast panels. One of the benefits of using UHPC as field joint material is that it has significantly higher tensile strength compared to the precast NSC panels. Consequently, no flexural cracks were

observed at the early stages of loading for both specimens as the first observed crack in the proprietary and NP-UHPC were at approximately 100 kips (444.8 kN) and 65 kips (289.1 kN), respectively. The reason for this difference is that the NP-UHPC has a relatively lower tensile strength compared to the proprietary UHPC.

The flexural cracks in both field joints (shown in Figure 6.9) were relatively limited to three or four main localized cracks with relatively narrow widths compared to cracks in the precast panels. Most of the flexural cracks at the bottom of the specimen were localized under the loading position in the middle of the specimen at the south precast panel as shown in Figures 6.9a and 6.9b for specimens S1-NP-UHPC and S2-P-UHPC, respectively. Crushing of concrete happened slightly before reaching the peak load capacity for both specimens as shown in Figures 6.9c and 6.9d for specimens S1-NP-UHPC and S2-P-UHPC, respectively. As mentioned earlier, concrete crushing happened only in the south precast panel as it started at the load pad location at mid-span and propagated to the west and east ends. It is worth noting that no interface cracks were observed between the joint and the precast panels up to the AASHTO ultimate load. However, a short-length interface crack was observed at the bottom of specimen S1-NP-UHPC between the south concrete panel and the joint at approximately 70 kips (311.4 kN). On the other hand, specimen S2-P-UHPC had only experienced interface cracking at the end of the test. One more key observation for both tested specimens is that there is no bar slip happened to the lap splices within the field joints throughout the test, this can be a good conclusion that the 5.5 in (13.97 cm) satisfied the lap length requirements and was adequate to transfer forces between both precast panels up to failure load. Moreover, no bar rupture was observed through the entire testing regime for both specimens. The test was stopped upon reaching a certain criterion when a specimen lose at least 20% of the observed peak load capacity.

#### *6.4.1.2 Load-Deflection Relationship*

The second aspect of assessing the global behavior of both tested specimens is investigating the load versus the vertical displacement behavior. The main aim of this section is to establish a comparison and detailed discussion of the flexural behavior of both specimens as evaluated at different load levels and highlight the key observations from the tests.

Figure 6.10 shows the load-deflection relationships for both tested specimens as it shows deflection readings at three different locations, i.e. two quarter-span locations and at mid-span.

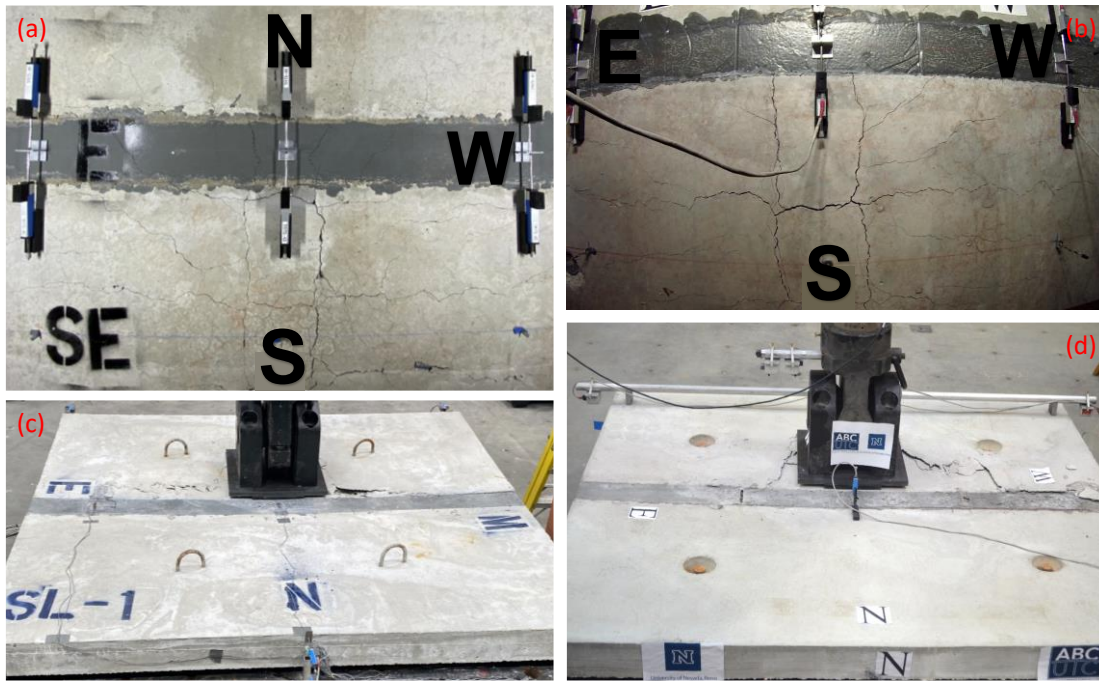


**Figure 6-9** Flexural crack pattern and concrete crushing at: (a) bottom of S1-NP-UHPC; (b) bottom of S2-P-UHPC; (c) top of S1-NP-UHPC; and (d) top of S2-P-UHPC.

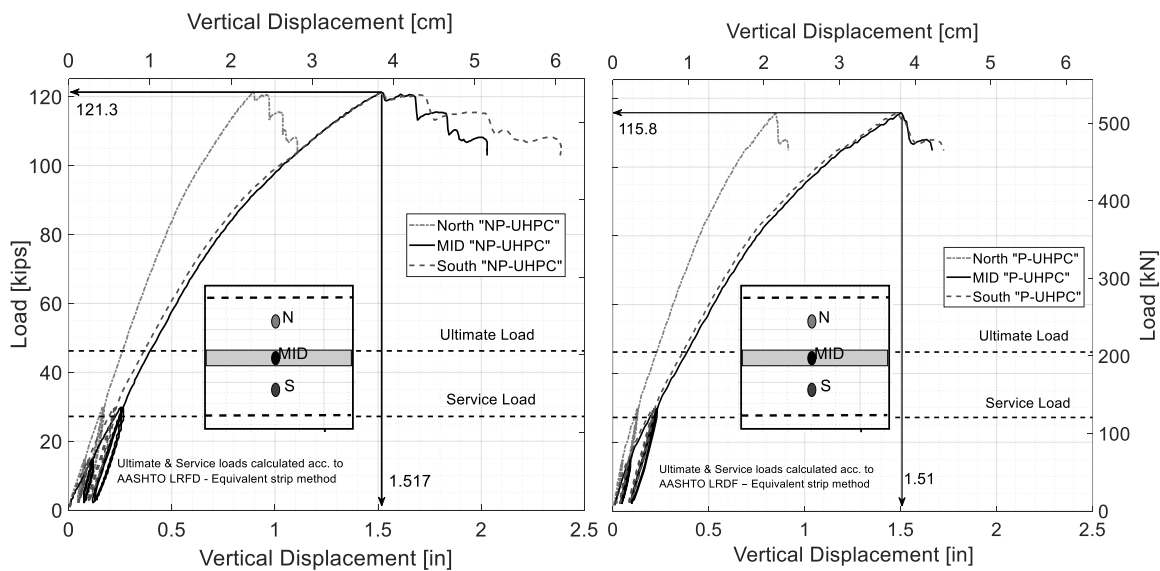


**Figure 6-10** Load versus vertical displacements at quarter- and mid-span locations of the non-proprietary S1-NP-UHPC specimen (left) and proprietary S2-P-UHPC specimen (right).

In general, it can be seen from Figure 6.10 that both specimens have a very comparable flexural behavior. As mentioned earlier, specimen S1-NP-UHPC has a slightly higher peak load capacity compared to specimen S2-P-UHPC because of the higher compressive strength of the precast panels of this specimen. On the other hand, specimen S2-P-UHPC has a slightly higher initial stiffness because of two main reasons. First, the stress distribution over the specimen cross-section was still within the linear elastic range when looking at the initial stiffness. Hence, the difference in the compressive strength of the NSC did not have any significant contribution to the stiffness and global initial flexural behavior of the specimens. Second, the integrated system (precast panels plus UHPC joint) at the beginning of the test was still fully-engaged and the mechanical properties and stiffness of the proprietary UHPC in the joint were comparably higher than the NP-UHPC. In such a case, the proprietary UHPC acted as a rigid beam in the middle of the specimen that helped more in uniformly distributing the load over the specimen. Consequently, the initial deflections of specimen S2-P-UHPC were smaller than S1-NP-UHPC and the initial stiffness was higher. Another key observation from Figure 6.10 is that the flexural capacity of both specimens significantly exceeded the AASHTO LRFD ultimate limit state. From the above key observations, both proprietary and NP-UHPC were capable of providing viable solutions for use in the precast deck field joints in which the deck systems can satisfy the target behavior of conventional cast-in-place monolithic decks in terms of strength and load distribution requirements.

The load-deflection responses for both tested specimens change with increasing the applied loads. Initially, the flexural behavior of both specimens started as linear elastic up to the service load limit, i.e. up to 15 kips (66.7 kN). During this linear behavior, no cracks were observed in the precast panels or the field joints as both specimens did not yet reach the cracking moment. Moreover, no interface debonding or bar slippage was observed up to this service limit loading. Then, as loading increased, the flexural response started to be a nonlinear behavior where the precast panels in both specimens started to have cracks and lost stiffness but the main steel was not yet yielded. During this stage, the load-deflection relationship behaved slightly non-linear in which both specimens had only small value deflections corresponding to the largely applied load increments. Moreover, and more



importantly, no interface cracks or flexural cracks were observed in both joints due to the high tensile strength of both closure joint materials compared to the NSC in the precast panels. This initial part of non-linearity continued as the load increased to the onset of yielding of the main bars for both tested specimens. Upon reaching the yielding limit, the flexural stiffness of both specimens was significantly decreased because of the extensive flexural cracking in the precast panels associated with the yielding of the transverse bottom bars.

The flexural behavior of both specimens then showed global softening in which large deflection values were associated with small applied load increments. During this severe non-linear response, flexural cracks were observed in the NP-UHPC joint and a small length interface crack was also observed in that specimen S1-NP-UHPC. However, specimen S2-P-UHPC had only severe cracks in the precast panels without any cracking in the joint or at the joint interface. It is worth noting that no bar slip or bar rupture happened through the test. At the end of this non-linear response and just before reaching the peak load capacity, concrete crushing started to take place in the NSC of the south precast panel at the loading location and propagated to the east and west sides. After then, a degradation in the load capacity of the specimens was observed. For specimen S2-P-UHPC, sudden loss of the load capacity of the specimen was observed with increasing the applied displacements due to the crack localization in the UHPC and propagation of concrete crushing. However, for specimen S1-NP-UHPC, the failure was more ductile. Again, the main goal of loading the specimens beyond the code loading limits was to determine the modes of failure and to make sure that the weakest link in the integrated system is not expected to be the field joint, and instead, the failure should be governed by the precast panels.

It can be seen from Figure 6.10 above that the measured deflections at the middle and under the loading pad are almost identical. However, the measured deflections at the north side panels were comparably smaller. There are two main reasons for this difference in deflections. First, the asymmetry of loading in the north-south direction as the load was applied on the south precast panel and adjacent to the connection. Second, the capability

of the field joint to provide the continuity of load transfer between both precast panels. This difference in deflections can be used as a useful tool in assessing the performance of the field joints in terms of load transfer capabilities. The less this difference indicates the better field joint performance. It can also be seen that this difference in deflections is increasing with the increase of the applied loads due to the increase of the flexural cracking that leads to a significant reduction in the stiffness of the specimens. The reason for this behavior complies with the research findings from a previous analytical study as a part of the NCHRP 10-71 project [14] which proves that the demands on the field joint decreases with the stiffness reduction associated with the extensive flexural cracking of the precast panel. It can be seen that the difference in deflections between the middle and north panel deflections for specimen S2-P-UHPC is slightly bigger than that of specimen S1-NP-UHPC. The difference between the middle and north side deflections at the measured peak loads were 0.62 in (1.57 cm) and 0.66 in (1.67 cm) for specimens S1-NP-UHPC and S2-P-UHPC, respectively.

To further illustrate the aforementioned deformed shape observations, a three-dimensional graph of the deflected shape is shown for one of the specimens at peak load. Figure 6.11 provides the deflection shape and deflection values (reported in inches) for S1-NP-UHPC at peak load.

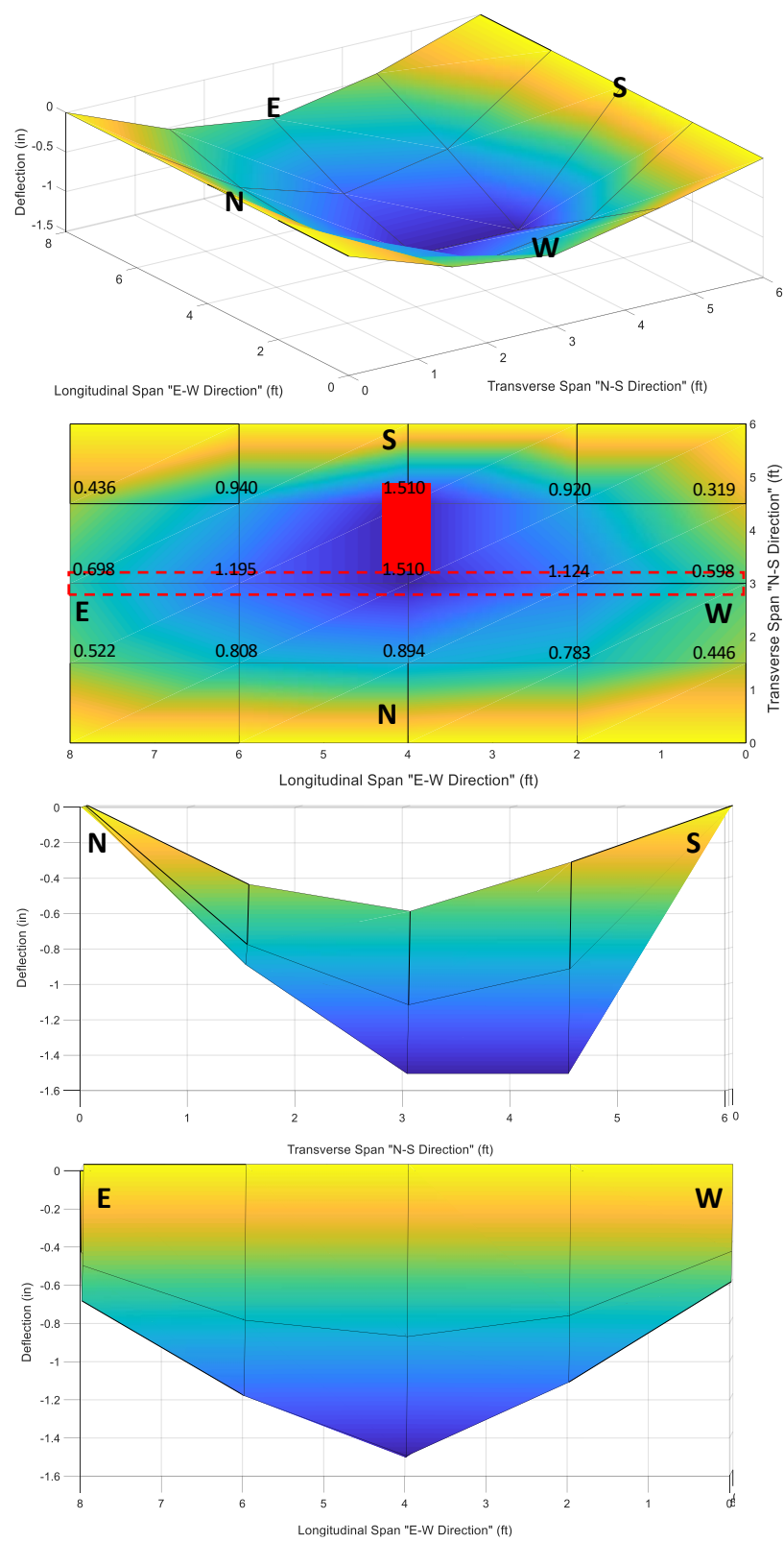


**Figure 6-11** Deflected shape of specimen S1-NP-UHPC at peak load.

## 6.4.2 Local Behavior of Specimens

This section provides selected results from the measured strains of the transverse and longitudinal reinforcement in addition to measurements of the interface crack opening between the field joints and the adjacent precast panels.

### 6.4.2.1 Transverse Reinforcement Strains

The load versus the measured strain readings from selected bottom transverse reinforcement strain gages that were located near the mid-span location are shown in Figure 6.12 and discussed in this subsection. It is worth noting that some of the strain gages were eventually damaged during the tests at higher load levels. Figure 6.12 indicates which strain gages used for the presented results were damaged and at which load level.

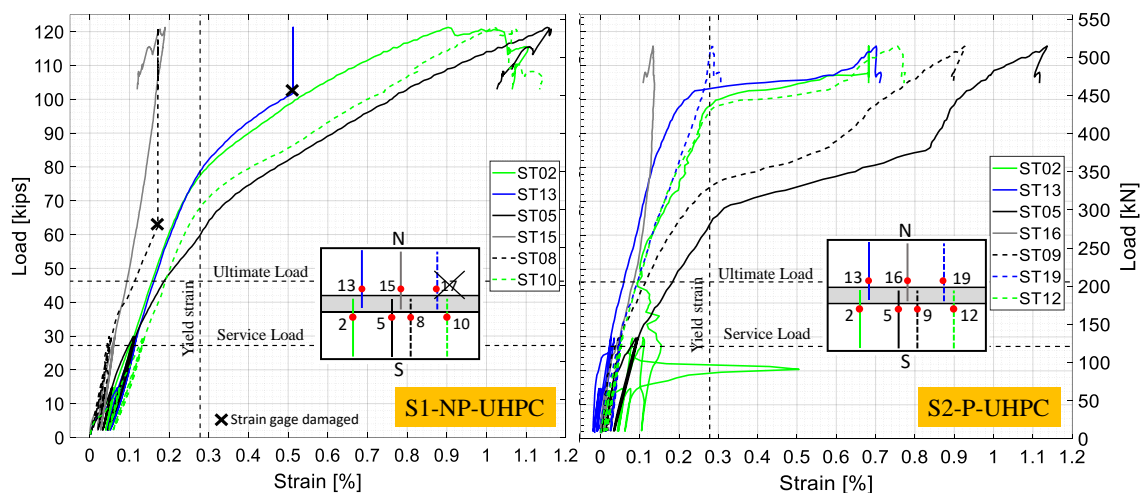


**Figure 6-12** Load versus strain of selected bottom transverse reinforcement.

It can be seen from Figure 6.12 that the strains of the bottom reinforcement for both specimens were very comparable. However, the strain distribution of specimen S1-NP-UHPC was more uniform than specimen S2-P-UHPC as the middle bars in the south precast panel were more strained than the other adjacent bars. As shown in Figure 6.12, the bars in the south precast panel, on which the load, was applied had the highest recorded strains, especially at the middle two bars. The onset of yielding for both tested specimens was observed in one of the middle bars of the south precast panel at 60 kips (266.9 kN) and

64 kips (284.7 kN) for specimen S1-NP-UHPC and S2-P-UHPC, respectively. The calculated yielding load values based on the curvature analysis of the precast slab cross-section are 57 kips (253.6 kN) and 55.2 kips (245.5 kN) for specimens S1-NP-UHPC and S2-P-UHPC, respectively. Based on the transformed section method, the yielding load values were 68.4 kips (304.3 kN) and 67.2 kips (298.9 kN) for specimens S1-NP-UHPC and S2-P-UHPC, respectively. It can be seen that the main steel for both specimens yielded after satisfying the AASHTO ultimate load level. This was expected because of many reasons such as the use of the nominal values for steel yielding strength and concrete compressive strength when calculating the AASHTO ultimate load and the use of a reduction factor ( $\Phi$ -factor) of 0.9 that magnifies the ultimate moment and consequently increase the required steel area. However, it can be concluded that the proposed deck systems with proprietary and NP-UHPC field joints remained elastic up to the code limit.

As mentioned earlier, the load-deflection response of both specimens (see Figure 6.10 above) completely changed to severe non-linear after many bars of the transverse bottom reinforcement were yielded. It can be seen that most of the transverse bottom bars were yielded at approximately 80 kips (355.9 kN) and 100 kips (444.8 kN) for specimens S1-NP-UHPC and S2-P-UHPC, respectively. This non-linearity in behavior associated with yielding of the main reinforcement and severe cracking has resulted in global softening of specimens with large deflection increments with the application of small load intervals. After yielding all the main transverse reinforcement, crushing of concrete was observed at the south precast panel as shown previously in Figure 6.9. It is worth mentioning that the bottom transverse reinforcement of both specimens has yielded inside both proposed field joints as shown in Figure 6.13. This can provide a good idea that both the proposed proprietary and NP-UHPC field joints with 6 in width can sufficiently provide a proper development length for the bars inside the joint. This in turn will ensure adequate load transfer between both precast panels.

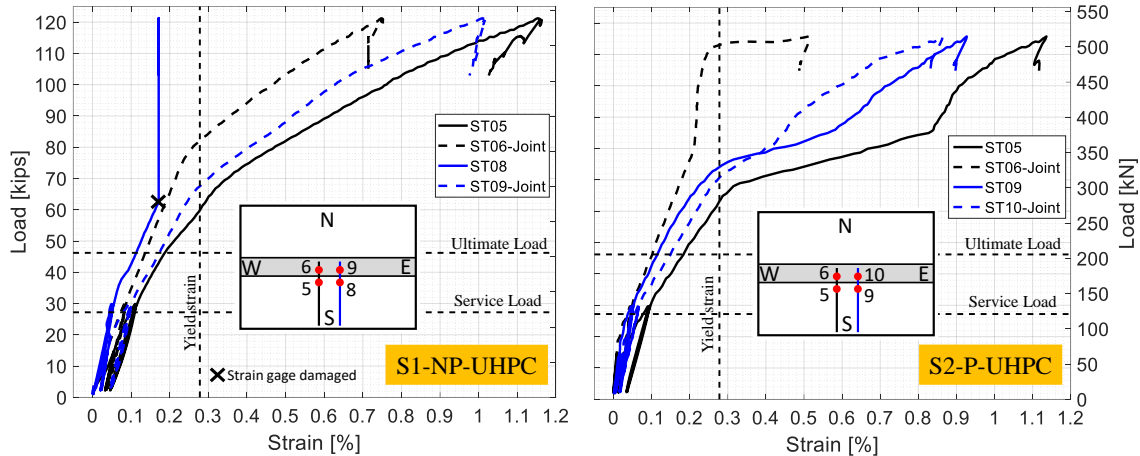


**Figure 6-13** Load versus strain of selected transverse reinforcement inside and outside the joint

#### 6.4.2.2 Longitudinal reinforcement strains

While the previous section was focused on strains of the transverse bottom bars (main steel), the load versus strain readings of the longitudinal bars (secondary steel) at the middle of both tested specimens is presented in Figure 6.14 for completeness. The figure shows that the strains of the middle longitudinal bars for both specimens were again very comparable, like the other aspects of behavior. Specimen S2-P-UHPC seemed to have slightly higher strain values after yielding than specimen S1-NP-UHPC. This can be attributed to the fact that specimen S2-P-UHPC suffered from more bending in the longitudinal direction than the other specimen. The difference in compressive strength of NSC of the precast panels can be one of the possible reasons for having a more rigid behavior of specimen S2-NP-UHPC in the longitudinal direction and consequently less bending in this direction. It can also be seen that the longitudinal bars inside the field joints and the precast panels were yielded after reaching the AASHTO ultimate load limit. Hence, the proposed deck systems were confirmed to have remained elastic up to the specified code limits. As can be seen from Figure 6.14, the strains of the bottom longitudinal bars inside the field joint and the south precast panels were comparably higher than the strains of the longitudinal bar in the north precast panel because of the position of the loading pad at the middle of the south precast panel and adjacent to the joint.

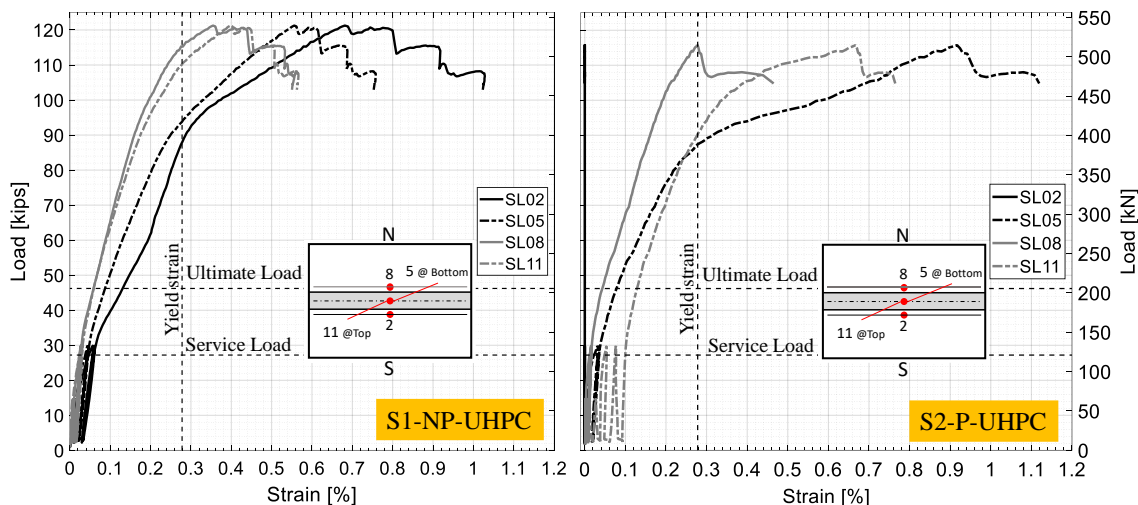


**Figure 6-14** Load versus strain at the middle of the top and bottom longitudinal bars.

#### 6.4.2.3 Field joint interface

As mentioned earlier, six horizontal LVDTs were used to monitor the interface crack opening between the joint and the adjacent panels at the bottom of both tested specimens. Table 6.5 reports the measured values for the interface opening of both specimens at the AASHTO service and ultimate loads. The table is arranged in a comparative way to verify if the bond properties of the NP-UHPC joint are adequate and are comparable to that of the proprietary UHPC joint. The AASHTO LRFD does not specify any limitations for the maximum allowable values for the interface crack opening. However, the AASHTO LRFD Article 5.6.7 [31] specifies a maximum spacing between the reinforcing bars to limit the width of the flexural cracks. These maximum spacing limitations were set based on the maximum allowable flexural crack width of 0.017 in (0.43 mm) for “class 1” exposure and 0.013 in (0.33 mm) for “class 2” exposure. The “class 2” exposure is typically used for situations in which the concrete is subjected to severe corrosion conditions.

**Table 6-5** Interface crack opening at the AASHTO LRFD service and ultimate loads

LVDT Name (See Figure 6.6)	S1-NP-UHPC				S2-P-UHPC			
	Service load		Ultimate load		Service load		Ultimate load	
	in ( $\times 10^{-3}$ )	mm	in ( $\times 10^{-3}$ )	mm	in ( $\times 10^{-3}$ )	mm	in ( $\times 10^{-3}$ )	mm
LVDT-NW	12.6	0.32	19.9	0.51	8.8	0.22	17.6	0.45
LVDT-SW	11.7	0.3	21.3	0.54	6.8	0.17	11.6	0.29
LVDT-N	11.6	0.29	20.5	0.52	8.6	0.22	18.5	0.47
LVDT-S	13.7	0.35	25.5	0.65	7.6	0.19	17.9	0.45
LVDT-NE	11.8	0.3	18.1	0.46	N/A	N/A	N/A	N/A
LVDT-SE	10.9	0.28	16.8	0.43	7.4	0.19	12.2	0.31

It can be seen from the previous table that the interface crack width of specimen S1-NP-UHPC is slightly higher than that of specimen S2-P-UHPC. This is an indication that the bond strength of the proprietary UHPC is relatively better than the NP-UHPC. However, the interface crack width of both specimens at the AASHTO service load satisfied the crack width limitations for class 1 and class 2 exposures. This can confirm that the interface bond between the proprietary or NP-UHPC joints and the adjacent precast panels satisfied the design requirements and the code service load limits.

## 6.5 Summary and Conclusions

This paper presented results from comprehensive large-scale testing of representative DBT girder panels with both non-proprietary and commercial proprietary UHPC-filled longitudinal joint as alternative closure pour materials. The presented study is part of a bigger collaborative project among the ABC-UTC consortium that aims at providing and demonstrating the viability of a NP-UHPC mix for ABC applications. In this study, we used NP-UHPC with ingredients sourced from the western United States and extended its application to bridge deck field connections for first-hand large-scale implementation. This paper first provided briefly the main mechanical properties of the proposed NP-UHPC mix. The paper then discussed the structural performance of the proposed NP-UHPC longitudinal field joint in comparison to a readily implemented commercial proprietary



UHPC product. The study compared both global and local experimental behavior of two identical full-scale specimens with proprietary and NP-UHPC field joints to verify the adequacy of using the newly developed UHPC as a closure material. The specimens considered representative DBT top flange parts and a 6-in (15.2-cm) wide diamond-shaped shear key joint and were tested under static vertical loading. The following observations and conclusions can be drawn from this comparative experimental study:

- Based on the conducted material characterization of the proposed non-proprietary UHPC mix, the local sources in Nevada and California that have been identified for the various material components used in the mix are confirmed to be adequate. The main mechanical properties of the mixes sourced from different regions of the country at UNR and OU were very comparable. Hence, the non-proprietary UHPC mix is deemed acceptable and insensitive to local resourcing as suggested by repeatable mechanical properties and is ready to be further extended to large-scale implementation.
- Overall, the structural behavior and joint performance of the representative DBT girder's top flange parts with full-depth longitudinal non-proprietary UHPC field joints are demonstrated to be a viable alternative for ABC. The performance of the longitudinal non-proprietary UHPC joint was very comparable to that of the currently acceptable and adopted practice using robust proprietary/commercial UHPC mixes.
- Both proprietary and non-proprietary UHPC proposed field joints were able to maintain the AASHTO LRFD service and ultimate load requirements without any flexural or interface cracking due to the high tensile and bond strength of both materials. Both joints were able to provide adequate load distribution over the joined precast panels until the end of the test. The UHPC joints are then confirmed not to be the weak link in the integrated deck system, which eventually failed in an emulative flexure manner as cast-in-place monolithic decks.
- Flexural load capacities of both tested specimens were found to be much higher than the AASHTO LRFD service and ultimate load limits. Moreover, the peak load capacity of the non-proprietary UHPC specimen was slightly higher than that of the proprietary UHPC, which was attributed to the higher compressive strength of the NSC used in the precast panels of the non-proprietary UHPC specimen.

- The initial stiffness of the deck system with proprietary UHPC field joint was slightly higher than that of the deck system with non-proprietary UHPC joint, which is attributed to the higher mechanical strength of the proprietary UHPC. However, both specimens still had a very comparable performance in terms of overall load and deflection capacities as well as joint performance.
- Strain values of the reinforcement of both specimens confirmed that both specimens remained essentially elastic up to the AASHTO LRFD ultimate load level. But, the bottom transverse reinforcement of both specimens has eventually yielded inside both proposed field joints. Thus, the proposed non-proprietary and proprietary UHPC field joints with 6-inch width can sufficiently provide a proper development length for the bars inside the joint.
- The interface crack width of the non-proprietary UHPC specimen appeared to be slightly higher than that of the other specimen. This suggests that the bond strength of the proprietary UHPC is better than the non-proprietary UHPC, but with no further implications as the interface crack width of both specimens was well below the AASHTO LRFD specified crack width limitations for class 1 and class 2 exposures.
- In summary, non-proprietary UHPC mix sourced from Nevada and California local materials can be effectively used for closure pours for full-depth DBT girders field joints without requiring any post-tensioning or mechanical splicing. This paper demonstrated that the 6 in [15.2 cm] field joint width, typically used for proprietary UHPC, is also sufficient for non-proprietary UHPC to provide monolithic-equivalent deck systems in terms of load distribution.

### **Acknowledgments**

This study is funded by the US DOT through the ABC-UTC (2016 cycle) headed at Florida International University. The authors would like to thank Lehigh Southwest Cement Co. for the cement slag donation, Martin Marietta Inc. for the crushed aggregate sand donation. The authors also thank the laboratory staff at the Earthquake Engineering Laboratory at the University of Nevada, Reno for their assistance with the testing and experimental program.

## References

- [1] American Road and Transportation Builders Association (ARTBA) 2020 bridge report.
- [2] Haber, Z. B., & Graybeal, B. A. (2018). Performance of Grouted Connections for Prefabricated Bridge Deck Elements (No. FHWA-HIF-19-003). United States. Federal Highway Administration. Office of Infrastructure Research and Development.
- [3] Qiao, P., Zhou, Z., & Allena, S. (2016). Developing Connections for Longitudinal Joints between Deck Bulb Tees-Development of UHPC Mixes with Local Materials (No. WA-RD 869.1). Washington (State). Department of Transportation.
- [4] Graybeal, B. A. (2010). Behavior of field-cast ultra-high performance concrete bridge deck connections under cyclic and static structural loading (No. FHWA-HRT-11-023). United States. Federal Highway Administration.
- [5] Peruchini, T. J. (2017). Investigation of Ultra-High Performance Concrete for Longitudinal Joints in Deck Bulb Tee Bridge Girders (Doctoral dissertation).
- [6] Hartwell, D. R. (2011). Laboratory testing of Ultra High Performance Concrete deck joints for use in accelerated bridge construction.
- [7] Hwang, H., & Park, S. Y. (2014). A study on the flexural behavior of lap-spliced cast-in-place joints under static loading in ultra-high performance concrete bridge deck slabs. *Canadian Journal of Civil Engineering*, 41(7), 615-623.
- [8] Coufal, R., Vitek, J. L., Rehacek, S., Kolisko, J., & Citek, D. (2016, July). UHPC Connection of Precast Bridge Deck. In *International Interactive Symposium on Ultra-High Performance Concrete* (Vol. 1, No. 1). Iowa State University Digital Press.
- [9] Abokifa, M., M.A. Moustafa, A. Itani, “Comparative Behavior of Precast Bridge Deck Panels with UHPC and Polymer Concrete Transverse Field Joints”, *Composites Part B: Engineering* (*under review*)
- [10] Abokifa, M., M.A. Moustafa, “Experimental Behavior of Poly Methyl Methacrylate Polymer Concrete for Bridge Deck Bulb Tee Girders Longitudinal Field Joints”, *Construction and Building Materials* (*under review*)
- [11] Zhu, P., Ma, Z. J., Cao, Q., & French, C. E. (2012). Fatigue evaluation of transverse U-bar joint details for accelerated bridge construction. *Journal of Bridge Engineering*, 17(2), 191-200.

- [12] Li, L., & Jiang, Z. (2016). Flexural Behavior and Strut-and-tie Model of Joints with headed bar details Connecting Precast Members. *Perspectives in Science*, 7, 253-260.
- [13] Verger-Leboeuf, S., Charron, J. P., & Massicotte, B. (2017). Design and behavior of UHPFRC field-cast transverse connections between precast bridge deck elements. *Journal of Bridge Engineering*, 22(7), 04017031.
- [14] French, C. E., Shield, C. K., Klaseus, D., Smith, M., Eriksson, W., Ma, Z. J., ... & Chapman, C. E. (2011). Cast-in-place concrete connections for precast deck systems (No. NCHRP Project 10-71).
- [15] Perry, V., Krisciunas, R., & Stofko, B. (2014). Mackenzie River Twin Bridges: North America's Largest Field-Cast Ultra-High-Performance Concrete Connections Project. *PCI Journal*, 59(2).
- [16] Sritharan, S., Aaleti, S., Garder, J., Bierwagen, D., & Abu-Hawash, A. (2012). Use of ultra-high performance concrete in bridge design. *US-Japan Cooperative Program in Natural Resources*.
- [17] Graybeal, B. (2013). Development of non-proprietary ultra-high performance concrete for use in the highway bridge sector. FHWA Publication No. FHWA-HRT-13-100.
- [18] Wille, K., Naaman, A. E., & Parra-Montesinos, G. J. (2011). Ultra-High Performance Concrete with Compressive Strength Exceeding 150 MPa (22 ksi): A Simpler Way. *ACI materials journal*, 108(1).
- [19] Wille, K., Naaman, A. E., El-Tawil, S., & Parra-Montesinos, G. J. (2012). Ultra-high performance concrete and fiber reinforced concrete: achieving strength and ductility without heat curing. *Materials and structures*, 45(3), 309-324.
- [20] Alsalman, A., Dang, C. N., & Hale, W. M. (2017). Development of ultra-high performance concrete with locally available materials. *Construction and Building Materials*, 133, 135-145.
- [21] Berry, M., Snidarich, R., & Wood, C. (2017). Development of Non-Proprietary Ultra-High Performance Concrete (No. FHWA/MT-17-010/8237-001). Montana. Dept. of Transportation. Research Programs.

- [22] Graybeal, B. (2014). Design and construction of field-cast UHPC connections (No. FHWA-HRT-14-084; HRDI-40/10-14 (750) E). United States. Federal Highway Administration.
- [23] Looney, T., Coleman, R., Funderburg, C., Volz, J., & Floyd, R. (2021). Concrete Bond and Behavior of Nonproprietary Ultrahigh-Performance Concrete Bridge Slab Joints. *Journal of Bridge Engineering*, 26(2), 04020128.
- [24] Looney, T., McDaniel, A., Volz, J., & Floyd, R. (2019). Development and Characterization of Ultra-High Performance Concrete with Slag Cement for Use as Bridge Joint Material. *Development*, 1(02).
- [25] Yuan, J., & Graybeal, B. (2015). Bond of reinforcement in ultra-high-performance concrete. *ACI Structural Journal*, 112(6), 851.
- [26] ASTM, C. (2006). 1437, "Standard test method for flow of hydraulic cement mortar", Annual Book of ASTM Standards, vol. 04-01. West Conshohocken, PA, USA.
- [27] ASTM C230/C230M. (1998). Standard specification for flow table for use in tests of hydraulic cement.
- [28] ASTM. (2017). Standard practice for fabricating and testing specimens of ultra-high performance concrete. ASTM C1856/C1586-17.
- [29] ASTM C39. Standard Test Method for Compressive Strength of Cylindrical Concrete Specimens. American Society for Testing and Materials Standard Practice C39, Philadelphia, PA, 2001.
- [30] Banthia, N., & Islam, S. T. (2013). Loading rate concerns in ASTM C1609. *Journal of Testing and Evaluation*, 41(6), 1032-1036.
- [31] AASHTO (American Association of State Highway and Transportation Officials). AASHTO LRFD Bridge Design Specifications, 7th ed.; American Association of State Highway and Transportation Officials: Washington, DC, USA, 2014.
- [32] PCI (Precast/Prestressed Concrete Institute) PCI Bridge Design Manual, 3rd ed.; First Release, 2011.
- [33] Graybeal, B. A. (2010, February). Behavior of Ultra-High Performance Concrete connections between precast bridge deck elements. In *Proceedings of the 2010*

- Concrete Bridge Conference: Achieving Safe, Smart & Sustainable Bridges, Phoenix, AZ, USA (Vol. 24).
- [34] Graybeal, B. (2010). Field-cast UHPC connections for modular bridge deck elements (No. FHWA-HRT-11-022).
- [35] Mante, D. M., Abbas, H. H., Ramey, G. E., & Barnes, R. W. (2015). Full-Scale Implementation and Testing of Full-Depth Precast Bridge Deck Panels. *Transportation Research Record*, 2522(1), 3-17.
- [36] Badie, S. S., Baishya, M. C., & Tadros, M. K. (1998). NUDECK-An efficient and economical precast prestressed bridge deck system. *PCI journal*, 43(5).
- [37] Aboukifa, M., Moustafa, M. A., Itani, A. M., & Naeimi, N. (2019). Durable UHPC Columns with High-Strength Steel (No. ABC-UTC-2013-C3-UNR02-Final). Accelerated Bridge Construction University Transportation Center (ABC-UTC).
- [38] Aboukifa, M., Moustafa, M. A., & Itani, A. M. (2020). Comparative Structural Response of UHPC and Normal Strength Concrete Columns under Combined Axial and Lateral Cyclic Loading. *ACI SP 341*. 71-96.

## **7 COMPARISONS AND DESIGN AND CONSTRUCTION RECOMMENDATIONS**

This chapter provides a general comparison between the key results, the global and local behaviors of all the tested transverse and longitudinal test specimens. The purpose of this comparison is to arrive at design recommendations for the design of the field cast bridge deck joints. Moreover, this chapter provides recommendations for the mixing of the used field joint materials and construction of the field cast bridge deck joints.

### **7.1 Comparison of the Transverse Specimens**

Total number of six transverse specimens have been tested in this study. They only vary in the type of the material used inside the joints and the splice type. Three identical specimens with straight splices and different joint materials (i.e., P-UHPC, NP-UHPC, and PC) were compared together in the following subsection. The other two identical specimens with loop splices and different joint materials (NP-UHPC, and PC) were compared together in a different subsection. The last specimen has a straight non-contact lap splice with relatively wider NP-UHPC joint with only 1% steel fibers and it has no duplicate with different joint material. Hence, it was not included in any of the comparisons.

#### ***7.1.1 Transverse specimens with straight splice***

##### ***7.1.1.1 Summary of the results***

The summary of the experimental results of the three transverse specimens with straight splices is reported in Table 7-1. The UHPC and the NP-UHPC has 2% steel fibers by volume in their mixtures while the PC has no fibers. The compressive strength at the day of test of the joint materials and the conventional concrete that was used for the fabrication of the deck panels are shown in Table 7-2. The table also shows the flexural strength of the joint material measured at the day of test.

The UHPC and PC specimens were fabricated using a single conventional concrete batch. Hence, the compressive strength of the deck panels were the same. The NP-UHPC specimen was fabricated using different batch that had a relatively higher compressive strength. To be able to compare the results of specimens, the compressive strength of the

specimens should be normalized based on some approximations. Each specimen was fabricated from two different components (i.e., conventional concrete panels and field joints). The weighted average of the compressive strength of the specimens was calculated based on the width of the elements (i.e., perpendicular to the bending direction) and the compressive strength of each element. The UHPC, NP-UHPC, and PC specimens have weighted average compressive strengths of 45.5 MPa, 58.3 MPa, and 37.5 MPa, respectively. Hence, the NP-UHPC specimen has approximately 28% and 55% higher average compressive strength than the UHPC and PC specimens, respectively. The 28% higher compressive strength between the NP-UHPC and UHPC specimens has resulted in 22% increase in the initial stiffness and only 13% increase in the load capacity. The 55% higher average compressive strength between the NP-UHPC and PC specimens has resulted in 53% increase in the initial stiffness and only 18% increase in the load capacity.

**Table 7-1** Summary of the experimental results of the transverse specimens with straight splices.

Specimen Name	Peak Load (kN)	Load @ 1 <sup>st</sup> Yield (kN)	Load @ 1 <sup>st</sup> Interface Crack (kN)	Mid-span Deflection (cm)			Initial Stiffness, (kN/cm)
				Peak Load	Service Load	Ultimate Load	
UHPC	524.5	≈ 290	520	5.920	0.444	0.975	420.3
NP-UHPC	592.0	≈ 320	335	6.217	0.349	0.811	510.6
PC	503.5	≈ 205	Post-peak load	6.426	0.521	1.168	332.7

**Table 7-2** Summary of the compressive strength and flexural strength of the utilized materials.

Specimen Name	Compressive strength (MPa)		Weighted Average Compressive Strength per Specimen (MPa)	Flexural Strength of Joint Material (MPa)
	Joint Material <sup>(1)</sup>	Deck Panel <sup>(2)</sup>		
UHPC	191.7	35.8	45.5	NA
NP-UHPC	146.4	52.4	58.3	20.7 <sup>(3)</sup>
PC	62.4	35.8	37.5	20.0 <sup>(4)</sup>

<sup>(1)</sup> Compression testing of  $7.6 \times 15.2$  cm cylinders according to ASTM C39 [1]

<sup>(2)</sup> Compression testing of  $15.2 \times 30.5$  cm cylinders according to ASTM C39 [1]

<sup>(3)</sup> Four point bending of  $7.6 \times 7.6 \times 30.5$  cm prisms according to ASTM C1609 [2]

<sup>(4)</sup> Three point bending of  $7.6 \times 7.6 \times 30.5$  cm prisms according to ASTM C580 – C [3]



The weighted average compressive strength of the field joint material and the conventional concrete has a slight effect on the peak load capacity of the specimens but a higher impact on the initial stiffness and the early behavior. The weighted average compressive strength of the UHPC specimen is approximately 22% higher than that of the PC specimen. This was mainly due to the higher compressive strength of the UHPC joint as the deck panels of both specimens were fabricated from the same batch. The 22% higher compressive strength between the UHPC and PC specimens has resulted in 9% increase in the initial stiffness and only a 4% increase in the load capacity. This indicates that the compressive strength of the joint material has no significant effect on the initial stiffness and the peak load capacity of the transverse specimens.

The results of Table 7-1 shows that the PC specimen has the best interface bond strength between the field joint and the deck panels, while the NP-UHPC has the least bond strength. Nonetheless, the NP-UHPC specimen was able to sustain the AASHTO LRFD design loads without any interface cracking. Hence, all the proposed materials for the field joints are considered acceptable in terms of the interface bond behavior. It is noted that no interface preparation was used for any of the specimens to test the worst case scenario. However, it is still recommended to use exposed aggregate surface at the interface of the deck panels to enhance the bond behavior, especially in the case of using NP-UHPC inside the joint.

#### *7.1.1.2 Load-deflection relationship*

The load versus the middle deflections of the three transverse specimens with straight non-contact lap splices are shown in Figure 7-1. As mentioned earlier, the NP-UHPC and UHPC materials used inside the joints include 2% steel fibers by volume in their mixtures, while the PC did not have fibers. Nonetheless, the PC specimen showed a comparable results to the NP-UHPC and UHPC specimens in terms of load capacity and flexural behavior as shown in Figure 7-1. The load capacity and stiffness of the NP-UHPC specimen are higher than that of the other two specimens because of the higher compressive strength of the conventional concrete which was used in the fabrication of the precast panels (see Table 7-2).

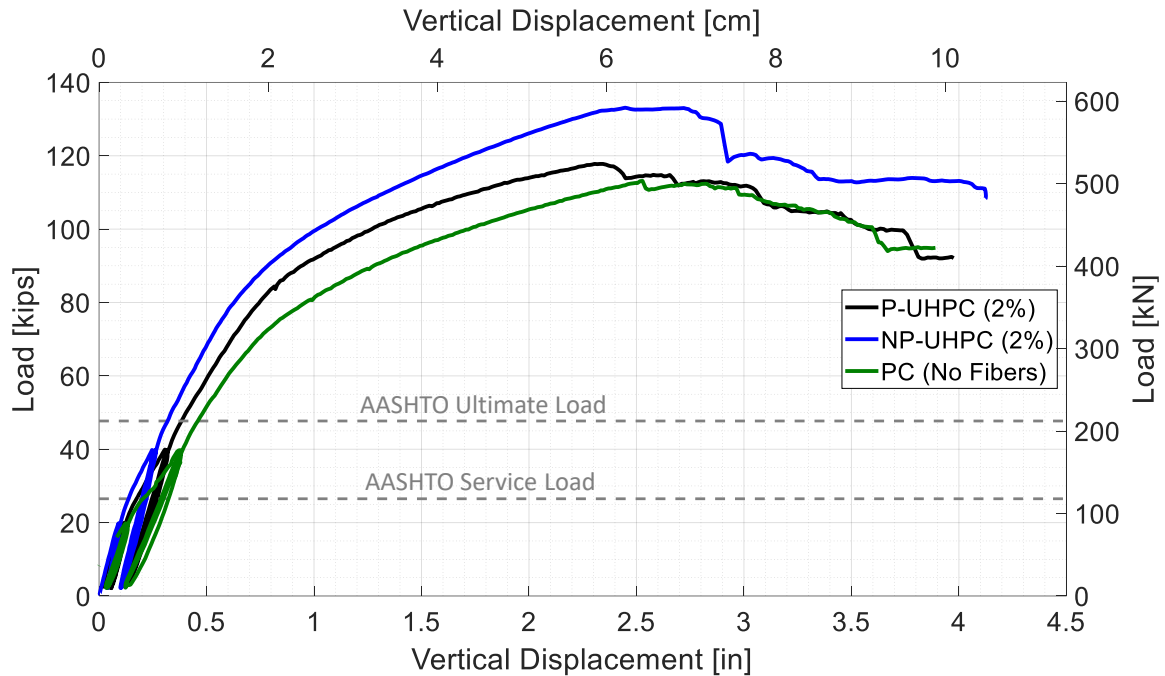


**Figure 7-1** Load versus middle deflection relationships of the transverse specimens with straight lap splice.

The load deflection relationship of all the test specimens are very comparable. All specimens failed in pure flexure behavior in which the main bars yielded then crushing of concrete took place just before the failure of the specimens. This happened without any major interface cracking that could have affected the behavior or slippage of the reinforcing bars that may have caused drops in the load-deflection relationships. The AASHTO LRFD service and ultimate loads were derived based on the equivalent strip method which takes into account the highest expected live load effects for a given bridge deck. The flexural capacities of all specimens have exceeded the AASHTO LRFD ultimate and service loads. This was expected because of many reasons such as the use of the nominal values for steel yielding strength and concrete compressive strength when calculating the AASHTO service and ultimate loads, the use of a reduction factor ( $\Phi$ -factor) of 0.9 that increases the difference between nominal and ultimate moments and consequently increases the required steel area, and neglecting the contribution of the top transverse reinforcement to the moment capacity while calculating the required area of the bottom transverse steel. From the above key observations, the proposed field joint materials were capable of providing viable solutions for use in the precast deck field joints in which the deck systems can satisfy

the target behavior of conventional cast-in-place monolithic decks in terms of strength and load distribution requirements.

### 7.1.2 Transverse specimens with loop splice

#### 7.1.2.1 Summary of the results

The summary of the experimental results of the two transverse specimens with loop splices is reported in Table 7-3. The NP-UHPC had 2% steel fibers by volume in their mixtures while the PC had no fibers. The compressive strength at the day of test of the joint materials and the conventional concrete that was used for the fabrication of the deck panels are shown conforms also to Table 7-2.

**Table 7-3** Summary of the experimental results of the transverse specimens with loop splices.

Specimen Name	Peak Load (kN)	Load @ 1 <sup>st</sup> Yield (kN)	Load @ 1 <sup>st</sup> Interface Crack (kN)	Mid-span Deflection (cm)			Initial Stiffness, (kN/cm)
				Peak Load	Service Load	Ultimate Load	
NP-UHPC	598.1	≈ 298	445	6.697	0.345	0.805	545.3
PC	544.9	≈ 300	NA	6.680	0.450	1.008	385.3

As mentioned earlier, the precast panels of both specimens were fabricated using different concrete batches. Hence, the weighted average compressive strength of both specimens were calculated (see Table 7-2) to be able to normalize the results and compare them together. The NP-UHPC, and PC specimens have weighted average compressive strengths of 58.3 MPa, and 37.5 MPa, respectively. Hence, the NP-UHPC specimen has approximately 55% higher average compressive strength than the PC specimen. The 55% higher average compressive strength between the NP-UHPC and PC specimens has resulted in 42% increase in the initial stiffness and only 10% increase in the load capacity. The weighted average compressive strength of the field joint material and the conventional concrete has a slight effect on the peak load capacity of the specimens while it has a higher impact on the initial stiffness and the early behavior. The results of Table 7-3 shows that the PC specimen has better interface bond strength between the field joint and the deck panels compared to the NP-UHPC specimen. Nonetheless, both specimens were able to sustain the AASHTO LRFD design loads without any interface cracking. Again, the

proposed filler materials for the field joints are considered acceptable in terms of the interface bond behavior. It is recommended to use exposed aggregate surface at the interface of the deck panels to enhance the bond behavior, especially in the case of using NP-UHPC inside the joint. The use of the loop splice for the NP-UHPC specimen has delayed the occurrence of the interface crack (i.e., 335 kN versus 445 kN for the straight and loop splices, respectively) and slightly enhanced the joint behavior.

#### 7.1.2.2 Load-deflection relationship

The load versus the middle deflection relationships of both transverse specimens with loop splices are shown in Figure 7-2. Both specimens had very comparable behavior in terms of the stiffness and peak load capacity. The load capacity and stiffness of the NP-UHPC specimen are higher than that of the PC specimen because of the higher compressive strength of the conventional concrete which was used in the fabrication of the precast panels (see Table 7-2).

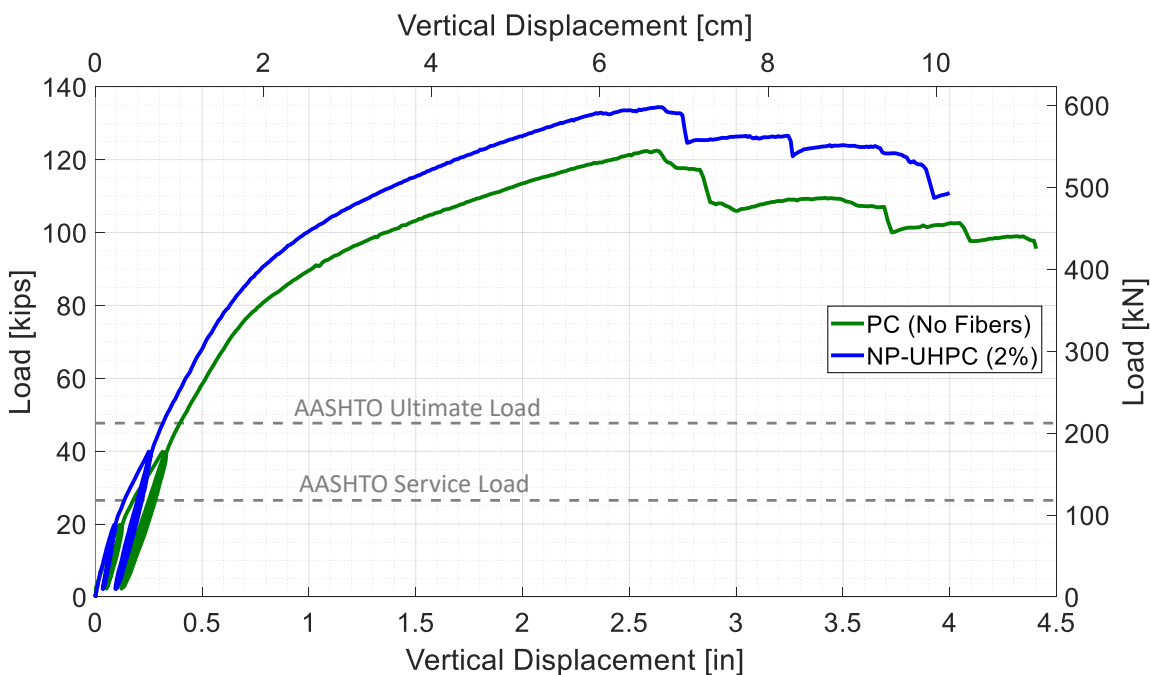


**Figure 7-2** Load versus middle deflection relationships of transverse specimens with loop splice. The load deflection relationship of both specimens are very comparable. Again, both specimens failed in pure flexure behavior without any major interface cracking that affected the behavior or slippage of the reinforcing bars. The peak load capacities of both

specimens exceeded the AASHTO LRFD ultimate and service loads. From the above observations, the use of the loop splice inside the deck joints is defined as a viable solution for the reinforcement splicing inside the bridge deck joints. Moreover, the loop splices enhanced the overall performance of the decks and the joint interface bond.

## 7.2 Comparison of the Longitudinal Specimens

Total number of three longitudinal specimens have been tested in this study. They only vary in the type of the material used inside the joints while they all implemented straight splice type for their joints. The closure materials which were used inside the field joints are UHPC, NP-UHPC, and PC. The UHPC and the NP-UHPC had 2% steel fibers by volume in their mixtures while the PC had no fibers.

### 7.2.1 Summary of Results

The summary of the experimental results of the three longitudinal specimens is reported in Table 7-4. The compressive strength at the day of test of the joint materials and the conventional concrete that was used for the fabrication of the deck panels were reported previously in Table 7-2.

**Table 7-4** Summary of the experimental results of the longitudinal specimens

Specimen Name	Peak Load (kN)	Load @ 1 <sup>st</sup> Yield (kN)	Load @ 1 <sup>st</sup> Interface Crack (kN)	Mid-span Deflection (cm)			Initial Stiffness, (kN/cm)
				Peak Load	Service Load	Ultimate Load	
UHPC	515.1	≈ 285	Post-peak load	3.83	0.49	0.98	420.3
NP-UHPC	539.6	≈ 267	311.4	3.85	0.57	0.99	376.5
PC	436.8	≈ 334	391.4	3.58	0.59	1.08	367.8

The results of Table 7-4 shows that the P-UHPC specimen had the best interface bond strength between the field joint and the deck panels, while the NP-UHPC had the least bond strength. Nonetheless, the NP-UHPC specimen was able to sustain the AASHTO LRFD design loads without any interface cracking. Hence, all the proposed materials for the field joints are considered acceptable in terms of the interface bond behavior. The compressive strength of the deck panels of the UHPC and PC specimens is equal to 35.8 MPa. The deck panels of the NP-UHPC specimen have compressive strength of 52.4 MPa at the day of

test. Again, the difference between the compressive strength of the specimens was calculated to be able to normalize the experimental results with respect to the compressive strength of the panels. This approximate normalization is essential for the comparison of the results. In the case of the transverse specimens, the longitudinal axis of the joint was parallel to the direction of bending. Hence, the field joint is acting as a beam with flexural stiffness at the middle between the two deck panels. Consequently, the compressive strength of the field joint material was taken into account and the weighted average compressive strength of each specimen was calculated and used for the approximate normalization. The longitudinal axis of the longitudinal field joint is perpendicular to the direction of bending of the specimen. This will add more stiffness to the direction which is perpendicular to the bending while it will have a negligible effect on the bending stiffness of the specimen. Consequently, the compressive strength of the field joint materials was not used for the approximate normalization of the results. The values of the initial stiffness and peak loads of the specimens, which were reported in Table 7-4, are normalized with respect to the compressive strength of the deck panels and are shown in Table 7-5. Table 7-5 also shows the actual load capacities in comparison to the calculated peak load values of the longitudinal specimens. The theoretical or the calculated peak load values, as shown in Table 7-5, were calculated based on the moment curvature analysis of the slab cross-section using the actual material properties and assuming a monolithic deck panel system without field joints.

**Table 7-5** Normalization of the experimental results of the longitudinal specimens.

Specimen Name	Compressive Strength of Panels, $f_c$ (MPa)	Peak Load / $f_c$	Initial Stiffness / $f_c$	Peak Load, $P_{act}$ (kN)	Calculated Peak Load, $P_{calc}$ (kN)	$P_{act} / P_{calc}$
UHPC	35.8	14.4	11.7	515.1	413.7	1.25
NP-UHPC	52.4	10.3	7.2	539.6	462.6	1.17
PC	35.8	12.2	10.3	436.8	413.7	1.06

The NP-UHPC specimen had approximately 46% higher compressive strength than the UHPC and PC specimens. While there was a 46% higher compressive strength between the NP-UHPC and UHPC specimens, the initial stiffness of the NP-UHPC specimen was

10% less than that of the P-UHPC specimens. Nonetheless, the peak load capacity of the NP-UHPC specimen was only 5% higher than that of the P-UHPC. The slight differences in the initial stiffness and the load capacity of the NP-UHPC and UHPC specimens may be attributed to the higher mechanical properties of the UHPC field joint material. As the mechanical properties of the UHPC increase, this may have added longitudinal stiffness to the specimen and helped with the distribution of the load in the longitudinal direction. This behavior can be also deduced from the difference in deflection between the middle of the joint and the deflections at the east or west sides along the joint. Figure 7-3 shows the relationship between the load and the difference in deflection between the middle and the east side of the joint. The specimen was loaded symmetrically, hence the east and west deflections of the joint were almost similar. If the flexural stiffness of the joint is large, the difference in deflections between the middle of the joint and the end of the joint is small and the load distribution along the longitudinal direction is better.

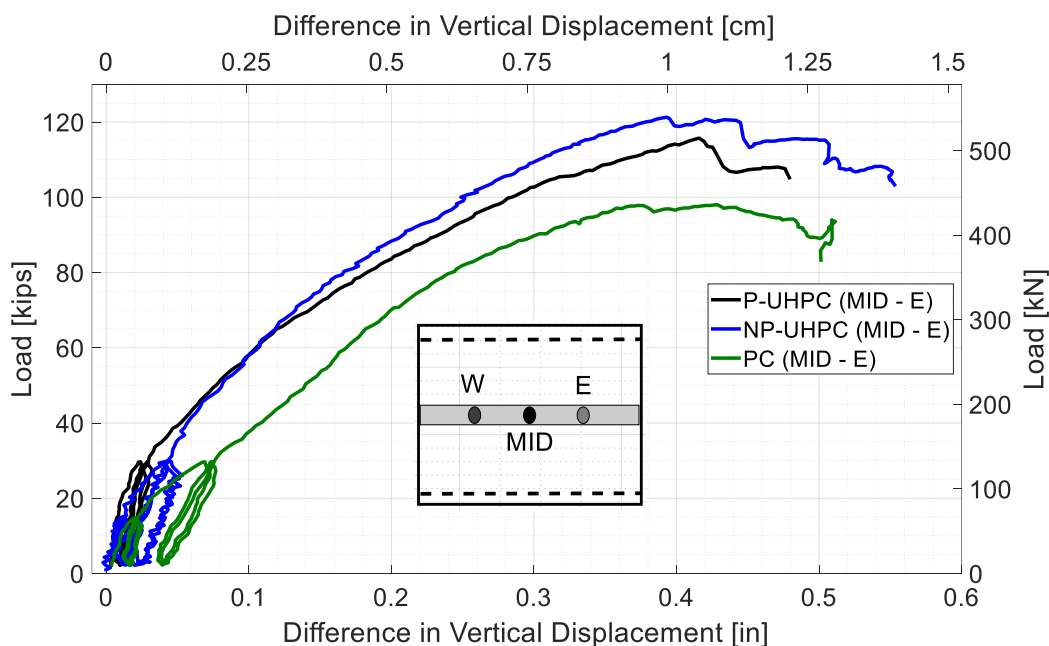


**Figure 7-3** Load versus difference between the middle and east side deflections relationships of the longitudinal specimens.

The deck panels of the NP-UHPC specimen were fabricated from conventional concrete with 46% higher strength than that of the P-UHPC specimen. However, the P-UHPC

specimen had a higher initial flexural stiffness compared to the NP-UHPC specimen, i.e. 420.3 kN/cm versus 376.5 kN/cm, respectively. This opposite behavior was expected because of the higher longitudinal flexural stiffness of the P-UHPC joint compared to the NP-UHPC joint. This higher longitudinal flexural stiffness of the joint enhanced the load distribution along the longitudinal direction of the specimen. As shown in Figure 7-3, the difference in deflections along the P-UHPC joint was smaller than that of the NP-UHPC joint up to 60 kips. This indicates that the P-UHPC specimen is more rigid in the longitudinal direction than NP-UHPC joint and proves the higher initial stiffness of the P-UHPC specimen.

Figure 7-3 shows that the PC joint had the least flexural stiffness in the longitudinal direction, while it was very comparable to the other two specimens at the beginning of the test. The deck panels of the NP-UHPC had 46% higher compressive strength than those of the PC specimens, while the initial stiffness of both specimens was almost equal. Nonetheless, the peak load capacity of the NP-UHPC specimen was 24% higher than that of the PC because of the interface crack between the PC joint and the south deck panel that forced the specimen to fail early.

The peak load values of all specimens have exceeded the calculated load values (see Table 7-5) assuming the continuity of the deck specimen, or in other words, monolithic deck systems. From the calculated and measured peak load values, the over strength of specimen P-UHPC is higher than that of the NP-UHPC and the PC specimens, i.e. 25% versus 17% and 6%, respectively. This higher over strength is the result of the higher mechanical properties of the P-UHPC material compared to the NP-UHPC and PC.

### ***7.2.2 Load-Deflection Relationship***

The load versus the middle deflections of the longitudinal specimens with straight non-contact lap splices are shown in Figure 7-4. All specimens had very comparable behavior in terms of the stiffness and peak load capacity. The load capacity of the NP-UHPC specimen was higher than that of the P-UHPC and PC specimens because of the higher compressive strength of the precast panels.



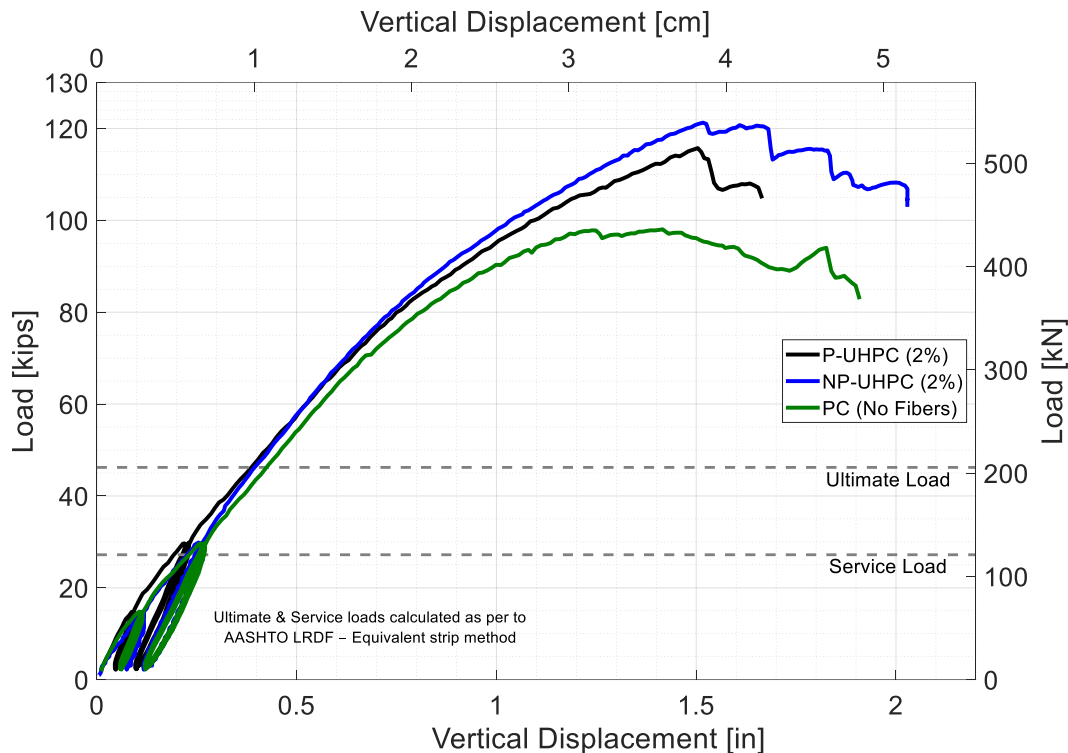


**Figure 7-4** Load versus middle deflection relationships of the longitudinal specimens.

The load deflection relationships of all specimens were very comparable up to approximately 400 kN where the PC specimen started to soften and lose stiffness due to the interface crack that happened between the PC joint and the south loaded side of the slab as mentioned before. The other two specimens failed in pure flexure behavior without any major interface cracking that affected the behavior or slippage of the reinforcing bars. The peak load capacities of all specimens exceeded the AASHTO LRFD ultimate and service loads. From the above key observations, the proposed field joint materials were capable of providing viable solutions for use in the longitudinal deck field joints in which the deck systems can satisfy the target behavior of conventional cast-in-place monolithic decks in terms of strength and load distribution requirements.

### 7.3 Design and Construction Recommendations of the FDBD Field Joints

This section provides guidance for the design and construction of the full-depth bridge deck (FDBD) joints based on the findings from the present research study along with previous

studies found in the literature. The recommendations provided herein are applicable to the transverse and longitudinal field joints in bridge decks.

FDBD deck panels are widely used to expedite bridge deck erection and accelerate bridge construction. FDBD with concave shear key type are currently common in bridge decks, with proprietary ultra-high performance concrete (P-UHPC) widely used for the closure pours of such joints. The unparalleled mechanical properties of UHPC mixes have gained the material popularity for ABC connections. However, the proprietary and relatively expensive nature of robust UHPC mixes pose some limitations, which motivated many researchers along with states departments of transportation to find other alternative advanced construction materials. The present study proved the applicability of using Poly-methyl methacrylate polymer concrete (PMMA-PC) and a newly developed non-proprietary UHPC mix (NP-UHPC) for bridge deck field joints. The objective of this section is to provide design and construction guidance on the deck field joints constructed using either of P-UHPC, NP-UHPC or PMMA-PC.

### ***7.3.1 Field Joint Materials***

This section provides general information about the field joint materials and their main mechanical and physical characteristics. Moreover, this section provides guidance on the mixing process and cost of each material.

#### ***7.3.1.1 Proprietary UHPC (P-UHPC)***

Ultra-high performance concrete (UHPC) is a new class of advanced construction materials with enhanced mechanical and durability properties due to steel fiber reinforcement, low water to binder ratio, and optimized particle packing density [4–6]. UHPC typically consists of a well-graded mixture of Portland cement, silica fume, ground quartz, high-range water reducer (HRWR), fine sand, and discontinuous steel fiber reinforcement [7,8]. Typical compressive strength of UHPC may exceed 21.7 ksi (150 MPa) with a sustained post-cracking tensile strength of at least 0.72 ksi (5 MPa) [9]. The unparalleled properties of UHPC have motivated the bridge engineering community to implement it in various applications, such as accelerated bridge construction (ABC) field joints, over the past two decades [10]. The proprietary UHPC (P-UHPC) products are commercially available

across the United States and Europe in pre-packed bags of proprietary blend of dry components, steel fibers, and plasticizer buckets. The type of P-UHPC that was used in this study is Ductal® JS1000. This product has been used for closure joints to connect pre-fabricated structural elements on-site for several projects across the United States. Its flowability, high strength, and enhanced bond properties make it ideal for this application.

#### 7.3.1.1.1 Material Properties of Ductal® JS1000

The main material properties of P-UHPC (i.e., Ductal® JS1000) with 2% steel fibers by volume, as reported by the manufacturer, are shown in Table 7-6. These values should be used as guidance for the design of the UHPC deck field joints. These values could also be used for comparison purposes with the actual test values of the quality control tests of the utilized UHPC inside the joints.

**Table 7-6** Main material properties of the P-UHPC, i.e. Ductal® JS1000

Material Characteristic (According to ASTM C1856 [11])	Average Result
Density	155 lb/ft <sup>3</sup> (2,480 kg/m <sup>3</sup> )
Flow	8.5 in. (21.6 cm) diameter
Working Time / Set Time	approx. 120 min. / 16.5 hrs
Compressive Strength (28 days)	> 21 ksi (150 MPa)
Modulus of Elasticity (28 days)	> 6,500 ksi (45 GPa)
Direct Tensile Cracking Strength	1.2 ksi (8.5 MPa)
Splitting Tensile Cracking Strength	1.3 ksi (9.0 MPa)
Long Term Shrinkage (28 days)	< 800 microstrain
Chloride Ion Penetrability (56 days)	< 250 coulombs (very low)

#### 7.3.1.1.2 P-UHPC Mixing Instructions

The mixing, placing, finishing and curing of the UHPC should conform to the recommendations provided by the FHWA [12] in addition to the instructions provided herein. Ductal® JS1000 is commonly packed into three different components as follows: (1) dry components that are packed in 50-lbs (22.7 kg) bags and consist of proprietary pre-blended cement, sand, ground quartz, and silica fume (see Figure 7-5a); (2) liquid admixture that is packed in 5-gallon (19 liter) pails and consists of a high range water

reducer (HRWR) in addition to an accelerator (see Figure 7-5b); and (3) steel fibers that are packed in 44-lbs (20 kg) bags and the single steel fiber has dimensions of 0.008 in (0.02 mm) diameter and 0.51 in (13 mm) long with tensile strength greater than 290 ksi (2,000 MPa) (see Figure 7-5c).



**Figure 7-5** Ductal® UHPC components (a) dry premix, (b) superplasticizer, and (c) steel fibers.

Table 7-7 shows the mixing proportions of the Ductal® JS1000 UHPC based on the number of dry premix bags used on a single batch. Table 7-8 shows the mix components and quantities per cubic yard and cubic meter of the Ductal® JS1000 UHPC. It is recommended to use a high shear mixer to mix UHPC such as the types of mixers shown in Figure 7-6. The UHPC can also be mixed using other types of equipment such as conventional rotary drum mixer, hand mixing in buckets, and ready mix truck mixers. However, such ways of mixing needs are not yet common for use. Hence, it is strictly recommended to do material tests such as flow, compression, and flexure tests on the produced UHPC to test the uniformity and consistency of the properties of the developed mixes.

**Table 7-7** Ductal® UHPC mixing proportions according to the number of dry premix bags

No. of bags per batch	5	6	7	8	9
Dry premix (lb)	250	300	350	400	450
Water or ice (lb)	14.37	17.24	20.12	22.99	25.86
Superplasticizer (lb)	3.43	4.11	4.80	5.48	6.17
Steel fibers (lb)	17.77	21.32	24.88	28.43	31.99
Batch volume (ft <sup>3</sup> )	1.82	2.19	2.55	2.92	3.28

**Table 7-8** Ductal® UHPC mixing proportions per cubic yard and cubic meter

	kg/m <sup>3</sup>	lb/yd <sup>3</sup>	Percentage per weight (%)
Dry premix	2195	3700	87.6
Water or ice	130	219.1	5
Superplasticizer	30	50.6	1.2
Steel fibers (2% volume)	156	263	6.2



**Figure 7-6** Examples of the UHPC mixer types (a) IMER high shear mixer, (b) high shear pan mixer [13], and (c) portable concrete pan mixer [12].

The mixing procedure of the UHPC is divided into three main steps as follows: (1) the dry premix blend is added to the mixer to mix for about one minute; (2) water mixed with the full amount of superplasticizer are then added gradually over the course of two minutes to the dry premix; (3) the components are then left to mix for about 10-13 minutes; (4) finally, the steel fibers are then added gradually to the UHPC paste over the course of one minute and then left for 2-4 minutes to ensure uniform distribution of the fibers inside the mix.

It is recommended to use 100% ice instead of the required quantity of water if the daytime temperature exceeded 25°C (77°F). The water replacement with ice is mainly to ensure that the mix will have sufficient working time for mixing, placing, and forming. UHPC is a flowable material, hence it is not required to use mechanical vibrators after placing to avoid any fibers segregation. The UHPC is recommended to be continuously poured inside the field joints from one location and left to flow to the other end of the joint. The UHPC usually form a thin solid crust at the top surface after approximately 10-20 minutes depending on temperature. It is recommended to break this crust using a steel rod before pouring the following UHPC batch to avoid the formation of any cold joints between separate flows. The typical mixing time for one UHPC batch is around 25-30 minutes.

#### 7.3.1.1.3 Placing of UHPC

Based on practical experience, the initial shrinkage of the UHPC joints usually cause settlement of the top surface of the joint. This settlement should be avoided by providing excess UHPC amount inside the joint. This extra amount of UHPC is also required to account for the top weak crust of the UHPC which should be grinded. The grinding of the UHPC joints is not required unless the project documents specifies that the joint surface is the final ride surface of the bridge and no deck overlays are used. The UHPC joint should be poured to an extra thickness of 0.25 in (0.64 cm) more than the adjacent deck panels. This extra quarter inch thickness should be grinded as soon as the UHPC reaches the compressive strength value which allow the structure to carry the grinding equipment safely without causing inelastic damage to the UHPC joint or the interface of the joint. The FHWA has recommended a threshold of 14 ksi (97 MPa) compressive strength for the UHPC joints before the structure being subjected to construction and traffic live loads [12]. The compressive strength of 14 ksi (97 MPa) is usually reached between 3-5 days depending on temperature and type of curing. The UHPC is recommended to be grinded before it reaches the full-strength to minimize the time and effort required for this process.

#### 7.3.1.1.4 Curing of UHPC

The UHPC does not required to be moist cured because of its low permeability. The FHWA has recommended that the UHPC should not freeze before reaching a compressive strength of 10 ksi (70 MPa). There are some issues with pouring UHPC joints in cold environment as the initial setting is delayed and this may cause non uniform fiber distribution along the depth of the joint. The steel fibers may settle at the bottom of the joints, this behavior was reported by project engineers in the Pulaski Skyway project in NY. Hence, it is recommended to start heat curing of the joints immediately after placing of UHPC. The heat curing could be applied to the field joints and the adjacent precast members using several types such as thermal heating mats and resistance heating wires [12]. It is prohibited to expose the surface of the freshly mixed UHPC to a forced hot air to prevent the loss of moisture of the mix. As mentioned earlier, the joint formwork removal or any construction

activities that includes the incorporation of heavy equipment are not recommended before the UHPC reaches 14 ksi (97 MPa) to avoid the damage of the joints.

#### 7.3.1.1.5 Cost and Availability of P-UHPC

According to the FHWA, the average cost of the P-UHPC products is about 20 times more expensive than conventional concrete, which is about \$100/yd<sup>3</sup> (\$130/m<sup>3</sup>). The P-UHPC is sold for about \$2,000/yd<sup>3</sup> (\$2,600/m<sup>3</sup>). This price includes the material costs of the proprietary blend and the fiber reinforcement, as well as costs associated with the development and delivery of the material. The complexity of mixing, surface grinding, and heat curing may increase the final cost of UHPC. According to the FHWA, there is limited numbers of commercial suppliers of UHPC in the transportation infrastructure market in the United States [14]. The proprietary nature, increased quality control, and high material costs are some factors that have limited the wide spread use of UHPC in the U.S. infrastructure [14].

#### 7.3.1.2 *Non-Proprietary UHPC (NP-UHPC)*

The proprietary nature of UHPC along with the high cost and limited availability of the material have motivated transportation agencies along with academic and industrial research to find other alternative materials for deck field joints [e.g. 15]. Some of these research efforts focused on making UHPC more accessible and less expensive through the development of non-proprietary UHPC (NP-UHPC) mixes using locally available materials. Former studies [e.g. 16] demonstrated that it is possible to develop NP-UHPC with a compressive strength greater than 30 ksi (200 MPa) without requiring any special treatment conditions. Due to the high number of these research efforts, a FHWA report was published to summarize some of these research findings to accelerate the use of NP-UHPC and promote more resilient US transportation infrastructures [14]. Many state departments of transportation (DOTs) have funded research on developing and testing several NP-UHPC mixes using locally available materials in their states for use in different bridge applications [e.g. 17–19]. A recent contribution in this area is the multi-institutional collaboration in the U.S. between the five consortium universities within the ABC

university transportation center (ABC-UTC), where the University of Oklahoma (OU) led the ABC-UTC NP-UHPC mix design [20–22].

The final NP-UHPC mix design was developed after establishing a wide parametric study that included evaluation of the particle packing density of a large number of different mix designs and comparison with the optimum packing curve generated from the Modified Andreasen and Andersen particle packing equation [23]. The mix design process investigated the effect of using different mixing proportions and combinations of various material ingredients. The final mix design included the replacement of the high cement ratio with almost 30% cement slag by weight to reduce the overall NP-UHPC mix cost. Research at OU used the final mix design in precast bridge deck joints and demonstrated acceptable behavior when compared to commercial UHPC formulations [24]. The final NP-UHPC mix developed by OU was selected as the main candidate for the ABC-UTC NP-UHPC initiative. As part of the ABC-UTC collaborative effort, the University of Nevada, Reno (UNR) reproduced the original OU mix using the locally-sourced Oklahoma set of materials, then identify and employ comparable materials from western US regions such as Nevada and California.

As part of this study, four NP-UHPC mixes were developed by UNR using the local materials in the Nevada and California states. Only two of them were selected for use in the bridge deck field joints. All information regarding the mix design, mixing methodology, and main material properties of the two mixes can be found on chapter 4. The name of the mixes, which were used inside the deck field joints, are B1 and B3. The only difference between both mixes is the amount of the steel fibers used in their compositions. B1 has 2% steel fibers by volume of the mix, while B3 has 1% steel fibers by volume. B1 has been suggested for use inside the transverse and longitudinal deck field joints. However, B3 has been used only inside the transverse field joints with a slightly wider joints. The recommendations, which have been suggested earlier for the mixing, placing and curing of the P-UHPC, do also apply to the NP-UHPC.



#### 7.3.1.2.1 Cost and Availability of NP-UHPC

The cost of the NP-UHPC is almost equal or slightly below half the typical cost of the P-UHPC products. The typical cost of the NP-UHPC is estimated to be around \$1,000/yd<sup>3</sup> (\$1,300/m<sup>3</sup>) [25,26]. One of the main objective of the study reported in chapter 4 is to study the variability effects on the main mechanical properties of the developed NP-UHPC mixes. The sought variability had two components: (1) material sourcing variability associated with utilizing different material sources from different regions of the country, and (2) aggregate type and grading variability through the using of fine masonry sand or sieved and non-sieved crushed aggregate sand in the NP-UHPC mixes. The reason for this study is to confirm if the proposed base mix design of the NP-UHPC could be reproduced with different construction teams using materials from different locations without affecting the main properties of the developed mixes. The study concluded that the effect of these variabilities could be negligible if the proposed mixing instructions and mixing proportions were closely applied. As mentioned earlier, the developed NP-UHPC mix was reproduced by the five consortium universities of the ABC-UTC using local materials in different regions of the country. This collaboration research investigation and reproduction of the proposed ABC-UTC NP-UHPC mixes would help this material gain significance in the U.S. transportation industry.

#### 7.3.1.3 *Poly-Methyl Methacrylate Polymer Concrete (PMMA-PC)*

PMMA-PC has physical and mechanical material properties that are arguably comparable to that of the high strength concrete and a gray color similar to cementitious concretes. However, PMMA-PC is not a cementitious material. PMMA-PC is created by mixing Methyl Methacrylate resin with a Benzoyl Peroxide initiator in addition to optional graded aggregate of 3/8 in × 3/16 in (9.5 mm × 4.8 mm) nominal maximum size. Adding of aggregate to the mix is only recommended for applications in which the thickness of the patch exceeds about 1.25 in (4 cm) and a concrete should be used rather than a mortar. Examples of these applications are bridge full-depth deck joints and DBT longitudinal field joints. PMMA-PC without aggregate can be used for thin patches such as bridge deck overlays but thicker and larger patches should be mixed with the addition of aggregate. The

utilized PMMA-PC has a specified compressive strength of 8–9 ksi (55– 62 MPa) after 24 h, and specified tensile strength of 1.0-1.2 ksi (6.9–8.3 MPa). PMMA-PC is designed for use on new construction and rehabilitation of bridge decks, expansion joints, bearing pads, airport runways and other concrete structures due its fast setting, high bond strength and early strength. The type of PMMA-PC which was used in this study is Transpo<sup>®</sup> T–17 PC and it is one of the commercial products of Transpo Industries Incorporation. Commercial PMMA-PC products are typically provided in pre-packed bags and pails. It is worth noting that the type of the PMMA-PC, which was used in this study, is not mixed with any type of fiber reinforcement. While the tensile properties of this material are very comparable to that of the fiber reinforced UHPC.

#### 7.3.1.3.1 Material Properties of Transpo<sup>®</sup> T–17 PC

The main material properties of the PMMA-PC (i.e., Transpo<sup>®</sup> T–17 PC), as reported by the manufacturer, are shown in Table 7-9. These values could be used as guidance for the design of the PMMA-PC deck field joints. These values could also be used for comparison purposes with the actual test values of the quality control tests of the utilized PMMA-PC inside the joints.

**Table 7-9** Main material properties of the PMMA-PC, i.e. Transpo<sup>®</sup> T–17 PC

Material Characteristic	Method	Average Result
Dynamic Flow	ASTM C1437/230	9 in. (22.9 cm) diameter
Initial Set Time	ASTM C191	17 min
Compressive Strength	ASTM C579	> 8 ksi (55 MPa)
Compression Modulus	ASTM C469	> 2,800 ksi (19.3 GPa)
Tensile Strength	ASTM D638	> 1 ksi (6.9 MPa)
Flexural Strength	ASTM D790	> 1.8 ksi (13 MPa)
Tensile Adhesion	ACI 503R	> 250 psi (1.7 MPa)
Linear Shrinkage	DuPont	< 0.2%

#### 7.3.1.3.2 P-UHPC Mixing Instructions

The PMMA-PC is commonly packed into two different components as follows: (1) proprietary blend of dry components, which are packed in 50-lbs (22.7 kg), and consists of

sand, inert fillers, polymers, and initiators (see Figure 7-7a); and (2) liquid admixture, which is packed in 5-gallon pails (19 liters) and consists of a solvent-free 100% reactive, low viscosity methyl methacrylate (MMA) (see Figure 7-7b). As mentioned earlier, a small-sized coarse aggregate shall be added to the PMMA-PC mortar if the depth or thickness of the PMMA-PC patch exceeds 1 in (2.54 cm). The coarse aggregate is also commercially available and offered from the same material supplier in 50-lbs bags (22.7 kg).



**Figure 7-7** Transpo® T-17 PC components (a) dry premix, and (b) liquid component.

Table 7-10 shows the mixing proportions of the Transpo® T-17 PC based on the number of powder bags that are used on a single batch. Table 7-11 shows the mix components and quantities per cubic yard and cubic meter of the Transpo® T-17 PC. The T-17 PC can be easily mixed in less than five minutes using the conventional rotary drum mixers. The mixing procedure is less complicated and requires less time compared to the UHPC. Hence, this material is recommended for the contractor teams who have limited experience with the complicated mixing of the UHPC. Moreover, this material is recommended for bridge projects in which a large amount of field joint material is needed. This material can be easily mixed in buckets using hand driller mixers for small-scale applications and patching. It can be also mixed in large quantities up to 4 ft<sup>3</sup> (0.11 m<sup>3</sup>) using the conventional rotary drum mixers. Based on the practical experience of the research team with mixing and testing this material, the test results from 12 different batches were very comparable and

more consistent compared to the UHPC. This consistency is mainly due to the less complexity of the mixing process and the absence of the random distribution of the steel fibers effects on the properties of the material when compared with the UHPC. Hence, it is recommended to verify the adequacy of the T-17 PC mixes by only testing the compression strength of the material at several ages and compare the results with the allowable results in Table 7-9.

**Table 7-10** Transpo® T-17 PC mixing proportions according to number of powder bags

No. of bags per batch	1	2	3	4	5	6
Dry components (lb)	50	100	150	200	250	300
Liquid component (lb)	5.72	11.44	17.16	22.88	28.6	34.32
Liquid component (gallon)	0.75	1.5	2.25	3	3.75	4.5
Aggregate (3/8 x 3/16) (lb)	25	50	75	100	125	150
Batch volume (ft <sup>3</sup> )	0.56	1.12	1.68	2.24	2.8	3.36

**Table 7-11** Transpo® T-17 PC proportions per cubic yard and cubic meter

	kg/m <sup>3</sup>	lb/yd <sup>3</sup>	Percentage per weight (%)
Dry components (lb)	3153	2411	61.95
Liquid component (lb)	361	276	7.10
Liquid component (gallon)	47	36	-
Aggregate (3/8 x 3/16) (lb)	1577	1205	30.95

The mixing procedure of the PMMA-PC is divided into four main steps as follows: (1) prior to mixing, the inside of the mixer should be clean and dry, then the mixer should be pre-wet with a quart of the liquid component; (2) the liquid component is added to the mixer; (3) the powder bags are then added gradually over the course of half minute and then left to mix with the liquid for about 2-3 minutes until uniform consistency to ensure appropriate PC paste; (4) finally, the coarse aggregate is then added gradually to the mix over the course of half minute and then left for one minute to ensure uniform distribution of the aggregate inside the concrete. The total mixing time of the PMMA-PC batch is typically around 5-6 minutes compared to approximately 25 minutes for the typical mixing of UHPC. The mixing time required for the PMMA-PC could save 80% of the time needed for the mixing of the same amount of UHPC. Moreover, the mixing of the PMMA-PC is not complicated and it is almost similar to the mixing of the grout or the conventional

concrete. Hence, potential money and labor savings are associated with the use of the PMMA-PC compared to UHPC.

It is recommended not to over-mix the PMMA-PC after adding the coarse aggregate to avoid segregation. The PMMA-PC has a wide application temperature range between 14-100 °F and its strength gain is less dependent on the ambient temperature. However, the UHPC needs more setting time in cold environments and requires additional heat curing to speed up the strength gaining. In addition, UHPC requires replacement of the mixing water to ice during the hot temperatures. It is preferred to use PMMA-PC as a joint material in the extreme hot or cold temperature conditions as it does not require any heat curing or special considerations for mixing as UHPC.

#### 7.3.1.3.3 Placing of PMMA-PC

The placing of PMMA-PC is similar to the placing of conventional concrete and the surface finish can be maintained easily using the same tools used for the conventional concrete. Steel trowels, floats, or screeds can be used to obtain a closed PC surface while tinning or broom finishing is not recommended. The PMMA-PC material does not experience any initial shrinkage as in the case of UHPC and the top surface can be used directly as the final riding surface of the bridge. Hence, it is not required to provide extra thickness of the material to account for the initial shrinkage or the grinding of the surface. As a result, there is another potential cost and labor savings associated with the placing and the surface finish activities of the PMMA-PC. PMMA-PC is a flowable material and it is not required to use a vibrator with the fresh mix of PMMA-PC to avoid any coarse aggregate segregation. PMMA-PC requires less mixing time, which is favorable to reduce the chances of having cold joints between successive batches. PMMA-PC is well known for its rapid strength gain as it can reach the full strength in about 24 hours. On the other hand, this advantage has resulted in a less working time for the PMMA-PC fresh mixes. Hence, it is recommended to do the mixing of PMMA-PC near to the location of application (i.e., field joints) to save the time needed for the transportation of the material to the pouring location.

As mentioned earlier, the FHWA has recommended a threshold of 14 ksi (97 MPa) compressive strength for the UHPC joints before the structure being subjected to

construction and traffic live loads [12]. This threshold was recommended by the FHWA for UHPC only, while it has to be investigated for the other field joint materials. The 14 ksi (97 MPa) threshold is determined in order for the UHPC to be able to provide the required bond strength for the reinforcement inside the joint. The maximum compressive strength of the PMMA-PC is typically below this threshold. While the compressive strength of the PMMA-PC is almost one third that of the P-UHPC, the PMMA-PC has a very comparable tensile and bond strengths as the P-UHPC. Hence, the PMMA-PC can gain full strength and develop the full bond strength to reinforcement in less than 24 hours. This is compared to a typical waiting time of 3-5 days for the UHPC in order to reach the 14 ksi (97 MPa) limit and be able to provide the adequate bond strength.

#### 7.3.1.3.4 Curing of PMMA-PC

There are no special considerations required for the curing of the PMMA-PC. The PMMA-PC usually gains strength based on the chemical reactions between its components (i.e., polymers, monomers, and initiators) without the need for moist or heat curing. The PMMA-PC is less susceptible to freezing because there is no water in the mix. The joint formwork removal or any construction activities can be done after few hours from pouring the joints without the need to wait for the 14 ksi (97 MPa) threshold which has been recommended for UHPC. The PMMA-PC can reach more than 80-90% of its full strength after only 3-6 hours.

#### 7.3.1.3.5 Cost and Availability of PMMA-PC

The material cost of PMMA-PC is equal to half the cost of the commercial products of the UHPC. The overall cost of the PMMA-PC including the mixing, placing, and finishing of the material is expected to be cheaper than the UHPC because of many reasons such as the ease of mixing and placing using the conventional mixers, less mixing time, and the speed of finishing using the traditional ways to maintain acceptable surface. Moreover, the PMMA-PC does not require any special treatment or curing regimes, unlike the UHPC that may require special heat curing in cold weather. A previous study by Mantawy et al. [27] has included a detailed design example and cost analysis of a practical precast bridge deck with PMMA-PC and UHPC field joints. The study considered the cost of one cubic yard

of PMMA-PC and UHPC per factory directions is \$2,000 and \$4,000, respectively. The study concluded that using the PMMA-PC instead of the commercial UHPC in the bridge deck field joints will ensure direct and indirect cost savings.

To provide more insight into the cost of applying PC and UHPC, the Caltrans Contract Cost Database [28] was checked for two recent projects that used PC and UHPC but for different applications. The average overall cost of two recently awarded bids for using polymer concrete for overlays and UHPC for deck joints were found to be \$2,790 and \$18,290 per cubic yard, respectively. This is not a direct comparison since the UHPC cost include the much involved labor and material furnishing costs as well as quality control. However, it gives an idea about the higher cost of UHPC applications that is attributed to higher material cost in addition to the extra costs UHPC vendors charge for material mixing, furnishing, and quality control. Unlike UHPC, different PMMA-PC products have been commonly used for decades around the nation as they are locally available and can be distributed to any place in North America for instance.

### ***7.3.2 Full-Depth Deck Panels (FDDP)***

The reinforcement of the full depth deck panels (FDDP) can be ordinary or conventional reinforcement or it could be pre-tensioned. The focus of this study is on the ordinary or conventional reinforced FDDP. The design of the FDDP are usually done according to the AASHTO LRFD design specifications [29]. However, the AASHTO LRFD assumes a fully composite cast in place (CIP) bridge deck systems and does not have a specific recommendations or design guidelines for the design of the FDDP. The AASHTO LRFD utilizes the equivalent strip method for the design of FDDP. The strip design method could be either a transverse strip design (i.e., perpendicular to traffic flow direction) or longitudinal strip design (parallel to traffic flow direction). The equivalent strip method assumes the largest expected bending moments experienced by the bridge decks based on the finite loading conditions. With the recent introduction and the large implementation of the precast members in the transportation industry, the AASHTO has provided a guide specification for accelerated bridge construction [30]. That document specified that the design of the FDDP should follow the same procedure for design of the CIP decks using

the AASHTO LRFD design specifications. The Precast/Prestressed Concrete Institute (PCI) code also provides more recommendations and specifications for the design, handling and erection of the FDDP [31].

In the present study, the FDDP has been designed according to the transverse equivalent strip method. The main reinforcement was provided in the transverse direction while the secondary reinforcement was provided in the longitudinal direction. The longitudinal reinforcement is mainly provided to control shrinkage and allow for more distribution of the load in the longitudinal direction.

For the transverse field joints, the longitudinal reinforcement is required to overlap inside the field joints. The amount of steel required for the longitudinal reinforcement is usually smaller than the transverse reinforcement, which may result in wide spacing between reinforcing bars. Based on the findings from the present study, it is shown that decreasing the bar size to #4 bars instead of #5 bars to provide denser reinforcement inside the joint has enhanced the load transfer across the FDDP. In addition, the narrow spacing between reinforcement is usually better for the concrete cracking control. However, the narrow spacing between the longitudinal reinforcement should be checked against the minimum specified limits by the AASHTO LRFD design specifications. Nonetheless, the FHWA has provided minimum limits for the clear spacing between the adjacent discrete reinforcement inside the UHPC joint.

For UHPC joints, the minimum clear spacing should be at least 1.5 times the length of the longest fiber reinforcement in the UHPC. In case of steel fibers with length of 0.5 in (13 mm), the minimum clear spacing of reinforcement inside the UHPC joint is equal to 0.75 in (20 mm). In case of non-contact lap splices, the minimum clear spacing between the longitudinal reinforcement inside the FDDP is equal to the greatest of; (1) double the minimum clear spacing of reinforcement inside the UHPC joint plus one bar diameter, i.e.  $3 \times \text{longest fiber reinforcement} + d_b$ ; (2) the minimum clear spacing required for the concrete crack control according to the AASHTO LRFD, section 5.7.3.4; (3) the minimum clear spacing between reinforcement according to the ACI 318-14, section 25.2.1. The FHWA has also specified a maximum limit for the clear spacing between the adjacent



reinforcement splices. The maximum clear spacing should be less than or equal to the lap splice length of reinforcement as provided in section 7.3.5 later in this chapter.

For PMMA-PC joints, there is no steel fibers used inside the mix. Hence, the minimum clear spacing between the longitudinal reinforcement is equal to the greatest of: (1) the minimum clear spacing required for the concrete crack control according to the AASHTO LRFD, section 5.7.3.4; and (2) the minimum clear spacing between reinforcement according to the ACI 318-14, section 25.2.1. It is recommended to use the larger aggregate size used either in the conventional concrete of the FDDP or the PMMA-PC joint to calculate the minimum clear spacing. The PMMA-PC is a new material which is recently tested for the FDDP field joint applications. Thus, more research investigations are required to study the bond behavior of PMMA-PC and provide guidance for the minimum or maximum clear reinforcement spacing, minimum reinforcement clear cover, minimum non-contact lap splice length, and minimum required development length in contact and non-contact splice assemblies.

### ***7.3.3 Field Joint Interface***

The interface bond between the field joint and the FDDP is one of the critical aspects for the joint design. The interface surface should be prepared to ensure the long term performance of the system. The interface cracks are one of the main issues that was previously experienced by the old systems with conventional joint materials (i.e., high strength concrete and non-shrink grouts). These interface cracks lead to ingress of moisture and deicing chemicals to the reinforcement and causes damage and less durability of the full deck system. The advanced joint materials such as UHPC and PMMA-PC have a higher bond strength to the adjacent concrete surfaces. Hence, these materials are ideal for such applications and less susceptible to interface cracking.

Research studies along with the FHWA design guidelines have recommended the diamond shaped shear key or the female-female joint detail as it provides the best interface cracking resistance compared to the flat joints. Nonetheless, the present study has recommended a modified version of the diamond shaped shear key to eliminate the need for the joint formwork. The modified shaped shear has only half inch gap at the bottom that was filled

with a backer rod. This type of joints showed a similar behavior and adequate interface bond as the basic diamond shaped shear key.

The interface surface of the joint should be prepared before the pouring of the joint material. The preparation includes removing any debris or dust from the interface of the joint. For the case of UHPC joints, it is preferred to ensure a wet surface dry condition for the joint interface. This is mainly done to ensure that the water of the UHPC mix is not going to be absorbed by the FDDPs. This condition does not apply to the PMMA-PC joints as there is no water inside the PMMA-PC mixture. The PMMA-PC supplier recommends brushing the interface joint surface with a primer before pouring the PMMA-PC into the joint. The application of primer is important to enhance the bond of the PMMA-PC. The FHWA has also recommended roughening of the surface to the nearest 0.25 in (6.4 mm) amplitude to enhance the interface bond. The present study has shown that there were no interface cracks experienced by any of the proposed joint systems up to the AASHTO LRFD ultimate loads. Hence, all joint materials had adequate joint interface bond. For more conservative approach, it is also recommended to do roughening of the interface to eliminate the likelihood of having interface cracking.

#### ***7.3.4 Full-Depth Deck Field Joints***

The width of the field joints should be large enough to accommodate the required overlap length of reinforcement inside the joint. This yields in a typical joint width for UHPC and PMMA-PC joints that ranges between 6 to 8 in (15.24 to 20.32 cm) for #4 or #5 bars overlapped reinforcing bars. The lap splice lengths required for the uncoated reinforcing bars in PMMA-PC and PC joints are equal to 4.1 and 4.5 times the bar diameter, respectively [27]. The minimum development length required for the uncoated reinforcing bars inside PMMA-PC ranges between 3.6 to 4.1 times the bar diameter [27]. The minimum development length required for the uncoated or epoxy coated reinforcing bars inside UHPC is equal to 8 times the bar diameter [12]. The required development length for UHPC is determined based on a UHPC compressive strength of about 14 ksi. Hence, a 14 ksi minimum compressive strength of UHPC limit was selected to be the threshold for resuming construction and removing the joint formwork. The P-UHPC typically reaches

14 ksi after approximately 3 days. The NP-UHPC mix, which were used in the present study, reaches a compressive strength of 14 ksi after approximately 7 days.

The results of the present study showed that it is not critical to provide the full development length for the reinforcement inside the transverse joints. This was mainly because the strains of the overlapped longitudinal (i.e., secondary) reinforcement inside the joint were typically far below the yielding strains at the AASHTO LRFD ultimate loads. However, it is still recommended to provide the full development length of reinforcement inside the transverse joints to account for the unusual loading conditions or unexpected shorter development lengths developed from inaccurate fabrication. Examples of the unusual loading conditions includes the load demands developed from the composite action between the girders and deck. The composite action may subject the bridge deck to high tensile demands at the negative moment location for the girders, i.e. over the support of the main girder. For the longitudinal field joints, the overlapped reinforcement is the transverse main reinforcement. Therefore, it is expected to have higher tensile strain values for the overlapped reinforcement inside the joints. Consequently, it is recommended to provide the minimum development length for the reinforcement inside the longitudinal joints plus a factor of safety.

The non-contact lap splices have been used and tested inside the bridge deck field joints in many research studies as they are easier to be constructed and they also could accommodate larger construction tolerances when connecting the FDDPs in field. Research studies showed that the non-contact lap splice specimens exhibit higher bond strength than contact lap splice specimens, due to the fact that the tight spacing in contact lap splice limits the ability of the fiber reinforcement to locally enhance the mechanical resistance of the UHPC [32].

Using loop bar splice provides less splice length when compared to the straight splice. The loop bar splice could provide slight better performance and force transfer between precast panels than the straight splice [33]. The present study showed that the use of the loop splice inside the transverse field joints has enhanced the structural performance and increased the flexural stiffness of the deck slabs. The choice of the reinforcing bar size should be adjusted

to accommodate the minimum bend diameter specified by the ACI 318. For #5 reinforcing bars or smaller, which are made of conventional steel, the minimum bend diameter should be six times the bar diameter  $6 d_b$  [34]. It is practically impossible to use loop splices for bridge decks with a thickness less than 8 in because of the bend diameter limitations. The typical thickness of the top flange of the DBT girders ranges from 6 to 8 in. Therefore, it is only recommended to use loop splice for the longitudinal field joints of the DBT girders if the minimum thickness of the top flange is more than or equal to 8 in and # 4 bars are used for reinforcement.

### ***7.3.5 Target Performance of Precast Bridge Deck with Full-Depth Field Joints***

The performance of the precast bridge deck systems with field joints should satisfy the following conditions:

- 1- The precast deck systems with field joints should act compositely as CIP bridge decks.
- 2- The overall behavior of the precast deck systems with field joints should be dominated by flexure. Therefore, at hypothetical ultimate states, yielding of the main reinforcement is expected before the crushing of concrete happens. More importantly, behavior at failure should not be dominated by the failure of the either the joint or the shear key.
- 3- The deck systems should remain essentially elastic up to the AASHTO LRFD design load limits without yielding of any reinforcing bars.
- 4- The precast deck systems, which are subjected to the AASHTO LRFD design loads, should not experience any interface cracks or slippage of spliced reinforcing bars inside the joint.
- 5- If interface cracking occurred, resulting cracks should be checked against leaking to avoid the corrosion of reinforcement due to the ingress of moist and chemicals. The interface cracks should also not affect the overall behavior or performance of the deck system.
- 6- It is preferred that the deck joint remain below its cracking load up to the AASHTO LRFD design load limits to ensure adequate load distribution across the precast panels.

## References

- [1] ASTM C39, Standard Test Method for Compressive Strength of Cylindrical Concrete Specimens, American Society for Testing and Materials Standard Practice C39, 2001.
- [2] ASTM C1609/C1609M-07. Standard test method for flexural performance of fiber reinforced concrete (using beam with third-point loading). American Society of Testing and Materials (2007).
- [3] ASTM, C. C580 Standard Test Method for Flexural Strength and Modulus of Elasticity of Chemical-Resistant Mortars, Grouts, Monolithic Surfacing, and Polymer Concretes.
- [4] American Road and Transportation Builders Association (ARTBA) 2020 bridge report.
- [5] Garber, D., & Shahrokhinasab, E. (2019). Performance Comparison of In-Service, Full-Depth Precast Concrete Deck Panels to Cast-in-Place Decks (No. ABC-UTC-2013-C3-FIU03-Final). Accelerated Bridge Construction University Transportation Center (ABC-UTC).
- [6] Haber, Z. B., & Graybeal, B. A. (2018). Performance of Grouted Connections for Prefabricated Bridge Deck Elements (No. FHWA-HIF-19-003). United States. Federal Highway Administration. Office of Infrastructure Research and Development.
- [7] Graybeal, B. Behavior of Field-Cast Ultra-High Performance Concrete Bridge Deck Connections Under Cyclic and Static Structural Loading; Report No. FHWA-HRT-11-023; Federal Highway Administration, McLean, VA, 2010
- [8] Hartwell, D. R. "Laboratory testing of Ultra High Performance Concrete deck joints for use in accelerated bridge construction" (2011). Graduate Theses and Dissertations. 10420.
- [9] Hwang H., Park S. Y. "A study on the flexural behavior of lap-spliced cast-in-place joints under static loading in ultra-high performance concrete bridge deck slabs" (2014). Canadian Journal of Civil Engineering, 41:615-623.
- [10] Vitek, J.L., Kolisko, J., Citek, D., Rehacek S., Coufal R. "UHPC connection of precast bridge deck" (2016). First International Interactive Symposium on UHPC.

- [11] ASTM C1856/C1856M-17. (2017). Standard practice for fabricating and testing specimens of ultra-high performance concrete. ASTM International”, West Conshohocken, PA.
- [12] Graybeal, B. (2014). Design and construction of field-cast UHPC connections (No. FHWA-HRT-14-084; HRDI-40/10-14 (750) E). United States. Federal Highway Administration.
- [13] Abbas, S., Soliman, A. M., & Nehdi, M. L. (2015). Exploring mechanical and durability properties of ultra-high performance concrete incorporating various steel fiber lengths and dosages. *Construction and Building Materials*, 75, 429-441.
- [14] Graybeal, B. A. (2013). Development of Non-Proprietary Ultra-High Performance Concrete for Use in the Highway Bridge Sector: TechBrief (No. FHWA-HRT-13-100). United States. Federal Highway Administration.
- [15] Abokifa, M., & Moustafa, M. A. Experimental behavior of poly methyl methacrylate polymer concrete for bridge deck bulb tee girders longitudinal field joints. *Construction and Building Materials*, 270, 121840.
- [16] K. Wille, A.E. Naaman, G.J. Parra-Montesinos, Ultra-High Performance Concrete with Compressive Strength Exceeding 150 MPa (22 ksi): A Simpler Way, *ACI Mater. J.* 108 (1) (2011).
- [17] El-Tawil, S., Alkaysi, M., Naaman, A. E., Hansen, W., & Liu, Z. (2016). Development, characterization and applications of a non proprietary ultra high performance concrete for highway bridges (No. RC-1637). Michigan. Dept. of Transportation.
- [18] Berry, M., Snidarich, R., & Wood, C. (2017). Development of non-proprietary ultra-high performance concrete (No. FHWA/MT-17-010/8237-001). Montana. Dept. of Transportation. Research Programs.
- [19] Hernandez, J. A. A. (2016). Development and laboratory testing of Ultra High Performance Concrete (Doctoral dissertation).
- [20] Abokifa, M., & Moustafa, M. A. (2021). Development of Non-Proprietary UHPC Mix: Application to Deck Panel Joints. Quarterly Progress Report.

- [21] Shahrokhinasab, E., & Garber, D. (2021). Development of “ABC-UTC Non-Proprietary UHPC” Mix, Final Report # ABC-UTC-2016-C2-FIU01-Final, ABC-UTC, Miami, FL.
- [22] T. Looney, A. McDaniel, J. Volz, R. Floyd, Development and characterization of ultra-high performance concrete with slag cement for use as bridge joint material, *Development 1 (02)* (2019).
- [23] J.E. Funk, D.R. Dinger, Predictive process control of crowded particulate suspensions: applied to ceramic manufacturing, Springer Science & Business Media, 2013.
- [24] T. Looney, R. Coleman, C. Funderburg, J. Volz, R. Floyd, Concrete Bond and Behavior of Non-proprietary Ultra high-Performance Concrete Bridge Slab Joints, *J. Bridge Eng.* 26 (2) (2021) 04020128, [https://doi.org/10.1061/\(ASCE\)BE.1943-5592.0001669](https://doi.org/10.1061/(ASCE)BE.1943-5592.0001669).
- [25] Subedi, D.; Moustafa, M.A.; Saiidi, M.S. Non-Proprietary UHPC for Anchorage of Large Diameter Column Bars in Grouted Ducts; Report No. CCEER-19-03; Center for Civil Engineering Earthquake Research: Reno, NV, USA, 2019.
- [26] Tadros, M.K.; Gee, D.; Asaad, M.; Lawler, J. Ultra-High-Performance Concrete: A Game Changer in the Precast Concrete Industry. *PCI J.* 2020, 65, <https://doi.org/10.15554/pcij65.3-06>.
- [27] Mantawy, I.; Chennareddy, R.; Genedy, M.; Taha, M.R. Polymer Concrete for Bridge Deck Closure Joints in Accelerated Bridge Construction. *Infrastructures* 2019, 4, 31.
- [28] California Department of Transportation (Caltrans). Caltrans Contract Cost Data, 2014. <https://sv08data.dot.ca.gov/contractcost/>. Accessed May 1, 2021.
- [29] L. AASHTO, “Bridge Design Specifications (8th edition September 2017),” Am. Assoc. State Highw. Transp. Off. Wash. DC, vol. 4, 2017.
- [30] American Association of State Highway and Transportation Officials (AASHTO), “AASHTO LRFD (2018) - Guide Specification for Accelerated Bridge Construction,” 2018.

- [31] PCI Committee on Bridges and PCI Bridge Producers Committee, "PCI State-of-the-Art Report on Full-Depth Precast Concrete Bridge Deck Panels," SOA-01-1911, 2011.
- [32] Yuan, J., & Graybeal, B. (2015). Bond of reinforcement in ultra-high-performance concrete. *ACI Structural Journal*, 112(6), 851.
- [33] National Cooperative Highway Research Program. Cast-in-Place Concrete Connections for Precast Deck Systems. NCHRP Report 10-71. Transportation Research Board, Washington DC, 2011.
- [34] ACI Committee. (2008). Building code requirements for structural concrete (ACI 318-08) and commentary. American Concrete Institute.



## **8 SUMMARY, CONCLUSIONS AND FUTURE WORK**

This doctoral dissertation included five standalone chapters in research papers format. The summaries of each of these parts of the study along with the conclusions of each part can be found in each chapter. Nonetheless, the current chapter provides an overall summary for the work done through this doctoral study for completeness and the convenience of the readers. It also highlights the broader impact of this study on the deck field joint implementations using alternative joint materials. Moreover, this chapter provides the main conclusions, research findings, and recommendations for future work.

### **8.1 Summary**

Pre-fabricated full-depth bridge deck panels are widely used to expedite bridge deck erection and accelerate bridge construction. These pre-fabricated deck panels dictates the need for field cast joints at least in one direction of the bridge. The conventional construction materials such as conventional concrete, advanced grouts, high-performance concrete (HPC) have been used for long time as field joint materials. However, there were several issues that developed from using these materials that has resulted in less durable systems such as interface joint cracking, low early strength, and relatively wide joints. Researchers tried to improve the performance of the joints through addressing special reinforcement requirements such as mechanical splicing or post-tensioning. Nonetheless, the conventional materials have relatively lower rates for strength gain that usually result in delaying the bridge deck erection. Many of the proposed solutions for improving the field joint performance requires more on-site work in addition to higher labor costs that are not viable for accelerated bridge construction (ABC). Hence, the main conclusion after experiencing many years of research and practical implementations is that the advanced construction materials (especially UHPC) are the best solutions to most of these issues.

The implementation of UHPC in the deck field joints has been shown to solve most of the aforementioned issues and can provide emulative monolithic deck systems with higher performance and prolonged durability. The robust UHPC mixes have gained popularity for deck field joint applications because of their unparalleled mechanical properties, high early

strength, high bond strength and high durability. Large number of research studies were published through the FHWA to summarize and synthesize the state-of-the-art for the pre-fabricated concrete components with UHPC field joints. These efforts converged on recommending a typical UHPC field joints that are 6 to 8 inches wide without post-tensioning and use simplified reinforcement configuration inside the joint with diamond-shaped shear key type.

On the other hand, the proprietary nature and relatively expensive cost of the UHPC mixes may restrain their implementation for the US bridge industry. Therefore, research efforts should be done to identify alternative field joint materials to avoid the drawbacks associated with the proprietary UHPC (P-UHPC). There is an obvious knowledge gap in the experimental proof testing and validating the use of alternative emerging and advanced materials beyond P-UHPC for bridge deck field joints.

Therefore, the overall objective of this study is to fill the abovementioned knowledge gap and provide more choices for connecting the full depth deck panels, especially for the west coast and western states. This is through investigating and validating the structural performance of PMMA-PC and NP-UHPC, with domestic materials from western states, in transverse and longitudinal full-depth deck joints as compared to P-UHPC. Moreover, this study aims at developing a better understanding of the structural behavior of the newly proposed joints at the AASHTO service and ultimate load levels and developing design tools for the future applications of the proposed joints. To achieve the main objective of this study, large sets of material testing along with large scale experimental testing of deck specimens with P-UHPC, PMMA-PC, and NP-UHPC field joints were conducted. The material testing, including flow testing, compression, flexure and direct tension testing, was conducted to determine the main material properties and understand the main material behavior of the newly proposed joint materials. Then, large scale experimental testing of nine full-scale specimens was done to study the structural performance of the deck systems with PMMA-PC and NP-UHPC field joints and compare them with reference systems with proprietary UHPC (P-UHPC) field joints. The experimental program included testing of six deck specimens with transverse field joints, and three other full-scale deck specimens that represent the top flange of the deck-bulb tee girders (DBTs) with longitudinal field

joint at the middle. The specimens were subjected to vertical static loading up to failure to investigate the overall structural behavior of the deck specimens and the performance of the field joints. A brief overview of each of the six major parts of this doctoral study is provided next.

The first part of study aimed at investigating and validating the structural behavior and joint performance of PMMA-PC transverse field joints as compared to P-UHPC. The specific objective was to conduct experimental testing of representative full-scale full-depth precast deck panel assemblies with PMMA-PC and P-UHPC transverse field joints under static vertical loading. Three large-scale tests were conducted and presented in detail in this section. Two identical specimens that varied only in the field joint material, i.e. UHPC versus PMMA-PC, were tested. The third specimen used PMMA-PC but with different splice type (i.e., loop splice instead of straight splice) and a different shear key shape (i.e., modified diamond-shaped). The use of loop splice inside the joint has shown to provide better structural performance and better load distribution compared to the straight lap splice.

The main objective of the second part of study was to investigate and validate the structural performance of PMMA-PC longitudinal field joints in DBT girders as compared to P-UHPC. This part was subdivided into two sections as in this part, material tests were initially performed to characterize the main mechanical properties of PMMA-PC to provide a better understanding of the material behavior that helps interpret the large-scale application. The material tests included flowability, compression, flexure, and direct tension testing of PMMA-PC samples at 28 days. The provided material characterization can also be readily used for future analytical studies and finite element modeling of the experimental results of the large scale test specimens. The second section included the full-scale experimental testing of deck assemblies of representative DBT girder flanges (slabs) with PMMA-PC and UHPC longitudinal field joints under static vertical loading. Two identical specimens that varied only in the field joint material, i.e. UHPC versus PMMA-PC, were tested and presented in this section.

The overall objective of the third part of study was to characterize and document the main physical and mechanical properties of the developed NP-UHPC mixes using local materials in the western states to facilitate the use of the developed mixes in various ABC applications, mainly bridge deck field joints. A total of five NP-UHPC mixes have been considered to investigate the effect of varying material sources as well as nominal sizes of the aggregate types on the main mechanical properties. The flow properties of the developed mixes were tested and compared with the recommended flow values. Moreover, different sets of testing were conducted on the developed mixes to test the compressive, flexural, and direct tensile strength and full behavior of the different NP-UHPC mixes. The results from these tests are then compared with various proposed equations from the literature to verify their validity for use with the considered NP-UHPC mixes. The results reported in this paper provide guidance for bridge and field engineers and researchers to further replicate the proposed NP-UHPC mixes by establishing the baseline mechanical properties for assessment and modeling.

The previous part of study was mainly focused on the assessment of the material behavior of the developed NP-UHPC mix. As mentioned earlier, five different NP-UHPC mixes were tested. Based on the results from this study, only two NP-UHPC mixes were selected to be further investigated in the deck field joints. The fourth part of study summarizes the main results of the comprehensive full-scale experimental testing of representative precast bridge deck panels with NP-UHPC transverse field joints. In this part of study, two NP-UHPC mixes with ingredients sourced from the western states (Nevada and California) were used as a closure joint material. The two NP-UHPC mixes only differs in the amount of the steel fibers used in their mixtures (i.e., 1% versus 2% by volume). The experimental program included testing of three full scale bridge deck specimens with transverse NP-UHPC joints. The main objectives of this study were to investigate the structural behavior of the NP-UHPC transverse joints with varying the reinforcement splice type, using dense reinforcement in the joint, and using wider joints with a NP-UHPC of 1 % by volume steel fibers. The first specimen utilized the NP-UHPC with 2% steel fibers and a straight lap splice. The second specimen was slightly different as it utilizes a loop splice. However, the third specimen was designed to optimize the NP-UHPC through using 1% steel fibers with

relatively wider joints and denser reinforcement in the joint. The structural behavior of the tested specimens was evaluated and compared with a reference proprietary UHPC specimen in terms of load and deflection capacities as well as the field joint performances at the AASHTO service and ultimate load levels.

The fifth part of study presents results from comprehensive large-scale testing of representative DBT girder panels with both non-proprietary and commercial proprietary UHPC-filled longitudinal joint as alternative closure pour materials. This part of study aimed at providing and demonstrating the viability of a NP-UHPC mix for ABC applications. The relevant chapter initially provided a brief summary of the main mechanical properties of the proposed NP-UHPC mix. Then, a detailed discussion of the structural performance of the proposed NP-UHPC longitudinal field joint in comparison to a readily implemented commercial proprietary UHPC product. The study compared both global and local experimental behavior of two identical full-scale specimens with proprietary and NP-UHPC field joints to verify the adequacy of using the newly developed UHPC as a closure material. The specimens considered representative DBT top flange parts and a 6-in (15.2-cm) wide diamond-shaped shear key joint and were tested under static vertical loading.

The last part of the doctoral study focused on analyzing and comparing the experimental results from the six full-scale bridge deck specimens with transverse joints and the three full-scale specimens with longitudinal field joints. This last part also presents more information and recommendations regarding the mixing and placing of the different field joint materials along with recommendations for the construction and design of the full depth deck panels with field joints. Such information stems from and documents several years of experience and numerous material trials and batches throughout the course of this work. The overarching goal of this part of study was to utilize the findings and conclusions from this doctoral study to contribute to the current and future design codes and the FHWA design guidelines for the field cast deck joints.

## 8.2 Key Conclusions and Findings

Based on individual papers conclusions in Chapters 2 through 6, a collection of the main observations and key concluding remarks that can be drawn from this comprehensive experimental study is reiterated and summarized as follows:

- In general, the structural behavior and joint performance of the precast bridge decks with full-depth transverse PMMA-PC and NP-UHPC field joints are demonstrated to be acceptable and viable for ABC. The global and local behaviors of the test specimens with transverse PMMA-PC and NP-UHPC were very comparable to that of the currently implemented and acceptable practice of the specimens using the commercial or P-UHPC.
- Similarly, the structural behavior and joint performance of the representative DBT girder's top flange parts with full-depth longitudinal PMMA-PC and NP-UHPC field joints are demonstrated to be a viable alternative for ABC. The performance of the longitudinal PMMA-PC and NP-UHPC joint was very comparable, as in case of transverse joints as well, to that of the currently acceptable and adopted practice using robust proprietary/commercial UHPC mixes.
- All the proposed joint systems were able to adequately satisfy the service and ultimate load requirements specified in the AASHTO LRFD, where deck systems remained essentially elastic without any yielding of reinforcement or major flexural cracking or interface cracking or rebar slippage. This is mainly attributed to the high bond and tensile strength of the proposed joint materials that prevented cracking of the joint. Therefore, the field joints were able to distribute the loads uniformly and elastically between the precast panels up to the AASHTO LRFD load.
- All test specimens showed adequate load distribution capabilities all the way through failure without any shear failure or significant interface de-bonding. The P-UHPC and NP-UHPC deck system exhibited few localized main flexural cracks at failure as opposed to several and multiple flexural cracks in the PMMA-PC deck systems at failure.

- All test specimens had flexure-dominated failure in which yielding of reinforcement was observed before the concrete crushing and failure. None of the proposed field joints were confirmed to be the weakest links in the integrated deck system. This conclusion applies to all the proposed joint systems except the PMMA-PC longitudinal field joint as it was subjected to interface cracking at the peak load that was one of the main reasons for failure of the specimen.
- The initial stiffness of the P-UHPC deck system was found to be higher than that of the PMMA-PC or NP-UHPC systems, which is attributed to the higher mechanical properties of the P-UHPC.
- The flexural load capacities of the test specimens were found to be much higher than the AASHTO LRFD service and ultimate load limits. However, all specimens have a comparable behavior in terms of loads, deflections, and field joint performance at the AASHTO LRFD ultimate load level. Moreover, the peak load capacity of the NP-UHPC specimen was slightly higher than that of the P-UHPC and PMMA-PC, which was attributed to the higher compressive strength of the precast deck panels of the NP-UHPC specimen.
- The tensile strains of the reinforcement splices inside the longitudinal field joints indicated that the proposed overlap lengths were sufficient to yield the reinforcement inside the joint. The tensile strain values of the splices inside the transverse field joint at the AASHTO LRFD load were typically far below the yield strain.
- The transverse specimens with loop splice type and shorter splice length had more flexural strength and more displacement capacity in addition to better load distribution across the precast panels than the transverse specimens with straight splice. This is attributed to the denser reinforcement distribution inside the joint (i.e., #4 bars were used with smaller spacing instead of #5 bars) and the better splice mechanism of the loop splice.
- The compressive strength of the transverse field joint material appears not to have significant effect on the initial stiffness and the peak load capacity of the transverse specimens while they are mainly controlled by the strength of the precast deck panels.

- The PMMA-PC transverse field joints with straight splice types showed the best interface bond strength between the field joint and the deck panels, while the NP-UHPC transverse field joints has the least bond strength. Moreover, using the loop splice inside for the transverse NP-UHPC joints has delayed the occurrence of the interface cracks.
- The P-UHPC longitudinal field joint has the best interface bond strength between the field joint and the deck panels, while the NP-UHPC longitudinal field joint has the least bond strength.
- The comparison between the calculated and measured peak load values of the longitudinal specimens showed that the over the strength (i.e., measured divided by the calculated peak load) of the P-UHPC is higher than that of the NP-UHPC and the PMMA-PC specimens, i.e. 25% versus 17% and 6%, respectively. This higher over strength is the result of the higher mechanical properties of the P-UHPC material compared to the NP-UHPC and PMMA-PC.
- A new shear key type that provides elimination of formwork was proposed in this study and demonstrated a comparable performance with the existing shear keys.
- The initial stiffness and load capacities of the deck systems with NP-UHPC transverse joints, which have a 2% steel fibers amount, were slightly greater than that of the deck systems with NP-UHPC joints with only 1% steel fibers.
- The use of NP-UHPC mix with 1% steel fibers in a relatively wider transverse field joints has shown to provide equivalent behavior and performance to that of the NP-UHPC mixes with 2% steel fibers. However, this has resulted in a less efficient load distribution capabilities over the specimen.
- PMMA-PC and NP-UHPC mixes sourced from Nevada and California local materials can be effectively used for closure joint materials for full-depth bridge deck field joints without requiring any post-tensioning or mechanical splicing. This study demonstrated that the 6-8 in field joint width, typically used for P-UHPC, is also sufficient for NP-UHPC to provide monolithic-equivalent deck systems in terms of load distribution.
- From the conducted material characterization tests of the PMMA-PC, the PMMA-PC is shown to have larger compressive ultimate strain than conventional normal strength concrete and P-UHPC as well as enhanced post-peak behavior and strain deformation



- capacity. The flexural strength of PMMA-PC and corresponding modulus of rupture, as obtained from standard prisms, is higher than typical normal strength concrete values, and comparable to P-UHPC with 2% fibers. However, PMMA-PC prisms show brittle failure after first crack formation as in conventional concrete.
- Direct tensile strength of PMMA-PC, as obtained from dog-bone specimens, is almost double typical normal strength concrete values and only slightly less than typical values of P-UHPC with 2% fibers. Unlike UHPC, the failure of PMMA-PC in tension is brittle after the first crack is formed. However, the PMMA-PC still provides a sustained tensile capacity with increased strains and very adequate ductility up to the instant of main crack formation.
  - The basic characteristics of the ABC-UTC NP-UHPC mix originally designed at OU based on materials from the Midwest and South US regions can be successfully replicated using full independent set of materials and different aggregate types from Western US.
  - The flow properties of all different NP-UHPC mixes is acceptable according to the flow requirements specified by ASTM C1856 or emerging FHWA reports. However, the fresh mixes with non-sieved sand (i.e. B1 and B3 in this study) are shown to have less uniform steel fiber dispersion because of the accumulation of the steel fibers around bigger sand particles.
  - The developed NP-UHPC mixes with sieved and non-sieved sand both meet the minimum compressive strength requirements specified by ASTM C1856 (117 MPa). The equations for predicting UHPC compressive strength gain over time are validated for use for NP-UHPC mixes up to 56 days, but underestimate the strength at higher ages. Moreover, other equations for predicting compressive stress-strain behavior of UHPC are also validated for NP-UHPC.
  - The compressive strength of NP-UHPC with 2% steel fibers is less sensitive than the ones with 1% steel fibers to the variability in aggregate types or material sources. Meanwhile, NP-UHPC mixes with local materials from Western US and non-sieved sand (i.e. B1 and B3) have higher compressive strength and more rapid early strength gain compared to other mixes.

- The various equations proposed in the literature for estimating UHPC modulus of elasticity are shown to inaccurately overestimate that for the NP-UHPC mixes. Thus, based on the conducted test results, the following equation is proposed to use for estimating the ABC-UTC NP-UHPC modulus of elasticity:  $E_c = 2,860\sqrt{f'_c}$  (for  $f'_c$  in MPa), but more future testing is still needed.
- The flexural behavior and tensile behavior of the different NP-UHPC mixes are very comparable and they all have sustained strain hardening without brittle or sudden failure. Moreover, using 1% steel fibers by volume instead of the more common 2% is shown to reduce both flexural and direct tensile strengths only by about 15% and 30% for NP-UHPC mixes with sieved sand and non-sieved sand, respectively.
- Based on all the material characterization tests, comparisons, and assessment conducted in this study, the ABC-UTC NP-UHPC mix with 1% steel fiber and non-sieved sand (i.e. B3) strikes the best balance between acceptable mechanical properties and cost (less fibers, less work for sieving, etc.). Therefore, this mix provides a reasonable NP-UHPC candidate and hence, is recommended for future implementation and large-scale ABC applications.
- Based on the conducted material characterization of the proposed NP-UHPC mixes, the local sources in Nevada and California that have been identified for the various material components used in the mix are confirmed to be adequate. The main mechanical properties of the mixes sourced from different regions of the country at UNR and OU were very comparable. Hence, the NP-UHPC mixes are deemed acceptable and insensitive to local resourcing as suggested by repeatable mechanical properties and they can be further extended to field implementation.
- This study enriches the literature by providing full tensile and compressive stress-strain relationships for PMMA-PC and NP-UHPC which can be readily used for defining constitutive laws and future modeling to further explore more applications of these advanced materials.

### 8.3 Recommendations for Future Work

Building on all test results and the adopted research approach of this doctoral study, there are more opportunities for future work as well as new research questions that yet to be answered. Some examples for future recommended studies include:

- The results of this study demonstrated that the PMMA-PC and the ABC-UTC NP-UHPC mixes can be potentially used inside the transverse and longitudinal field joints in precast bridge deck systems. The experimental approach of the current study utilizes a static monotonic loading of the deck specimens, while the bridge decks are usually subjected to large numbers of cyclic loading in real life scenarios. Therefore, more research studies should be done to test the behavior and performance of the proposed PMMA-PC and NP-UHPC joints subjected to cyclic and fatigue loading to determine their long term performance.
- Larger number of analytical and finite element studies, which cannot be all conducted experimentally, are recommended to investigate different parameters such as the variation of the joint width, lap splice length, and reinforcement distribution inside the joints to determine their effect on the structural performance of the bridge decks and to provide new design recommendations for the reinforcement of the bridge decks based on the splicing requirements inside the field joints.
- This study focused on the precast deck field joints in the context of studying one of the most common ABC connections and applications. Thus, it is important to investigate the early behavior of the proposed joint materials. Many material properties should be investigated through the first week of age of the material to determine the appropriate time to remove the formwork, resume construction activities, and open the bridge for traffic. The material properties should include the compressive and tensile strength of the material along with the required development length at early stages and the interface bond strength between the joint materials and conventional concrete substrates.
- The FHWA has recommended a compressive strength of 14 ksi for the P-UHPC field joints to allow for the resumption of work over the bridge. This compressive strength threshold should be determined for the newly proposed joint materials (i.e. PMMA-PC

and NP-UHPC) and revisited for the P-UHPC. The determination of this limit should be dependent on the expected load demands at the construction and operation stages along with the early material strength and behavior determined from the previously mentioned study.

- The proposed NP-UHPC mixes have a relatively lower early strength compared to the other joint materials. This may limit the implementation of these mixes for the ABC applications. Thus, it is important to improve the early strength of such mixes through investigating adding accelerators to the mixture or using heat treatment to accelerate the strength gain of the material.
- It is of paramount importance at this point to assemble a database for the various developed NP-UHPC mixes across the nation, which utilize local materials in different parts of the country to facilitate and encourage the use of these mixes for the construction and bridge application. The database should include detailed information regarding the mix design, proportioning, mixing methodology, material sources, main material properties, early strength of the materials. The database should also include whether a given NP-UHPC mix has been experimentally used for any structural application or practically implemented in real construction projects. The information in such database can also be used to verify the developed equations for estimating the strength of the P-UHPC mixes. This might eventually yield to the development of unified or general equations that can predict the strength and behavior of a wider range of fiber reinforced concrete including the P-UHPC and NP-UHPC materials.